



# Plombylènes stabilisés par des phosphines : précurseurs de nouveaux phosphinidènes et cations plombyliumylidènes

Vladislava Timofeeva

## ► To cite this version:

Vladislava Timofeeva. Plombylènes stabilisés par des phosphines : précurseurs de nouveaux phosphinidènes et cations plombyliumylidènes. Chimie de coordination. Université Paul Sabatier - Toulouse III; Institut N.D. Zelinsky de chimie organique de l'académie des sciences de Russie, 2022. Français. NNT: 2022TOU30276 . tel-04117053

HAL Id: tel-04117053

<https://theses.hal.science/tel-04117053v1>

Submitted on 5 Jun 2023

**HAL** is a multi-disciplinary open access archive for the deposit and dissemination of scientific research documents, whether they are published or not. The documents may come from teaching and research institutions in France or abroad, or from public or private research centers.

L'archive ouverte pluridisciplinaire **HAL**, est destinée au dépôt et à la diffusion de documents scientifiques de niveau recherche, publiés ou non, émanant des établissements d'enseignement et de recherche français ou étrangers, des laboratoires publics ou privés.



# THÈSE

**En vue de l'obtention du  
DOCTORAT DE L'UNIVERSITÉ DE TOULOUSE  
Délivrée par l'Université Toulouse 3 - Paul Sabatier**

**Cotutelle internationale: Zelinsky Institute of Organic Chemistry**

**Présentée et soutenue par  
Vladislava TIMOFEEVA**

Le 14 décembre 2022

**Plombylènes stabilisés par des phosphines : précurseurs de  
nouveaux phosphinidènes et cations plombyliumylidènes**

Ecole doctorale : **SDM - SCIENCES DE LA MATIERE - Toulouse**

Spécialité : **Chimie Organométallique et de Coordination**

Unité de recherche :

**LHFA - Laboratoire Hétérochimie Fondamentale et Appliquée**

Thèse dirigée par  
**Tsuyoshi KATO et Syroeshkin Mikhail**

Jury

**M. Viatcheslav JOUIKOV, Rapporteur**

**M. Vladimir DODONOV, Rapporteur**

**M. Mikhail KINZHALOV, Examinateur**

**Mme Yulia GORBUNOVA, Examinatrice**

**M. Tsuyoshi KATO, Directeur de thèse**

**M. Mikhail SYROESHKIN, Co-directeur de thèse**

**M. Alexander DILMAN, Président**

## *Acknowledgments*

I would like to express a sincere thanks to my supervisors Prof. Dr. Tsuyoshi Kato and Dr. Mikhail Syroeshkin for giving me the opportunity to do my joint project in world-class laboratories and for the interesting research topics. I would like to thank the members of my jury Prof. Dr. Viatcheslav Jouikov, Dr. Dodonov Vladimir, Dr. Kinzhalov Mikhail, Prof. Dr. M. Dilman Alexander and Prof. Mme Yulia Gorbunova who kindly accepted the invitation to correct the manuscript and to come to the PhD defence. To M. Viatcheslav Jouikov and M. Dodonov Vladimir for accepting to be the referees of this work, as well as M. Dilman Alexander for accepting to be the jury president. A particular thanks to Professor Thomas Müller for accepting also to collaborate with us.

I would like to express deep gratitude for Tsuyoshi, for all the conversations about chemistry his optimism and his style of teaching. He was the person who helped me to keep lit the fire in my heart during really dark times with his encouraging attitude and his excellent guidance during the whole PhD time. It was the hardest journey I've undertook but I have learned a lot during my thesis. It was a big honour for me to work with Tsuyoshi.

A particular thanks to Antoine for all the advices and the suggestions he gave me during my thesis, especially for the shaping of my manuscript. Big thanks for administrative and logistic team of the LHFA Maryse, Serah, Florance, Olivier T., Olivier V., Romaric and Julien B. for their help during the whole time I spent in Toulouse. I want to tell big thank you to Romaric, who became my dear friend. Even when I called you from Siberia you always have been there for me =)

I want to express my gratitude to the MHT persons, Marc, Pierre, Claude and Caroline for your precious NMR spectres. You are always optimistic and full of energy, I'm happy to have an occasion to work with such people! I would like to say that I love your sense of humour, Caroline. Our discussions gave me always inspiration with the energy of life. I hope one day to participate in one of your carnivals as a ninja-chemist-pharmacist.

I would like to thank Nathalie (the Goddess of crystals!) for obtaining the crystal structures during all time of my thesis, especially for the advice on how to obtain crystals of the highly sensitive compounds I worked with. Your filigree work impressed me from the dept of my soul.

My thesis would not be possible to be done in vacuum. I would like to tell thank you to the people that became the air for me when I did my work in Toulouse. Aymeric, who became my sensei and taught me all the tricks and techniques, you are great teacher! Sometimes too much emotional, but I was not an easy student, so thank you that you didn't kill me before my defense. Thanks to Ugo, for all the time we spend together doing manipulations. I have an impression that you know answers on all the questions in the world! I'm happy to be the part of "sophisticated" parties with monsieur J.Petit, Alejandro and Luca. You changed my attitude toward the rules, making me much better-behave human being. Aswin, the person that gifted me the plumbylene project, Limiao (thank you for being so supportive and kind always), Deependra (I'm sad that I didn't get an opportunity to see your wedding in India), Cynthia (for instilling in me the vigilance and punctuality so necessary for a chemist), Maria (for encouraging me and training me always to fight for the final goal), Manuel (thank you for all your help with chemistry and for your jokes... "j'ai un couteau et je sais comme l'utiliser"), Shintaro (brilliant scientist with a great future! I believe in you!), Jose (my first «stagiaire». I feel so sorry for it... Especially for the toluene evaporation at Friday evenings, my favourite leisure type that I tried to transfer to you).

I also want to thank SHEN, SYMAC, COP and LPBP teams. In particular Alejandro-Sweet-Potato, who became my first best friend in Toulouse. You are an endless source of the energy, always ready to go for

crazy adventures. Also, I want to say thanks for Soukaina, who always smile and stayed at the evenings and weekends at the lab with me. Thanks for Julien P. (for your excursion to Lyon and for the evening of French culture with Fatal Bazooka), Ana and Corine (for all our discussions), Corentin (I'm always impressed by your spirit power!), and particular thanks for Enrico. I feel honoured of having a such great and beautiful person among my friends. Never give up, that was a simple idea that filled my existence after meeting you.

I also want to express gratitude for my Russian colleagues, in particular to Pasha, with whom we have started this path together four years ago. It was completely not easy, both of us changed so much after all these years, but I feel that it did not affect our sincere friendship. I want to tell thank for Pavel G., who appeared in my life the last year. I was so curious to know about your rocket-fuel chemistry =)

Also I want to tell thank for Ana S. with whom I was able to go through a storm. I am very grateful for Irina Krylova, for her excellent help and it has been a great experience working with her. Thanks to Artem F. for help with understanding the tricks of NMR (would be so great if one day you will meet Caroline). Lubov Nikolayevna, thank you for your excellent classes of English language. You are the best English teacher I've ever met.

I want to tell thank for my family who supported me enormously. Without them I would not have done even the first step. I feel a deep gratitude for my dear mother and father that were always with me, even when I left home to live in France for almost two years.

At the end, I want to tell thank for mon cheri Luca. You simply changed my world, always being with me and demonstrating that life is not as convoluted as me, as a highly paranoid person, always thought. Your words of support and motivation encouraged me always, making me strong enough to continue writing my own story. Even if we were forced to stay for some time on a distance I've never feel lonely. Thank you for all love and happy moments we share together.

# Summary

Foreword.....	7
General introduction.....	13
<b>Chapter I: Bibliography introduction.....</b>	15
<b>I. Carbenes .....</b>	17
<b>II. Tetrylenes (heavier analogues of carbenes, E = Si, Ge, Sn) .....</b>	19
-Stabilization of tetrylenes.....	20
-Substituent effect (size and $\sigma$ -donating character) on the HOMO-LUMO gap and reactivity of tetrylenes.....	21
- Activation of small molecules ( $H_2$ , $NH_3$ and others) by tetrylenes (E = Si, Ge, Sn) .....	23
• Small molecules activation by <b>stable silylenes</b> .....	23
Cyclodiaminosilylenes.....	23
NHSi with a 1,1'-ferrocenediyl backbone.....	23
• Small molecules activation by <b>Germylenes</b> .....	27
$H_2$ activation by stable diarygermylenes.....	27
$NH_3$ activation by germylenes substituted by bulky aryl groups.....	28
• Small molecules activation by <b>Stannylenes</b> .....	28
$H_2$ activation by Stannylenes substituted by bulky aryl groups.....	28
$NH_3$ activation by stannylenes substituted by bulky aryl groups.....	29
Small molecule activations by diboryl stannylenes.....	30
<b>III. Plumbylenes.....</b>	31
- <b>Synthesis of stable plumbylenes</b> .....	31
Diarylplumbylenes.....	31
Diaminoplumbulenes.....	32
- <b>Synthesis of donor-stabilized tricoordinate plumbylenes</b> .....	36
Stabilized diaminoplumbbylenes with a ferrocene ligand scaffold.....	36
Diaminoplumbbylenes stabilized by $\beta$ -diketiminate.....	37
Plumbylenes stabilized by a NON-backbone ligand .....	38
(Amino)(alkoxy) stabilized plumbylenes.....	39
<b>III.I Reactivity of plumbylenes .....</b>	39
<b>III.II Polymerization of lactide catalyzed by plumbylenes.....</b>	42
<b>IV. Plumbylene Cations.....</b>	42
<b>V. Amido-phosphine ligand supported metallylenes. ....</b>	45
V.I Phosphine stabilized silylenes and germylenes.....	45
<b>VI. Conclusions.....</b>	47

<b>Bibliographic references.....</b>	48
<b>Chapter II: Synthesis of Plumbylene-Substituted Phosphaketene and Decarbonylation reaction.....</b>	52
<b>I. Introduction .....</b>	53
I.I Phosphinidenes and base-stabilized singlet phosphinidenes.....	53
I.II Synthesis and reactivity of phosphine-stabilized phosphinidenes (phosphanylidene- $\sigma^4$ -phosphoranes) .....	53
I.II.I <i>Phosphanyl-phosphanylideneephosphoranes (R<sub>2</sub>P-P=P(X)R'</i> <sub>2</sub> ) .....	54
I.II.II <i>Aryl-substituted phosphanylideneephosphoranes (ArP=PR'</i> <sub>3</sub> ) .....	55
I.II.III <i>Cyclic phosphanylideneephosphoranes.....</i>	57
I.II Phosphaethynolate anion as a suitable source of anionic phosphorus .....	59
<b>II. Results and discussion.....</b>	61
II.I Synthesis and characterisation of iminophosphine-stabilized chloroplumbylene <b>29</b> .....	61
II.II Synthesis and characterisation of iminophosphine-stabilized lead phosphaketene <b>30</b> .....	62
<b>III. Decarbonylation reaction of the lead-phosphaketene <b>30</b>.....</b>	64
III.I Characterization of phosphanylidene- $\sigma^4$ -phosphoranes <b>35</b> and <b>36</b> .....	64
III.II Mechanistic study.....	66
III.IV Theoretical investigation of phosphanylidene- $\sigma^4$ -phosphorane <b>35</b> by DFT calculations.....	69
<b>IV. Reactivity of (amino)phosphanylidene-<math>\sigma^4</math>-phosphorane <b>35</b>.....</b>	70
IV.I. Reaction with BH <sub>3</sub> ·THF.....	70
IV.II. Reaction with 3,5-di-tertbutyl-o-benzoquinone (TCBQ) .....	71
IV.III. Reaction of <b>35</b> with of 2,6-Dimethylphenyl isocyanide.....	72
IV.IV. Reaction with of phenylsilane Ph <sub>3</sub> SiH.....	74
<b>V. First attempts for the synthesis of sulfide-stabilized phosphinidene <b>52</b>.....</b>	75
V.I. Synthetic strategy .....	75
V.II. First attempt for the synthesis of sulfide-stabilized chloroplumbylenes <b>50</b> .....	76
<b>VI. Conclusions and perspectives .....</b>	79
Bibliographic references.....	80
Experimental part.....	83
<b>Chapter III: Synthesis and reactivity of cationic plumbylenes.....</b>	93
<b>I. Introduction.....</b>	94
I.I Hydroamination .....	94
• Acid-catalysed hydroamination of alkenes and alkynes.....	94
• Base-catalysed hydroamination of alkenes and alkynes.....	95
• Hydroaminations Catalyzed by Transition Metals .....	97
❖ Early Transition Metal-Catalyzed Hydroamination.....	97
❖ Late Transition Metal-Catalyzed Hydroamination.....	98

Nucleophilic attack on a coordinated alkene or alkyne.....	99
Nucleophilic attack of amine nitrogen atom on allylic complexes.....	100
Insertion of the alkene/alkyne into metal-hydride bond .....	102
Oxidative addition of the amine to electron-rich metal center.....	105
❖ Rare Earth Metal-Based Catalysts.....	107
<b>II. Results and discussion:</b> .....	108
• Synthesis of cationic derivatives of plumbbylenes.....	109
<b>II.I Stabilisation of plumbbyliumylidenes with Lewis bases</b> .....	110
• Cationic plumbbyliumylidenes stabilized by tertiary phosphines <b>48-PR<sub>3</sub></b> ( <b>R = Me, Ph</b> ) .....	110
• Reactivity of complexes <b>48-PR<sub>3</sub></b> ( <b>R = Me, Ph</b> ) with an alkyne. ....	110
• Cationic plumbbyliumylidenes stabilized by secondary phosphines <b>48-HPR<sub>2</sub></b> ( <b>R = Ph, iPr</b> ) .....	113
• Cationic plumbbyliumylidenes stabilized by secondary amines <b>48-HNR<sub>2</sub></b> ( <b>R = iPr</b> ) .....	115
• Reactivity of complex <b>48-NHiPr<sub>2</sub></b> with alkynes. ....	116
• Cationic c stabilized by ammonia <b>48-NH<sub>3</sub></b> .....	117
<b>III. Conclusions and perspectives</b> .....	121
Bibliographic references.....	122
Experimental part.....	125
<b>General conclusion</b> .....	144
<b>Annexe</b> .....	146
<b>Résumé du projet</b> .....	167
<b>Abstract</b> .....	188

## **Foreword**

## **General handling conditions**

All manipulations were performed under inert atmosphere of argon by using Schlenk or high-pressure NMR tube techniques. The solvents used have been purified by the solvent purifier MBraun SPS-800 over filtrating columns filled with molecular sieves of 0.4 nm, and have been stocked under Argon atmosphere.

## **Equipment**

### Nucleus Magnetic Resonance (NMR)

$^1\text{H}$ ,  $^{11}\text{B}$ ,  $^{13}\text{C}$ ,  $^{19}\text{F}$ ,  $^{31}\text{P}$ ,  $^{29}\text{Si}$  and  $^{207}\text{Pb}$ : Bruker Avance II 300 MHz, Avance III HD 400 MHz and Avance I and III HD 500 MHz spectrometers. The complete characterization of the products has been done using 1D experiments, as well as 2D analysis, such as COSY ( $^1\text{H}$ - $^1\text{H}$ ,  $^{31}\text{P}$ - $^{31}\text{P}$ ), HSQC ( $^1\text{H}$ - $^{13}\text{C}$ ,  $^1\text{H}$ - $^{29}\text{Si}$ ), HMBC ( $^1\text{H}$ - $^{13}\text{C}$ ,  $^1\text{H}$ - $^{31}\text{P}$ ,  $^1\text{H}$ - $^{29}\text{Si}$ ).

$^1\text{H}$ ,  $^{29}\text{Si}$  and  $^{13}\text{C}$  NMR chemical shifts are reported in ppm relative to  $\text{SiMe}_4$  as internal standard.  $^{31}\text{P}$  NMR chemical shifts are expressed in ppm relative to 85 %  $\text{H}_3\text{PO}_4$ .  $\text{CFCI}^3$  for  $^{19}\text{F}$  and  $\text{BF}_3\text{OEt}_2$  for  $^{11}\text{B}$  (15 % solution in  $\text{CDCl}_3$ ).  $^{207}\text{Pb}$  chemical shifts are relative to  $\text{Me}_4\text{Pb}$  as external reference. The chemical shift have been counted positively verse the low field, and expressed in part per million (ppm). The coupling constant are expressed in Hz.

The following abbreviations and their combinations are used: br, broad; s, singlet; d, doublet; t, triplet; q, quartet; sept, septuplet m, multiplet, Ar (aromatic),  $J_{AB}$  (coupling constant between A and B).

### **Melting point.**

Digital device Electrothermal Stuart SMP40. The samples have been prepared in the glove-box before the analysis.

### **X-ray diffraction analysis.**

The X-ray diffraction analysis has been carried out by Nathalie Saffon-Merceron, using Bruker-AXS APEX II CCD Quazar and Bruker-AXS D8-Venture diffractometers. The structures were solved using SHELXT programs.<sup>[1]</sup>

### **Mass spectroscopy.**

ESI-HRMS data were obtained on a Waters Xevo G2 Q-TOF mass spectrometer.

### **Theoretical calculations**

The theoretical calculations have been carried out by Dr. Gül Altınbaş Özpinar, Dr. Saskia Rathjen and by Dr. Thomas Müller (professor in the Carl-von-Ossietzky University of Oldenburg, Germany), using the Gaussian 16<sup>[2]</sup> program package. The M06-2X/6-311+G(d,p)<sup>[3]</sup> computational level was used for structure optimizations.

The nature of transition states were characterized by frequency computations on M06-2X/6-311+G(d,p) computational level. Intrinsic reaction coordinate (IRC)<sup>[4]</sup> calculations for the transition states were performed at the same computational level. Integral Equation Formalism-Polarizable Continuum Model (IEF-PCM) method was used to investigate solvent effects. M062X/6-311G(d,p)//M062X/6-311+G(d,p) level used in order to perform molecular orbital computations. Natural Bond Orbital (NBO) and Natural Chemical Shift (NCS) analysis were done using the NBO<sup>[5]</sup> program as implemented in Gaussian 16 Rev C.01 program. GausView<sup>[6]</sup> and Jmol<sup>[7]</sup> program packages were applied to create molecular orbitals and NBOs.

## Abbreviations

2-Py	2-benzoyl pyridine
Ar	Aryl
BINAP	2,2'-bis(diphenylphosphino)-1,1'-binaphthyl
Cat	Catalyst
Cp*	pentamethylcyclopentadienyl
cAAC	Cyclic alkyl amino carbene
COD	1,5-Cyclooctadiene
DCM	Dichloromethane
DFT	Density Functional Theory
DMAP	4-(dimethylamino)pyridine
DMSO	Dimethyl sulfoxide
DTBM	3,5-di-tert-butyl-4-methoxy
Dipp	2,6-Diisopropylphenyl
Dppf	1,1'-Bis(diphenylphosphino)ferrocene
Equiv.	Equivalent
Et	Ethyl
eV	Electron volt
FLP	Frustrated Lewis pairs
FcPH <sub>2</sub>	ferrocenylphosphine
HBpin	Pinacolborane

HOMO	highest occupied molecular orbital
<i>i</i> Pr	<i>iso</i> -propyl
Kcal	Kilocalorie
LB	Lewis base
LUMO	lowest unoccupied molecular orbital
liq	liquid
MBTE	Methyl tert-butyl ether
MHz	Megahertz
Me	Methyl
<sup>Me</sup> IMe	1,3,4,5- tetramethylimidazolin-2-ylidene
MeOH	Methanol
Mes	1,3,5-Trimethylbenzene
NBO	Natural Bond Order
NHC	N-heterocyclic carbene
NHGe	N-heterocyclic germylene
NHSi	N-heterocyclic silylene
NICS -	Nucleus-Independent Chemical Shifts
NON	4,5-bis(2,6)-diisopropylphenyl-amino-2,7-di-tert-butyl-9,9-dimethyl-xanthene
Na(OCP)	Sodium phosphaethylnolate
NacNac	$\beta$ -diketiminate
<i>n</i> BuLi	<i>n</i> -butyllithium
Ph	Phenyl
Ppm	Parts per million
ROP	ring-opening polymerisation
RT	room temperature
Sergphos	5,5'-Bis(diphenylphosphino)-4,4'-bi-1,3 benzodioxole
TCBQ	3,5-di-tertbutyl-o-benzoquinone

TFA	Trifluoroacetic acid
THF	Tetrahydrofuran
TM	transition metal
TMEDA	N,N,N',N'-Tetramethylethylenediamine
TOF	turnover frequency
TS	Transition state
Tipp	2,4,6-triisopropylphenyl group
Tol	toluene
Triphos	1,1,1-Tris(diphenylphosphinomethyl)ethane
<i>t</i> Bu	<i>tert</i> -butyl
UV	Ultra-violet
XRD	X-Ray diffraction analysis

- [1] G. M. Sheldrick, *Acta Crystallogr. Sect. A Found. Crystallogr.* **2015**, *71*, 3–8.
- [2] G. M. J. Frisch, G. W. Trucks, H. B. Schlegel, G. E. Scuseria, M. A. Robb, J. R. Cheeseman, J. Scalmani, V. Barone, G. A. Petersson, H. Nakatsuji, X. Li, M. Caricato, A. V. Marenich, A. F. I. Bloino, B. G. Janesko, R. Gomperts, B. Mennucci, H. P. Hratchian, J. V. Ortiz, A. J. L. Sonnenberg, D. Williams-Young, F. Ding, F. Lipparini, F. Egidi, J. Goings, B. Peng, W. Petrone, T. Henderson, D. Ranasinghe, V. G. Zakrzewski, J. Gao, N. Rega, G. Zheng, Y. Liang, M. Hada, M. Ehara, K. Toyota, R. Fukuda, J. Hasegawa, M. Ishida, T. Nakajima, F. Honda, O. Kitao, H. Nakai, T. Vreven, K. Throssell, J. A. Montgomery, Jr., J. E. Peralta, R. L. Ogliaro, M. J. Bearpark, J. J. Heyd, E. N. Brothers, K. N. Kudin, V. N. Staroverov, T. A. Keith, R. Kobayashi, J. Normand, K. Raghavachari, A. P. Rendell, J. C. Burant, S. S. Iyengar, J. Tomasi, M. Cossi, J. M. Millam, M. Klene, C. Adamo, R. Cammi, J. W., and D. J. F. Martin, K. Morokuma, O. Farkas, J. B. Foresman, *Gaussian 16, Rev. C.01, Gaussian, Inc., Wallingford CT, 2016.*, **2016**.
- [3] Y. Zhao, D. G. Truhlar, *Theor. Chem. Acc.* **2008**, *120*, 215–241.
- [4] a) K. Fukui, *Acc. Chem. Res.* **1981**, *14*, 363–368. b) H. P. Hratchian and H. B. Schlegel, in Theory and Applications of Computational Chemistry: The First 40 Years, Ed. C. E. Dykstra, G. Frenking, K. S. Kim, G. Scuseria (Elsevier, Amsterdam, 2005) 195 – 249. S8 G. Scalmani, M. J. Frisch, *J. Chem. Phys.*, **2010**, *132*, 114110
- [5] E. D. Glendening, J. K. Badenhoop, A. E. Reed, J. E. Carpenter, J. A. Bohmann, C. M. Morales, P. Karafiloglou, C. R. Landis, and F. Weinhold, Theoretical Chemistry Institute, University of Wisconsin, Madison (2018).
- [6] GaussView, Version 6.1, Roy Dennington, Todd A. Keith, and John M. Millam, Semichem Inc., Shawnee Mission, KS, 2016
- [7] Jmol development team. (2022).

## **General Introduction**

## General introduction

The last few years have seen a major resurgence in Main group chemistry due to the development of low valence main group compounds featuring a transition metal behaviour.

Among these species, carbenes and their heavier analogues, tetrylenes, which possess a small HOMO-LUMO gap and transition metal-like boundary orbitals, are promising candidates to replace expensive transition metal complexes. Indeed, they are capable of activating small molecules through an oxidative addition step. However, tetrylenes tend to form very stable oxidative adducts in the high oxidation state (IV), which complicates the subsequent regeneration of the lower oxidation state species via a reductive elimination.

The relative stability of low oxidation states in group 14 species increases with increasing the atomic number of the corresponding element, and thus, the divalent state of plumbylenes is the most stable among the other tetrylenes. Besides, since Pb-C bonds are particularly weak, the substituents on the Pb atom are labile and can be easily exchanged. Thus, theoretically, plumbylenes could be the most suitable class among the other tetrylenes for catalysis. Moreover, the reactivity of these species could be enhanced by their transformation into cationic plumbylenes (plumbyliumylidene ions), which possess an additional vacant p-orbital and a cationic charge on the lead moiety, making them extremely reactive and electrophilic.

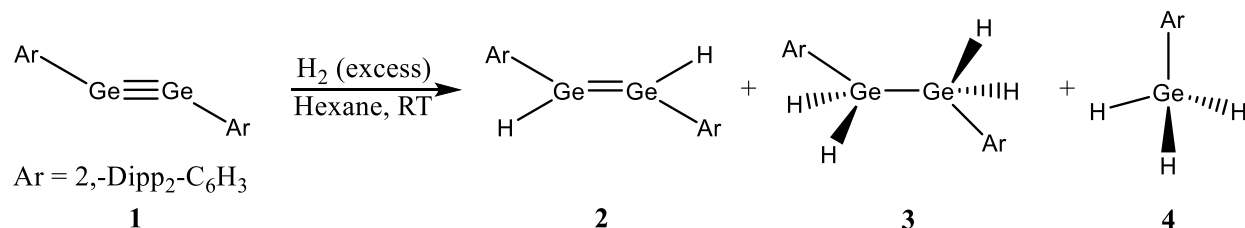
However, a detailed knowledge of the chemistry of plumbyliumylidenes and their reactivity is still lacking. This thesis aims to fill this gap by developing new ionic complexes of plumbylene and plumbyliumylidene stabilized by an original amido-phosphine ligand developed by our group, and to study their chemistry, aiming at new specific properties and reactivity that cannot be induced by other ligand systems.

## **Chapter I: Bibliography introduction**

## **Chapter I: Bibliography introduction:**

The cleavage of strong  $\sigma$ -bonds (such as C-H, C-C, N-H or C-O) has long been considered mainly as domain of transition metal complexes.<sup>[1][2][3]</sup> Due to weak E-M bonds compared to E-H or E-E bonds, transition metal complexes are capable to activate small molecules and implement catalytic cycles.

The landmark discovery of Philip P. Power in 2005 who reported the first example of small molecule activation by low valent main group species opened a new avenue in low valent main group chemistry.<sup>[4]</sup> Indeed, the stable digermyne **1** readily activated hydrogen under mild conditions (room temperature, 1 atmosphere), to give the mixture of digermene **2**, digermane **3** and primary germane **4** (Scheme 1).



**Scheme 1.** Activation of H<sub>2</sub> by digermyne **1**.

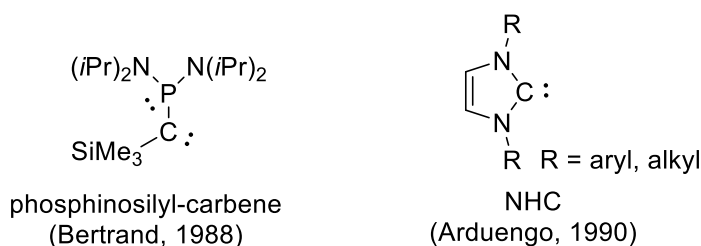
This breakthrough inspired a series of experiments that revealed the ability of main-group compounds to activate a range of small molecules containing strong bonds (e.g., H-H, N-H, C-F).<sup>[5,6]</sup> Thus, a question arises: can low-valent compounds of main group 14 become an effective alternative to rare and expensive transition metal complexes? Theoretical studies have revealed that low-valent group 14 compounds possessing a small HOMO-LUMO gap can potentially present a characteristic of transition metal-like molecular orbitals.<sup>[7-9]</sup> Such frontier orbitals with a small energy gap facilitate oxidative addition reactions at the center of the low-valent group 14,<sup>[6-9]</sup> despite the reductive elimination step for these species remains a challenge. Currently, this is the limiting factor for the development of main-group catalytic systems based on reversible oxidative addition/reductive elimination steps.<sup>[5,10-14]</sup>

Three types of main group based species, presenting transition metal like behaviour, can be distinguished: Frustrated Lewis pairs (FLP), heavier analogues of alkynes and stable singlet carbenes with its heavier analogues (tetrylenes).

In this chapter, we will focus on bibliographic research on carbenes and tetrylenes. We will review recent developments in this chemistry with emphasis on the chemistry of plumbylenes and their cationic derivatives - plumbylliumylidenes.

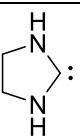
## I. Carbenes

Carbenes ( $R_2C:$ ) are neutral divalent carbon species, which possess only 6 valence electrons with two non-bonding electrons. They exist either in a singlet or triplet ground state, depending on the electronic and steric properties of the substituents.<sup>[15]</sup> For a long time, they were considered as short-lived reactive intermediates. However, since the discovery of two stable carbenes: (phosphino)(silyl)carbenes by G. Bertrand in 1988<sup>[16]</sup> and cyclic diaminocarbenes (NHCs) by Arduengo in 1990<sup>[17]</sup> the chemistry of stable carbenes has been remarkably developed.



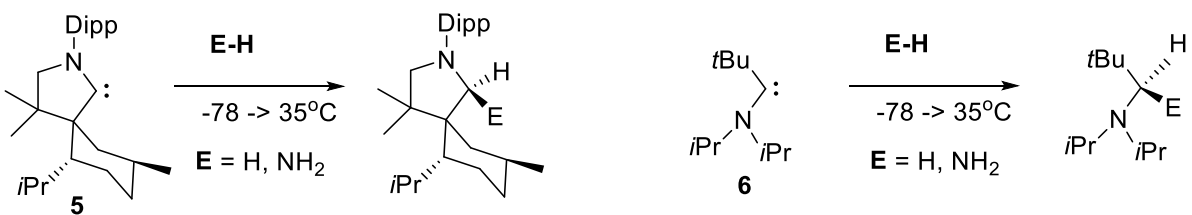
The types of substituents are particularly important to stabilize carbene both sterically (*via* kinetic protection and the control of the angle near the central carbene atom) and thermodynamically (*via* mesomeric and inductive effects).

The effects of amino-groups are especially substantial, which strongly affects the energy level of the frontier orbitals ( $\sigma$  and  $p_\pi$ ). Notably the introduction of amino groups considerably increases HOMO-LUMO gap and thus leads to their stabilisation, to their decreased reactivity as carbenes (ambiphilic reactivity). For instance, Arduengo-type carbenes (NHCs) stabilized by two strongly donating amino groups are unable to activate small molecules such as  $H_2$  or  $CO$  (Table 1).<sup>[5,18]</sup>

Carbene				
$\Delta E_{S-T}$ (kcal/mol)	68.1	51.1	46.2	33.2
$E_{HOMO}$ (eV)	-5.2	-5.1	-5.0	-5.0

**Table 1.** Singlet-triplet energy gap [ $\Delta E_{S-T}$ (kcal/mol)] for different types of carbenes.

On the contrary, carbenes stabilized by only one amino group such as the cyclic alkyl amino carbene **5** and acyclic alkyl amino carbene **6** are particularly reactive and are able to cleave H-H and N-H bond under mild conditions. The difference in reactivity of these amino-substituted carbenes is correlated to the differences of their singlet-triplet energy gaps ( $\Delta E_{S-T}$ ) which are calculated to be significantly smaller for the cAACs ( $46.2 \text{ kcal mol}^{-1}$ ) than NHCs ( $68.1 \text{ kcal mol}^{-1}$ ). Therefore, the activation energy for the insertion reaction is  $10 \text{ kcal mol}^{-1}$  lower for the cAACs. Additionally, alkyl amino carbenes **5** and **6** possess a higher lying HOMO than Arduengo-type carbenes due to the presence of  $\sigma$ -donating but not  $\pi$ -donating alkyl group instead of the electronegative and  $\pi$ -donor amino substituents of diaminocarbenes.<sup>[5]</sup>



**Scheme 2.** Activation of  $\text{H}_2$  and  $\text{NH}_3$  by cyclic (**5**) and acyclic (**6**) alkyl amino carbenes.

The activation of  $\text{H}-\text{H}$  and  $\text{N}-\text{H}$  bonds starts with the interaction of HOMO of carbene with the  $\sigma^*$ -orbital (LUMO) of  $\text{H}_2$  or  $\text{NH}_3$ . It leads to elongation and polarization of  $\text{E}-\text{H}$  bond. The hydridic hydrogen or  $\text{H}_2\text{N}$  of the polarized transition state subsequently attacks positively polarized carbene centre, resulting in complete cleavage of  $\text{E}-\text{H}$  bond (figure 1).<sup>[18]</sup>

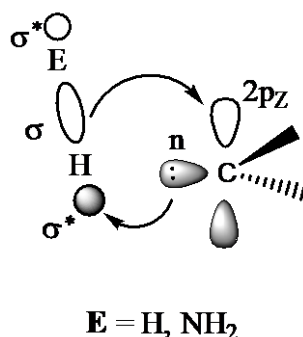
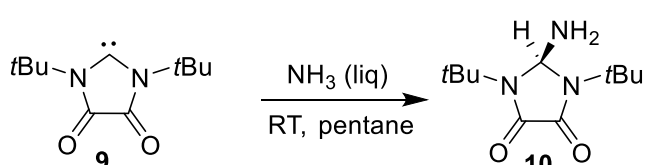
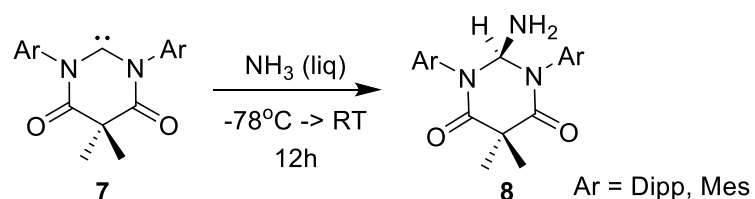


**Figure 1.** Mechanism of  $\text{E}-\text{H}$  ( $\text{E} = \text{H}, \text{NH}_2$ ) activation by cyclic or acyclic alkyl amino carbenes.

The computational study on the addition of  $\text{H}_2$  to a cyclic or acyclic alkyl amino carbenes by Ess et al.-revealed that the alkyl amino carbenes possess more ambiphilic nature but not solely a nucleophilic than NHCs.<sup>[19]</sup>

Although classical Arduengo-type NHCs are known to be inert toward ammonia, the introduction of electron withdrawing substituents on N atoms (to decrease the electron donation of amino groups to the carbene center), increases their reactivity. Indeed, the cyclic diaminocarbenes **7** and **9** with a carbonyl group at each nitrogen atom are able to activate  $\text{NH}_3$  to give the corresponding amines **8** and **10**.<sup>[20-22]</sup>



**Scheme 3.** Ammonia activation by di(amido) carbenes.

For **7**, an electrophilic activation of  $\text{NH}_3$  was proposed instead of the classical nucleophilic pathway proposed for cAACs.<sup>[23]</sup> In this case, the first step of the reaction is the interaction of the lone pair of ammonia with the vacant p orbital of carbene (Figure 2).

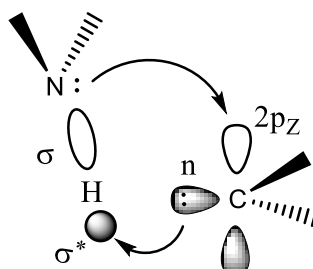
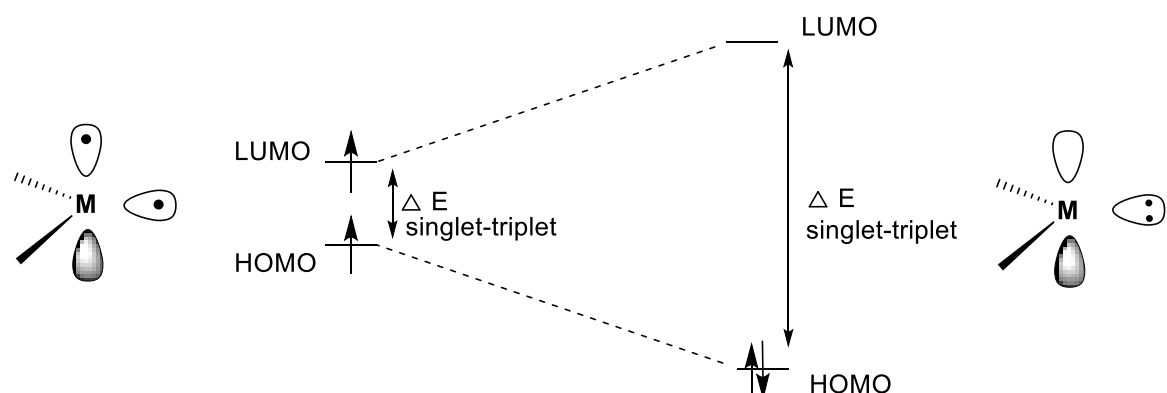


**Figure 2.** Electrophilic model of activation of  $\text{NH}_3$  by carbenes.

## II. Tetrylenes (heavier analogues of carbenes, E = Si, Ge, Sn)

Tetrylenes ( $\text{R}_2\text{E}:$ ) are the heavier analogues of carbenes featuring a divalent E atom ( $\text{E} = \text{Si, Ge, Sn, Pb}$ ).<sup>[24]</sup> Tetrylenes have found diverse application in small molecules activation<sup>[5,6,8,25,26]</sup>, catalysis,<sup>[7,14]</sup> and as ligands for transition metal complexes.<sup>[27]</sup>

Unlike carbon, the heavier counterparts have a lower ability to form hybrid orbitals (the inert lone pair effect is increasing down the group, which decreases the degree of sp-mixing at E atom and thus increases the HOMO-LUMO energy gap) and consequently tetrylenes ( $\text{H}_2\text{E}:$ ) preferably exist in singlet ground state, while classical carbenes ( $\text{H}_2\text{C}:$ ), are triplet (Figure 3).<sup>[28]</sup>



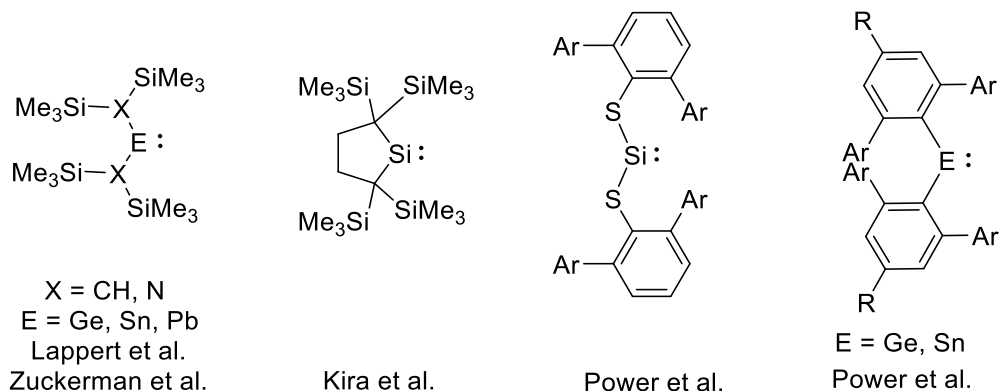
$\text{H}_2\text{M}: \quad \text{H}_2\text{C}: \quad \text{H}_2\text{Si}: \quad \text{H}_2\text{Ge} \quad \text{H}_2\text{Sn}: \quad \text{H}_2\text{Pb}: \quad \text{M} = \text{C, Si, Ge, Sn, Pb}$					
$\Delta E_{\text{S}-\text{T}} (\text{kcal/mol})$	-14.0	16.7	21.8	24.8	34.8

**Figure 3.** Electronic features of carbenes and its heavier analogues.

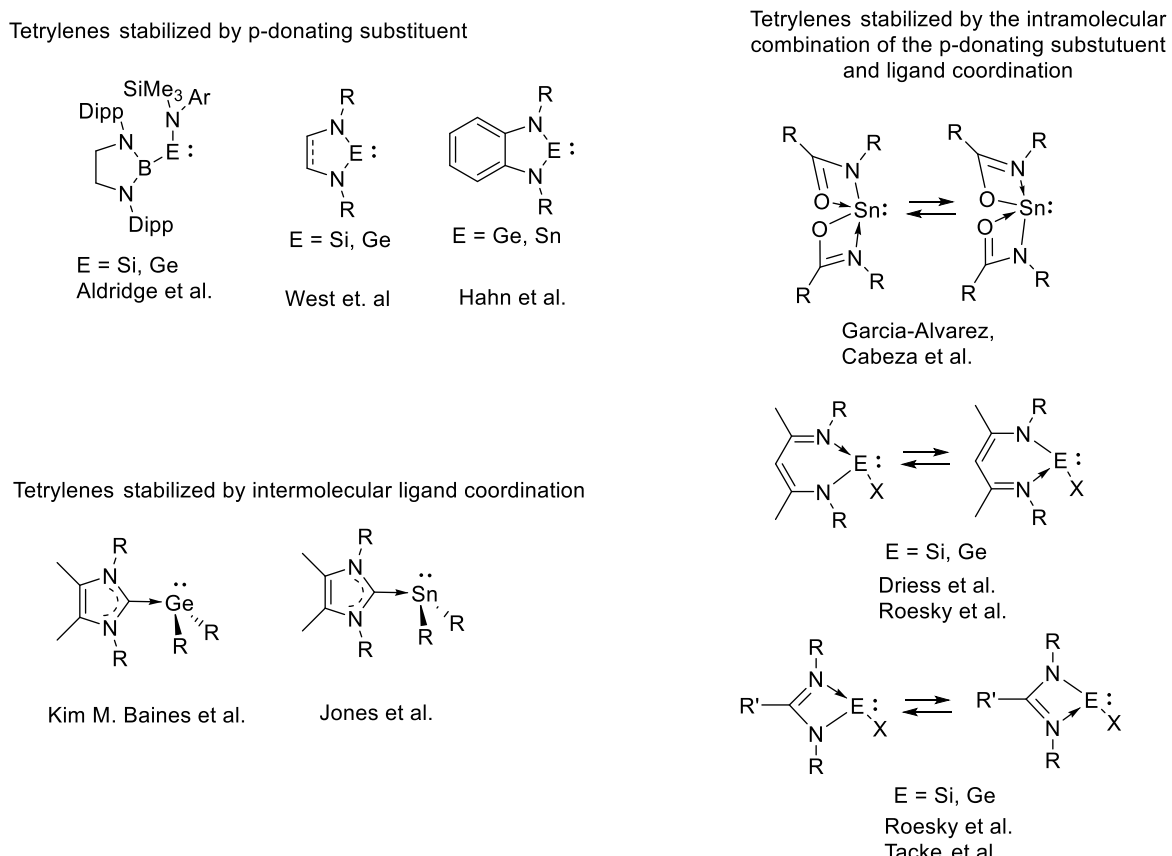
Thus,  $\text{R}_2\text{E}$  ( $\text{E} = \text{Si, Ge, Sn, Pb}$ ) have a vacant p-orbital and a lone pair with enhanced s-character at the same atom (figure 3). Due to their high electron deficiency (the lack of two electrons to satisfy the octet rule) and the presence of a lone pair of electrons they are highly reactive. In this regard, isolation of stable and monomeric tetrylenes is a challenge.

- Stabilization of tetrylenes

Two different strategies to stabilize tetrylenes are known to date.<sup>[29]</sup> The first one is the steric protection (kinetic stabilization) of their reactive site by bulky substituents (Scheme 4).<sup>[30–36]</sup>



The second one is a thermodynamic stabilization of electron deficient E atom by electron donation. Like in the case of carbenes, this can be achieved by introducing  $\pi$ -donating substituents such as amino groups. It could be also implemented by electron donation from the inter- or intramolecular coordination of donating ligands (for example from imine ligand,<sup>[33]</sup>  $\beta$ -diketiminate,<sup>[37–41]</sup> NHC,<sup>[42,43]</sup> amide,<sup>[44]</sup> amidinates,<sup>[45–47]</sup> guanidinates<sup>[48]</sup>) on the E atom. The integration of the E(II) atom into aromatic systems also provides an additional stabilization (for example amides NHGe<sup>[49–51]</sup>).



Thus, thermodynamic stabilisation implies the partial filling of the electron deficient p-orbital of the tetrylene molecule by intra- or intermolecular electron donating substitents or ligands. This mode of stabilisation allows tuning the electrophilicity and therefore chemical behaviour of the corresponding tetrylene divalent atom E(II) while changing the nature of the donating atoms of the substituents. However thermodynamic stabilisation leads to the perturbation of the frontier orbitals of the E(II) atom and their heteroatom substituents, modifying the intrinsic nature of the divalent atom of the tetrylenes. Furthermore, due to increased size of the central E(II) atom going down the group compared to the carbon atom of carbenes, the bond lengths E(II)-R elongates, which leads to the less effective orbital overlap and therefore limited intramolecular stabilization.

While kinetic stabilisation protects reactive site of the molecule by steric shielding of the empty p-orbital, avoiding self-oligomerization reactions and external nucleophilic attacks. The kinetic stabilisation is well suited for the study of the intrinsic nature of a highly reactive species, but on the other hand, the reactivity is limited due to the steric volume introduced by the bulky substituents. The combination of both types of the stabilization (kinetic and thermodynamic) is the most effective way to stabilize tetrylenes, since it allows obtaining the balance between stability of the highly reactive species and its reactivity.

#### -Substituent effect (size and $\sigma$ -donating character) on the HOMO-LUMO gap and reactivity of tetrylenes

The HOMO of  $R_2E$ : is typically associated with the E-centered lone pair, while the LUMO corresponds to p-orbital of  $\pi$ -symmetry.<sup>[28,52]</sup> The energy difference between HOMO and LUMO determines the balance between the reactivity and stability of the tetrylenes. A larger HOMO-LUMO gap relates to higher stability and low chemical reactivity of the corresponding compounds, while a smaller HOMO-LUMO gap results in decreased stability and higher chemical reactivity. Small HOMO-LUMO gap leads also to increasing of the triplet ground state character of the corresponding tetrylenes. Thus, the factors that can influence the HOMO-LUMO gap are the key for the fine tuning of the reactivity of tetrylenes. Indeed, the ability of tetrylenes to activate small molecules has been shown to be attributed to the small HOMO-LUMO gap and the composition of the boundary orbitals which are somewhat similar to those of transition metals (figure 4).

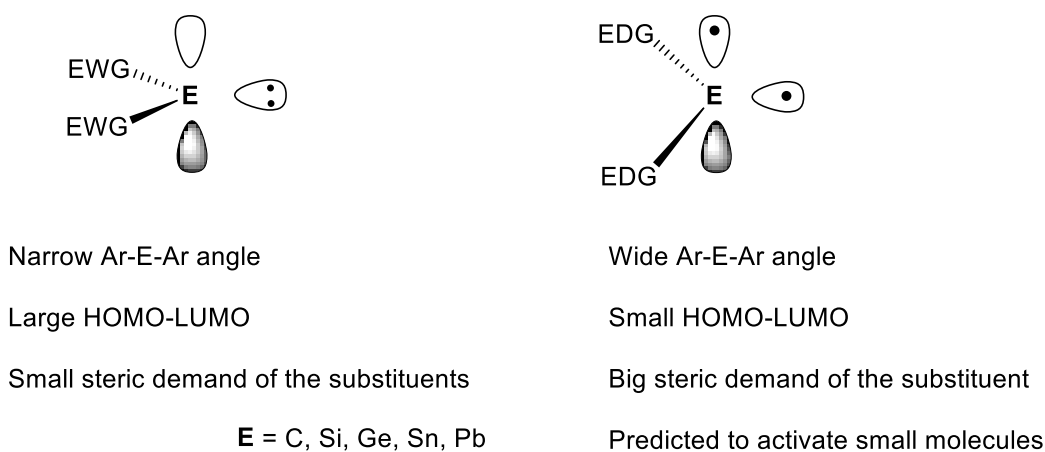
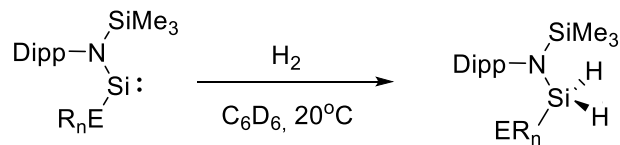


**Figure 4.** The factors that can influence the reactivity of tetrylenes.

The HOMO-LUMO gap is strongly influenced not only by structural and steric parameters but also by electronic properties of the substituents, which are interdependent. Bulky substituents, forcing larger R-E-R angle, decrease the HOMO-LUMO gap and thus enhance the tetrylene reactivity, while the less-hindered

substituents or small cyclic structures, that minimize R-E-R angle, increase their thermodynamic stability. Therefore, acyclic metallylenes generally show higher reactivity towards small molecules activation compared to cyclic ones.

Strongly  $\sigma$ -electron donating substituents also tend to increase the R-E-R angle and thus decreases the HOMO-LUMO gap. On the contrary, tetrylenes with  $\sigma$ -electron withdrawing substituents present smaller R-E-R angles and larger HOMO-LUMO gaps.<sup>[28]</sup> For instance, the introduction of strongly  $\sigma$ -electron donating and bulky silyl or boryl substituents with an electropositive element [electronegativity: Si (1.9), B (2.0)] destabilizes silylenes minimizing the HOMO-LUMO gap, and therefore such boryl- or silyl-substituted tetrylene show a higher reactivity (figure 4).<sup>[33,53]</sup> Indeed, the groups of Aldridge, Jones and Mountford have demonstrated that the boryl- and silyl-substituted aminosilylene **11**<sup>[54]</sup>, **12**<sup>[55]</sup> show a large silylene angle (109.7°, N-Si-Si angle of 116.9°) and a small HOMO-LUMO gap (2.04 eV and 1.99 eV). As a consequence, they are particularly reactive and able to activate H<sub>2</sub> even at room temperature (Scheme 6).<sup>[33,55]</sup>



**11** ER<sub>n</sub> = B(N(Dipp)CH=)<sub>2</sub>

**12** ER<sub>n</sub> = Si(SiMe<sub>3</sub>)<sub>3</sub>

**13** ER<sub>n</sub> = B(N(Dipp)CH=)<sub>2</sub>

**14** ER<sub>n</sub> = Si(SiMe<sub>3</sub>)<sub>3</sub>

**Scheme 6.** H-H activation by stable mixed amido boryl silylenes **11**, **12**.

In contrast, disulfino and cyclic diamino-silylene (**15**<sup>[26]</sup> and **16**<sup>[56,57]</sup>), presenting much smaller silylene angle (93.9° and 90.5°) and larger HOMO-LUMO gaps (4.26 eV and 3.76 eV), are not capable of activating hydrogen.<sup>[58]</sup>

Compound	<b>11</b>	<b>12</b>	<b>15</b>	<b>16</b>
X-Si-X angle [°]	109.7	116.9	90.5	93.9
HOMO-LUMO gap [eV]	2.04	1.99	4.26	3.76

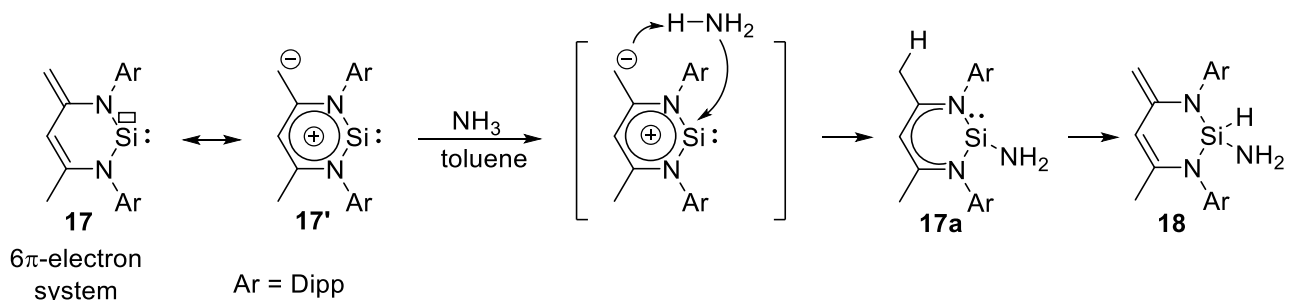
**Table 2.** HOMO-LUMO energy gaps and X-Si-X angles for different types of silylenes.

**- Activation of small molecules ( $\text{H}_2$ ,  $\text{NH}_3$  and others) by tetrylenes (E = Si, Ge, Sn)**

- Small molecules activation by stable silylenes:

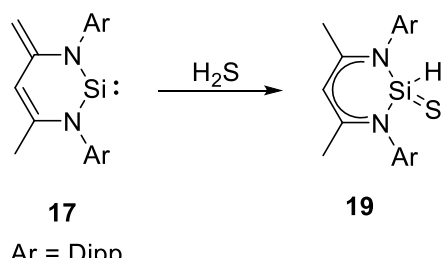
Cyclodiaminosilylenes

Although cyclic tetrylenes are less reactive toward small molecules, there are still some examples of successful  $\sigma$ -bond activation. Indeed, stabilized  $\beta$ -diketiminato silylene **17** is able to activate N-H or S-H  $\sigma$ -bonds of  $\text{NH}_3$  or  $\text{H}_2\text{S}$  under mild conditions. Due to  $\pi$ -electron delocalization silylene **17** exhibits a more pronounced ambiphilicity than other cyclic diaminosilylenes<sup>[49,59]</sup> and it can be represented as the allyl-like mesomeric form **17** as well as the  $6\pi$ -heterofulvene ylide mesomeric form **17'**, featuring a strongly polarized exocyclic C-C bond. Thus, N-heterocyclic silylene **17** possess two reactive sites: the first one is the amphiphilic silylene center with one lone pair and an empty p-orbital, and the second one is the strongly polarised exocyclic C-C bond. When it reacts with the excess of ammonia, the primary kinetic product of 1,4-addition **17a** undergoes an isomerisation and affords the thermodynamically favoured 1,1-addition product **18** (Scheme 7).<sup>[39]</sup>



**Scheme 7.** Activation of  $\text{NH}_2\text{-H}$  bond by  $\beta$ -diketiminato silylene **17**.

The reaction of base stabilized  $\beta$ -diketiminato silylene **17** with gaseous  $\text{H}_2\text{S}$  resulted in the formation of donor-stabilized silathioformamide **19**, which is the first isolable silathioformamide stabilised by intramolecular donor stabilization (Scheme 8).<sup>[39]</sup>

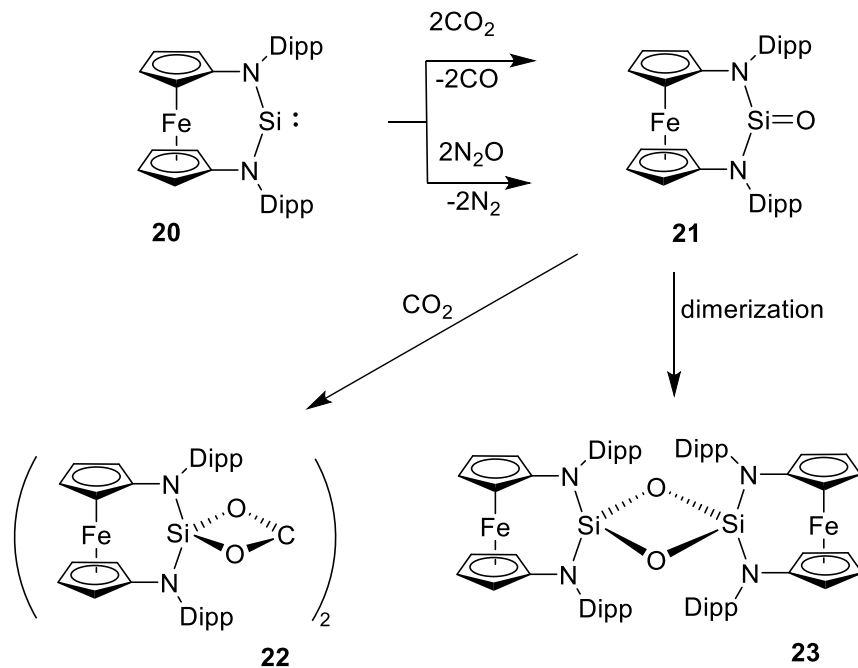


**Scheme 8.** Activation of S-H bond by  $\beta$ -diketiminato silylene **17**.

NHSi with a 1,1'-ferrocenediyl backbone

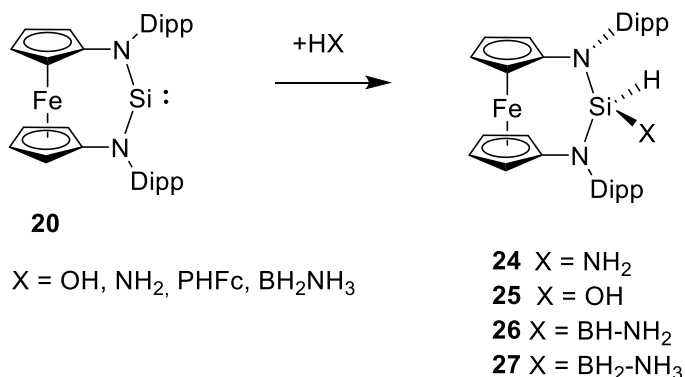
As already mentioned in the section of carbenes, one of the possible strategies for increasing the reactivity of silylenes is the decrease the electron donation of amino groups to the silylene center by the introduction of strongly electron-withdrawing substituents on N atoms. Indeed, in 2021, Siemeling et al. had shown that the ferrocene-based N-heterocyclic silylene **20** possess an increased reactivity compared to that of cyclic dialkylsilylene **17**, which is the only other stable cyclic diaminosilylene with a ring size

larger than five.<sup>[60,61]</sup> Silylene **20** also possesses a wide N-Si-N angle 106° which is larger than other cyclic silylenes (85 - 99°<sup>[49,56,59,62-64]</sup>) indicating an increased reactivity. For example, silylene **20** readily reacts with CO<sub>2</sub> and N<sub>2</sub>O under mild conditions, while cyclic dialkylsilylene **17** is inert (Scheme 9).<sup>[60]</sup> Probably, the first step is the formation of a transient silanone **21** with the CO elimination, which undergoes a subsequent cycloaddition with CO<sub>2</sub> to give orthocarbonate **22**. The same silanone **21** could be formed by the reaction with N<sub>2</sub>O in benzene at room temperature with further dimerization to **23** (Scheme 9).<sup>[61]</sup>



**Scheme 9.** Reactions of **20** with CO<sub>2</sub> and N<sub>2</sub>O under ambient conditions in benzene.

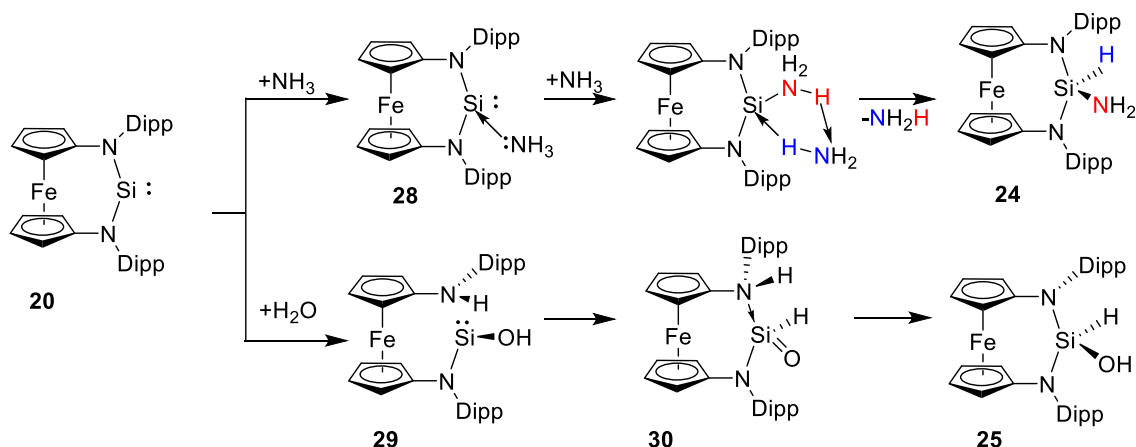
Ferrocene-based N-heterocyclic silylene **20** is also capable of activating strong H-X bonds with different polarities. Albeit it is inert toward H<sub>2</sub>, it reacts with H<sub>2</sub>O, NH<sub>3</sub> and FcPH<sub>2</sub> under ambient conditions furnishing the corresponding oxidative addition products (Scheme 10).<sup>[61]</sup>



**Scheme 10.** Activation of X-H bonds by 1,1'-ferrocenediyl stabilized silylene **20**.

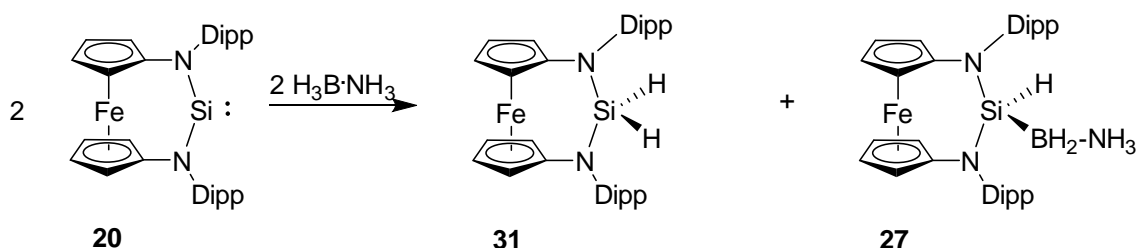
The reactions of silylene **20** with both NH<sub>3</sub> and H<sub>2</sub>O afforded the H-X insertion products. However, DFT studies revealed high kinetic barriers for the direct oxidative addition pathway in both cases (42 and 35 kcal/mol respectively). Two different alternative mechanisms were proposed. The NH<sub>3</sub> activation by **20** proceeds through the formation of the datively bonded intermediate **28** with subsequent proton transfer from a second molecule of NH<sub>3</sub> and formation of the experimentally observed oxidative addition product **24** in a strongly exergonic step with an overall barrier of 20 kcal/mol (Scheme 11, top). While in

the case of H<sub>2</sub>O, the reaction occurs via direct addition of the H<sub>2</sub>O across the Si-N bond with formation of the intermediate hydroxysilylene **29**. Then the product **25** is formed in a strongly exergonic step through the transient silanone **30** via water assisted proton transfer (Scheme 11, bottom)<sup>[61]</sup>.



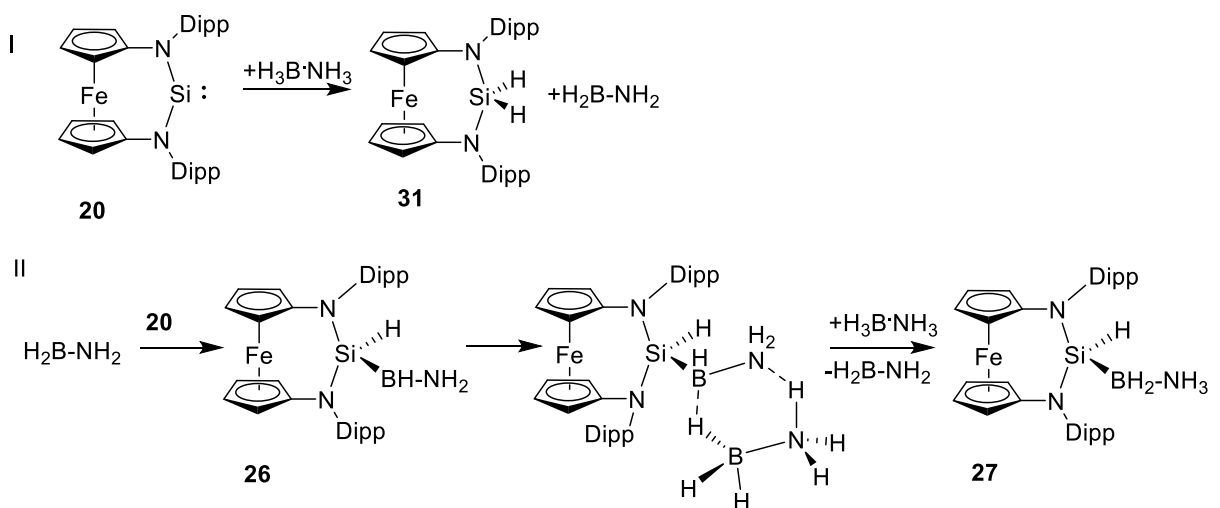
**Scheme 11.** Computed reaction mechanisms for the activation of N-H and H-O bonds by 1,1'-ferrocenediyl stabilized silylene **20**.

The cyclic silylene **20** reacts with H<sub>3</sub>B·NH<sub>3</sub> to afford the dihydrogenated product **31** and the B-H bond insertion product **27** in a 1 : 1 ratio (Scheme 12).



**Scheme 12.** Activation of B-H bond by 1,1'-ferrocenediyl stabilized silylene **20**.

The reaction of two equivalents of H<sub>3</sub>B·NH<sub>3</sub> with silylene **20** consists of two key elementary steps. The first one is the dehydrogenation of H<sub>3</sub>B·NH<sub>3</sub> by silylene **20** to generate H<sub>2</sub>B·NH<sub>2</sub> and silane **31**. The highly reactive dihydrogeno(amino)borane H<sub>2</sub>B·NH<sub>2</sub>, featuring a vacant p-orbital, then reacts with **20** via silylene insertion reaction into the B-H bond affording a transient silylborane **26**, which dehydrogenate a second equivalent of H<sub>3</sub>B·NH<sub>3</sub> to give the final product **27** (Scheme 13).<sup>[61]</sup>

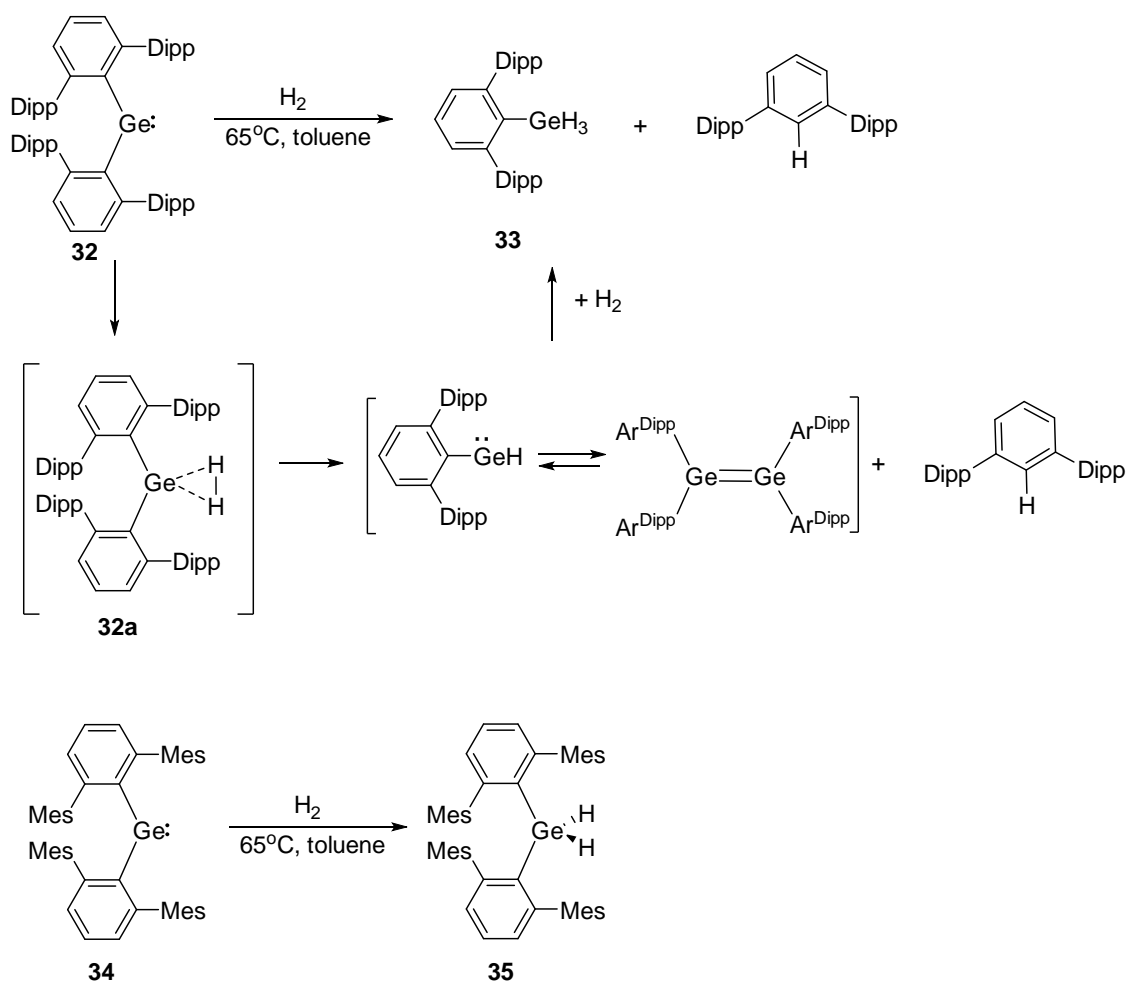


**Scheme 13.** The mechanism of B-H activation by 1,1'-ferrocenediyl stabilized silylene **20**.

- Small molecules activation by Germynes:

### H<sub>2</sub> activation by stable diarygermylenes

As already mentioned, the first example of small molecules activation by main-group species has been implemented by Power in 2005 using stable diarylgermylenes. The reaction affords germane ArGeH<sub>3</sub> (**33**), suggesting the transient formation of germylene Ar-Ge-H, which is able to react with H<sub>2</sub>. Indeed, the stable diarygermylenes **32** and **34** react with H<sub>2</sub> and depending on the steric hindrance around Ge(II) centre two different products were isolated. With the bulkier diisopropylphenyl substituted germylene **32**, the reaction with H<sub>2</sub> resulted in the formation of trihydride **33** along with subsequent elimination of HAr<sup>Dipp</sup>, while with the less hindered germylene **34** dihydride **35** was formed in high yield (Scheme 14).<sup>[65]</sup>

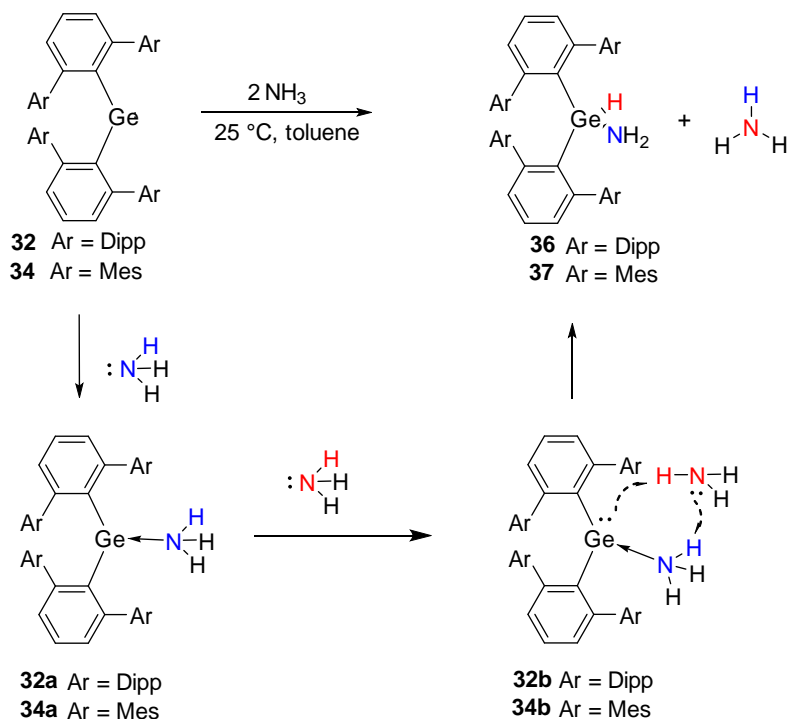


Scheme 14. H-H bond activation by diarylgermylenes **32** and **34**.

Calculations revealed that the initial step for both reactions is the interaction of the σ-orbital of the H<sub>2</sub> with the LUMO of germylene. Then, in the case of **34**, the H-H bond rupture gives the energetically favoured oxidative addition product **35**. While in the case of more sterically hindered germylene **32**, the intermediate **32a** is formed upon addition of the H<sub>2</sub>, and the considerable steric congestion due to the two bulky aryl groups induces the energetically preferred elimination of HAr<sup>Dipp</sup>. Then the transient monoarylgermylene Ar<sup>Dipp</sup>-GeH formed, in the equilibrium with its Ge=Ge bonded dimer, reacts with H<sub>2</sub> to give the final product **33**.<sup>[65]</sup>

### NH<sub>3</sub> activation by germynes substituted by bulky aryl groups

Power et al. have also investigated the reactivity of diaryl germynes **32** and **34** towards ammonia. Interestingly, in both cases, the reaction with NH<sub>3</sub> afforded Ge(IV) oxidative addition products **36** and **37**.



**Scheme 15.** N-H bond activation by diarylgermylenes **32** and **34**.

DFT calculations indicate that two molecules of NH<sub>3</sub> are involved in this reaction. The initial step is the coordination of NH<sub>3</sub> to the germylene leading to transient complexes **32a** or **34a**, which subsequently react with a second molecule of NH<sub>3</sub> *via* an intermolecular N–H interaction, which evolve to give the isolated products **36** or **37**. This pathway is thermodynamically favoured over the arene elimination to give Ar-Ge-NH<sub>2</sub> and H-Ar by 5.7 kcal mol<sup>-1</sup> (Scheme 15).<sup>[65]</sup>

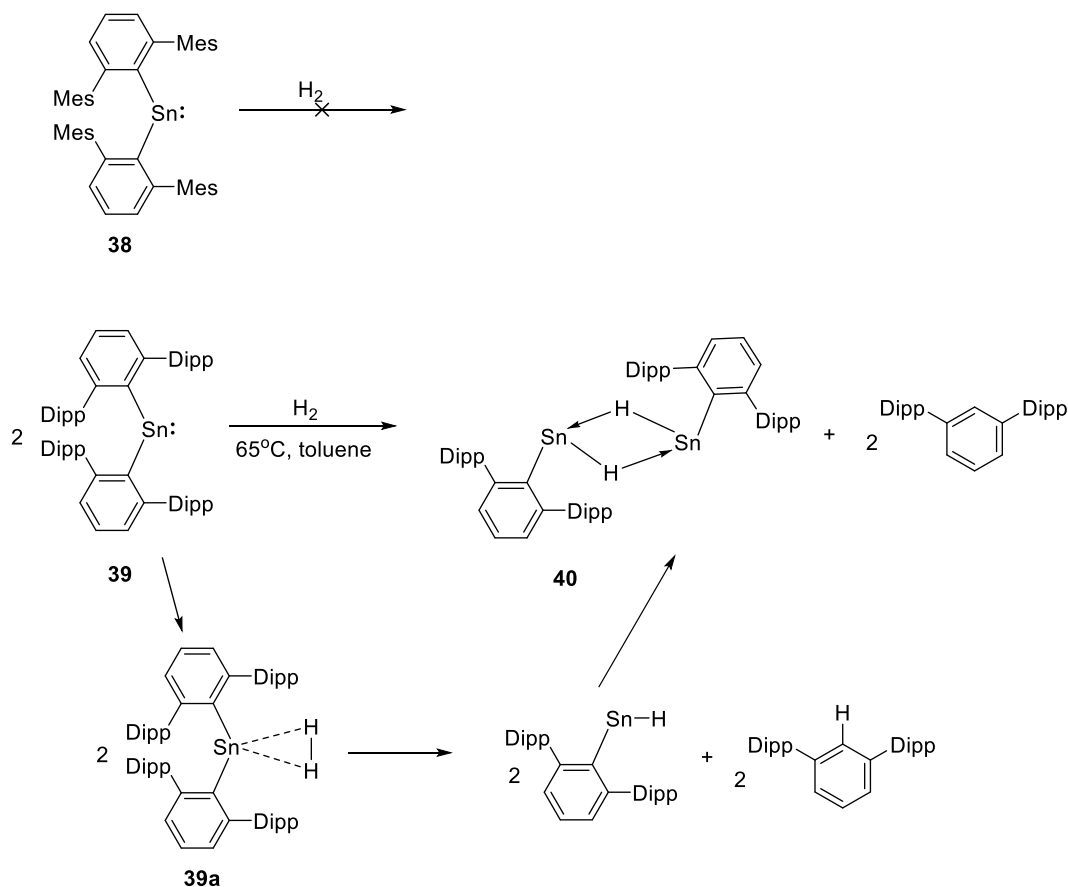
- Small molecules activation by Stannylenes:

### H<sub>2</sub> activation by Stannylenes substituted by bulky aryl groups

In contrast to germylene **34**, the analogous diarylstannylene **38** doesn't react with H<sub>2</sub> even upon heating to 70 °C. However, the more sterically hindered one **39** successfully reacts with dihydrogen at 65 °C affording a dimer of (aryl)(hydrogeno) stannylenes **40** along with elimination of arene. Such difference of reactivity between stannylenes **38** and **39** can be attributed to a widened stannylenes bond angle of **39** compared to that of **38** (117.6° vs 114.7°), leading to a higher reactivity due to a smaller HOMO-LUMO gap (Scheme 16).<sup>[5,65]</sup>

The reaction starts with the addition of H<sub>2</sub> to stannylenes **39** and formation of the H<sub>2</sub>-complex intermediate **39a**. The sufficient strain of the bulky aryl groups in addition to the labile character of Sn-C bond (weaker than Ge-C bond) favours the arene elimination along with formation of the hydrogenostannylene Ar<sup>Dipp</sup>SnH, which subsequently dimerize to the product **40**. The dimerization process is strongly favoured (-20.0 kcal mol<sup>-1</sup>) and facilitates the arene elimination pathway. Thus, larger size of tin

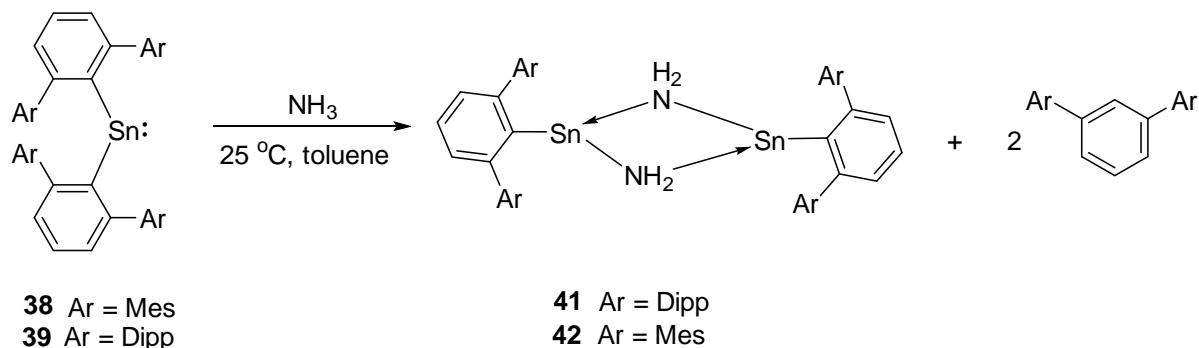
versus germanium together with the greater stability of the divalent Sn(II) state makes the arene elimination more favoured for tin compounds.



**Scheme 16.** H-H bond activation by diaryl stannylenes **39**.

#### NH<sub>3</sub> activation by stannylenes substituted by bulky aryl groups

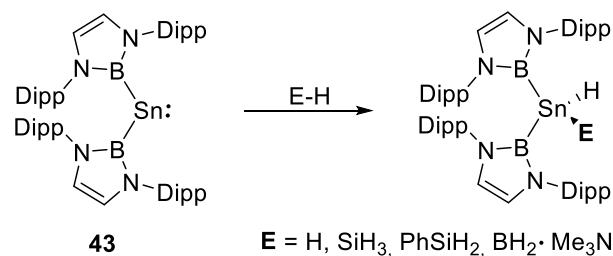
The reactions of stannylenes **38** and **39** with NH<sub>3</sub> leads to the formation of (amino)(aryl)stannylenes **41** and **42** with concomitant arene elimination (Scheme 17). Unlike germylene analogues, the arene elimination and formation of the tin dimer **41** is thermodynamically favoured by 20.3 kcal mol<sup>-1</sup> while the oxidative addition product Ar<sup>Mes</sup>Sn(H)NH<sub>2</sub> is energetically disfavoured by 2.2 kcal mol<sup>-1</sup>. The bulkier species **39** behaves similarly and the formation of dimer **42** is also strongly favoured.<sup>[5,6,65]</sup> It should be noted that these reactions of stannylenes (with H<sub>2</sub> and NH<sub>3</sub>) can be seen as successive oxidative addition/reductive elimination processes, and can take place more easily than with germylenes because Sn-C bonds are weaker. As already mentioned, oxidative addition and reductive elimination are the two key steps associated with many catalytic processes. These two stages are usually facilitated by the M<sup>n+</sup>/M<sup>(n+2)+</sup> redox shuttle of transition metal complexes, which made such species ubiquitous for the catalysis.<sup>[2,3,5,6]</sup>



**Scheme 17.** NH<sub>2</sub>-H bond activation by diarylstannylene **38** and **39**.

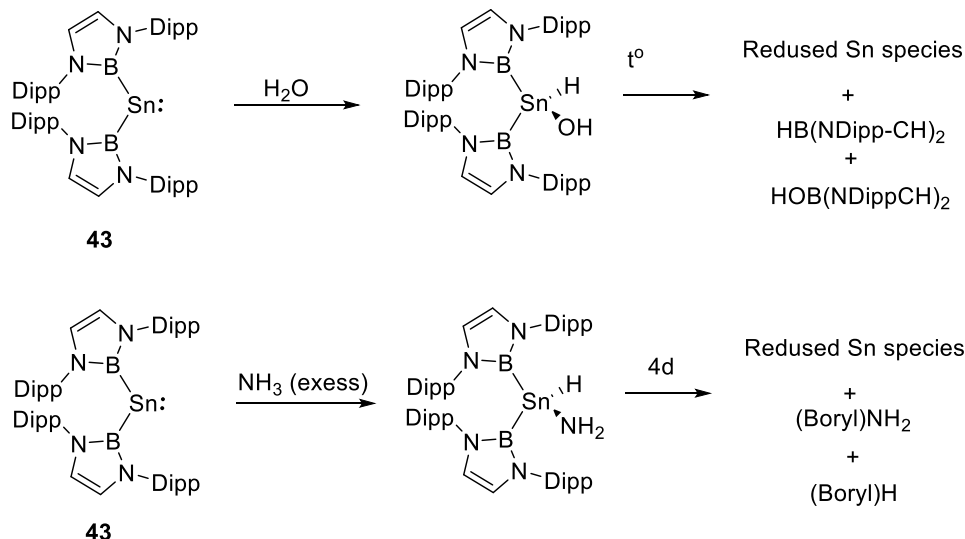
#### Small molecule activations by diborylstannylene

As already mentioned, the incorporation of strong  $\sigma$ -donating substituents results in a low HOMO-LUMO gap and thus would facilitate the oxidative addition reactions.<sup>[66]</sup> Indeed, Aldridge et al. reported the highly reactive stannylene **43** with two electropositive boryl-substituents capable of activating wide a range of small molecules by oxidative addition reactions to give the corresponding tin(IV) products (Scheme 18).<sup>[66]</sup>



**Scheme 18.** Reactivity of diborylstannylene towards E-H bonds

With ammonia and water, the products resulting after the oxidative addition are not stable and evolve further by the reductive elimination of boryl-alcohol and –amine respectively (Scheme 19).<sup>[66]</sup> Thus, stoichiometric oxidative addition/reductive elimination based bond cleavage/formation was demonstrated for a heavier tetrylene at room temperature.



**Scheme 19.** Reactivity of diborylstannylene **43** towards H<sub>2</sub>O and NH<sub>3</sub>: oxidative additions followed by reductive eliminations.

### III. Plumbylenes

**Plumbylenes ( $R_2Pb:$ )** are the heaviest analogues of carbenes among other tetrylenes (figure 5). As it was already mentioned, the stability of the tetrylenes (divalent state relative to tetravalent state) increasing as principal quantum number ( $n$ ) increases due to relativistic effects. For instance, dihalogenosilylenes  $SiCl_2$  are barely isolable unstable compounds, dichlorogermylene stable as a dioxane-complex  $GeCl_2 \cdot (\text{dioxane})^3$ , while dichlorostannylene  $SnCl_2$  and dichloroplumbulene  $PbCl_2$  are stable compounds.<sup>[28]</sup> It means that within all other tetrylenes, the plumbylenes shows the highest stability. One could say that it makes these species boring and uninteresting among the whole family, but it would be a dramatic mistake. The high stability of the divalent state makes plumbylenes the most promising species for catalysis, since the reductive elimination step, theoretically, would be more facile.

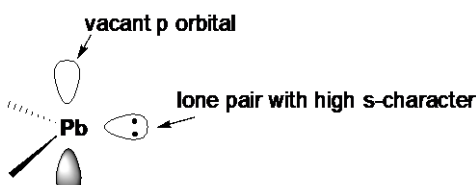


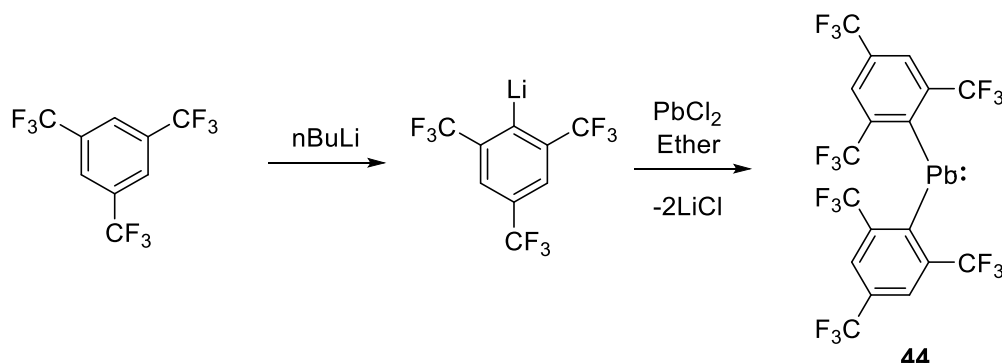
Figure 5. Singlet ground state of plumbylenes.

#### - Synthesis of stable plumbylenes

##### *Diarylplumbylenes*

The first attempts to synthesize low-valent lead complexes date back to 1956, when the first well-characterized sandwich complex  $Pb(\text{II}) - Pb(\eta^5-C_5H_5)_2$  was synthesized.<sup>[67]</sup> Twenty years later another example of successful stable  $\sigma$ -bonded  $Pb(\text{II})$  compound synthesis was reported by Lappert et al. Indeed, dialkyl and diamino plumbylenes  $Pb[\text{CH}(\text{SiMe}_3)_2]_2$  and  $Pb(\text{NR})_2$  are easy to obtain and they can be stored under inert atmosphere for a long time. These features made them a widely used precursors for the new plumbylenes.<sup>[68,69]</sup>

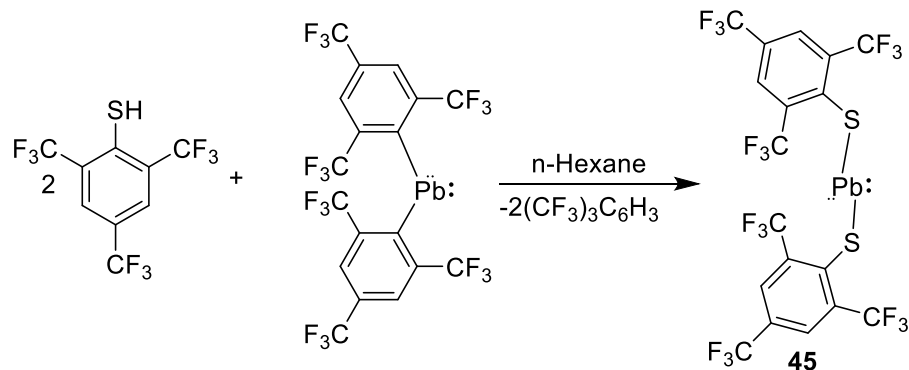
In 1991, Edelmann et al. have synthesized the first stable diaryl plumbylene **44**.<sup>[69]</sup> The reaction of 2 equivalents of lithiated 2,4,6-tris-(trifluoromethyl)phenyl ligand with  $PbCl_2$  and subsequent recrystallization from n-hexane solution furnished large yellow crystals of **44** (scheme 20).



Scheme 20. Synthesis of diaryl plumbylene **44**.

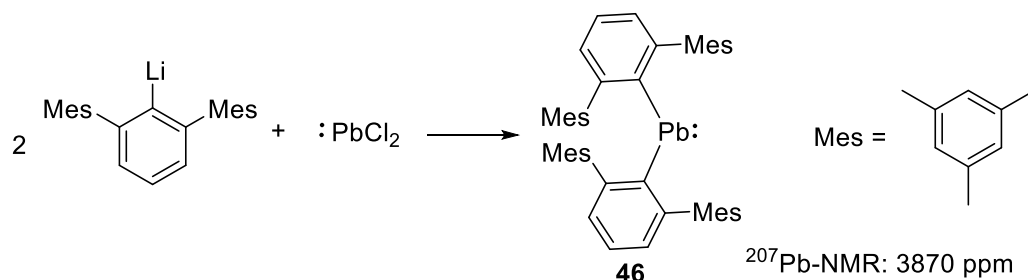
Plumbylene **44** is thermally stable up to its melting point at 58 °C, and is not light sensitive in the solid state, although it slowly decomposes in solution when exposed to light. The XRD analysis of **44**

revealed a monomeric structure, as a result of an additional stabilization of four weak Pb<sup>++</sup>F intermolecular interactions (Pb<sup>++</sup>F = 2.785 - 2.966 Å). The compound has a strongly bent geometry with an obtuse angle Ar-Pb-Ar of 94.5°. Plumbylene **44** readily reacts with two equivalents of 2,4,6-(CF<sub>3</sub>)C<sub>6</sub>H<sub>2</sub>SH, affording bis-thiolate plumbylene **45** and concomitant elimination of tris(trifluoromethyl)benzene (Scheme 21).<sup>[69]</sup>



**Scheme 21.** Synthesis of bis-thiolate plumbylene **45**.

In 1997, P. Power also described the synthesis of another stable diarylplumbylene **46**. Similarly to compound **44**, plumbylene **46** was obtained by the reaction of PbCl<sub>2</sub> with two equivalents of LiC<sub>6</sub>H<sub>3</sub>-2,6-Mes<sub>2</sub> (Scheme 22). Compare to **44**, plumbylene **46** presents a significantly better thermal stability, with a higher melting point (175 - 199 °C). Probably such increased thermal stability of **46** is a consequence of a more efficient kinetic stabilization by two crowded -C<sub>6</sub>H<sub>3</sub>-2,6-Mes<sub>2</sub> groups. The UV-vis spectrum of **46** shows an absorption peak at around 526 nm, and the <sup>207</sup>Pb NMR spectroscopy indicates signal at 3870 ppm. Violet crystals, stable in the absence of air and moisture, suitable for XRD analysis were obtained from a toluene solution. In the solid state, plumbylene **46** exists in isomorphic and isostructural form, and it has a V-shaped geometry with the shortest Pb-Pb bond length of 8.409(1) Å and a L-Pb-L angle of 114.5(6)°.<sup>[35]</sup>



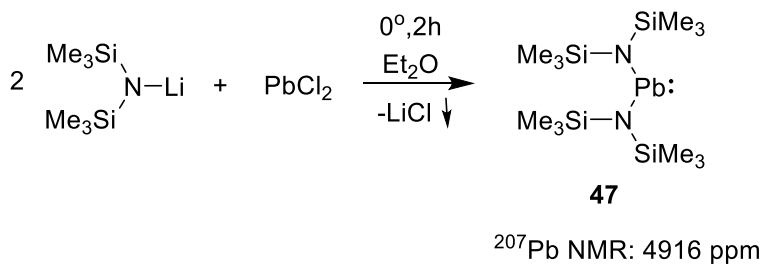
**Scheme 22.** Synthesis of diaryl plumbylene **46**.

#### Diaminoplumblyenes

Lappert's plumbylene **47** can be easily obtained by the reaction of lithiated hexamethyldisilazane, NLi(SiMe<sub>3</sub>)<sub>2</sub> with PbCl<sub>2</sub> in diethyl ether in a good yield (69%) as a yellow crystalline solid (Scheme 23).<sup>[34,70]</sup>

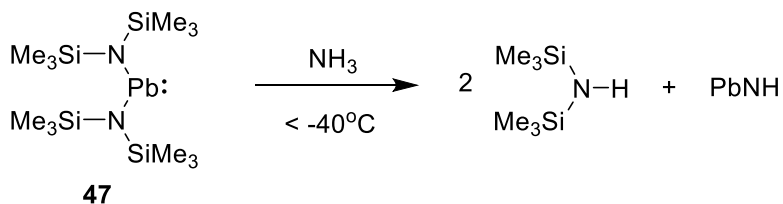
Compound **47** is monomeric in both solution and solid state, which reflects the efficient thermodynamic and kinetic stabilization of the electron deficient lead moiety by bis(trimethylsilyl)amino substituents.<sup>[70,71]</sup> The <sup>207</sup>Pb NMR spectrum shows a singlet signal at low field ( $\delta$  = 4916 ppm) corresponding to the dicoordinate lead atom.<sup>[68,72]</sup> This value is significantly low field shifted compared to the <sup>207</sup>Pb resonance of Lappert's dialkyl plumbylene Pb[CH(SiMe<sub>3</sub>)<sub>2</sub>]<sub>2</sub> ( $\delta$  = 9110 ppm).<sup>[73]</sup> It could be a

consequence of the intramolecular electron donation from the adjacent nitrogen atoms to the p $\pi$ -orbital of the **47**.



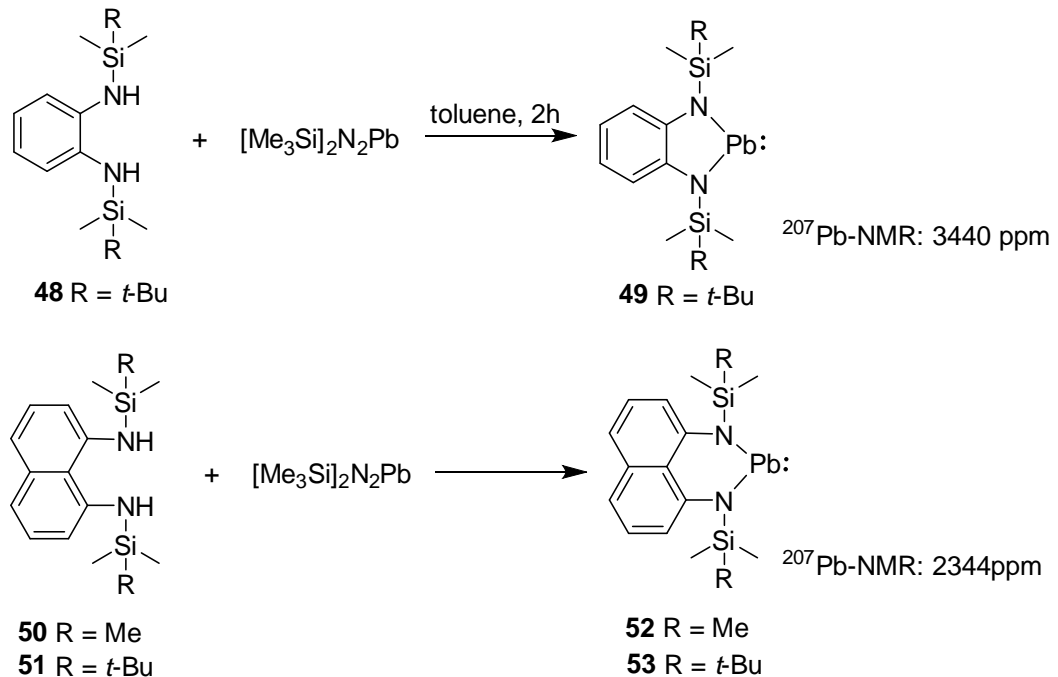
**Scheme 23.** Synthesis of the Lappert's diaminoplumbylene **47**.

According to XRD analysis data plumbylene **47** possess an V-shaped monomeric structure with a N-Pb-N bond angle of 103.6°.<sup>[71]</sup> It is well established, that the reactivity of the tetrylenes correlates with the value of the bond angle around the divalent atom. Thus, taking into account the large N-Pb-N angle of **47**, an increased potential of diaminoplumbylene **47** for the activation of the small molecules could be expected. Indeed, in 2020, Siemeling et al. during the course of the correlation study of the bond angle at lead atom and the reactivity of the different diaminoplumblenes toward ammonia showed that **47** immediately underwent ammonolysis reaction with the subsequent formation of lead imide PbNH as an orange solid (Scheme 24).<sup>[74]</sup>



**Scheme 24.** Reactivity of the Lappert's diaminoplumbylene **47** toward NH<sub>3</sub>.

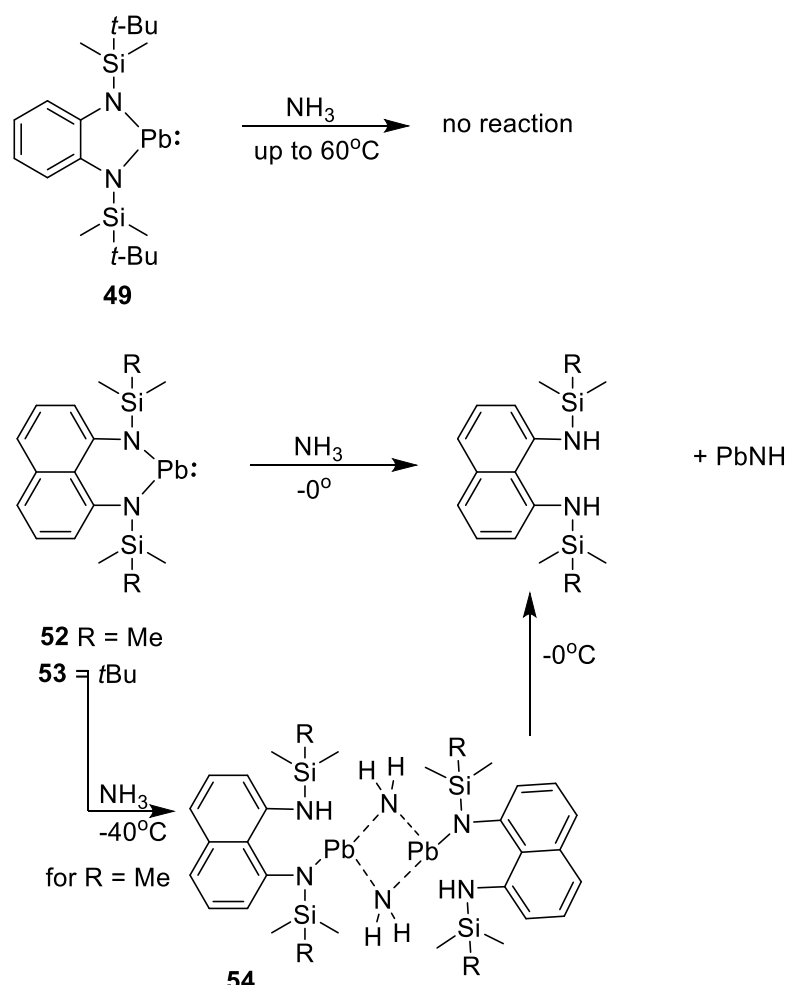
During same research project, the authors reported also the synthesis of a series of a stable diaminoplumblenes **49**, **52** and **53** (Scheme 25). Five-membered cyclic plumbylene **49** was obtained as yellow crystals by the reaction of "Lappert plumbylene" **47**<sup>[34]</sup> with o-C<sub>6</sub>H<sub>4</sub>[N(H)Si(*t*-Bu)Me<sub>2</sub>]<sub>2</sub> in good yield (71%). In the <sup>207</sup>Pb NMR spectrum a singlet signal corresponding to the lead(II) atom was observed at  $\delta$  = 3440 ppm. The N1-Pb-N2 angle around the central lead moiety was found to be equal 78°. The six-membered plumbylenes **52** and its bulkier analogue **53** were obtained using the same synthetic way as solids in good yields (88% and 85% respectively). The more sterically hindered one **53** has been fully characterized by NMR and XDR analysis. The <sup>207</sup>Pb NMR spectrum of **53** shows a singlet signal at  $\delta$  = 2344 ppm corresponding to the lead moiety.<sup>[74]</sup> Such significant difference between <sup>207</sup>Pb NMR shifts of **49** and **53** could be a consequence of the enlarged aromatic system in the case of **53**, which strongly affects the geometry of the molecule and, thus, the effective p-donation from the adjacent nitrogen atoms. The N1-Pb-N2 bond angles of **52** and **53** are ca 83°.



**Scheme 25.** Synthesis of the five-membered diaminoplumblylene **49** and six-membered diaminoplumblylenes **52, 53**.

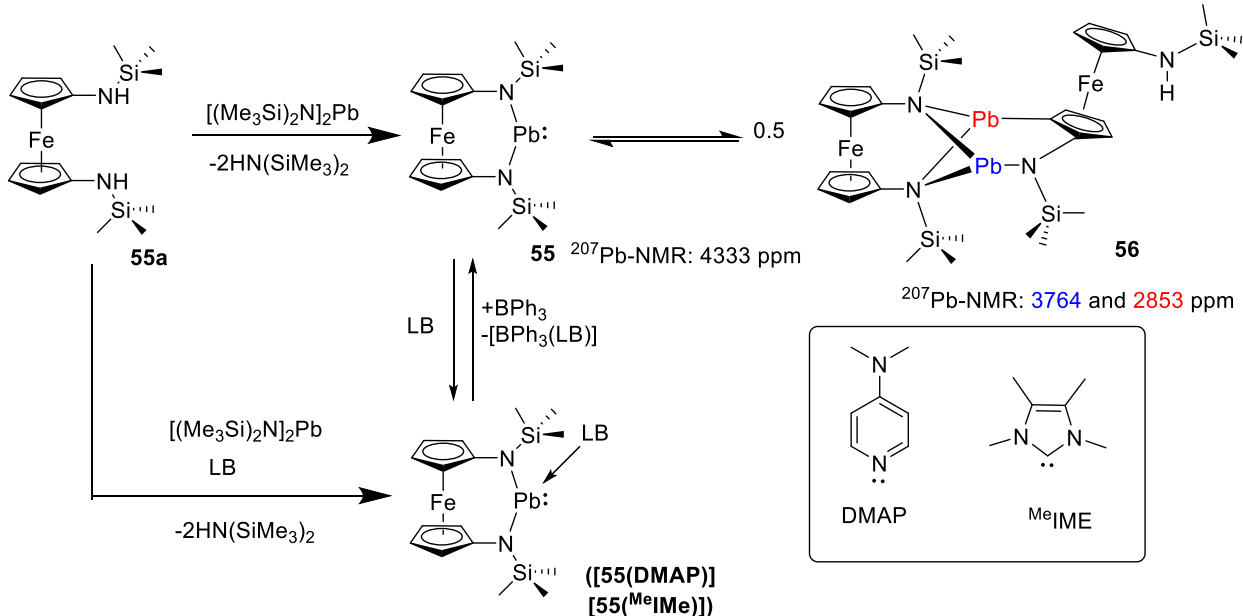
The interdependence of the bond angle around lead atom and the reactivity of the reported plumbylenes were studied by the reactions with ammonia. The five-membered plumbylene **49** didn't react with ammonia even at elevated temperatures, while the six membered plumbylenes **52** and **53** underwent ammonolysis. In the case of plumbylene **52**, Siemeling et al. were able to isolate an intermediate dimer **54**, keeping the temperature below -40 °C (Scheme 26).<sup>[74]</sup>

Thus, as it was mentioned in section I.II, the bond angle around the central divalent atom in tetrylenes strongly influences the reactivity. An increased value of this angle causes small HOMO-LUMO gaps and therefore small singlet-triplet energy gap and therefore an increased potential for the activation of the small molecules. Siemeling et al. clearly demonstrated this correlation for the heaviest tetrylenes – plumbylenes.<sup>[74]</sup>



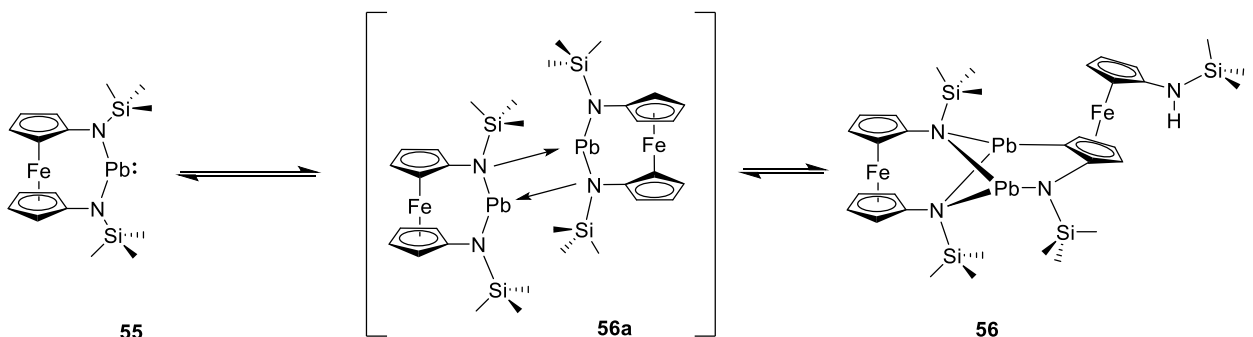
**Scheme 26.** Reactivity tests of five-membered diaminoplumblylene **49** and six-membered diaminoplumblylenes **52**, **53** with ammonia.

Another example of N-heterocyclic plumbylene **55**, stabilized by a ferrocene ligand scaffold, was reported in 2018. Attempts to synthesize it directly by transamination between diamine **55a** and Lappert's plumbylene **47** led to the reversible formation of the unsymmetrical dimer **56** from the initially formed monomeric plumbylene **55**. However, in the presence of a Lewis base (DMAP or  ${}^{\text{Me}}\text{IMe}$ ) the corresponding monomeric complexes [**55**(DMAP)] or [**55**( ${}^{\text{Me}}\text{IMe}$ )] were obtained. Attempts to liberate the free plumbylene **55** by adding one equivalent of Lewis acid  $\text{BPh}_3$  led to the formation of a 1 : 1 mixture of **55** and the corresponding Lewis-base- $\rightarrow\text{BPh}_3$  complex (Scheme 27). The  ${}^{207}\text{Pb}$  NMR spectrum showed a singlet signal corresponding to the lead atom of **55** at  $\delta = 4333$  ppm, which is in the same range of other reported chemical shifts of diaminoplumblylenes.<sup>[73]</sup> When the Lewis acid-base adducts were removed from the reaction mixture the formation of the dimer **56** was observed. Probably, the [LB- $\rightarrow\text{BPh}_3$ ] complex stabilizes the highly reactive plumbylene **55** via a secondary interaction (Scheme 27).<sup>[75]</sup>



**Scheme 27.** Synthesis and monomer–dimer equilibrium between plumbylene **55** and its dimer **56**. Plumbylene stabilization by adding a Lewis base.

According to computational data, the dimerization process proceeds via cleavage of the C-H bond along with formation of the Pb-C and N-H bonds rather than the insertion of the lead atom into C-H bond. This is the first example of a C-H activation by a plumbylene (Scheme 28). The two  $^{207}\text{Pb}$  NMR signals associated with the dimer **56** appear at  $\delta = 3764$  and  $2853$  ppm. In  $^{13}\text{C}$  NMR spectrum, the signal corresponding to the C-Pb(II) atom is a doublet at  $\delta = 182$  ppm with a large coupling constant ( $^1J_{\text{CPb}} = 1280$  Hz).<sup>[75]</sup> This dimerization is reversible.

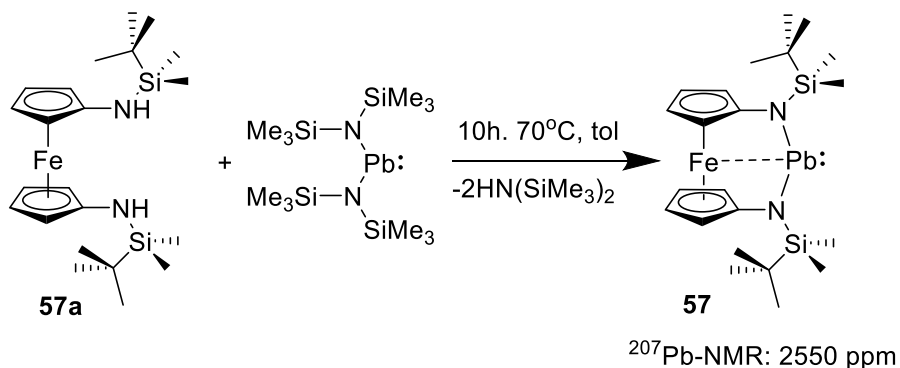


**Scheme 28.** Dimerization of the plumbylene **55**.

#### - Synthesis of donor-stabilized tricoordinate plumbylenes

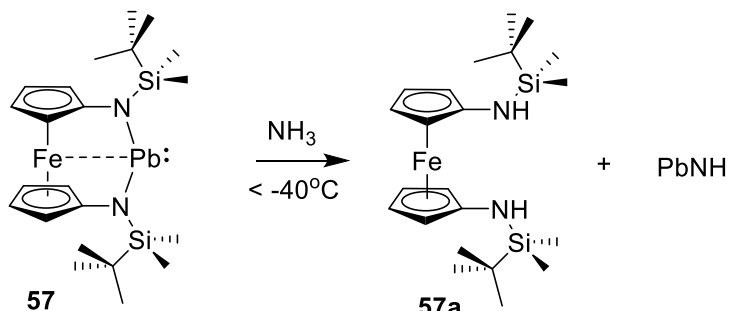
##### *Stabilized diaminoplumbylenes with a ferrocene ligand scaffold*

Six-membered cyclic plumbylene **57** was reported by Siemeling et al. in 2018 along with the analogues **55**. However, in contrast to **55**, the more sterically encumbered **57** was easily obtained by a simple transamination reaction between diamine **57a** and diaminoplumbylene  $[(\text{Me}_3\text{Si})_2\text{N}]_2\text{Pb}$  (Scheme 29).



**Scheme 29.** Synthesis of stable diaminoplumbylene **57**.

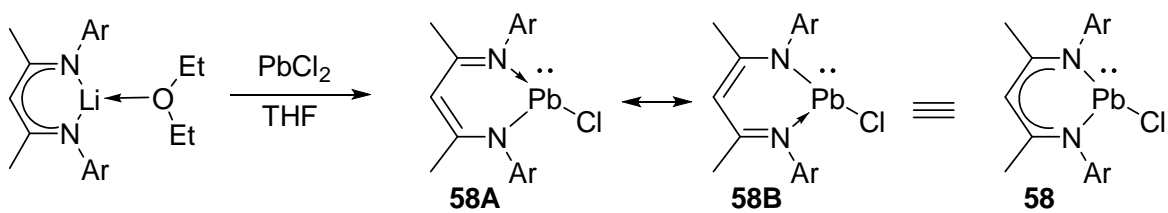
In the  $^{207}\text{Pb}$  NMR spectrum, **57** shows a singlet signal at  $\delta = 2550$  ppm, which is in the range of species with a tricoordinate lead atom rather than dicoordinate, in agreement with an additional stabilization interaction at the deficient lead Pb(II) via the intramolecular coordination of the electron-rich Fe(II) fragment. Indeed, the XRD data revealed a short Fe-Pb distance of 3.27 Å which is only slightly longer than van der Waals radii for Fe (1.32 Å) and Pb (1.46 Å). DFT calculations confirm a weak covalent metal-metal bond. The angle around Pb centre was found  $\text{N1-Pb-N2} = 99.2(4)^\circ$ <sup>[75]</sup> which is larger compared to other six-membered-ring plumbylene systems **52** and **53** (ca.  $83^\circ$ ).<sup>[74]</sup> As a consequence, the ability to activate small molecules increases (large angles cause a small HOMO-LUMO gap), and plumbylene **57** easily reacts with ammonia at low temperature (Scheme 30).<sup>[74]</sup>



**Scheme 30.** Reaction of **57** with ammonia.

#### Diaminoplumblyenes stabilized by $\beta$ -diketiminate

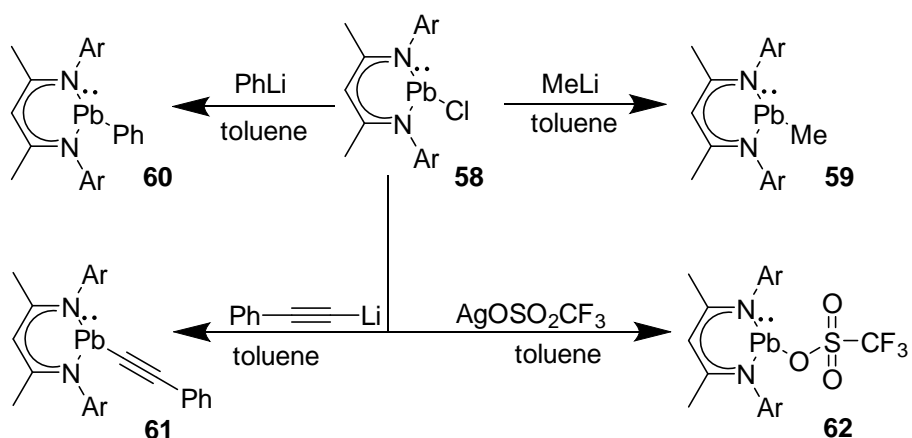
$\beta$ -diketiminate is commonly used as a ligand to efficiently stabilize metals in low oxidation states by intramolecular coordination of donating imine fragment. In the case of tetrylenes an additional stabilization occurs through the involvement of the tetrylene lone pair in the aromatic system. In 2009, Roesky group reported the synthesis NacNac-stabilized chloroplumbylene **58**, which was obtained by the reaction of lithium  $\beta$ -diketiminate ligand with 1 equivalent of lead dichloride in THF (Scheme 31).<sup>[68]</sup> In the  $^{207}\text{Pb}$  NMR spectrum **58** shows a singlet signal corresponding to Pb(II) at  $\delta = 1413$  ppm. Due to the resonance effect, both nitrogen atoms behave as donating ligands to stabilize the Pb(II) atom (**58A** and **58B** in Scheme 31). Indeed, the XRD study of **58** shows a symmetric structure because of this effect. The central lead atom in **58** exhibits a distorted trigonal-pyramidal geometry.



$^{207}\text{Pb-NMR}$ : 1413 ppm

**Scheme 31.** Synthesis of the  $\beta$ -diketiminate stabilized plumbylene **58**.

Due to the presence of chloride substituent, **58** readily reacts with various nucleophilic reagents such as MeLi, PhLi and Ph-CC-Li to give the corresponding plumbylenes **59-62** (Scheme 32).



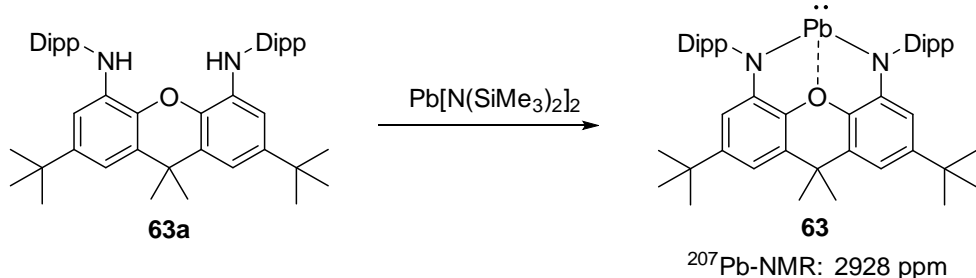
$^{207}\text{Pb-NMR}$ : 1334 ppm

**Scheme 32.** Reactivity of  $\beta$ -NacNac stabilized plumbylene **58**.

The chloride abstraction reaction of **58** with silver triflate results in the formation of **62** with a triflate anion coordinated on the Pb(II) atom, instead of Pb(II) cation. This triflate-substituted plumbylene **62** is interesting as a potential precursor for further reactions, since triflate anion is known to be unrivalled leaving group. The  $^{207}\text{Pb}$  NMR spectrum of **62** shows a singlet signal at  $\delta = 1334$  ppm, which is similar to the chemical shift of chloro-plumbylene **58**.<sup>[68]</sup>

#### Plumbylenes stabilized by a NON-backbone ligand

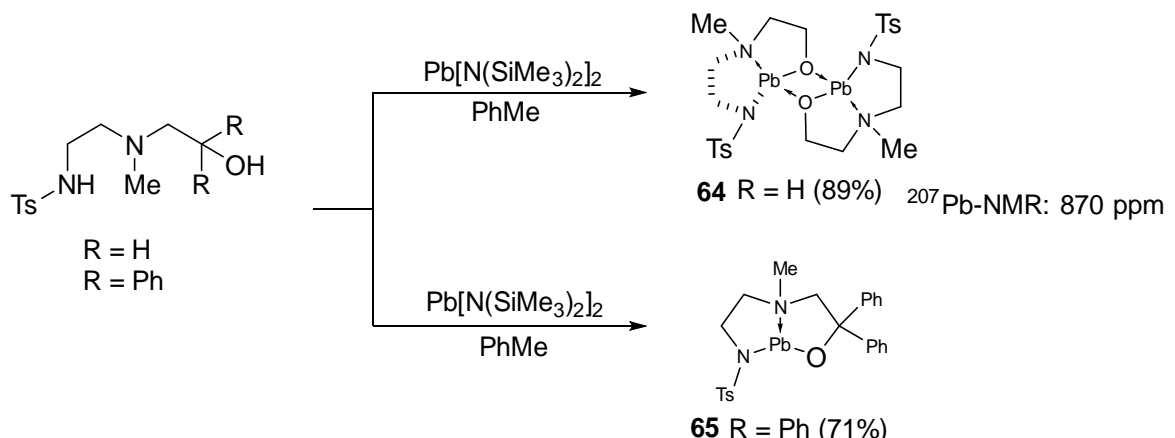
The NON-backbone flexible and labile ligand (NON = 4,5-bis(2,6)-diisopropylphenyl-amino-2,7-di-tert-butyl-9,9-dimethyl-xanthene) has been employed by the Breher group to prepare a new type of plumbylene.<sup>[81]</sup> The desired donor-stabilized diaminoplumbylene **63** has been synthesized by the transamination reaction between the ( $\text{Pb}[\text{N}(\text{SiMe}_3)_2]_2$ ) and NON-H **63a** (scheme 33). In the  $^{207}\text{Pb}$  NMR spectrum, a singlet signal at  $\delta = 2928$  ppm corresponds to the divalent lead atom in **63**. Plumbylene **63** has been isolated in good yield (81%) as violet crystals. The electrophilic Pb(II) centre interacts with the O atom as indicated by a Pb-O distance of 2.486(2) Å, which is nevertheless relatively long (covalent Pb-O bonds observed for lead alkoxides 2.17-2.24 Å) indicating a weak interaction.<sup>[76-81]</sup>



**Scheme 33.** The synthesis of NON-plumbylene **63**.

#### (Amino)(alkoxy) stabilized plumbylenes

Zaitsev et al. reported a new family of plumbylenes stabilized by NNO-ligands. The (amino)(alkoxy)plumbylenes **64** and **65** were synthesized by metathesis reactions between  $[(\text{Me}_3\text{Si})_2\text{N}]_2\text{Pb}$  and the corresponding protonated NNO-ligand (Scheme 34). The products were obtained in high yields (71 - 89%) as colourless crystalline powders which were stable under inert atmosphere. The structure analysis of **64** shows a dimer structure with a planar  $\text{Pb}_2\text{O}_2$  fragment. On the other hand, the introduction of a bulkier phenyl group in the ligand backbone leads to the formation of plumbylene **65** in a monomeric form. The geometry around lead atom in this case is tetrahedral with the lone pair of electrons at the one of the vertices. A weak coordination of the solvent (DMSO)  $\text{S}=\text{O} \rightarrow \text{Pb}$  is observed, showing enhanced electrophilicity of the compound compared to its Ge analogues.  $^{207}\text{Pb}$  NMR signal for plumbylene **64** appears at  $\delta = 870$  ppm, which is in the range chemical shifts for tetracoordinated lead atom.<sup>[82]</sup>

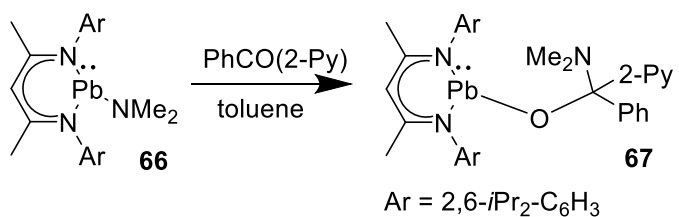


**Scheme 34.** The synthesis of plumbylenes based on NNO-ligands.

#### III.I Reactivity of plumbylenes

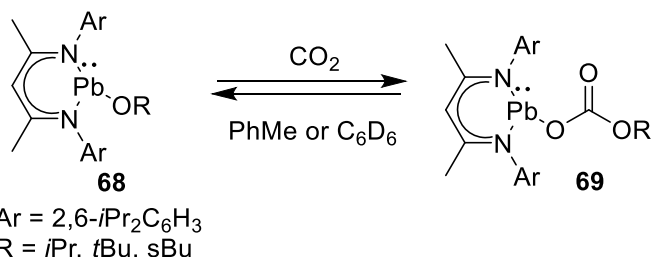
As it was already mentioned (section I.II) the electron donating ability of tetrylenes is decreasing upon descending down the group. As a consequence, plumbylenes are weaker  $\sigma$ -donors and stronger  $\pi$ -acceptors compared to lighter congeners.<sup>[28,81]</sup> Taking into account that Pb has a tendency to favour the +2 oxidation state, one can predict that for plumbylenes, insertion reactions would be the most characteristic. Indeed, wide diversity of reported reactions for plumbylenes are among the insertion type.<sup>[24,59,83-88]</sup> For example, base-stabilized dimethylamino plumbylene **66** reacts with 2-benzoyl pyridine at low temperatures (-20 to -10 °C) through a carbonyl insertion into Pb-N bond. The final product is best described as an alkoxy plumbylene **67**. The  $^1\text{H}$  NMR spectrum of **67** exhibits a singlet signal at  $\delta = 4.77$

ppm corresponding to the  $\text{NMe}_2$  group. The  $^{207}\text{Pb}$  NMR signal for **67** appears as singlet at  $\delta = 1093$  ppm corresponding to the Pb(II) atom (Scheme 35).<sup>[88]</sup>



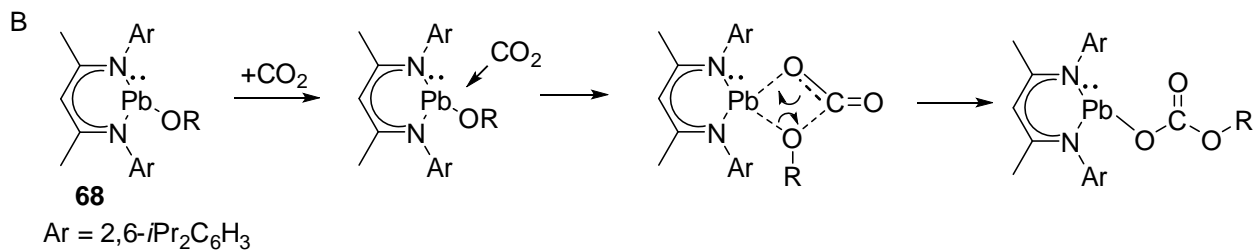
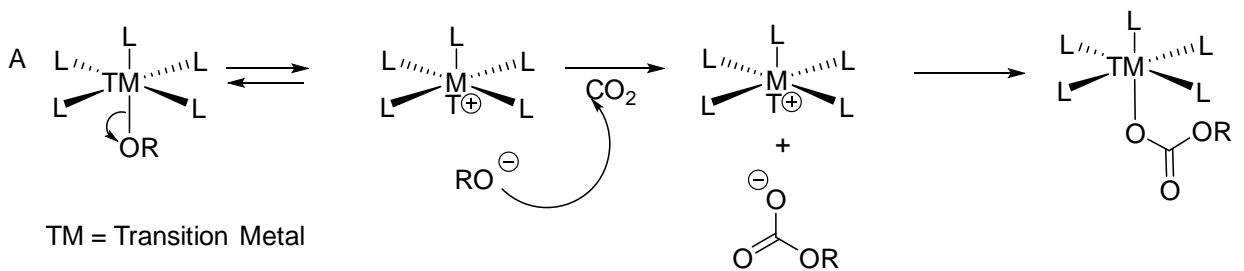
**Scheme 35.** The reaction of plumbylene **66** with pyridyl phenyl ketone.

Fulton et al. reported a series of monomeric divalent three-coordinate lead-alkoxides, stabilized by  $\beta$ -diketiminate scaffold, which readily but reversibly insert carbon dioxide (Scheme 36).<sup>[86]</sup> Interestingly, the degree of reversibility of the reaction depends on the nature of the R group. For example, if the lead-carbonate <sup>i</sup>Pr**69** is subjected to the reduced pressure, the elimination of the CO<sub>2</sub> and the formation of the initial lead-alkoxide was not observed. In the case of carbonate <sup>s</sup>Bu**68**, under vacuum for 10 minutes, 20 % of the molecules have released CO<sub>2</sub>. While, with the bulkiest carbonate fragment of the series <sup>t</sup>Bu**69**, under the same vacuum conditions, an almost complete reversion to the initial lead-alkoxide <sup>t</sup>Bu**68** was observed. The degree of reversibility for the listed compounds could be assigned to the stability of the related lead-alkoxides, which correlates with the pKa value of the corresponding alcohols. The higher the pKa of the alcohol, the more stable is the lead alkoxide. For example, pKa = 30.2 for isopropanol, and pKa = 32.2 for tert-butanol,<sup>[89]</sup> and thus, <sup>i</sup>Pr**68** is less stable among the series <sup>i</sup>Pr**68** - <sup>s</sup>Bu**68** - <sup>t</sup>Bu**68**, while <sup>t</sup>Bu**68** is the most stable.<sup>[86]</sup>



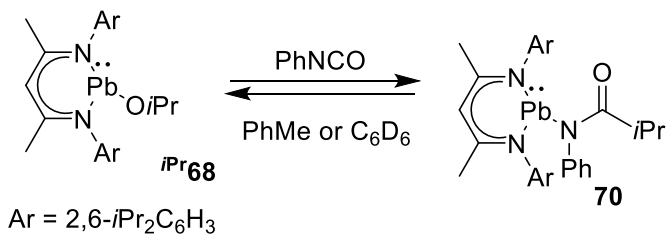
**Scheme 36.** Reactivity of alkoxy substituted plumbylenes **68**.

Fulton et al. supposed, that the mechanism for the CO<sub>2</sub> insertion into Pb-O bond could be different compared to the classical mechanism considered for transition-metal alkoxides. Generally, in the case of transition-metal alkoxides the insertion reaction of carbon dioxide is thought to proceed through a concerted mechanism in which the new carbon-oxygen and metal-carbonate bonds forming along with the cleavage of the metal-alkoxide bond (Scheme 37 A).<sup>[90-92]</sup> However, in the case of the lead-alkoxides <sup>t</sup>Bu**68**, the reaction probably starts with the initial coordination of the CO<sub>2</sub> to the lead atom, which consequently induces the alkoxide to react with CO<sub>2</sub> (Scheme 37B).<sup>[86]</sup> The reasons for such mechanism differences could be the lack of the nucleophilicity of the alkoxide-oxygen atom in <sup>t</sup>Bu**68**. Indeed, in this case the oxygen atom is masked by the pocket formed by two nitrogen-isopropyl groups along with the alkyl group on the O atom, and thus, the nucleophilicity of alkoxide decreases for steric reasons.<sup>[86]</sup>



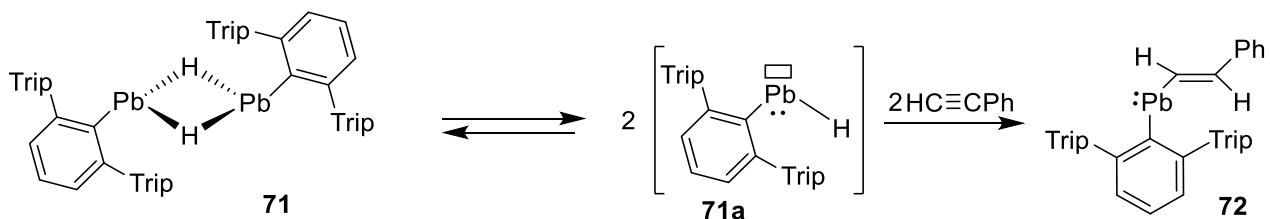
**Scheme 37.** Proposed mechanisms for the CO<sub>2</sub> insertion reaction: A – with transition-metal-alkoxide complexes; B – with alkoxide-plumbbylenes.

Similarly, Isopropoxyplumbylene <sup>iPr</sup>**68** reversibly reacts with phenyl isocyanate at room temperature to give carbamate **70** (Scheme 38).<sup>[86]</sup>



**Scheme 38.** Reactivity of isopropoxyplumbylene **68** with phenyl isocyanate

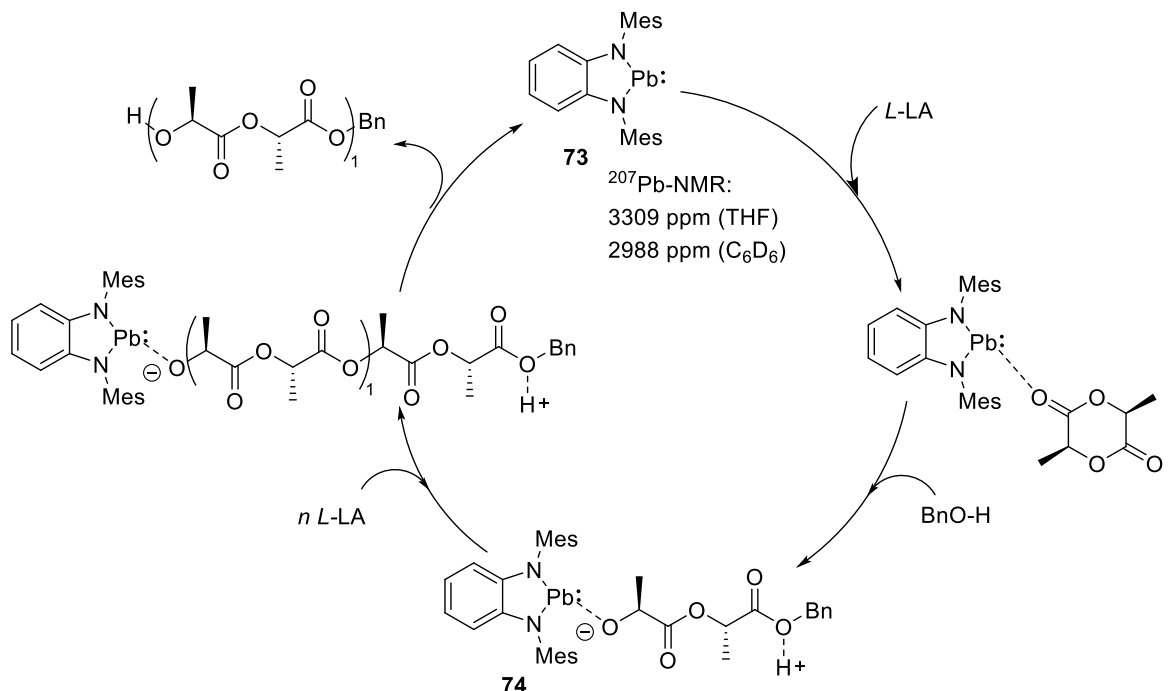
Another interesting reactivity of plumbylenes was reported recently by the group of Lars Wesemann. The first example of a lead hydride complex, hydrogenoplumbylene dimer [(Ar<sub>2</sub>PbH)<sub>2</sub>] (Ar<sub>2</sub> = 2,6-Trip<sub>2</sub>C<sub>6</sub>H<sub>3</sub>, Trip = 2,4,6-triisopropylphenyl) **71** reacts with phenylacetylene via a 1,2-addition of Pb-H (**71a** generated by the dissociation of dimer **71**) to the triple bond to give a vinyl plumbylene **72**. The product was isolated in good yield (65%) by crystallization from a hexane solution at a low temperature (Scheme 39).<sup>[84]</sup>



**Scheme 39.** Reaction of the lead hydride **71** with phenylacetylene.

### III.II Polymerization of lactide catalyzed by plumbylenes

Chiua and Chen have recently demonstrated the ability of benzannulated N-heterocyclic plumbylene **73** to catalyse the ring-opening polymerisation reaction (ROP) of lactide. ROP is a widely used method for the synthesis of biopolymers. Plumbylene **73** in THF, displays a  $^{207}\text{Pb}$  NMR signal at  $\delta = 3309$  ppm in the range of chemical shifts of dicoordinate lead atom. Using a non-coordinative solvent such as  $\text{C}_6\text{D}_6$  the signal shifts to high-field ( $\delta = 2988$  ppm), which confirms the Lewis acidic character of the plumbylene **73**.



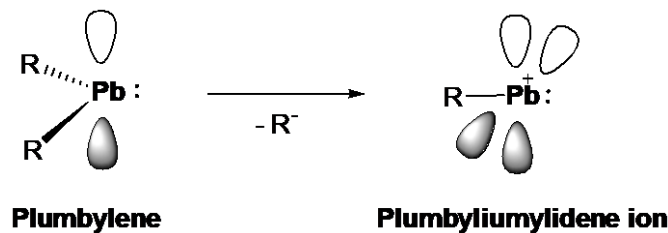
**Scheme 40.** *L*-lactide polymerization with **73** as the catalyst in the presence of benzyl alcohol.

Plumbylene **73** efficiently catalyzes the ROP of *L*-lactide at room temperature,<sup>[93]</sup> leading to 97 % of conversion of *L*-lactide in the presence of 0.3 mol% of catalyst **73** and benzyl alcohol as initiator. Chiua and Chen suggested that the first step of catalytic cycle is the activation of the *L*-lactide by the Lewis acidic plumbylene **73**, which activates the carbonyl group. Subsequently the nucleophilic attack of benzyl alcohol to the carbonyl group induces the ring opening reaction of monomer to initiate the polymerization. The generated alkoxide-coordinated anionic complex **74** reacts with another *L*-lactide to continue the ROP process. As the last step to terminate the ROP, self-protonation of the  $[\text{NHPb}--\text{PLA-O}^+(\text{H})\text{Bn}]$  takes place to give the desired product along with the regeneration of the catalyst (Scheme 40).

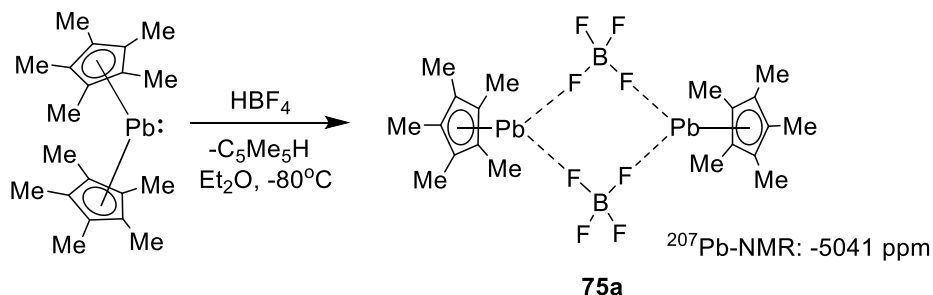
### IV- Plumbylene Cations

One of the general ways to increase the reactivity of molecules is to use their transformation into corresponding cationic derivatives,<sup>[94]</sup> providing an additional vacant orbital and a positive charge to increase their electrophilic character. Therefore, we can easily imagine that the mono-coordinate plumbylene cation (Plumbyliumylidene ion), generated by the abstraction of the anionic substituent ( $\text{R}'$ ) from the corresponding plumbylene, would exhibit an enhanced reactivity and electrophilic character and thus be an attractive target molecule. In this section, we will review the recent development of

plumbbyliumylidene ion (cationic plumbylene or Pb(II) cation) chemistry, although the chemistry of cationic plumbylenes is far underdeveloped compared to that of plumbylenes.

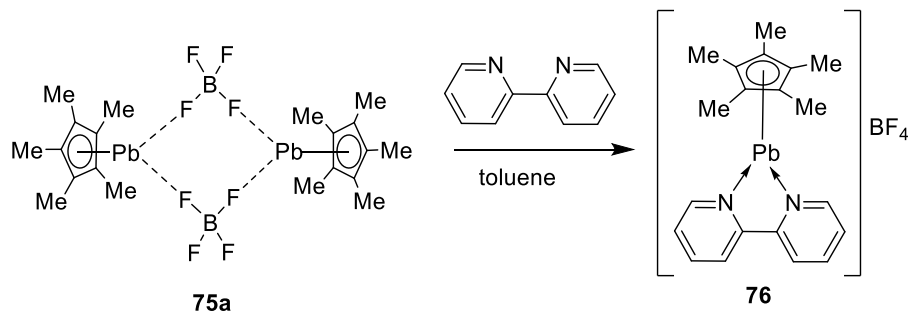


The first stable Pb(II) cations **75a** were reported by the group of Jutzi in 1980. The *nido*-cluster type cations  $[(\eta^5\text{-C}_5\text{Me}_5)\text{Pb}]^+\text{BF}_4^-$  **75a** and  $[(\eta^5\text{-C}_5\text{H}_5)\text{Pb}]^+\text{BF}_4^-$  **75b** were synthesized by the treatment of corresponding plumbylene  $[\text{Cp}_2^*\text{Pb}]$  with  $\text{HBF}_4$  (Scheme 41).<sup>[95]</sup>



**Scheme 41.** Synthesis of the first isolable plumbbyliumylidene **75a**.

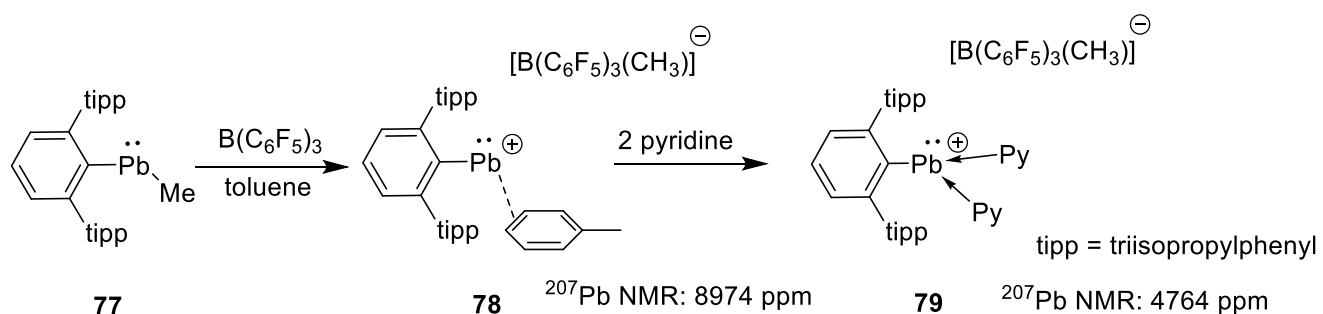
Due to the  $\eta^5$ -coordination of the Cp ring to the Pb(II) centre, the  $^{207}\text{Pb}$  NMR spectra exhibit extremely high-field chemical shifts ( $\delta = -5041$  ppm for **75a**, and  $\delta = -4961$  ppm for **75b**). Compound **75a** was structurally characterized showing a pentagonal-pyramidal geometry around lead center. The cationic Pb(II) weakly interacts with the counter anion  $\text{BF}_4^-$  as suggested by a long Pb-F distance [2.831(9) Å]. The Lewis acid character of **75a** was confirmed by the reaction with a Lewis base such as 2,2'-bipyridine, to form a stable donor-acceptor adduct **76** (Scheme 42).<sup>[95]</sup>



**Scheme 42.** The reaction of **75a** with 2,2'-bipyridine with formation of the adduct **76**.

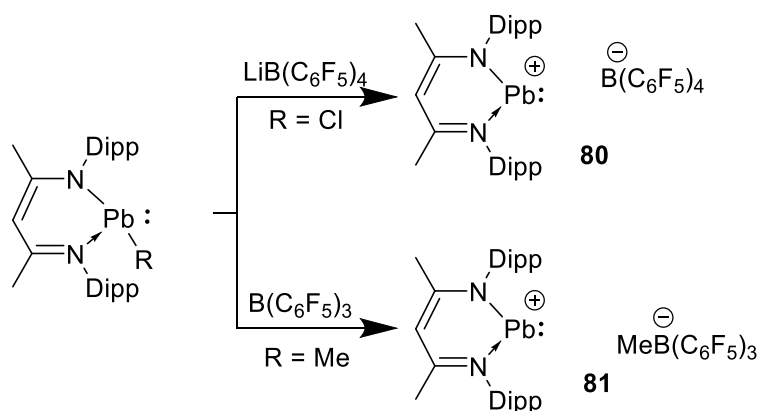
Power et al., elegantly synthesized quasi-mono-coordinate cationic plumbylene **78** complexed with a molecule of toluene via  $\eta^2$ -coordiantion by the methyl abstraction from  $\text{Ar}^*\text{PbMe}$  using a Lewis acid  $\text{B}(\text{C}_6\text{F}_5)_3$  (Scheme 43).<sup>[96]</sup> The  $^{207}\text{Pb}$ -NMR signal for **78** appears at remarkably low-field at  $\delta = 8974$  ppm, and compared to the pentacoordinate plumbbyliumylidenes of Jutzi **75**, there is a huge chemical shift gap of about 13 500 ppm. Such tremendous difference could be a consequence of the weak interactions with toluene in the case of **78**. As expected, the weakly coordinating toluene molecule could be easily replaced upon the treatment of **78** with pyridine, affording bis-pyridine stabilized Pb (II) cation **79**. The formation of

**79** was evidenced by an up-field shifted  $^{207}\text{Pb}$  NMR chemical shift ( $\delta = 4764 \text{ ppm}$ ) compared to that of **78** due to the increased coordination number.<sup>[96]</sup>



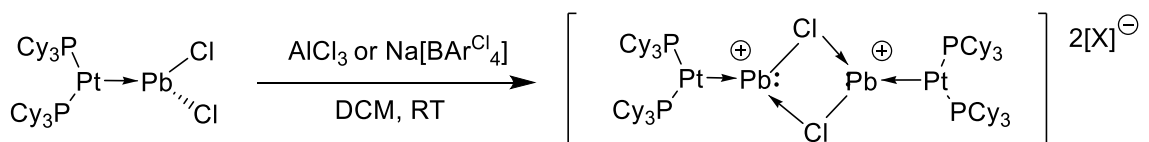
**Scheme 43.** Quasi-mono-coordinate cationic plumbylenes **78** and **79**.

Later Fulton et al., reported the synthesis of  $\beta$ -diketiminato substituted two-coordinate plumbyliumylidenes **80** and **81** (stabilized by imine coordination). Chloroplumbylene and methylplumbylene complexes react with  $\text{LiB}(\text{C}_6\text{F}_5)_4$  via chlorine abstraction and with  $\text{B}(\text{C}_6\text{F}_5)_3$  via methyl abstraction respectively to give the corresponding  $\text{Pb}(\text{II})$  cations **80** and **81** (Scheme 44). The structural analysis of both compounds do not show close interactions with counter anions (the shortest  $\text{Pb}-\text{F}$  was found 3.319 Å). Probably due to the fast relaxation of lead nuclei no  $^{207}\text{Pb}$  NMR signal were detected.<sup>[97]</sup>

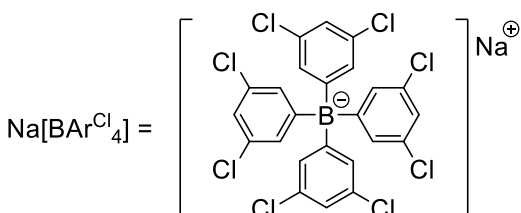


**Scheme 44.** Synthesis of  $\beta$ -diketiminato stabilized plumbyliumylidenes **80** and **81**.

As a special case, in 2015, Braunschweig et al. synthesized chloroplumbylene cations stabilized by a  $\sigma$ -coordination of  $\text{Pt}(0)$  complex with a counter anion of  $\text{AlCl}_4^-$  **83a** or  $[\text{BAr}^{\text{Cl}}_4]^-$  **83b** ( $\text{Ar}^{\text{Cl}} = 3,5\text{-Cl}_2\text{C}_6\text{H}_3$ ).<sup>[98]</sup> They are synthesize by halide abstraction of the corresponding  $(\text{Cy}_3\text{P})_3\text{Pt} \rightarrow \text{PbCl}_2$  complex using  $\text{AlCl}_3$  or  $\text{NaBAr}^{\text{Cl}}_4$ . (Scheme 45). All attempts to obtain the  $^{207}\text{Pb}$  NMR spectra failed, probably due to increased electric field gradient and large chemical shift anisotropy at the lead atom. The XRD analysis revealed a distorted T-shaped geometry around the platinum atom in **83a**. Theoretical calculations indicate that, compared to the plumbylene **82**, which possess  $\text{Pt} \rightarrow \text{Pb}$  dative bond, the cationic complexes **83a** and **83b** have  $\text{Pt} \rightarrow \text{Pb}$  electron sharing bond.



82

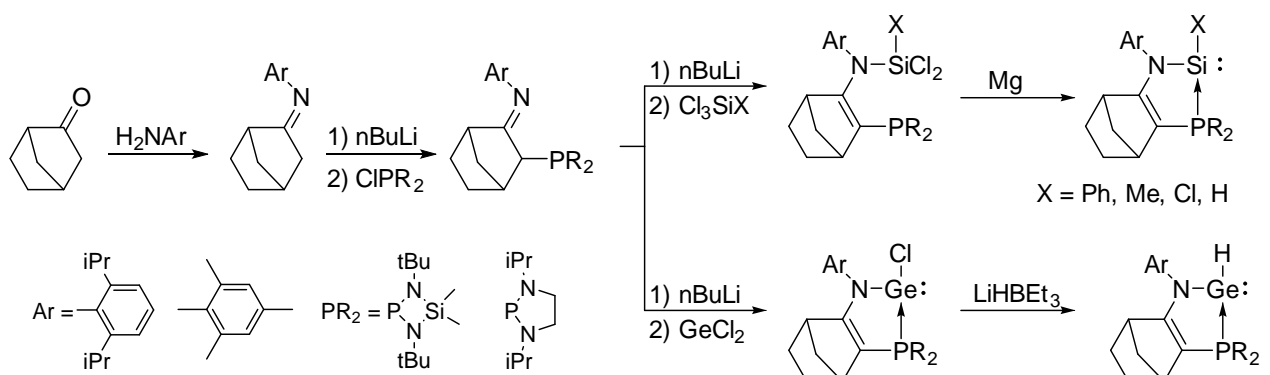
83a: X = AlCl<sub>4</sub>  
83b: X = BArCl<sub>4</sub>**Scheme 45.** Synthesis dicationic diplatinum complexes **83a** and **83b**.

## V- Amido-phosphine ligand supported metallylenes.

### V.I Phosphine stabilized silylenes and germynes

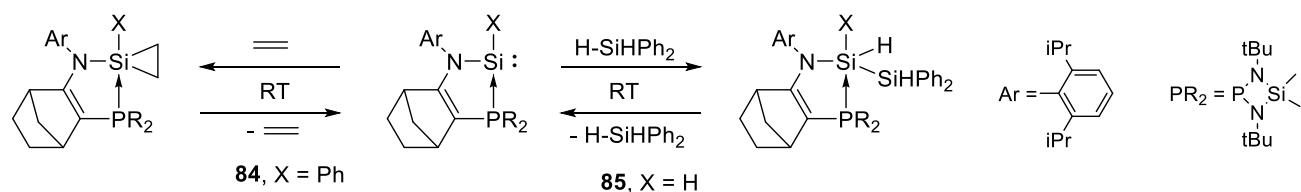
The Kato/Baceiredo's group has developed an amido-phosphine ligand which presents a particular ligand effect and efficiently stabilizes metallylenes (silylenes and germynes). A key feature of this ligand is the rigid and stable bicyclic olefin bridge connecting an amido and phosphine fragment. Due to its rigidity, despite the coordination of the P-fragment to the reactive site of metallylenes (the labile P→Si and P→Ge interaction), the ligand stays on the reactive metallylene center to stabilize it. On the other hand, the amido-phosphine ligand possesses high level of steric hindrance thanks to the bulky amido substituent (Ar) and phosphine ligand (PR<sub>2</sub>), which provides an efficient kinetic stabilization. Thus, highly reactive metallylenes bearing small substituents E(II)-H and E(II)-Cl could be obtained as stable complexes.

Moreover, the substituents on the N and P atoms of the ligand system can be easily modulated and thus allow to tune the ligand properties. Such ability to set the nature of the substituents on the ligand system is a consequence of the easy stepwise synthesis of iminophosphine ligand starting from the commercially available norcamphor (Scheme 46).<sup>[99–103]</sup>

**Scheme 46.** Synthesis of silylenes and germynes supported by an amido-phosphine ligand.

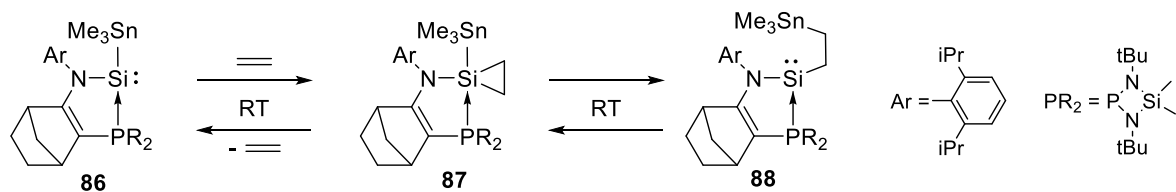
Due to relatively weak ligand coordination, the corresponding iminophosphine stabilized silylenes remain highly reactive. For example, Si(II) complex **84** readily reacts with ethylene at room temperature via [2+1] cycloaddition reaction.<sup>[100]</sup> Besides, silylene **85** also reacts with silanes via silylene insertion into Si-H σ-bond affording the Si(IV) species.<sup>[102]</sup> Interestingly, these reactions are reversibly at room temperature

(oxidative addition/reductive elimination), which clearly demonstrates unique transition-metal complexes like behaviour (Scheme 47).



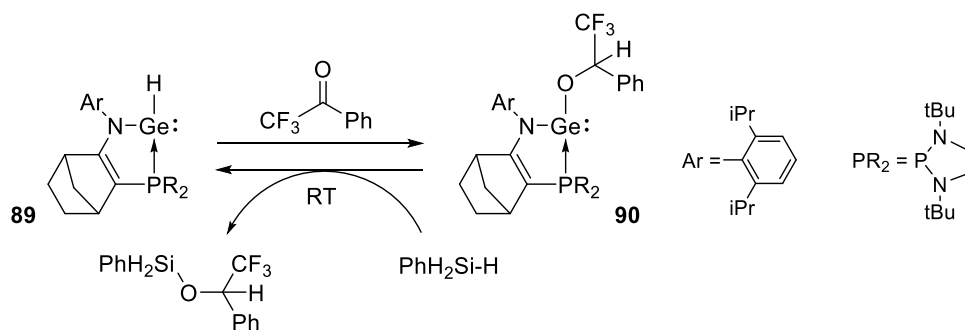
**Scheme 47.** Reversible reactions of phosphine stabilized silylenes with an olefin and a silane.

Besides, the silylene, bearing the labile Si(II)-Sn bond is able to reversibly react with ethylene through the olefin insertion into Si-Sn bond (olefin insertion/β-elimination) (Scheme 48).<sup>[102,104]</sup> According to the DFT calculations data, the reaction proceeds in two steps. The first step is the formation of intermediate [2+1]-cycloadduct **87**. On the second step of the reaction, the intermediate **87** readily evolves via migratory insertion of ethylene with the final formation of the alkyl substituted silylene **88**. These results demonstrate the peculiar ligand effect on the amido-phosphine-stabilized silylenes, which makes the Si(II)- and Si(IV)-complexes close in energy, enabling the Si(II)/Si(IV) redox shuttle.<sup>[104]</sup>



**Scheme 48.** Reversible olefin insertion reactions of Me<sub>3</sub>Sn-substituted silylene complex.

The germylenes supported by the same amido-phosphine ligand also show a particular reactivity. The hydrogen-germylene complex **89** can react with ketones such as trifluoromethyl acetophenone at room temperature via the insertion reaction into Ge-H bond, affording the corresponding alcoxygermylene product **90**. This product can react with silanes by metathesis reaction to give the hydrosilylation product along with the regeneration of the starting hydrogenogermylene **89**. Thus, the hydrogeno- and alcoxygermylene complexes stabilised by amido-phosphine ligand are capable of catalysing the hydrosilylation reactions of various ketones in the presence of phenylsilane under mild conditions (Scheme 49).

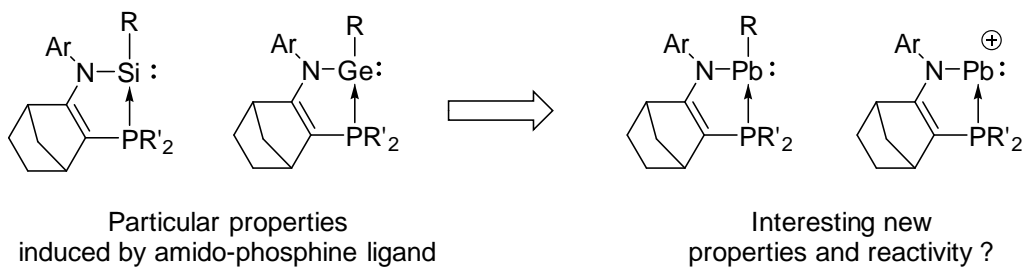


**Scheme 49.** Hydrosilylation of a ketone catalysed by phosphine-stabilized germylene **89**.

## VI. Conclusions

In this chapter, we have discussed the latest recent advances in tetrylene chemistry. Due to the small HOMO-LUMO energy gaps and transition metal-like frontier orbitals, tetrylenes are capable of activating small molecules through oxidative addition reactions. However, due to the high stability of oxidative adducts in higher oxidation state (IV), the subsequent regeneration of lower oxidation state species by reductive elimination is less common. Because the stability of the divalent species in group 14 relative to the tetravalent species increases down the column of the periodic table, the divalent state of plumbylenes is the most stable among all other tetrylenes. Thus, in theory, the reduction elimination step should be easier with plumbylenes and therefore, they could be the most suitable metallylene to be used in catalysis. We have also seen in this chapter that a possible strategy to increase the reactivity of plumbylenes is to transform them into cationic derivatives - plumbylumylidenes. These cationic plumbylenes have an extra vacant p-orbital and a cationic charge on the lead moiety, which makes plumbylumylidenes extremely reactive and electrophilic.

As shown in Section V, the amido-phosphine ligand developed by the Baceiredo/Kato group not only effectively stabilizes the reactive metallylenes (silylene and germynes) but also induces their interesting properties (transition metal-like properties) due to the particular steric and electronic effect of the ligand. We were therefore interested in applying this ligand system to synthesize the corresponding plumbylene- and plumbylumylidene ionic complexes and study their chemistry during this PhD thesis, hoping for new peculiar properties and reactivity that cannot be induced by other ligand systems.



## **Bibliographic references**

- [1] C. C. C. Johansson Seechurn, M. O. Kitching, T. J. Colacot, V. Snieckus, *Angew. Chemie - Int. Ed.* **2012**, *51*, 5062–5085.
- [2] I. P. Beletskaya, A. V. Cheprakov, *Chem. Rev.* **2000**, *100*, 3009–3066.
- [3] V. P. Ananikov, *Nat. Catal.* **2021**, *4*, 732–733.
- [4] G. H. Spikes, J. C. Fettinger, P. P. Power, *J. Am. Chem. Soc.* **2005**, *127*, 12232–12233.
- [5] T. Chu, G. I. Nikonov, *Chem. Rev.* **2018**, *118*, 3608–3680.
- [6] C. Weetman, S. Inoue, *ChemCatChem* **2018**, *10*, 4213–4228.
- [7] S. Yadav, S. Saha, S. S. Sen, *ChemCatChem* **2016**, *8*, 486–501.
- [8] P. P. Power, *Nature* **2010**, *463*, 171–177.
- [9] R. L. Melen, *Science (80-.)* **2019**, *363*, 479–484.
- [10] J. C. L. Walker, H. F. T. Klare, M. Oestreich, *Nat. Rev. Chem.* **2020**, *4*, 54–62.
- [11] T. J. Hadlington, M. Hermann, G. Frenking, C. Jones, *J. Am. Chem. Soc.* **2014**, *136*, 3028–3031.
- [12] R. K. Siwatch, S. Nagendran, *Chem. – A Eur. J.* **2014**, *20*, 13551–13556.
- [13] P. G. B. C. F. Adducts, A. L. Pair, M. Sites, N. Del Rio, M. Lopez-reyes, A. Baceiredo, N. Saffon-mercero, D. Lutters, T. Müller, T. Kato, **2016**, 1–7.
- [14] T. J. Hadlington, M. Driess, C. Jones, *Chem. Soc. Rev.* **2018**, *47*, 4176–4197.
- [15] W. Kirmse, *Angew. Chem - Int. Ed.* **2003**, *42*, 2117–2119.
- [16] A. Igau, H. Grutzmacher, A. Baceiredo, G. Bertrand, *J. Am. Chem. Soc.* **1988**, *110*, 6463–6466.
- [17] A. J. Arduengo, R. L. Harlow, M. Kline, *J. Am. Chem. Soc.* **1991**, *113*, 361–363.
- [18] G. D. Frey, V. Lavallo, B. Donnadieu, W. W. Schoeller, G. Bertrand, *Science* **2007**, *316*, 439–441.
- [19] D. Devarajan, C. E. Doubleday, D. H. Ess, *Inorg. Chem.* **2013**, *52*, 8820–8833.
- [20] U. Siemeling, F. Christian, C. Bruhn, M. Leibold, D. Selent, W. Baumann, M. Von Hopffgarten, G. Frenking, *Chem. Sci.*, **2010**, *1*, 697–704.
- [21] T. W. Hudnall, J. P. Moerdijk, C. W. Bielawski, *Chem. Commun.*, **2010**, *46*, 4288–4290.
- [22] J. P. Moerdijk, C. W. Bielawski, *Chem. Commun.*, **2014**, *50*, 4551–4553.
- [23] J. P. Moerdijk, G. A. Blake, D. T. Chase, C. W. Bielawski, *J. Am. Chem. Soc.* **2013**, *135*, *50*, 18798–18801.
- [24] N. Tokitoh, R. Okazaki, *Coord. Chem. Rev.* **2000**, *210*, 251–277.
- [25] P. Frisch, S. Inoue, *Dalt. Trans.* **2020**, *49*, 6176–6182.
- [26] S. Fujimori, S. Inoue, *Eur. J. Inorg. Chem.* **2020**, 3131–3142.
- [27] Y. Zhou, M. Driess, *Angew. Chem.*, **2019**, *131*, 3753–3766.
- [28] Y. Mizuhata, T. Sasamori, N. Tokitoh, *Chem. Rev.* **2009**, *109*, 3479–3511.
- [29] J. Barrau, G. Rima, *Coordination Chemistry Reviews*, **1998**, *180*, 593–622.
- [30] P. J. Davidson, M. F. Lappert, *J. Chem. Soc., Chem. Commun.* **1973**, 317.
- [31] M. Timko, *J. Am. Chem. Soc.* **1974**, *96*, *22*, 7160–7162.
- [32] P. Wil, K. Schittelkopf, M. Flock, R. H. Herber, P. P. Power, R. C. Fischer, *Organometallics* **2015**, *34*, *11*, 2222–2232.
- [33] A. V. Protchenko, K. H. Birjkumar, D. Dange, A. D. Schwarz, D. Vidovic, C. Jones, N. Kaltsoyannis, P. Mountford, S. Aldridge, *J. Am. Chem. Soc.* **2012**, *134*, *15*, 6500–6503.
- [34] D. H. Harris, M. F. Lappert, *J. Chem. Soc. Chem. Commun.* **1974**, 895–896.
- [35] R. S. Simons, L. Pu, M. M. Olmstead, P. P. Power, *Organometallics* **1997**, *16*, 1920–1925.
- [36] P. Vargas del Valle, M. S. Piñeiro Becerra, H. Palomino Montenegro, M. a. Torres-Quintana, L. Balducci, A. Ramachandran, J. Hao, K. Narayanan, C. Evans, A. George, et al., *Am. J. Orthod. Dentofac. Orthop.* **2016**, *20*, 1–8.
- [37] I. Saur, S. G. Alonso, H. Gornitzka, V. Lemierre, A. Chrostowska, J. Barrau, *Organometallics* **2005**, *24*, 2988–2996.
- [38] J. R. Fulton, P. B. Hitchcock, N. C. Johnstone, E. C. Y. Tam, *Dalt. Trans.* **2007**, 3360–3362.
- [39] A. Meltzer, S. Inoue, C. Präsang, M. Driess, *J. Am. Chem. Soc.* **2010**, *132*, 3038–3046.
- [40] E. C. Y. Tam, M. P. Coles, J. D. Smith, J. R. Fulton, *Polyhedron* **2015**, *85*, 284–294.
- [41] M. J. Taylor, E. J. Coakley, M. P. Coles, H. Cox, J. R. Fulton, *Organometallics* **2015**, *34*, 2515–2521.

- [42] S. M. I. Al-Rafia, M. R. Momeni, R. McDonald, M. J. Ferguson, A. Brown, E. Rivard, *Angew. Chem. Int. Ed.* **2013**, *52*, 6390–6395.
- [43] A. J. Ruddy, P. A. Rupar, K. J. Bladek, C. J. Allan, J. C. Avery, K. M. Baines, *Organometallics* **2010**, *29*, 1362–1367.
- [44] L. Álvarez-Rodríguez, J. A. Cabeza, P. García-Álvarez, D. Polo, *Organometallics* **2013**, *32*, 3557–3561.
- [45] A. Stasch, C. M. Forsyth, C. Jones, P. C. Junk, *New J. Chem.* **2008**, *32*, 829–834.
- [46] S. S. Sen, H. W. Roesky, D. Stern, J. Henn, D. Stalke, *J. Am. Chem. Soc.* **2010**, *132*, 1123–1126.
- [47] S. S. Sen, J. Hey, R. Herbst-Irmer, H. W. Roesky, D. Stalke, *J. Am. Chem. Soc.* **2011**, *133*, 12311–12316.
- [48] T. Chlupatý, Z. Růžičková, M. Horáček, J. Merna, M. Alonso, F. De Proft, A. Růžička, *Organometallics* **2015**, *34*, 2202–2211.
- [49] M. Denk, R. Lennon, R. Hayashi, R. West, A. V. Belyakov, H. P. Verne, A. Haaland, M. Wagner, N. Metzler, *J. Am. Chem. Soc.* **1994**, *116*, 2691–2692.
- [50] A. V. Zabula, F. E. Hahn, *Eur. J. Inorg. Chem.* **2008**, 5165–5179.
- [51] S. Krupski, C. Schulte To Brinke, H. Koppetz, A. Hepp, F. E. Hahn, *Organometallics* **2015**, *34*, 2624–2631.
- [52] P. P. Gaspar, M. Xiao, D. H. Pae, D. J. Berger, T. Haile, T. Chen, D. Lei, W. R. Winchester, P. Jiang, *J. Organom. Chem.* **2002**, *646*, 68–79.
- [53] M. Usher, A. V. Protchenko, A. Rit, J. Campos, E. L. Kolychev, R. Tirfoin, S. Aldridge, *Chem. - A Eur. J.* **2016**, *22*, 11685–11698.
- [54] A. V. Protchenko, K. H. Birjkumar, D. Dange, A. D. Schwarz, D. Vidovic, C. Jones, N. Kaltsoyannis, P. Mountford, S. Aldridge, *J. Am. Chem. Soc.* **2012**, *134*, 6500–6503.
- [55] A. V. Protchenko, A. D. Schwarz, M. P. Blake, C. Jones, N. Kaltsoyannis, P. Mountford, S. Aldridge, *Angew. Chem.*, **2013**, *125*, 596–599.
- [56] Kira N, Ishida S, Iwamoto T, Kabuto C, *J. Am. Chem. Soc.* **1999**, *121*, 9722–9723
- [57] T. Kosai, S. Ishida, T. Iwamoto, *Angew. Chem. Int. Ed.* **2016**, *55*, 15554–15558.
- [58] Y. Wang, J. Ma, *J. Organomet. Chem.* **2009**, *694*, 2567–2575.
- [59] M. Asay, C. Jones, M. Driess, *Chem. Rev.* **2011**, *111*, 354–396.
- [60] N. Weyer, M. Heinz, C. Bruhn, M. C. Holthausen, U. Siemeling, *Chem. Commun.* **2021**, *57*, 9378–9381.
- [61] U. Siemeling, N. Weyer, M. Heinz, J. Schweizer, C. Bruhn, M. Holthausen, *Angew. Chem. Int. Ed.*, **2021**, *60*, 2624–2628.
- [62] M. Haaf, T. A. Schmedake, R. West, *Acc. Chem. Res.* **2000**, *33*, 704–714.
- [63] B. Gehrhus, M. F. Lappert, *J. Organomet. Chem.* **2001**, *617–618*, 209–223.
- [64] N. J. Hill, R. West, *J. Organomet. Chem.* **2004**, *689*, 4165–4183.
- [65] Y. Peng, J. D. Guo, B. D. Ellis, Z. Zhu, J. C. Fettinger, S. Nagase, P. P. Power, *J. Am. Chem. Soc.* **2009**, *131*, 16272–16282.
- [66] A. V. Protchenko, J. I. Bates, L. M. A. Saleh, M. P. Blake, A. D. Schwarz, E. L. Kolychev, A. L. Thompson, C. Jones, P. Mountford, S. Aldridge, *J. Am. Chem. Soc.* **2016**, *138*, 4555–4564.
- [67] E.O. Fischer, H. Grubert, Z. anorg. allg. Chem., **1956**, *286*, 237–242.
- [68] A. Jana, S. Pillai Sarish, R. W. Herbert, C. Schulzke, A. Döring, M. John, *Organometallics* **2009**, *28*, 2563–2567.
- [69] S. Brooker, J. Buijink, F. T. Edelmann, *Organometallics*, **1991**, *10*, *1*, 25–26.
- [70] B. M. J. S. Gynane, D. H. Harris, M. F. Lappert, P. P. Power, P. Rividre, *J. Chem. Soc., Dalton Trans.*, **1977**, 2004–2009.
- [71] T. Fjeldberg, A. J. Thornc, *Chem. Commun.* **1983**, 639–641.
- [72] B. Wrackmeyer, *J. Magn. Reson.* **1985**, *61*, 536–539.
- [73] B. Wrackmeyer, K. Horchler, H. Zhou, *Spectrochim. Acta Part A Mol. Spectrosc.* **1990**, *46*, 809–816.
- [74] R. Guthardt, C. Bruhn, C. Färber, U. Siemeling, *Organometallics* **2020**, *39*, 4174–4177.
- [75] R. Guthardt, J. Oetzel, J. I. Schweizer, C. Bruhn, R. Langer, M. Maurer, J. Vícha, P. Shestakova, M. C. Holthausen, U. Siemeling, *Angew. Chem. Int. Ed.* **2019**, *58*, 1387–1391.
- [76] J. Barrau, G. Rima, T. El Amraoui, *J. Am. Chem. Soc. Chem. Soc.* **1998**, *466*, 607–614.

- [77] W. Van Zandt, J. C. Huffman, J. L. Stewart, *Main Gr. Met. Chem.* **1998**, *21*, 237–240.
- [78] R. Papiernik, L. G. Hubert-Pfalzgraf, M. C. Massiani, *Polyhedron* **1991**, *10*, 1657–1662.
- [79] R.C.Mehrotra, A.K.Rai, A.Jain, *Polyhedron*, **1991**, *10*, 1103-1104.
- [80] B. D. Rekken, T. M. Brown, M. M. Olmstead, J. C. Fettinger, P. P. Power, *Inorg. Chem.*, **2013**, *52*, 6, 3054–3062.
- [81] F. Krämer, M. S. Luff, U. Radius, F. Weigend, F. Breher, *Eur. J. Inorg. Chem.*, **2021**, 3591–3600.
- [82] K. V. Zaitsev, V. S. Cherepakhin, A. V. Churakov, A. S. Peregovodov, B. N. Tarasevich, M. P. Egorov, G. S. Zaitseva, S. S. Karlov, *Inorganica Chim. Acta* **2016**, *443*, 91–100.
- [83] N. Kano, N. Tokitoh, R. Okazaki, *Yuki Gosei Kagaku Kyokaishi/Journal Synth. Org. Chem.* **1998**, *56*, 919–930.
- [84] S. Weiß, H. Schubert, L. Wesemann, *Chem. Commun.* **2019**, *55*, 10238–10240.
- [85] M. M. Al-Ktaifani, P. B. Hitchcock, M. F. Lappert, J. F. Nixon, P. Uiterweerd, *Dalt. Trans.* **2008**, *2*, 2825–2831.
- [86] E. C. Y. Tam, N. C. Johnstone, L. Ferro, P. B. Hitchcock, J. R. Fulton, *Inorg. Chem.*, **2009**, *48*, 18, 8971–8976.
- [87] U. S. Robin Guthardt, Jan Oetzel, Julia I. Schweizer, Clemens Bruhn, Robert Langer, Martin Maurer, Jan Vícha, Pavletta Shestakova, Max C. Holthausen, and U. S. Robin Guthardt, Jan Oetzel, Julia I. Schweizer, Clemens Bruhn, Robert Langer, Martin Maurer, Jan Vícha, Pavletta Shestakova, Max C. Holthausen, *Angew.Chem.Int.Ed.*, **2019**, *58*, 1387–139.
- [88] A. Jana, H. W. Roesky, C. Schulzke, P. P. Samuel, D. Alexander, *Inorg. Chem.*, **2010**, *49*, 12, 5554–5559.
- [89] N. Olmstead, Z. Margolin, F. G. Bordwell, *J. Org Chem.* **1980**, *45*, 3295–3299.
- [90] R. D. Simpson, R. G. Bergman, *Organometallics* **1992**, *11*, 4306–4315.
- [91] H. E. Bryndza, W. Tam, *Chem. Rev.* **1988**, *88*, 1163–1188.
- [92] D. J. Dahrenbourg, K. M. Sanchez, A. L. Rheingoldib, *J. Am. Chem. Soc.*, **1987**, *109*, 290-292.
- [93] T. Lin, G. Lee, S. Peng, C. Chiu, H. Chen, *Polymer*, **2019**, *180*, 121748.
- [94] V. S. V. S. N. Swamy, S. Pal, S. Khan, S. S. Sen, *Dalt. Trans.* **2015**, *44*, 12903–12923.
- [95] C. K. and Y.-H. T. P. Jutzi, F. Kohl, P. Hofmann, *Chem. Ber.* **1980**, *113*, 757–769.
- [96] S. Hino, M. Brynda, A. D. Phillips, P. P. Power, *Angew. Chem.* **2004**, *116*, 2709–2712.
- [97] M. J. Taylor, A. J. Saunders, M. P. Coles, J. R. Fulton, *Organometallics* **2011**, *30*, 1334–1339.
- [98] H. Braunschweig, M. A. Celik, R. D. Dewhurst, M. Heid, F. Hupp, S. S. Sen, *Chem. Sci.* **2015**, *6*, 425–435.
- [99] R. Rodriguez, D. Gau, Y. Contie, T. Kato, N. Saffon-Merceron, A. Baceiredo, *Angew. Chem. Int. Ed.* **2011**, *50*, 11492–11495.
- [100] R. Rodriguez, D. Gau, T. Kato, N. Saffon-Merceron, A. De Cózar, F. P. Cossío, A. Baceiredo, *Angew. Chem. Int. Ed.*, **2011**, *123*, 10598–10600.
- [101] J. Berthe, J. M. Garcia, E. Ocando, T. Kato, N. Saffon-Merceron, A. De Cózar, F. P. Cossío, A. Baceiredo, *J. Am. Chem. Soc.* **2011**, *133*, 15930–15933.
- [102] R. Rodriguez, Y. Contie, R. Nougué, A. Baceiredo, N. Saffon-Merceron, J. M. Sotiropoulos, T. Kato, *Angew. Chem. Int. Ed.* **2016**, *55*, 14355–14358.
- [103] L. (FR) ANTOINE BACEIREDO, TOULOUSE (FR); TSUYOSHI KATO, TOULOUSE (FR); YANLI MAO, TOULOUSE (FR); JULIETTE BERTHE, PARIS (FR); MAGALI BOUSQUIE, United States (12) Patent Application Publication i 19, Ua 2013/0157174, **2017**, US 2017/0313729 Al.
- [104] R. Rodriguez, Y. Contie, D. Gau, N. Saffon-Merceron, K. Miqueu, J. M. Sotiropoulos, A. Baceiredo, T. Kato, *Angew. Chem. Int. Ed.* **2013**, *52*, 8437–8440.

**Chapter II: Synthesis of Plumbylene-Substituted**  
**Phosphaketene and Decarbonylation reaction**

## I. Introduction

### I.I Phosphinidenes and base-stabilized singlet phosphinidenes

Phosphinidenes ( $\text{RP}$ ) are mono valent organophosphorus compounds, analogous to nitrenes ( $\text{RN}$ ), with 6 electrons in their valence shell having only one substituent ( $\text{R}$ ) and two lone pairs on the phosphorus atom. They could exist either in singlet or in triplet ground states with a strong preference to the latter (figure 1).<sup>[1]</sup> Indeed, the triplet ground state of parent phosphinidene ( $\text{PH}$ ) is 22 kcal/mol lower in energy.<sup>[1,2]</sup> In the case of carbene, parent methylene ( $\text{CH}_2$ ) presents a significantly smaller (9 kcal/mol) single-triplet gap.<sup>[3]</sup> In the triplet state phosphinidenes can be considered as highly reactive diradicals,<sup>[4]</sup> which hampers the profound studies on their chemical properties.<sup>[4,5]</sup> However with right substituents that can provide both electronic stabilisation and kinetic protection, singlet phosphinidenes could be obtained.<sup>[1,4]</sup> Thus, according to theoretical calculations, amino and phosphinido substituents can lower the singlet-triplet energy difference, suggesting that the singlet species may be experimentally accessible.<sup>[1]</sup> However, the kinetic protection by bulky substituents in addition to electronic stabilisation is necessary to prevent dimerization of phosphinidene into a diphosphene.<sup>[4]</sup>

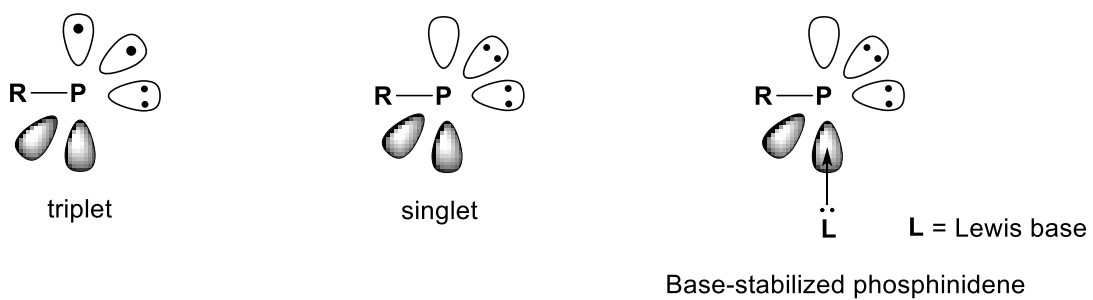


**Figure 1.** The two ground states of phosphinidenes: triplet and singlet.

One of the most efficient ways to stabilize singlet phosphinidenes is the coordination of a Lewis base to the vacant p-orbital of phosphorus atom, leading to the formation of stable adducts satisfying the octet rule of monovalent phosphorus atom.<sup>[1,6]</sup>

### I.II Synthesis and reactivity of phosphine-stabilized phosphinidenes (phosphanylidene- $\sigma^4$ -phosphoranes)

Among the most studied class of the stable phosphinidene derivatives are phosphanylidene- $\sigma^4$ -phosphoranes ( $\text{RP}=\text{PR}'_3$ ) (figure 2).<sup>[6]</sup>

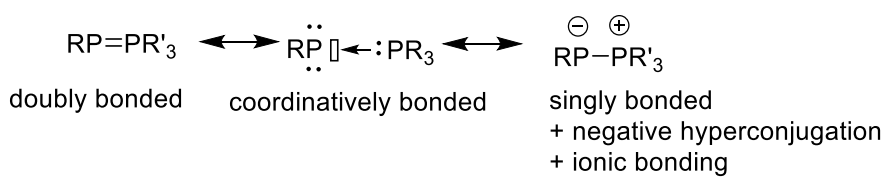
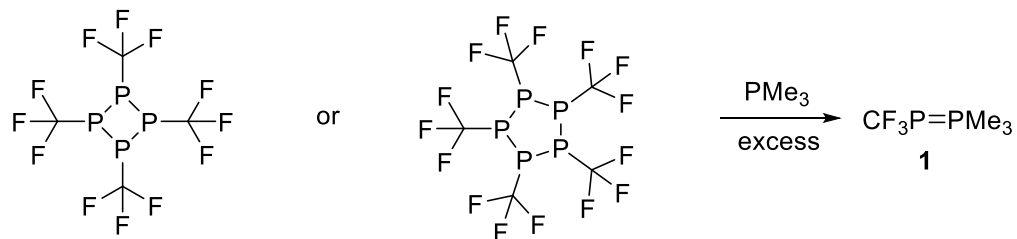


**Figure 2.** Phosphanylidene- $\sigma^4$ -phosphoranes: resonance structures.

The first attempts to isolate such compounds date back to 1961.<sup>[7]</sup> Burg and Mahler obtained  $\text{CF}_3\text{P}=\text{PMe}_3$  by the addition of an excess of  $\text{PMe}_3$  to cyclophosphanes  $(\text{CF}_3\text{P})_4$  or  $(\text{CF}_3\text{P})_5$  (Scheme 1).<sup>[8–10]</sup>

Nonetheless **1** was thermally unstable and was not structurally characterized.<sup>[7]</sup> In  $^{31}\text{P}$ -NMR spectrum the signal for  $\text{CF}_3\text{P}$  atom appears at high field ( $\delta = -81.0$  ppm) due to the strongly polarised ylidic  $\text{R}_3\text{P}^{\delta+}=\text{P}^{\delta-}\text{R}$  bond, and the phosphine fragment ( $\text{PMe}_3$ ) appears at lower field ( $\delta = 12.7$  ppm) with a large PP-coupling constant ( $^1\text{J}_{\text{PP}} = 436.5$  Hz), in agreement with a direct P-P bonding.<sup>[9]</sup>

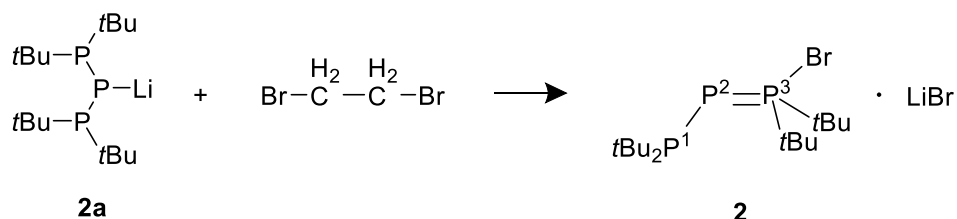


**Scheme 1.** Synthesis of phosphanylidene- $\sigma^4$ -phosphorane **1** by Burg and Mahler

After this pioneering report, phosphanylidene- $\sigma^4$ -phosphoranes received further attention and their chemistry was extensively studied. Depending on the substituent of dicoordinate phosphorus atom, three different types can be considered: phosphanyl-substituted ( $\text{R}_2\text{P}-\text{P}(\text{X})\text{R}'_2$ ), aryl-substituted ( $\text{ArP=PR}'_3$ ), and cyclic ones (e.g. diphosphete).

### I.II.I Phosphanyl-phosphanylideneephosphoranes ( $\text{R}_2\text{P}-\text{P}=\text{P}(\text{X})\text{R}'_2$ )

$\pi$ -donating substituents (e.g.  $-\text{NX}_2$ ,  $-\text{OX}$ ,  $-\text{PX}_2$ ,  $-\text{SX}$ ), generally stabilize singlet phosphinidenes.<sup>[5]</sup> In 1989 Fritz et al. reported a stable phosphanyl-phosphanylideneephosphorane **2** by the reaction of lithiated phosphine and 1,2-dibromoethane in toluene (Scheme 2). The formation of the ylidic P-P adduct was confirmed by  $^{31}\text{P}$ -NMR spectroscopy showing a typical signal for di-coordinate P atom at considerably high-field ( $\delta = -88.9$  ppm,  $J_{\text{P}2\text{P}3} = 683$  Hz), and an unusually low field signal for  $\text{P}^3$  ( $\delta = 175.6$  ppm), probably due to the halide substituent.



$^{31}\text{P}$  NMR:

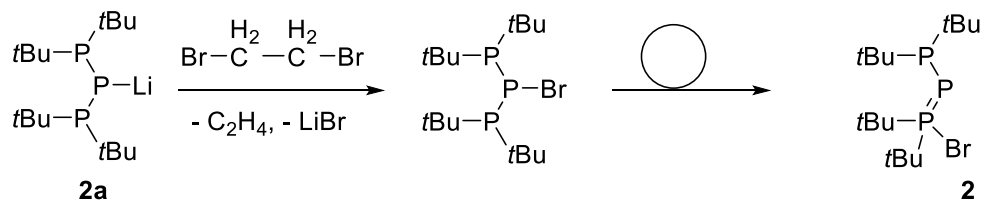
$\text{P}^1 = 20.6$  dd       $J_{\text{P}1\text{P}2} = 252$  Hz

$\text{P}^2 = -88.9$  dd       $J_{\text{P}1\text{P}3} = 40$  Hz

$\text{P}^3 = 175.6$  dd       $J_{\text{P}2\text{P}3} = 683$  Hz

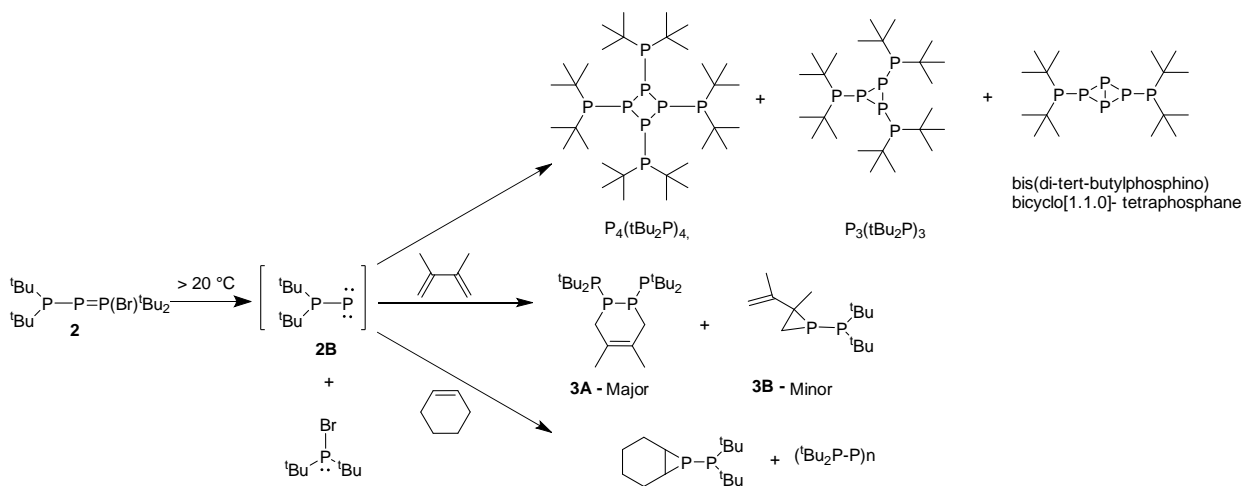
**Scheme 2.** The synthesis of **2** by the reaction of lithiated phosphine and 1,2-dibromoethane.

The reaction probably starts with the bromination at the central phosphorus atom of **2a** by 1,2-dibromoethane via Li-Br exchange reaction. Subsequent migration of the bromine atom to the adjacent terminal tricoordinate phosphorus atom leads to the formation of the phosphinidenoid-phosphane complex **2** (Scheme 3).<sup>[11]</sup>



**Scheme 3.** Mechanism of the formation of product **2**.

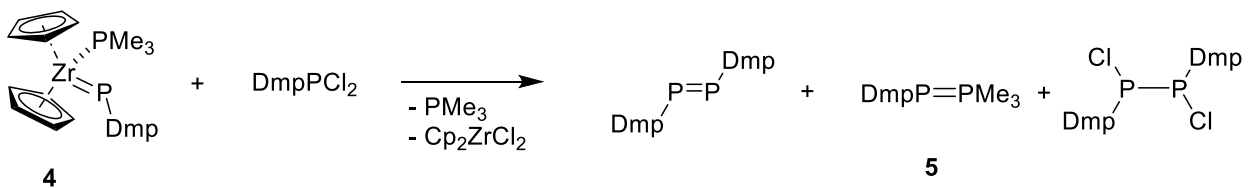
The dative  $\text{P}\rightarrow\text{P}$  bond in compound **2**, is thermally labile and **2** evolves above  $20^\circ\text{C}$  by phosphine ligand dissociation to give the  $\text{tBu}_2\text{PBr}$  and cyclic phosphorus oligomers  $(\text{tBu}_2\text{P-P})_n$  [e.g. cyclic tetramer  $\text{P}_4(\text{tBu}_2\text{P})_4$ , cyclic trimer  $\text{P}_3(\text{tBu}_2\text{P})_3$  or bis(di-*tert*-butylphosphino)bicyclo[1.1.0]- tetraphosphane with a butterfly structure] (Scheme 4), suggesting the transient formation of singlet phosphino-phosphinidene  $\text{tBu}_2\text{P-P}$  **2B**. All attempts to isolate this intermediate in an argon matrix failed.<sup>[12,13]</sup> Instead, the transient phosphinidene can be trapped in the presence of various reagents. For example, the reaction of **2** with 2,3-dimethyl-buta-1,3-diene gives two different products. The major product **3A** is the result of a Diels-Alder reaction between phosphinidene dimer  $\text{tBu}_2\text{P-P=P-PtBu}_2$  and diene, while the minor one **3B** is formed via a [2+1]-cycloaddition reaction between phosphinidene  $\text{tBu}_2\text{P-P}$  and an alkene moiety of diene. A similar cycloadduct is obtained by the reaction of **2** with cyclohexene leading to the formation of the phosphiranes.



**Scheme 4.** Reactivity of phosphanyl-phosphanylideneephosphorane **2** via the transient formation of phosphinidene **2B**.

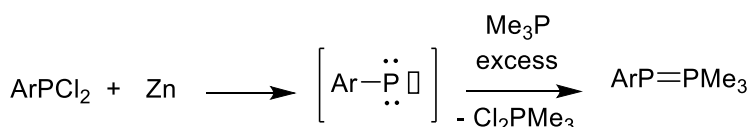
### I.II.II Aryl-substituted phosphanylideneephosphoranes ( $\text{ArP=PR}'_3$ )

The formation of Aryl-substituted phosphanylideneephosphoranes were initially observed by the group of Protasiewicz during the reactivity study of the cyclopentadienyl-substituted zirconium complex **4** with  $\text{DmpPCl}_2$  ( $\text{Dmp} = 2,6\text{-Mes}_2\text{C}_6\text{H}_3$ ). In this reaction, they obtained a mixture of products, one of which was identified as  $\text{DmpP=PMes}_3$  **5** (Scheme 5). The formation of the product **5** was evidenced by  $^{31}\text{P}$  NMR spectroscopy showing an AX system at  $-1.54$  ppm for  $\text{PMes}_3$  fragment and at  $-113.2$  ppm for two-coordinate phosphorus, with a large PP-coupling constant ( ${}^1J_{PP} = 572$  Hz), in a good agreement with a P-P direct bond.<sup>[6,14]</sup>



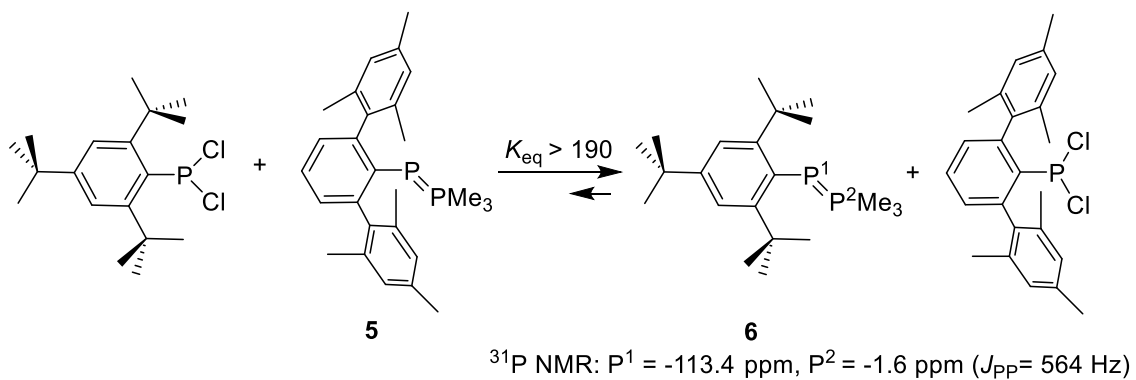
**Scheme 5.** The synthesis of Dmp-P=PMe<sub>3</sub>.

Later, Mathey and Le Floch reported the synthesis of the DmpP=PMe<sub>3</sub> and Mes\*P=PMe<sub>3</sub> (Mes\* = 2,4,6-tBu<sub>3</sub>C<sub>6</sub>H<sub>2</sub>) via the reduction of the corresponding dichlorophosphine Ar-PCl<sub>2</sub> with Zn dust in the presence of an excess of PMe<sub>3</sub> (Scheme 6).<sup>[14]</sup> It seems that PMe<sub>3</sub> acts as a reductant (with subsequent formation of the Cl<sub>2</sub>PMe<sub>3</sub>) and as a stabilizing base. However, when only PMe<sub>3</sub> is applied in the reaction, a lower yield was obtained, and therefore the use of Zn dust along with PMe<sub>3</sub> is necessary in these reactions.



**Scheme 6.** Synthesis of the Phospha–Wittig reagents.

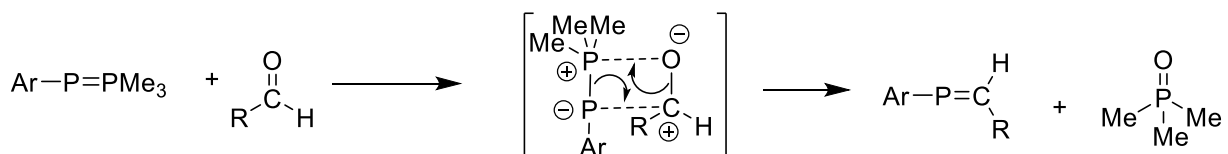
The two-coordinate phosphinidene fragment in the phosphanylidenephosphoranes **5** is exchanged by other in a reversible manner, when it reacts with a Ar'PCl<sub>2</sub> (scheme 7).<sup>[15]</sup>



**Scheme 7.** Phosphinidene fragment exchange in **5**.

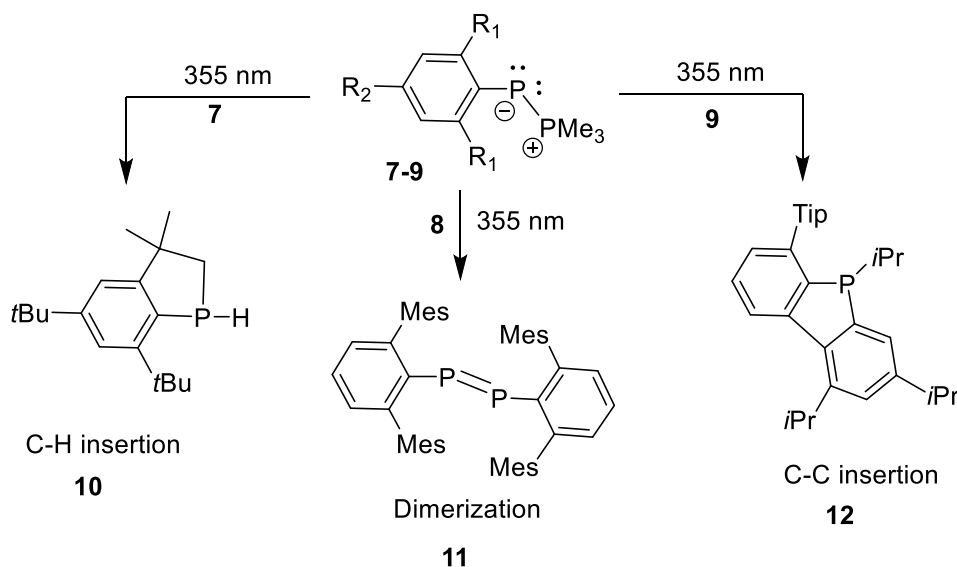
The reaction equilibrium depends on the steric hindrance of the Ar groups. Since the phosphanylidenephosphoranes are sterically less crowded than dichlorophosphines, the use of bulkier aryl groups on the corresponding dichlorophosphine favors phosphinidene exchange to give the new aryl-phosphanylidenephosphorane **6**.<sup>[15]</sup> These reactions can be catalysed by PMe<sub>3</sub> or Bu<sub>3</sub>PCl<sub>2</sub>. The PMe<sub>3</sub> probably reduces ArPCl<sub>2</sub> while R<sub>3</sub>PCl<sub>2</sub> oxidizes ArP=PMe<sub>3</sub>, acting as a catalyst for the chlorine atom transfer reaction.

The ArP=PMe<sub>3</sub> also react with aldehydes through a phospha-Wittig-type reaction, forming ArP=CR'H and Me<sub>3</sub>P=O as products. The driving force of this reaction is the formation of R<sub>3</sub>P=O (Scheme 8).<sup>[16]</sup>



**Scheme 8.** Proposed mechanism for the Phospha-Wittig reaction between phosphanylidene phosphoranes and an aldehyde.

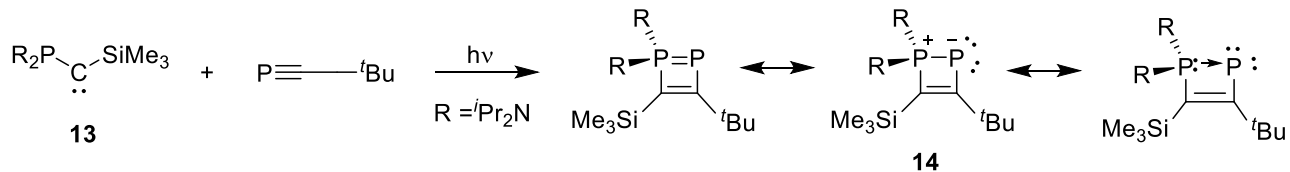
According to computational data, the LUMO of phosphanylidene phosphoranes **7-9** corresponds to the antibonding  $\sigma^*(P-P)$  orbital. Thus, the photochemical irradiation of these compounds, leading to a  $n(P)\rightarrow\sigma^*(PP)$  excitation, results in a photodissociation of the PMe<sub>3</sub> at 355 nm, via the cleavage of the ArP=PM<sub>3</sub> bond, to generate the free phosphinidene.<sup>[17]</sup> In the case of **7**, a C-H activation of one of the o-tBu groups results in the formation of phosphaindane **10** (Scheme 8).<sup>[18-20]</sup> While in the case of more bulky **8** the irradiation gives the dimer of phosphinidene **11**. When R<sub>1</sub>=Tip, cyclic phosphine **12** is formed via a C-C bond activation.<sup>[16,21]</sup>



**Scheme 8.** Photodissociation of **7** (R<sub>1</sub>, R<sub>2</sub> = tBu), **8** (R<sub>1</sub> = Mes, R<sub>2</sub> = H) and **9** (R<sub>1</sub> = Tip, R<sub>2</sub> = H)

### I.III.III Cyclic phosphanylidene phosphoranes

The first cyclic phosphanylidene phosphorane **14** was synthesized by Regitz and Bertrand in 1995 by the reaction of (phosphine)(silyl)carbene **13** with a tert-butylphosphaalkyne (Scheme 9).

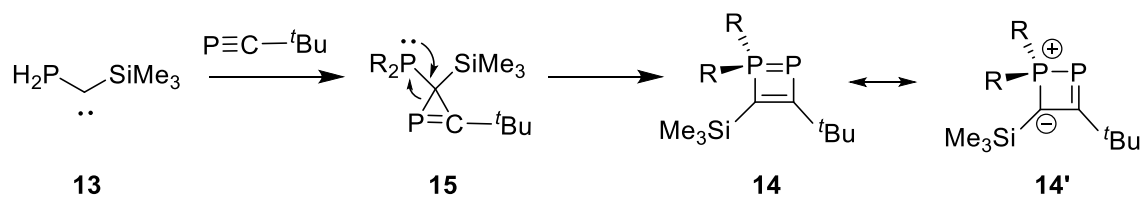


<sup>31</sup>P NMR: 49.2 ppm (PR<sub>2</sub>), 58.4 ppm (PC), <sup>1</sup>J<sub>PP</sub> = 201 Hz

**Scheme 9.** Synthesis of cyclic phosphanylidene phosphorane **14**.

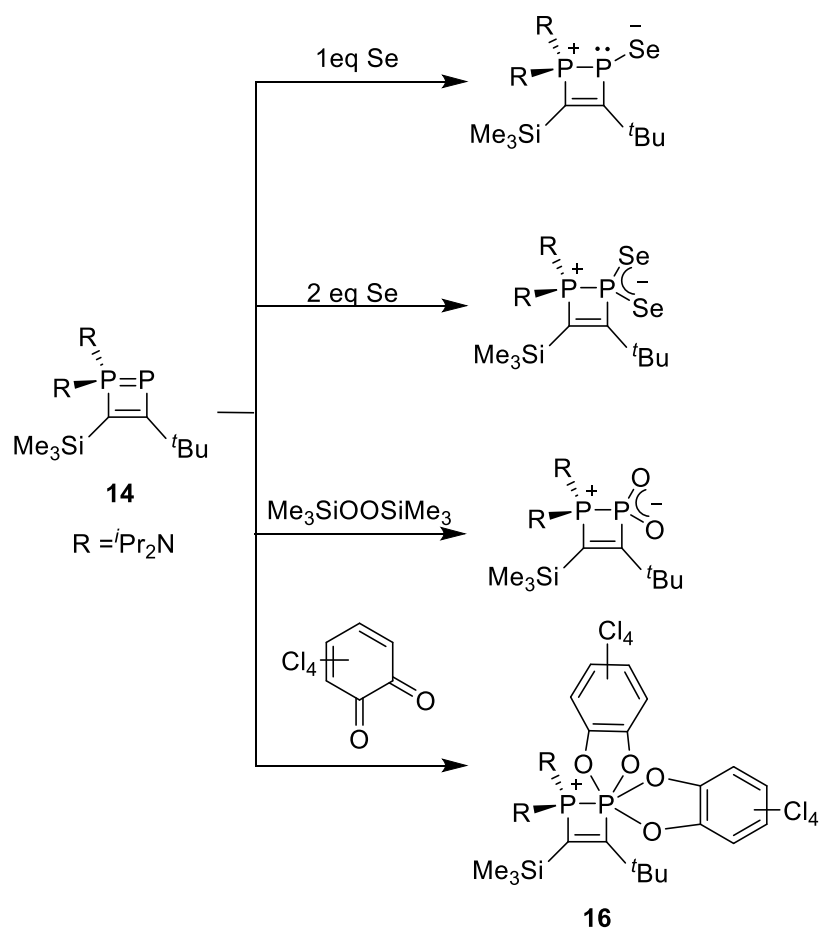
They suggested that the reaction starts with a [2+1]-cycloaddition between the stable (phosphine)(silyl)carbene **13** and a phosphaalkyne to generate the phosphirene **15** (Scheme 10). The

strained three-membered cyclic molecule **15** is unstable and undergoes further ring expansion furnishing **14**.<sup>[22]</sup>



**Scheme 10.** Proposed mechanism for the formation of cyclic **14**.

The stability of this molecule **14** is attributed to the amino-substituents on the tetracoordinate P atom, which enhances the basicity of phosphine ligand. Additionally, the presence of the  $\pi$ -accepting silyl substituent also contributes to the stabilisation of yliadic resonance form **14'**.<sup>[6]</sup> In contrast to acyclic analogues, the P-P bond in **14** is persistent to the phosphine ligand dissociation. Instead, **14** readily undergoes selective oxidation reactions of dicoordinate P atom (Scheme 11).<sup>[6,23]</sup>



**Scheme 11.** Reactivity study of cyclic phosphanylideneephosphorane **14**.

### I.II Phosphaethynolate anion as a suitable source of anionic phosphorus

Phosphaethynolate anion,  $\text{PCO}^-$  was found to be a versatile chemical reagent for the synthesis of a variety of unprecedented phosphorus-containing molecules. Recently Grützmacher's group reported a convenient synthesis of sodium phosphaethylolate salt  $[\text{NaOCP}(\text{dioxane})_x]$  from commercially available Na, red phosphorus and ethylene carbonate. This simple and efficient synthesis of  $\text{NaPCO}$  made it popular and a powerful chemical tool, allowing to easily synthesize various phosphinidene derivatives. Indeed, by reacting it with different electrophiles ( $\text{E-X}$ ,  $\text{X}$  = halogen), various phosphaketenes **17** ( $\text{E-P=C=O}$ ) can be readily obtained, which are thermally labile and easily release CO by photolysis or thermolysis to generate the corresponding phosphinidenes (figure 3).<sup>[24]</sup>

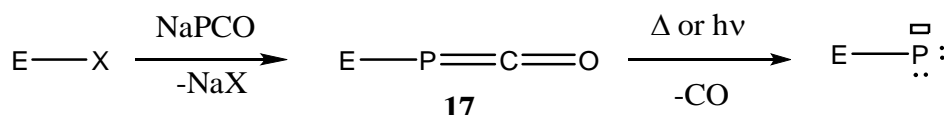
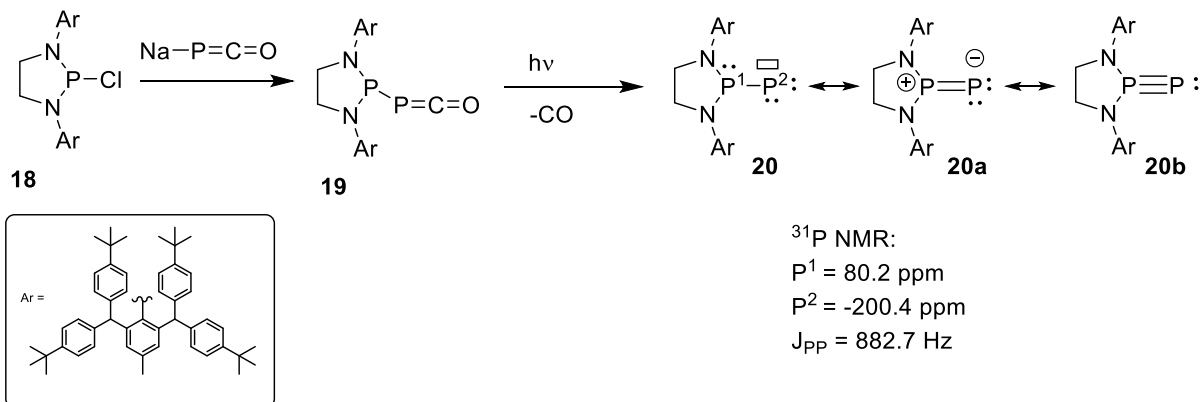


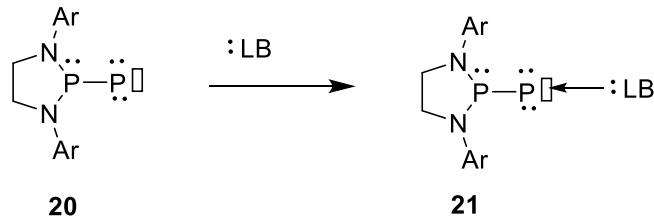
**Figure 3.** The decarbonylation reaction of phosphaketenes **17**.

Using this synthetic technique, in 2016, Bertrand et al. successfully synthetized the first stable singlet (phosphino)phosphinidene **20** (Scheme 12)<sup>[4]</sup> by the photolysis of the corresponding phosphine-phosphaketene **19**. The precursor **19** was prepared by the reaction of chlorodiazaphospholidine **18** with  $\text{NaP=C=O}$ . The phosphinidene **20** is efficiently stabilized by the  $\pi$ -donating and  $\pi$ -accepting effects of diaminophosphanyl substituent (resonance structures **20a** and **20b**).



**Scheme 12.** Synthesis of a stable singlet (phosphino)-phosphinidene **20**.

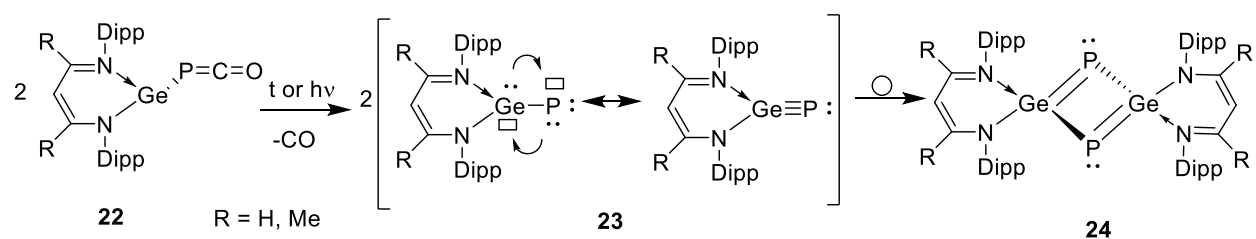
Despite its high thermal stability, phosphinidene **20** presents an extremely high electrophilic character and it reacts with various nucleophiles, even with CO (Scheme 13).<sup>[25]</sup>



**Scheme 13.** Reaction of the stable phosphinidene **20** with Lewis bases.

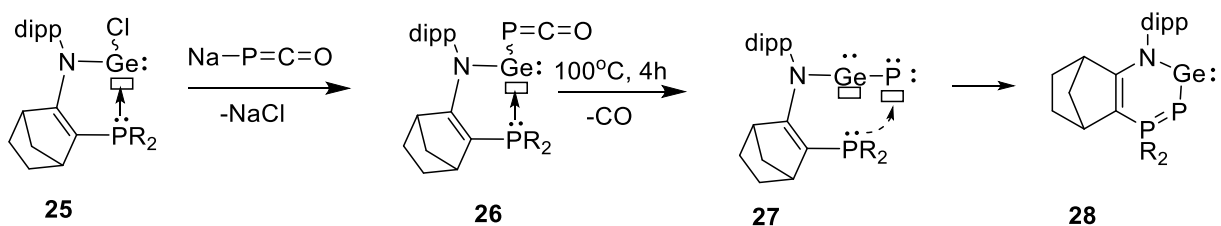
Using the same methodology, Driess et al. tried to obtain a germylene-substituted phosphinidene **23**. The photolysis of the corresponding germylene phosphaketene **22** led to the transient formation of the

germanium-phosphinidene derivative **23**. However, the product **23** subsequently dimerized affording four-membered cyclic dimer **24** (Scheme 14).<sup>[26]</sup>



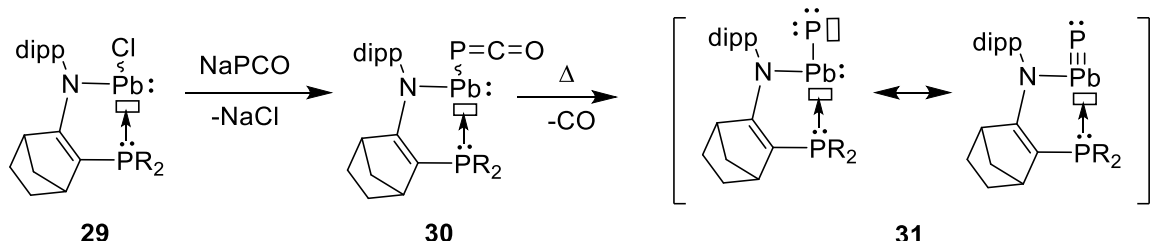
**Scheme 14.** Synthesis of the transient germanium-phosphinidene **23** via a decarbonylation reaction and subsequent dimerization affording **24**.

Following the same strategy, our group has also synthesized the phosphine-stabilized germylene-with a phosphaketene substituent **26** by the reaction of chlorogermylene **25** with NaPCO. This compound is thermally unstable and releases CO at 100 °C to generate the corresponding phosphinidene **27** which then isomerizes to give a phosphanylidene-phosphorane-substituted germylene **28** (Scheme 15).<sup>[27]</sup> Therefore, this can be regarded as a unique and simple new way to synthesize phosphanylidene-phosphorane derivatives.



**Scheme 15.** The synthesis of stable heterocyclic amino(phosphanylidene-phosphorane) germylene **28**.

Then, we have considered the synthesis of the heaviest plumbylene analogue **31** featuring an original iminophosphine ligand. The lead phosphaketene precursor **30** can be easily obtained by the reaction of chloroplumbylene derivative **29** with sodium phosphaethynolate (scheme 16).

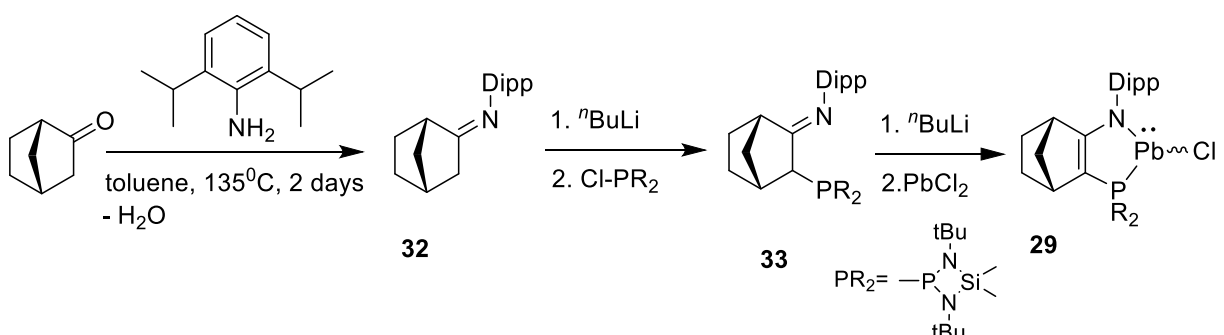


**Scheme 16.** Synthetic strategy to generate lead-phosphinidene complex **31**.

## II. Results and discussion

### II.I Synthesis and characterisation of iminophosphine-stabilized chloroplumbylene **29**

The phosphine-stabilized chloroplumbylene **29** was prepared following the synthetic strategy already established in our group (Scheme 17). The advantage of this strategy is that the synthesis does not require special equipment and it can be performed on a large scale (50 - 100 g). Besides, this strategy is remarkably modulable, since at each step each reagent (ketone, amine and phosphine) can be changed to adjust and optimize the steric hindrance, the donation of the Lewis base, or even change the Lewis base itself, without consequent modification of the experimental condition. The synthesis starts with the condensation reaction of a primary aryl-amine with norcamphor to give the corresponding imine **32**. Then, the  $\alpha$ -position of the imine undergoes deprotonation with *n*-butyl lithium at  $-80\text{ }^{\circ}\text{C}$  in THF, followed by the addition of one equivalent of chlorophosphine affording iminophosphine **33** in 93 % yield. The addition of the lithiated iminophosphine ligand to a suspension of  $\text{PbCl}_2$  in THF leads to the formation of the corresponding chloroplumbylene **29** in 77 % yield (Scheme 17).



Scheme 17. Synthesis of chloroplumbylene **29**.

The plumbylene **29** was characterized by NMR spectroscopy in solution and by X-ray diffraction analysis in the solid state. In the  ${}^{31}\text{P}\{{}^1\text{H}\}$  spectrum of **29** a singlet signal appears at 212.3 ppm. The presence of two satellites with a large PbP-coupling constant ( ${}^1J_{\text{Pb-P}} = 3619.2\text{ Hz}$ ) indicates the formation of a direct Pb-P bond (figure 4).

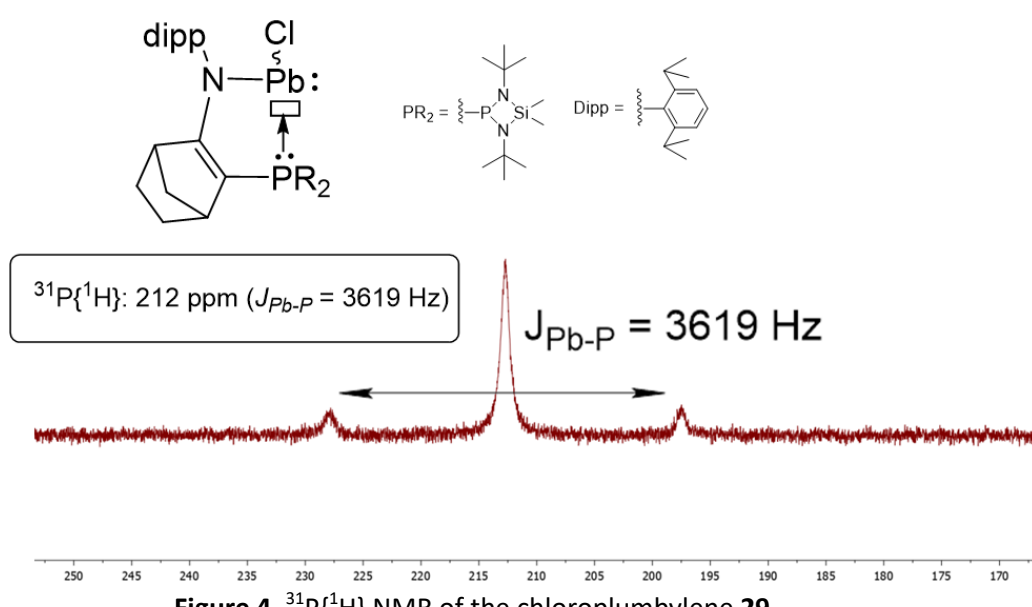
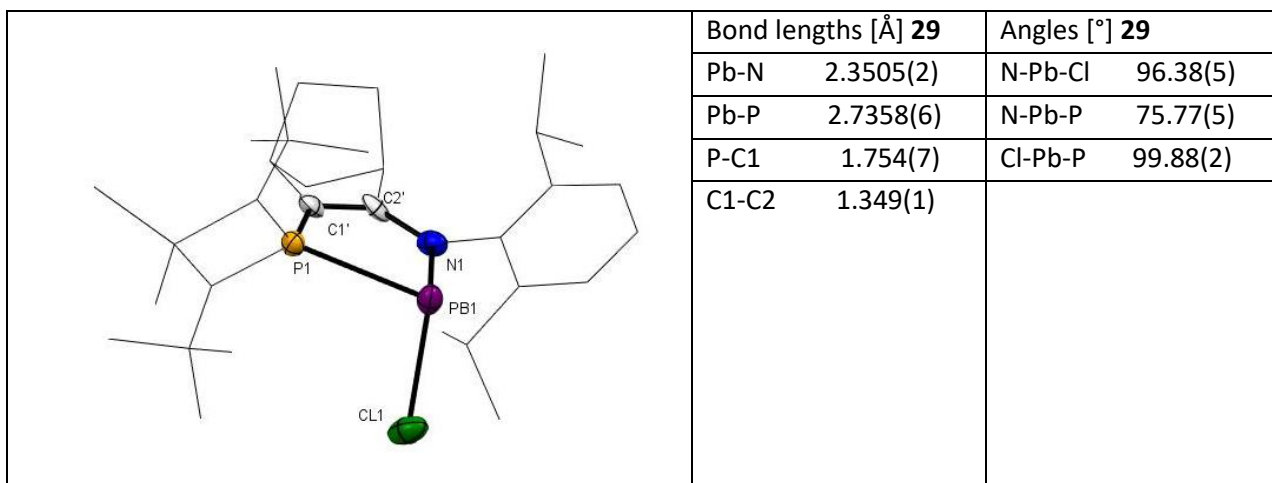


Figure 4.  ${}^{31}\text{P}\{{}^1\text{H}\}$  NMR of the chloroplumbylene **29**.

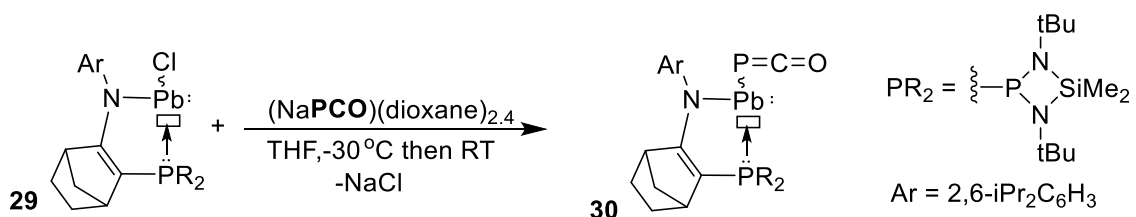
In the  $^1\text{H}$  NMR spectrum of **29**, the signal corresponding to the C-H moiety next to P disappeared, while the carbon atom at this position in the  $^{13}\text{C}$ -NMR shifted to 114.9 ppm from 66.6 ppm. The signal for carbon atom next to the nitrogen in the  $^{13}\text{C}$ -NMR shifted to 188.1 ppm, thus evidencing the formation of the enamine function. The molecular structure of compound **29** was confirmed by X-ray diffraction analysis (figure 5). The Pb-N bond distance [2.3505(2) Å] is in a range of those of other typical Pb-N single bond lengths reported for other diaminoplumbbylenes (2.0 - 2.9 Å).<sup>[28,29]</sup> The structure possess a pyramidalized geometry around divalent lead center ( $\Sigma^\circ_{\text{Pb}} = 272.03^\circ$ ), indicating the presence of the lone pair at the Pb(II) center (figure 5).



**Figure 5.** Molecular structure of chloroplumbulene **29** and selected bond lengths [Å] and angles [°]. Hydrogens and some atoms of disorder omitted for clarity.

## II.II Synthesis and characterisation of iminophosphine-stabilized lead phosphaketene **30**

The reaction of the iminophosphine-stabilized chloroplumbylene **29** with one equivalent of sodium phosphaethynolate  $\text{Na(OCP)(dioxane)}_{2.4}$  affords the desired lead phosphaketene **30**, which was isolated as an orange powder with moderate yield (66%) (Scheme 18).



**Scheme 18.** Synthesis of plumbylene-substituted phosphaketene **30**.

Phosphaketene **30** was obtained as a mixture of two diastereomers (55 : 45), due to the presence of two chiral centers in the molecule (the asymmetric bicyclic fragment and the three-coordinated pyramidalized lead atom) (figure 6).

For each product, in the  $^{31}\text{P}\{^1\text{H}\}$ -NMR spectrum, appear AX-systems due to the presence of two types of phosphorus atoms (phosphine ligand and the phosphaalkene fragment). All signals present satellites with large P-Pb-coupling constants (major isomer:  $J_{\text{PPb}} = 3716.1$  Hz, minor isomer:  $J_{\text{PPb}} = 3816.2$  Hz), that indicates the direct P-Pb interaction (table 1).

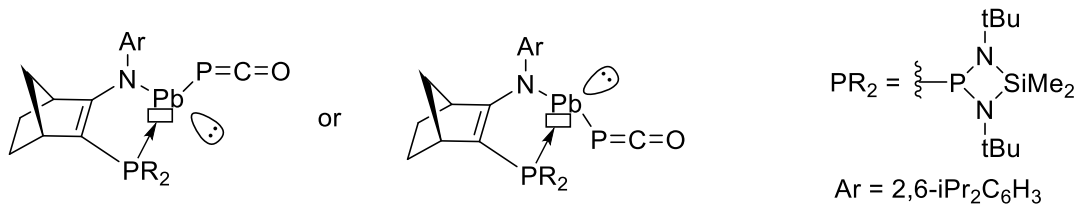


**Figure 6.** Two possible diastereomers of plumbylene-substituted phosphaketene **30**.

The signals, in the  ${}^{31}\text{P}\{{}^1\text{H}\}$ -NMR spectrum, for the  $-\text{P}=\text{C}=\text{O}$  moieties ( $\delta = -329.4/-333.2$  ppm) are downfield shifted compared to NaPCO ( $\delta = -392.0$  ppm). Indeed, the same tendency was observed for other reported phosphaketenes (table 1). The  ${}^{207}\text{Pb}$ -NMR spectrum displays two doublet of doublets at  $\delta = 2460$  ppm (major) and  $\delta = 2233$  ppm (minor), in the typical region for three-coordinate Pb(II) atoms, and featuring the same P-Pb-coupling constants which are observed in the  ${}^{31}\text{P}\{{}^1\text{H}\}$ -NMR spectrum.

${}^{31}\text{P}\{{}^1\text{H}\}$ NMR				$\text{Ph}_3\text{Ge-P}=\text{C}=\text{O}$ <b>34</b> <sup>[30]</sup>	NaPCO
<b>30 [55:45]</b>				$\text{Ph}_3\text{Ge-P}=\text{C}=\text{O}$ <b>34</b> <sup>[30]</sup>	NaPCO
( $\delta$ ) $\text{PR}_2$	182.2 / 189.9	90.7 / 90.1	-	-	
( $\delta$ ) $-\text{P}=\text{C}=\text{O}$	-329.4 / -333.2	-317.3 / -315.9	-298.9	-344	-392.0
${}^2J_{\text{P-P}}$ (Hz)	11.6 / 5.5	32.4 / 34.9			
${}^1J_{\text{P-Pb}}$ (Hz)	3716.1 / 3816.2				

**Table 1.**  ${}^{31}\text{P}$ -NMR chemical shifts and coupling constants of reported phosphaketenes.

	Bond lengths [ $\text{\AA}$ ] <b>30</b>	Angles [ $^\circ$ ] <b>30</b>
	Pb-P2 2.761(5)	Pb-P2-C3 87.3(3)
	Pb-N1 2.315(2)	P2-C3-O 177.1(8)
	Pb-P1 2.747(1)	N1-Pb-P1 76.6(1)
	P1-C1 1.715(3)	N1-Pb-P2 98.4(2)
	C1-C2 1.387(4)	P2-Pb-P1 93.1(1)
	C2-N1 1.318(4)	Pb-P1-C1 94.9(1)
	P2-C3 1.591(8)	P1-C1-C2 122.5(2)
	C3-O 1.176(9)	C1-C2-N1 128.5(3)
		C2-N1-Pb 116.1(2)

**Figure 7.** Molecular structure of **30** and selected bond lengths [ $\text{\AA}$ ] and angles [ $^\circ$ ]. (Hydrogen atoms and some distorted atoms are omitted for clarity).

The structure of **30** was established by single crystal X-ray diffraction analysis (figure 7), and exhibits a strongly pyramidalized Pb center ( $\Sigma^\circ_{\text{Pb}}=268.07^\circ$ ) and an almost planar PbNCCP ring ( $\Sigma\alpha = 535^\circ$ ). The C1-C2 distance (1.387  $\text{\AA}$ ) is slightly longer than classical double bond (1.34  $\text{\AA}$ ) while the P1-C1 (1.715  $\text{\AA}$ ) and C2-N1 (1.318  $\text{\AA}$ ) bond lengths are shorter than classical single bonds (1.84  $\text{\AA}$  and 1.47  $\text{\AA}$ , respectively). This bonding situation is very similar to that observed in the case of related Ge-phosphaketene **26** and suggests a  $\pi$ -electron delocalization of the cyclic nitrogen lone pair (figure 8). Besides, the structure exhibits an acute Pb-P2-C3 angle [87.3(3) $^\circ$ ] similar to the germylene analogues **26** Ge-P-C [86.01(12) $^\circ$ ]<sup>[27]</sup>.

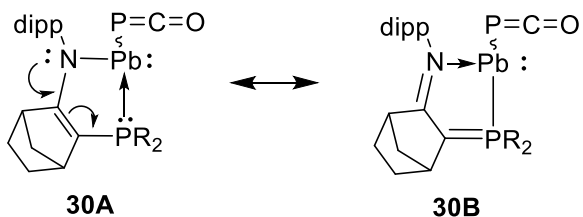
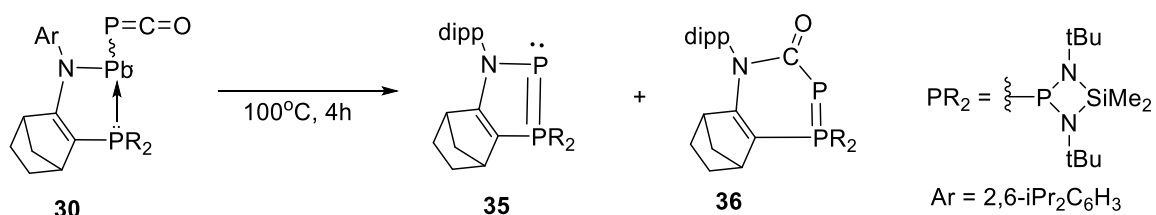


**Figure 8.** Mesomeric forms of lead phosphaketene **30**.

### III. Decarbonylation reaction of the lead-phosphaketene **30**

We have then studied the thermolysis of lead phosphaketene **30**. Monitoring the reaction by  $^{31}\text{P}$ -NMR spectroscopy indicates that the molecule **30** starts to evolve at 80 °C. Of particular interest, the reaction leads to the precipitation of metallic lead and the formation of the mixture of two phosphanylidene- $\sigma^4$ -phosphorane derivatives **35** and **36** without lead atom in the molecules (Scheme 19). The ratio between these two products is temperature dependent and the lower temperature favours the formation of the **35** [**35** : **36** = 80 : 20 ( $T = 80$  °C) and 50 : 50 ( $T = 100$  °C)]. In order to avoid the isolation of thermally unstable **30**, its thermolysis can be performed *in situ*, which is a more efficient process.



**Scheme 19.** Thermolysis of lead phosphaketene **30**.

#### III.I Characterization of phosphanylidene- $\sigma^4$ -phosphoranes **35** and **36**.

The minor product **36** was isolated by the precipitation as a yellow powder from a pentane solution (yield 39 %) and then the major product **35** was isolated by crystallization from a heptane solution at –30 °C in a moderate yield (31 %). The  $^{31}\text{P}\{\text{H}\}$ -NMR spectrum of the **35** shows an AX-system ( $\delta = 88.5$  and 75.5 ppm for dicoordinate and tetracoordinate phosphorus atoms respectively) with a large PP-coupling constant ( $^1J_{\text{PP}} = 518.0$  Hz) confirming the two directly bonded phosphorus atoms. Generally, the signal for the dicoordinate phosphorus atom of phosphanylidene phosphoranes appears at high field due to the strongly polarised ylidic  $\text{R}_3\text{P}^{\delta+}=\text{P}^{\delta-}\text{R}$  bond, which is in line with the  $^{31}\text{P}\{\text{H}\}$ -NMR signal of carbon monoxide substituted **36** (table 2). The signal for the  $\sigma^4$ -P atom appeared in typical range of  $^{31}\text{P}\{\text{H}\}$ -NMR chemical shifts for tetracoordinated phosphorus atoms.

<sup>31</sup> P{ <sup>1</sup> H} RMN				
	<b>35</b>	<b>36</b>	<b>37<sup>[31]</sup></b>	<b>38<sup>[32]</sup></b>
$\sigma^2\text{-P } (\delta)$ (ppm)	88.5	-69.3	-244.3	-157.7
$\sigma^4\text{-P } (\delta)$ (ppm)	75.5	69.8	56.7	76.7
$^1J_{\text{PP}}$ (Hz)	518.0	482	531.0	479.6

**Table 2.** <sup>31</sup>P{<sup>1</sup>H} NMR data for products **35** and **36** and selected phosphanylidene phosphoranes.

As discussed later (section II.V), the DFT calculations on **35** indicate that the p<sub>π</sub>–lone pair of a σ<sup>2</sup>-P is involved in cyclic π-delocalization (figure 9).

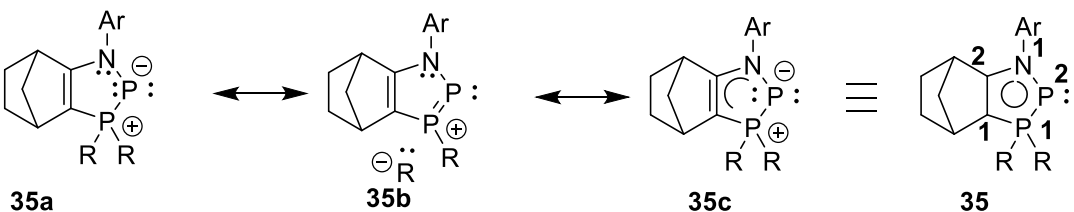


**Figure 9.** Some canonical structures of the cyclic phosphanylidene-σ<sup>4</sup>-phosphorane **35**.

According to single crystal diffraction analysis, the molecular structure of **35** shows an almost planar five-membered C<sub>2</sub>P<sub>2</sub>N ring ( $\Sigma\alpha = 537^\circ$ ) with the N1-P2 bond distance (1.778 Å) significantly longer than N=P double bonds (1.61 Å) (figure 10). A similar N-P bond length (1.779 Å) for 1,4,2-diazaphospholidine-3,5-dione anion was reported by Grützmacher and Goicoechea.<sup>[33]</sup> The P1-C1 [1.715(3) Å] and C2-N1 [1.320(3) Å] bonds lengths are slightly shorter than those of the CO-substituted **36** (P1-C1: 1.741 Å, C2-N1: 1.376 Å, C1-C2: 1.360 Å), while the P1-P2 distance in **35** [2.119(8) Å] is intermediate between PP-single and –double bonds (2.22 Å and 2.04 Å) (figure 11).<sup>[34]</sup> The P1=P2 bond length in **36** is similar to this value [2.1006(7) Å] (figure 10). These results suggest a cyclic 6π-electron delocalization across the C<sub>2</sub>P<sub>2</sub>N ring in the case of **35**.

	Bond lengths [Å] <b>35</b>	Angles [°] <b>35</b>
N1-P2	1.778(2)	N1-P2-P1 92.1(1)
P2-P1	2.119(1)	P2-P1-C1 95.5(1)
P1-C1	1.715(3)	P1-C1-C2 114.7(2)
C1-C2	1.368(3)	C1-C2-N1 121.8(2)
C2-N1	1.320(3)	C2-N1-P2 115.9(1)

**Figure 10.** Molecular structure of **35** and selected bond lengths [Å] and angles [°]. Hydrogen some distorted atoms are omitted for clarity.

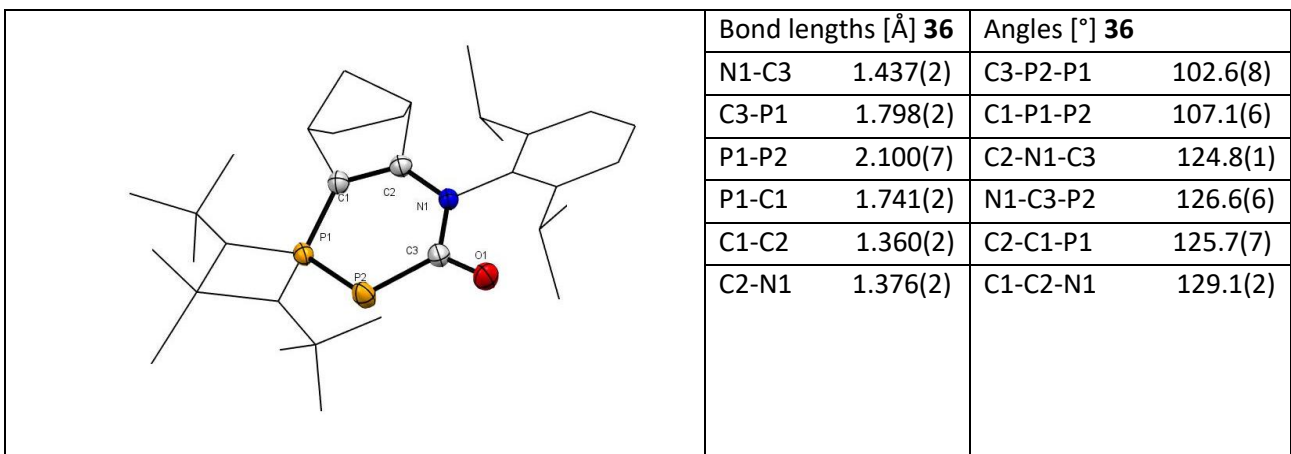


**Figure 11.** Molecular structure of **36** and selected bond lengths [Å] and angles [°]. Hydrogen some distorted atoms are omitted for clarity).

The natural bond orbital (NBO) analysis confirms the strong heteroallylic resonance across C1=C2-N1 fragment in **35** along with substantial delocalisation from occupied  $\pi$ -type orbitals ( $\pi_{C1-C2}$  and lone pair of P2) into  $\sigma^*_{P1-N2}$  and  $\sigma^*_{P1-N3}$ . This interplay between  $\pi$ -resonance and negative hyperconjugation (the donation of the lone pair of the P2 atom into antibonding  $\sigma^*_{P1-N2}$  and  $\sigma^*_{P1-N3}$  orbitals) leads to an aromatic character of the central C<sub>2</sub>P<sub>2</sub>N ring in **35**. Indeed, the nucleus independent chemical shift (NICS) value calculated for the simplified model **39** was found to be negative (-6.9), and therefore confirms the aromatic character of **35**. This value is 70 % of that predicted to aromatic cyclopentadienide (C<sub>5</sub>H<sub>5</sub>)<sup>-</sup> [NICS(1) = -9.9] and very close to the parent phosphole C<sub>4</sub>H<sub>4</sub>PH [NICS(1) = -6.2]. Besides, NICS(1) calculated for **39** is significantly bigger than that of parent phosphinine C<sub>5</sub>H<sub>5</sub>PH<sub>2</sub> [NICS(1) = -2.4] (Figure 12).

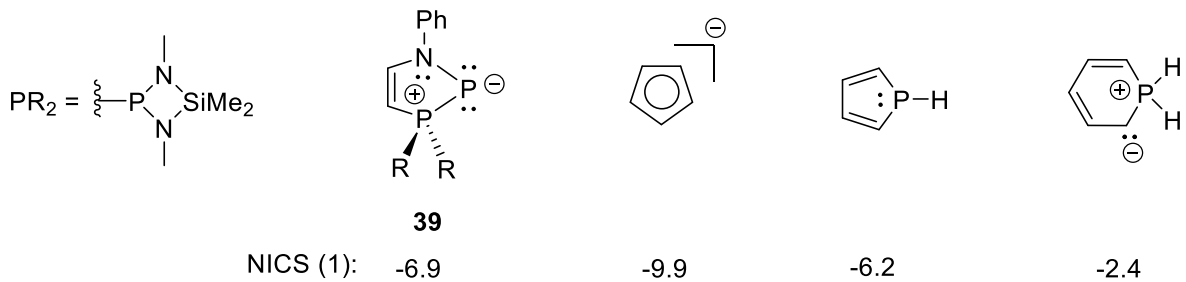
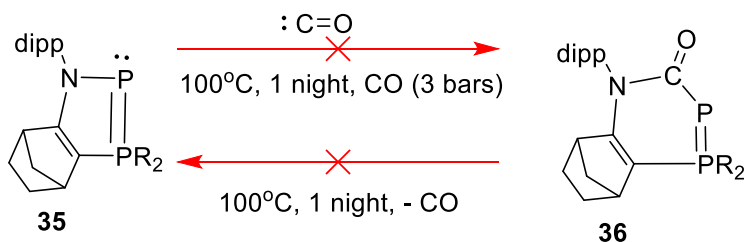


**Figure 12:** Calculated NICS(1) (total) values for compound **39**, cyclopentadienide (C<sub>5</sub>H<sub>5</sub>)<sup>-</sup>, phosphole C<sub>4</sub>H<sub>4</sub>PH and phosphinine C<sub>5</sub>H<sub>5</sub>PH<sub>2</sub> [at M06-2X/6-311+G(d,p) level].

The further natural chemical shift analysis (NCS) revealed strong deshielding from the  $\pi$ -type lone pair at P2. This deshielding is a consequence of an interaction between the orthogonal  $\pi$ -type lone pair on the  $\sigma^2$ -P atom and the  $\sigma^*_{P2-N1}$  orbitals.

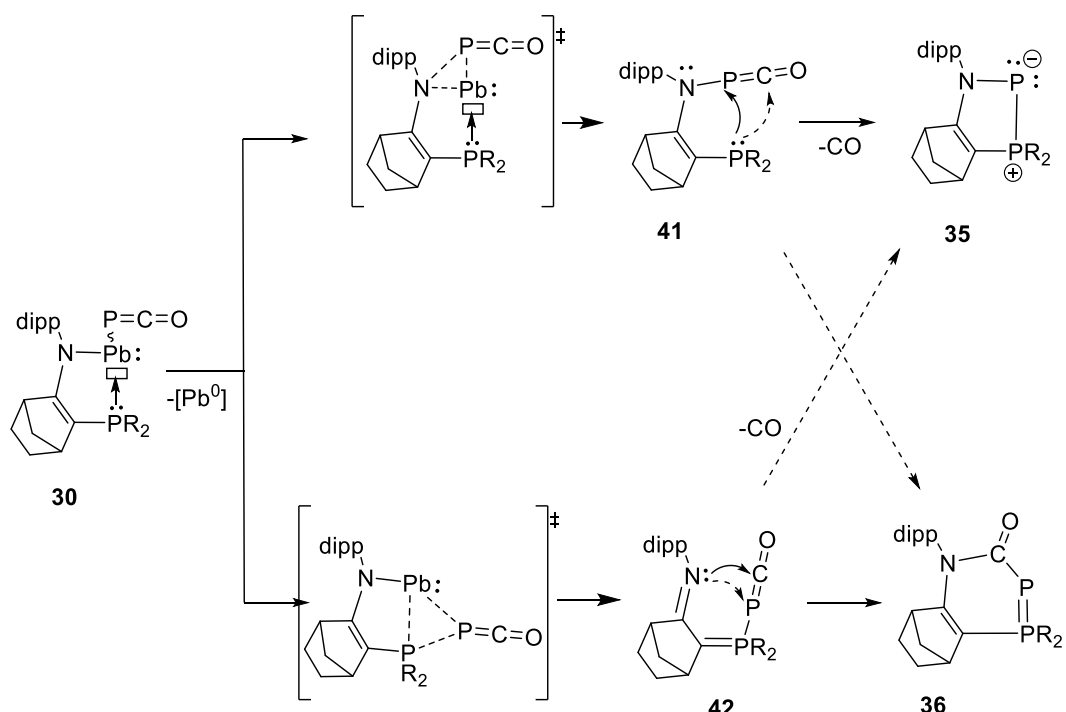
### III.II Mechanistic study

We have then investigated the mechanism of the reaction. To explain the formation of two similar products **35** and **36**, we first considered the formation of one product from the other, either by the addition or removal of CO. Therefore, we checked the reaction of the **35** with 3 bars of CO at 100 °C as well as the CO-elimination reaction of **36** under vacuum at 100 °C (scheme 20). However, both reactions did not take place, indicating that these two products come from two different pathways.



**Scheme 20.** Attempted reactions: (i) thermal reaction of **35** with CO, and (ii) thermal elimination of CO from **36**.

Given the formation of metallic Pb during the thermolysis of phosphaketene-substituted plumbylene **30**, the reaction probably starts with the reductive eliminations of Pb either to form a P-N bond to generate an N-phosphaketene intermediate **41** or to form a P-P bond to generate a P-phosphaketene intermediate **42**. Both intermediates **41** and **42** can be the precursors of final products **35** and **36**. Indeed, further evolution of **41** by CO elimination induced by phosphine attack on the P atom of phosphaketene gives phosphanylidene phosphorene **35** or evolution by phosphine attack on the C atom of phosphaketene gives **36**. Similarly, the attack of the imine function on the P or N atom of phosphaketene in **42** leads to the formation of **35** or **36** respectively.



**Scheme 21.** Proposed reaction pathways for the thermolysis of lead-phosphaketene **30**.

Therefore, two possibilities can be considered:

- 1) One of the two intermediates (**41** or **42**) is the precursor of the two final products (**35** and **36**).
  - 2) Each intermediate is the specific precursor of each of the final products.

To clarify the reaction mechanism of the thermolysis of the **30**, DFT calculations at the M062X/6-311+G(d,p) level were performed using simplified model compounds **39-40**. The calculated energy difference between the two simplified intermediates **43** and **44** were found  $\Delta G(398)_{7M/6M}=32$  kJ/mol to be

similar to the values calculated for the real molecules of intermediates **41** and **42** (figure 13), suggesting that the model compounds are suitable for our theoretical studies.

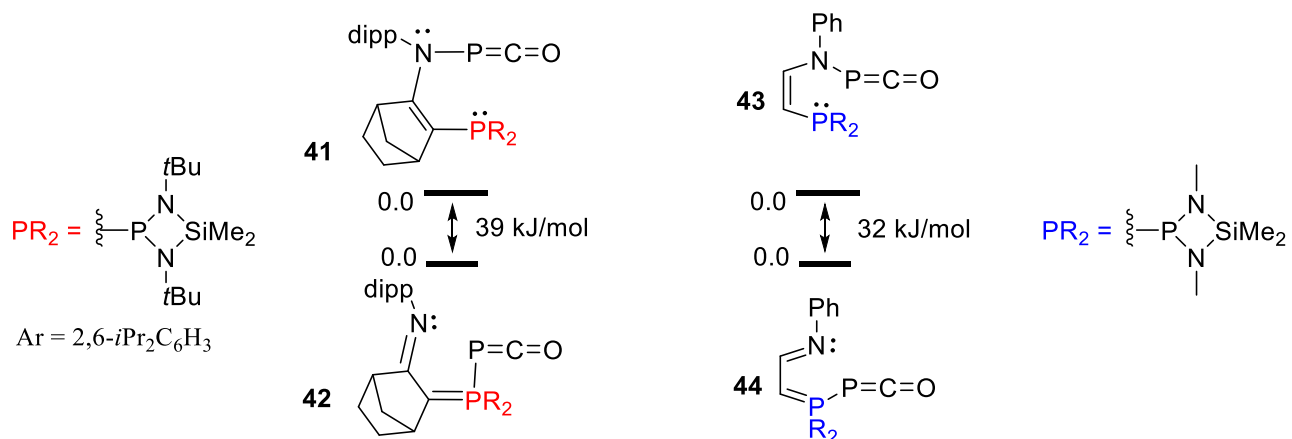


**Figure 13.** Relative Gibbs energies  $\Delta G(398)$  (kJ/mol) calculated for experimentally formed intermediates **41** and **42** and for model molecules **43** and **44**. DFT calculations performed at the M062X/6-311+G(d,p) level.

Although we could not calculate the energy barriers and the Gibbs free energies for the reactions to form the intermediates **43** and **44** from the phosphaketene-substituted plumblylene, as already mentioned, the energy difference between these intermediate is reasonably small (32 kJ/mol) and therefore both intermediates can be produced in a competitive manner.

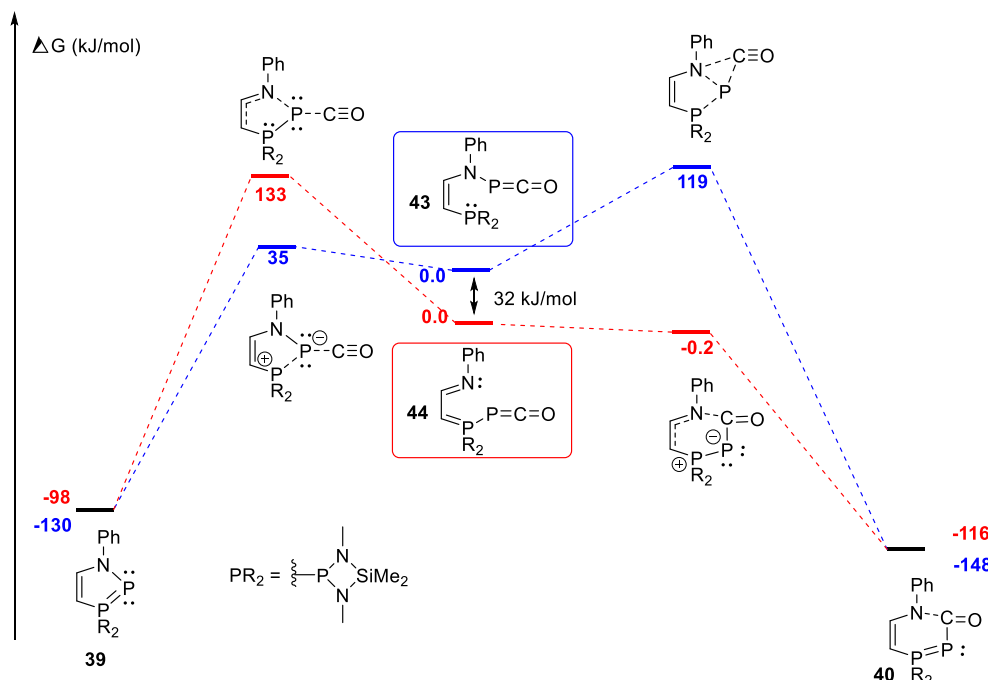


**Figure 14.** Proposed mechanism for the transformation of phosphaketene intermediates **43/44** into **39/40**. Calculated relative Gibbs energies at 398 K in toluene,  $\Delta G(398)$  in kJ/mol using M062X/6-311+G(d,p)) relative to the energy of intermediates **43** (in blue) and **44** (in red).

In both pathways, the formation of final products **39** and **40** from the intermediates **43** and **44**, are exergonic. The formation of the **39** from **43** via CO substitution by the attack of phosphine on the P atom of phosphaketene proceeds with a small energy barrier ( $\Delta G^\ddagger = 35 \text{ kJ/mol}$ ). In the same way, the formation of the **40** from the **44** through the nucleophilic attack of the imine to the C atom of phosphaketene proceeds

almost without barrier, the formation of **39** from **44** through the CO elimination requires much higher energy to proceed ( $\Delta G^\ddagger = 133$  kJ/mol). In contrast to these easy pathways (**43** → **39** and **44** → **40**), the calculated barriers of other pathways (**43** → **40** and **44** → **39**) are considerably higher in energy (133 kJ/mol and 119 kJ/mol, respectively). Thus, these pathways cannot compete with the formation of the **39** from **43** and **40** from the **44** which proceeds with significantly lower energy barriers (figure 14). These results confirm that each final product **39** and **40** (**35** and **36**) is obtained from a specific precursor **43** and **44** (**41** and **42** respectively).

### III.IV-Theoretical investigation of phosphanylidene- $\sigma^4$ -phosphorane **35** by DFT calculations

DFT calculations at the M062X/6-311+G(d,p) level were also performed to understand the electronic state of compound **35**. The computed structural parameters of **35** are very close to the values obtained by XRD analysis [no deviation in atomic distances larger than 3%] (table 3).

Compound	P1 -P2 [ $\text{\AA}$ ]	P1 -N4 [ $\text{\AA}$ ]	C7 -C8 [ $\text{\AA}$ ]	N4 - 8 [ $\text{\AA}$ ]	P2 -C7 [ $\text{\AA}$ ]	N4 -P1-P2 [°]
<b>35 (exp.)</b>	2.11	1.77	1.36	1.32	1.71	92
<b>35 (Comp.)</b>	2.14	1.79	1.37	1.33	1.73	90
<b>39</b>	2.11	1.78	1.36	1.35	1.74	89.6

**Table 3.** Comparison of the selected structural parameters for compound **35** computed using the level of M06-2X/6-311+G(d,p) with the experimental data.

The calculated HOMO of **35** is a typical  $\pi$ -orbital with dominant contributions from the dicoordinate P2 atom (figure 15). The LUMO of the **35** corresponds to the antibonding orbital of P2-N1  $\sigma$ -bond ( $\sigma^*PN$ ), implying a weak and polarized P-N bond. Notably, the orientation of the frontier orbitals (in-plane LUMO,  $\pi$ -type HOMO) is inverted compared to the classical orientation in regular carbene analogues. The HOMO-1 also possesses  $\pi$ -character, thus suggesting the delocalisation across  $\text{C}_2\text{P}_2\text{N}$  ring (**35** in Figure 9).

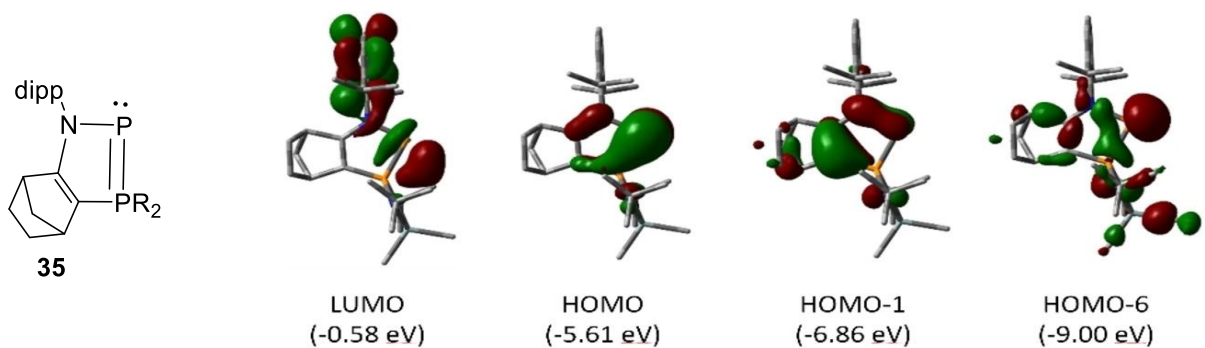


**Figure 15.** Computed surface diagrams of the frontier molecular orbitals of **35** and their corresponding energy values at the M06-2X/6-311G(d,p)//M06-2X/6-311+G(d,p) level (isosurface level =  $\pm 0.04$  e/(a.u.)<sup>3</sup>). Hydrogen atoms were omitted for the clarity.

Furthermore, the computed negative electron charge on the P2 atom (Natural charge: +0.02 a.u. at P2 vs. +1.58 a.u. at P1) and a strong negative electrostatic potential at this atom is in good agreement with a strongly polarized ylidic P-P bond and suggests the nucleophilic character of the dicoordinate P2 atom (Resonance structure **35a** on Figure 16).

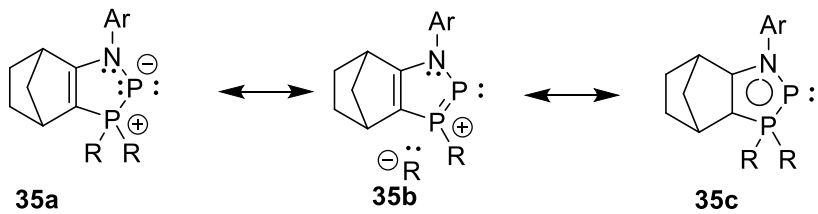


**Figure 16.** Suggested canonical structures of the obtained cyclic phosphanylidene- $\sigma^4$ -phosphorane **35** involving the  $\text{PR}_2$  group through negative hyperconjugation.

#### IV. Reactivity of (amino)phosphanylidene- $\sigma^4$ -phosphorane **35**

##### IV.I. Reaction with $\text{BH}_3 \cdot \text{THF}$

Due to the presence of an empty p-orbital, boranes are the typical Lewis acids of the p-block. They readily react with various phosphines leading to the formation of a strong P-B bond ( $\Delta H = 82.9 \text{ kcal/mol}$ )<sup>[35]</sup> and therefore a large number of stable phosphorus-boron adducts have been reported (figure 17).<sup>[36–38]</sup>

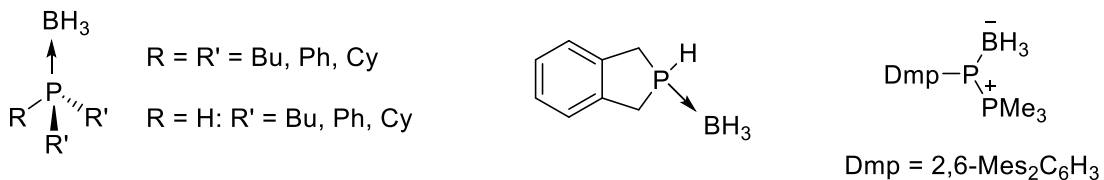
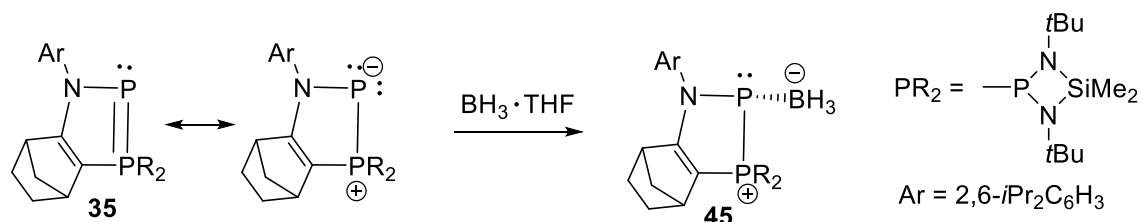


**Figure 17.** Selected examples of reported phosphino-borane complexes

The addition of borane–tetrahydrofuran complex,  $\text{BH}_3 \cdot \text{THF}$ , to a solution of **35** in toluene at room temperature afforded the formation of the corresponding donor-acceptor complex **45** which has been isolated in crystalline form in moderate yield (37 %) (scheme 22).



**Scheme 22.** Reaction of phosphanylidene- $\sigma^4$ -phosphorane **35** with  $\text{BH}_3 \cdot \text{THF}$ .

In the  $^{31}\text{P}\{\text{H}\}$ -NMR spectrum, a low-field chemical shift for the dicoordinate P atom ( $\delta = 101 \text{ ppm}$ ) relative to that of starting material **35** ( $\delta = 88.5 \text{ ppm}$ ) is observed, while chemical shift for the teracoordinate P atom ( $\delta = 77.8 \text{ ppm}$ ) is similar to that observed for **35** ( $\delta = 75.5 \text{ ppm}$ ). Moreover, the large PP-coupling constant ( ${}^1J_{\text{PP}} = 408.3 \text{ Hz}$ ) indicates the presence of a direct PP-bond in **45**. The  $^{11}\text{B}\{\text{H}\}$ -NMR spectrum shows a high field singlet signal at  $\delta = -32.4 \text{ ppm}$  which is in a good agreement with a tetracoordinated boron atom. Single crystals of compound **45**, suitable for the X-ray diffraction analysis, were obtained from a concentrated ether solution at room temperature. The P2-B1 bond distance ( $1.962(2) \text{ \AA}$ ) is in a good agreement with boron-phosphorus single bond involving three-coordinate boron and phosphorus atoms ( $1.93 \text{ \AA}$ ) (Figure 19).<sup>[39]</sup> The P1-P2 bond length [ $2.181(1) \text{ \AA}$ ] is longer than those for **35** [ $2.119(1) \text{ \AA}$ ] and CO substituted **36** [ $2.100(7) \text{ \AA}$ ] but still shorter, than typical P-P-single bonds [ $2.20 - 2.35 \text{ \AA}$ ] and longer than P=P-double bonds [ $2.04 \text{ \AA}$ ] (Figure 19), which indicates a weakened PP  $\pi$ -interaction.<sup>[34,40]</sup> The strong

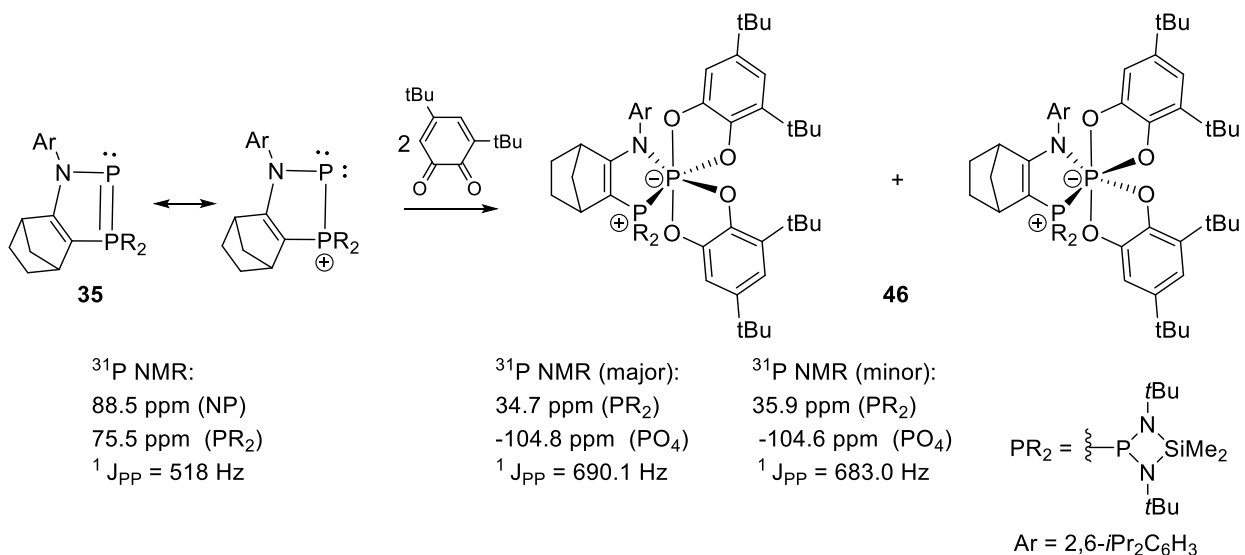
pyramidalization around the tricoordinate P atom ( $\Sigma_p^\circ = 315.42$ ) indicates the presence of a remaining lone pair localized on this P atom.

Bond lengths [Å] <b>45</b>		Angles [°] <b>45</b>	
N1-P1	1.775(1)	N1-P2-B	113.49(8)
N2-B2	1.962(2)	B-P2-P1	110.54(7)
P2-P1	2.181(1)	N1-P2-P1	91.39(4)
P1-N2	1.676(1)	P2-P1-C1	95.21(5)
P1-N3	1.682(2)	N2-P1-N3	86.55(6)
P1-C1	1.714(2)	P1-C1-C2	113.92(10)
C1-C2	1.382(2)	C1-C2-N1	123.19(12)
C2-N1	1.339(2)	C2-N1-P2	115.35(9)

**Figure 19.** Molecular structure of **45** and selected bond lengths [Å] and angles [°]. (Hydrogens and some distorted atoms are omitted for clarity).

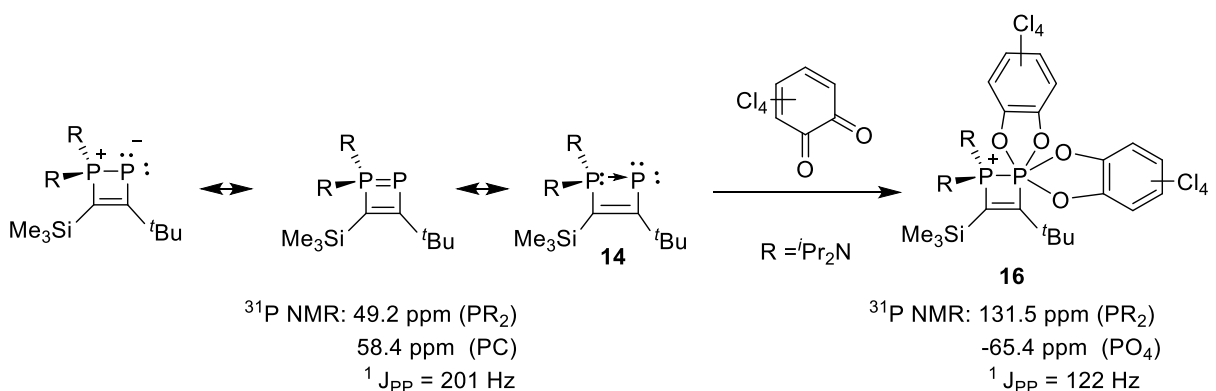
#### IV.II. Reaction with 3,5-di-tertbutyl-o-benzoquinone (TCBQ)

The reaction of **35** with two equivalents of 3,5-di-tertbutyl-o-benzoquinone (TCBQ) in toluene afforded the corresponding hexa-coordinated phosphorus product **46** which has been isolated as a white solid in a moderate yield (40 %) (Scheme 23).



**Scheme 23.** Reaction of phosphanylidene- $\sigma^4$ -phosphorane **35** with 3,5-di-tertbutyl-o-benzoquinone

In the  ${}^{31}\text{P}\{{}^1\text{H}\}$ -NMR spectrum, two AX-systems with large P-P-coupling constants ( ${}^1\text{J}_{\text{PP}} = 690.1 \text{ Hz}$  and  $683.0 \text{ Hz}$ ) were observed, which suggest the formation of a mixture of two diastereomers in a [78 : 22] ratio due to the chiral hexacoordinate phosphorus center and asymmetric bicyclic fragment (Scheme 23). The chemical shifts for the hexacoordinate P atom of two diastereomers appeared at  $\delta = -104.8 \text{ ppm}$  and  $-104.6 \text{ ppm}$ . Such high field shifted chemical shifts are typical for hexacoordinate phosphorus compounds.<sup>[23,41]</sup> Similar reactions of cyclic phosphanylidene-phosphoranes **14** with were reported by Guy Bertrand (Scheme 24).<sup>[40]</sup>



**Scheme 24.** Reaction of cyclic phosphanylidene-phosphoranes **14** with 3, 5-di-tertbutyl-o-benzoquinone

Single crystals suitable for a crystal diffraction analysis were obtained from a heptane solution at RT (Figure 18). The P-P bond distance [2.293(3) Å] is in the range of typical P-P-single bonds [2.20 – 2.35 Å] and is similar to that observed for compound **16** [2.2962(6) Å] (Table 9).<sup>[40]</sup> The geometry around P1 atom is slightly distorted octahedral (Figure 20), which is typical for hexacoordinate phosphorus. A similar geometry was observed for **16**.<sup>[40]</sup>

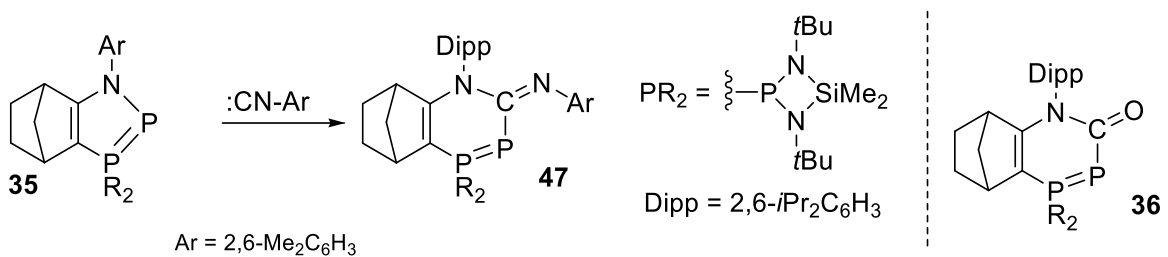
The molecular structure of **46** is shown on the left, featuring a central hexacoordinate phosphorus atom (P1) coordinated to two phenoxide oxygens (O3, O4), one carbonyl oxygen (O1), and two tert-butyl groups (C1, C2). The structure also includes a nitrogen atom (N1) and a quinone-like ring system. On the right, a table lists selected bond lengths and angles for **46**.

	Bond lengths [Å] <b>46</b>	Angles [°] <b>46</b>
C1-C2	1.338(1)	P2-P1-N1 90.0
C2-N1	1.324(9)	O1-P1-O4 88.8
N1-P2	1.700(5)	O4-P1-O2 92.3
P1-P2	2.293(3)	O1-P1-O3 176.3
P1-C1	1.670(7)	O4-P1-O3 90.2

**Figure 20.** Molecular structure of **46** and selected bond lengths [Å] and angles [°]. (H and disordered atoms are omitted for clarity).

#### IV.III. Reaction of **35** with of 2,6-Dimethylphenyl isocyanide

As suggested by DFT calculations the P2-N1 bond in **35** is labile and reactions involving the rupture of this bond can be favoured. Indeed, **35** reacts with the ambiphilic 1,3-dimethylbenzo isonitrile via an insertion reaction into the P2-N1 bond to afford a new phosphanylidene phosphorane **47** (Scheme 25).



**Scheme 25.** Reaction of **35** with of 2,6-Dimethylphenyl isocyanide.

The  $^{31}\text{P}\{\text{H}\}$ -NMR spectrum shows an AX-system with a large P-P-coupling constant ( $\delta = 66.2$  and -87.6 ppm,  $^1J_{\text{PP}} = 483$  Hz) which is similar to that observed for the related molecule **36** ( $\delta = 69.8$  and -69.3 ppm,  $^1J_{\text{PP}} = 482$  Hz). Single crystals of **47** suitable for the X-ray diffraction analysis were obtained from a concentrated heptane solution at room temperature (yield = 53.3 %). Not surprisingly, the structural geometry of six-membered heterocycle in **47** is almost identical to that of **36**. The P1-P2 bond length [2.083(9) Å] is slightly shorter than that observed for **36** [2.100(7) Å] probably due to the less electrophilic C=N-Ar than C=O function in **36** (Figure 21). The C1-N1 bond distance [1.42 Å]<sup>[42]</sup> is intermediate between classical C-N-single bonds [1.47 Å] and C=N-double bonds [1.25 Å]<sup>[43,44]</sup> which suggests some degree of  $\pi$ -delocalisation of lone-pair on the P atom toward the imine moiety (figure 21).

Bond lengths [Å] 47		Angles [°] 47	
C2-C3	1.365(5)	P2-P1-C1	102.6
C2-P2	1.730(4)	P1-P2-C2	108.4
P2-P1	2.083(9)	C3-N1-C1	125.0
P1-C1	1.822(4)	N1-C1-N4	114.3
C1-N1	1.420(4)	P1-C1-N1	126.6
N1-C3	1.973(4)	P1-C1-N4	118.9
		C1-N4-C31	122.2

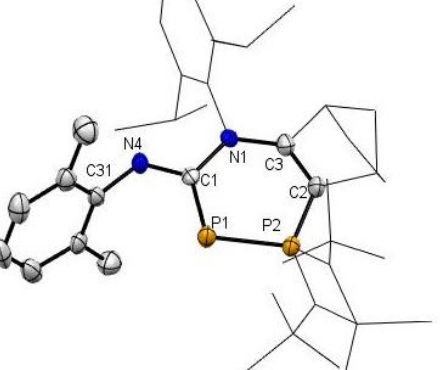
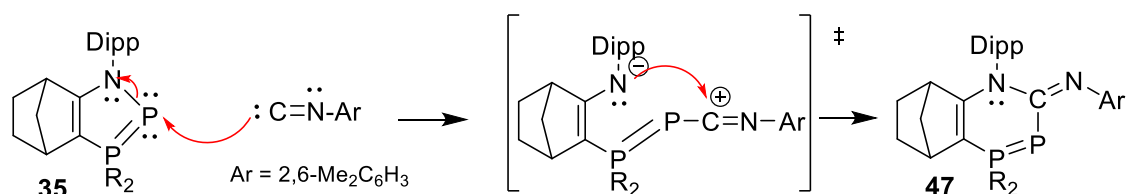


**Figure 21.** Molecular structure of **47** and selected bond lengths [Å] and angles [°] (Hydrogen atoms omitted for clarity).

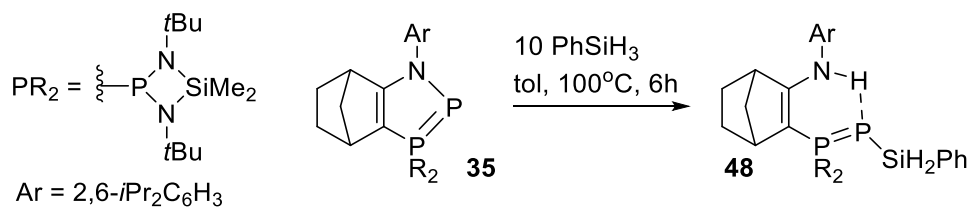
Probably, the reaction starts with a nucleophilic attack of the isocyanide to the vacant orbital on the dicoordinate P-atom (LUMO of **35**). Subsequent nucleophilic attack of the nitrogen atom to the C atom of isocyanide moiety leads to the formation of **47** (Scheme 26).



**Scheme 26.** Proposed mechanism for the reaction of **35** with 2,6-Dimethylphenyl isocyanide.

#### IV.IV. Reaction with of phenylsilane $\text{Ph}_3\text{SiH}$

The lability of the P2-N1 bond in **35** is also demonstrated by the reaction with phenylsilane which results in a formal metathesis of the Si-H/P-N  $\sigma$ -bonds to give a new P-silylated phosphanylidene phosphorene **48** (Scheme 27).



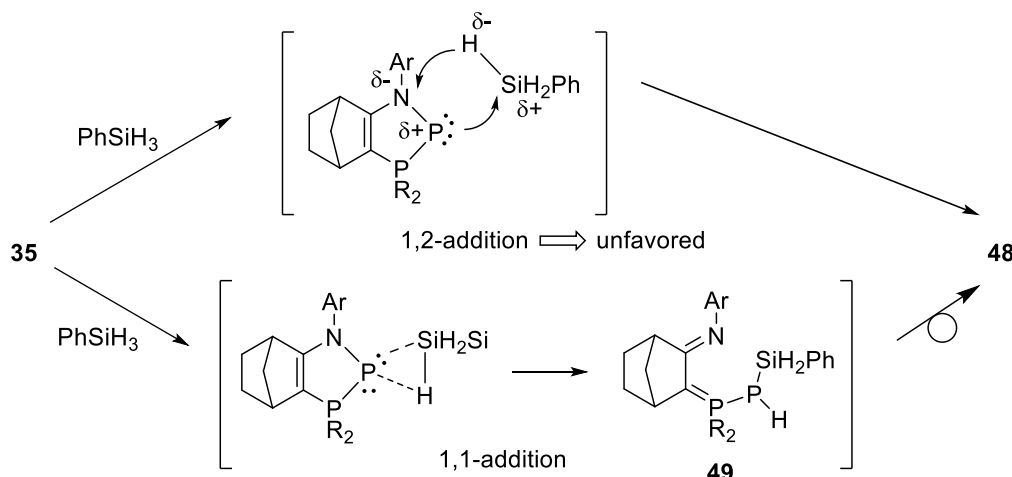
Scheme 27. The reaction of the **35** with phenylsilane.

In the  $^{31}\text{P}\{^1\text{H}\}$ -NMR spectrum, an AX system with a large PP-coupling constant similar to those observed for other phosphinidene- $\sigma^4$ -phosphoranes is observed ( $\delta = 72.7$  and  $-216.4$  ppm,  $^1J_{\text{PP}} = 526.1$  Hz). As expected for phosphanylidene phosphoranes, the signal for the tetracoordinated P atom appeared at low field ( $\delta = 72.7$  ppm), while that for the dicoordinated P atom appears in high field ( $\delta = -216.4$  ppm). In the  $^{29}\text{Si}\{^1\text{H}\}$ -NMR spectrum, the silicon atom of the P-SiH<sub>2</sub>Ph fragment appears as doublet of doublets at  $\delta = -38.9$  ppm with two PSi-coupling constants ( $^1J_{\text{PSi}} = 71.2$  Hz,  $^2J_{\text{PSi}} = 10.0$  Hz). In the  $^1\text{H}$  NMR spectrum, the two geminal protons of SiH<sub>2</sub>Ph moiety appeared as doublet of doublets at  $\delta = 5.39$  ppm ( $J_{\text{HH}} = 6.6$  Hz,  $J_{\text{HP}} = 12.2$  Hz) and at  $\delta = 5.45$  ppm ( $J_{\text{HH}} = 6.6$  Hz,  $J_{\text{HP}} = 10.7$  Hz). The  $^1\text{H}$ - $^{29}\text{Si}$  HSQC NMR indicates the correlation between two geminal protons of SiH<sub>2</sub>Ph moiety and Si atom of the SiH<sub>2</sub>Ph fragment with a large silicon-proton coupling constant ( $^1J_{\text{SiH}} = 195.9$  Hz and  $^1J_{\text{SiH}} = 196.1$  Hz) which is within a range of  $^1J$  for Si-H bonds (420 - 475 Hz).<sup>[45]</sup> The signal for the N-H proton was also observed at low-field ( $\delta = 8.75$  ppm) with a large PH-coupling constant ( $J_{\text{HP}} = 18.6$  Hz) suggesting the intermolecular interaction of N-H with the dicoordinate phosphorus atom. Single crystals, suitable for X-ray diffraction analysis, were obtained from a saturated CH<sub>3</sub>CN/Ether solution at room temperature (Figure 22). The P-P bond length [2.085(1) Å] is similar to those of related compounds **35**, **36**, **45** and **47**, indicating a strongly polarised ylidic  $\text{R}_3\text{P}^{\delta+}\text{P}^{\delta-}\text{R}$  bond in **48**. The Si-P-P angle [102.56(3) $^\circ$ ] is larger than similar angles reported for other acyclic phosphanylidene- $\sigma^4$ -phosphoranes (90.3 - 93.1 $^\circ$ ) probably due to the bulkiness of the molecule (Figure 22).<sup>[6]</sup>

	Bond lengths [Å] <b>48</b>	Angles [°] <b>48</b>	
Si1-P2	2.207(1)	Si1-P2-P1	102.56(3)
P2-P1	2.085(1)	P2-P1-C1	105.17(7)
P1-N2	1.693(2)	P1-C1-C2	131.17(16)
P1-N3	1.687(2)	C1-C2-N1	130.38(19)
P1-C1	1.766(2)		
C1-C2	1.368(3)		
C2-N1	1.351(3)		

Figure 22. Molecular structure of **48** and selected bond lengths [Å] and angles [°]. Hydrogens, except N-H and SiH<sub>2</sub> are omitted for clarity.

The reaction probably starts with 1,1-addition (oxidative addition) of  $\text{Ph}_3\text{SiH}$  to the phosphinidene-phosphorus atom in **35**, leading to the formation of intermediate **49**, which subsequently undergoes an intramolecular deprotonation of the P-H group by the adjacent imine-phosphazene function. Indeed, the direct 1,2-addition of phenylsilane to the P1-N1 moiety is unlikely due to the polarity of  $\text{Si}^{(\delta+)}\text{-H}^{(\delta-)}$  and  $\text{N}^{(\delta-)}\text{-P}^{(\delta+)}$  bonds (Scheme 28).

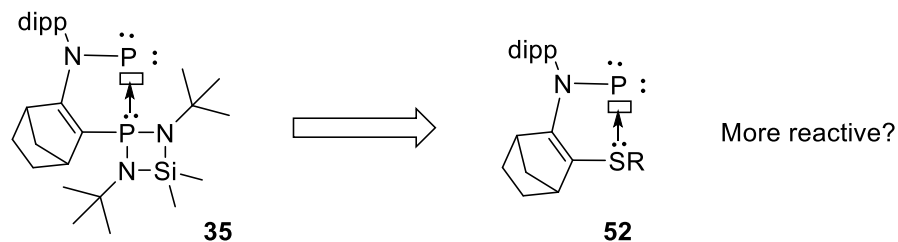


**Scheme 28.** Formation of the 1,1-addition intermediate **49** in the reaction of **35** with  $\text{Ph}_3\text{SiH}$ .

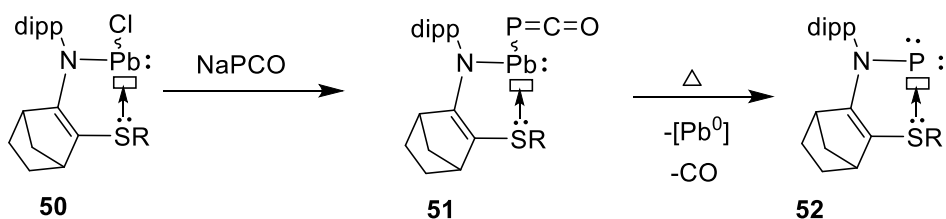
## V. First attempts for the synthesis of sulfide-stabilized phosphinidene **52**

### V.I Synthetic strategy

The phosphanylidene- $\sigma^4$ -phosphorane **35**, presented in the previous section, possess a persistent PP-bond, which reduces its behaviour as a phosphinidene. This is probably due to the strong nucleophilic character of diaminophosphine ligand as well as the significant  $\pi$ -back donation leading to a strong P=P double bond character in **35**. In order to increase the reactivity, we have considered to replace the phosphine ligand (the P-P bond dissociation energy is 490(11) kJ/mol)<sup>[46]</sup> by a less electron-donating ligand such as a sulfide (P-S bond dissociation energy is 346.0(17) kJ/mol).<sup>[46]</sup>



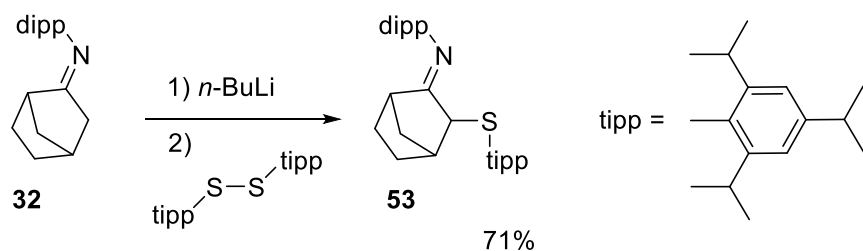
To synthesize of such a sulfide-stabilized phosphinidene **52**, we have considered to use the same synthetic strategy: the thermolysis of the corresponding phosphaketene substituted by a sulphide-stabilized plumbylene **51**. We can easily imagine that the precursor **51** can be readily prepared by the reaction of the corresponding sulfide-stabilized chloroplumbylene **50** and NaPCO. Therefore, we first considered the synthesis of stable chloroplumbylene **50** (Scheme 29).



**Scheme 29.** Synthetic strategy for the synthesis of the novel sulphide-stabilized phosphinidene **52**.

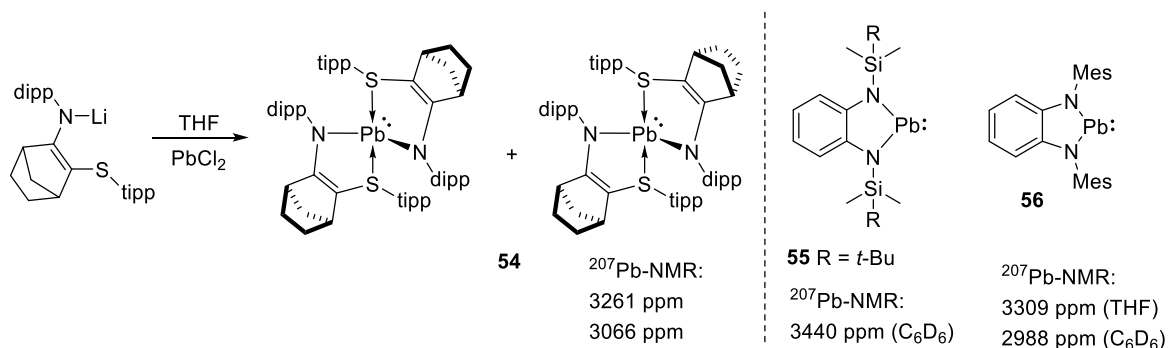
*V.II. First attempt for the synthesis of sulfide-stabilized chloroplumblylenes **50***

First, we have considered the synthesis of the sulfur-stabilised chloroplumbulene **50** with a bulky aryl group ( $R = 2,4,6$ -triisopropylphenyl group) on the S atom. The synthesis started with the preparation of the iminosulfide ligand **53** by the reaction of bis(2,4,6-triisopropylphenyl) disulphide with the lithiated imine **32**. Compound **53** was obtained in relatively good yield (Scheme 30). The iminosulfide **53** is insoluble in methanol and therefore it can be easily separated from the 2,4,6-triisopropylphenyl thiolate by-product by precipitation in MeOH. The NMR analysis indicates that the compound was obtained as a mixture of two diastereomers in 67 : 33 ratio. In the  $^1\text{H}$  NMR spectrum, the proton signal for the CH-S moiety was observed at  $\delta = 3.67$  ppm (major) and  $\delta = 3.16$  ppm (minor).



**Scheme 30.** Synthesis of iminosulfide **53**.

Then, the lithiated ligand, prepared by the reaction of **53** with  $n\text{BuLi}$ , was reacted with one equivalent of  $\text{PbCl}_2$  hoping to get the formation of the corresponding sulphide-stabilized chloroplumbylene (type **50**). However, instead of chloroplumbylene **50**, this reaction affords the diaminoplumbylene **54** with two fragments of enaminosulfide moiety as a mixture of two diastereomers (scheme 31).



**Scheme 31.** The reaction of lithiated enaminosulfide with lead dichloride.

The  $^{207}\text{Pb}$  NMR spectrum displays two singlets at  $\delta = 3261$  ppm and  $\delta = 3066$  ppm, which appear in the same range as the previous reported dicoordinate diaminoplumblyenes. The replacement of  $\text{C}_6\text{D}_6$  solvent by THF leads to a high-field shift of  $^{207}\text{Pb}$ -NMR signals ( $\delta = 2988$  ppm) (scheme 31).

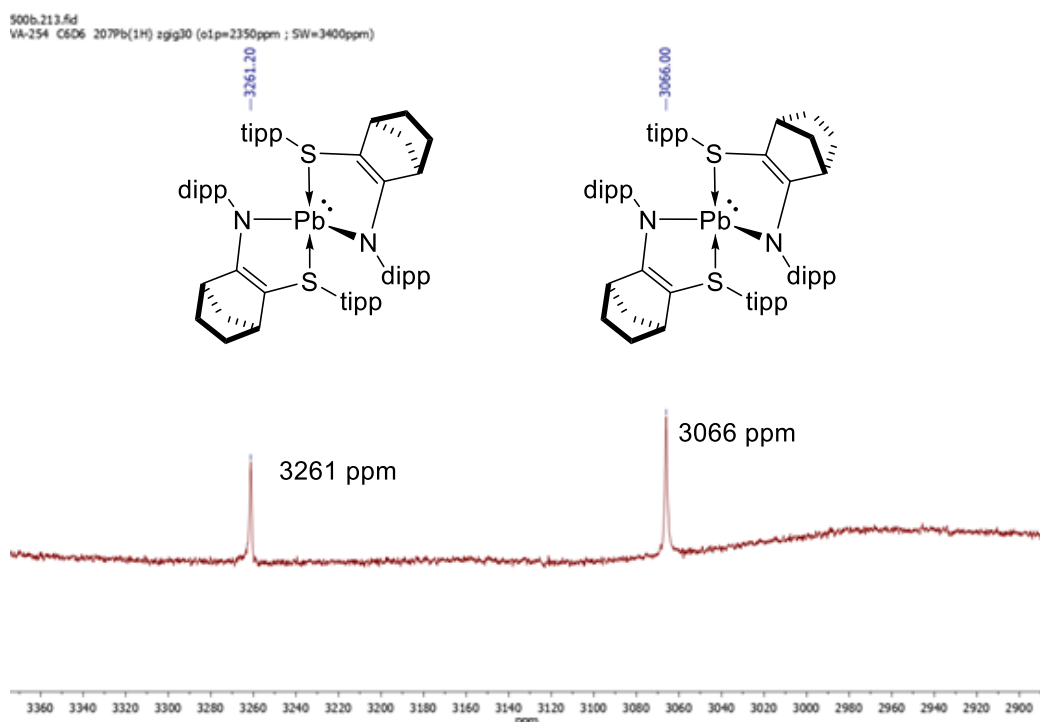


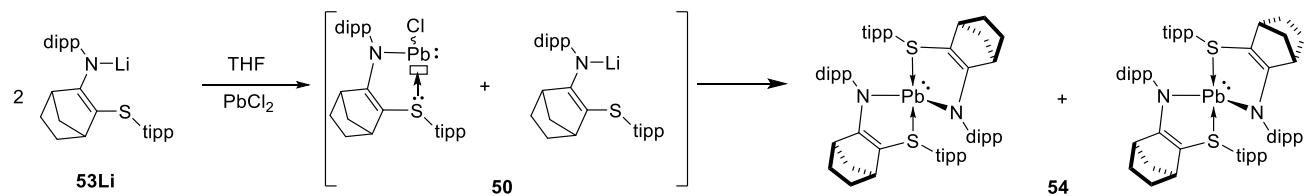
**Figure 23.**  $^{207}\text{Pb}$  NMR for compound **54** (THF-d8, 500MHz).

The structure of **54** was indeed confirmed by X-ray diffraction analysis (Figure 24). The two diastereomers of **54** co-crystallized and, therefore, we were able to confirm the structures of the major and minor diastereomers as shown in Figure 54. The Pb-N(1) and Pb-N(2) bond lengths in **54** are in the range of typical Pb-N single bond lengths reported for other diaminoplumbbylenes (2.0 - 2.9 Å).<sup>[28,29]</sup> The Pb-S(1) and Pb-S(2) bond lengths are significantly longer than distances reported for other covalent Pb-S single bond values of dicoordinate lead(II) thiolates (2.49 - 2.56 Å), indicating the dative bond character of these bonds.<sup>[47,48]</sup>

		Bond lengths [Å] <b>54</b>	Angles [°] <b>54</b>
Pb – N(1)	2.290(18)	N(1)-Pb(1)-S(2)	86.85(5)
Pb – N(2)	2.324(17)	N(1)-Pb(1)-S(2)	86.85(5)
Pb-S(1)	2.9838(6)	N(2)-Pb(1)-S(2)	73.19(4)
Pb- S(2)	2.9541(5)	N(1)-Pb(1)-S(1)	73.91(5)
		N(2)-Pb(1)-S(1)	90.23(4)
		N(1)-Pb-N(2)	103.75(7)
		S(1)-Pb-S(2)	150.99(15)

**Figure 24.** Molecular structure of **54** and selected bond lengths [Å] and angles [°] (Hydrogens and some disordered atoms have been omitted for clarity).

These results suggest that the stabilisation of the chloroplumbbylene by the aryl-sulfide (tipp-S) ligand **53** is not efficient enough, and therefore, it subsequently reacts with a second equivalent of lithiated ligand to afford the experimentally obtained diaminoplumbbylene derivatives **54** (Scheme 32).



**Scheme 32.** Proposed mechanism for the reaction of the **53Li** with **50**.

Taking into account these results, to increase the stability of plumbylenes, we can consider as alternative models: (i) a more nucleophilic amino-sulfide ligand leading to the more thermodynamically stabilized **model A**, (ii) and a more hindered aryl-sulfide ligand, leading to the kinetically stabilized **model B** (Figure 25). The synthesis of stable chloroplumbbylenes with such ligand systems (model **A** and **B**) could give an easy access to the corresponding sulfide-stabilized  $\text{Pb}(\text{II})$ -substituted phosphaketenes and therefore to the corresponding phosphinidenes.

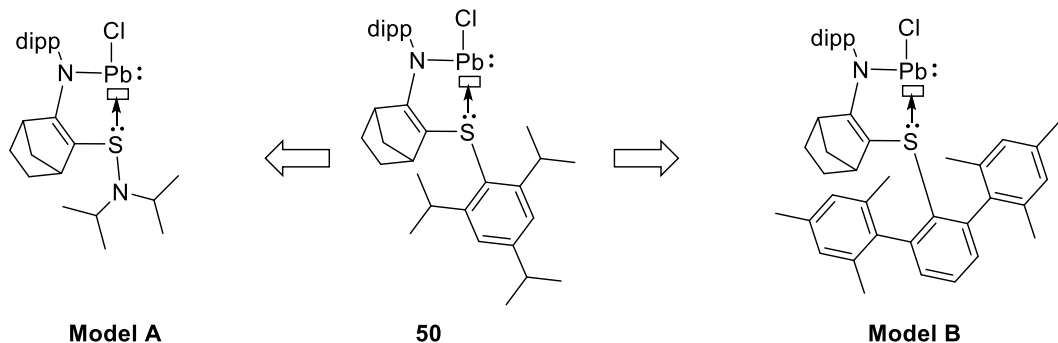


**Figure 25.** Proposed methods to improve the stabilisation ability of the iminosulfide ligand scaffold.

## VI. Conclusions and perspectives

The first stable phosphine-stabilized plumbylene substituted by a phosphaketene function **30** has been synthesized by the reaction of chloroplumbylene and NaPCO and fully characterized in solution and in the solid state. Phosphaketene **30** thermally evolves in an unusual manner by reductive elimination at the divalent lead center, affording new phosphanylidene- $\sigma^4$ -phosphoranes **35** and **36**, and lead metal. Particularly the five-membered cyclic phosphanylidene phosphorane **35** shows a unique reactivity due to the highly polarized phospha-ylide function and labile P(II)-N bond. Mechanistic studies indicate that the reaction starts with the reductive eliminaton of Pb metal to form new amino- and phosphonio-phosphaketene derivatives which evolve further to give the experimentally obtained phosphanylidene phosphoranes **35** and **36**. Particularly, the amino-phosphaketene evolves via CO-elimination to generate a phosphinidene intermediate which stabilized by the coordination of phosphine to produce the cyclic phosphanylidene phosphorane **35**. Since this process produces only inert by-products such as Pb metal precipitate and CO gas, the plumbylene-substituted phosphaketene **30** can be an ideal and useful phosphinidene precursor.

To investigate further the potential of the proposed synthetic method, we have considered the synthesis of a new sulfide-stabilised plumbylene **50**. However, the formed chloroplumbylene **50** is not enough stable and, thus, readily reacts with an additional equivalent of the ligand to give the corresponding diaminoplumbylene with two sulfide-ligand fragments, **54**. To obtain more efficiently stabilized derivatives, we should consider new models, either with a more nucleophilic aminosulfide ligand or with a more sterically hindered aryl sulfide ligand. Once we obtain a stable sulfide-stabilized chloroplumbylene, we should be able to explore more interesting derivatives such as the phosphaketene precursor and the corresponding sulfide-stabilized phosphinidene, which should exhibit an enhanced phosphinidene reactivity.

## **Bibliographic references:**

#### IV. Bibliographic references:

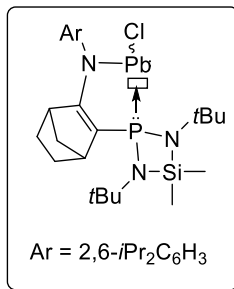
- [1] K. Lammertsma, *Top Curr Chem.*, **2003**, 229, 95–119.
- [2] Z. Benkő, R. Streubel, L. Nyulászi, *J. Chem. Soc. Dalt. Trans.* **2006**, 4321–4327.
- [3] S. Gronert, J. R. Keefe, R. A. More O’Ferrall, *J. Am. Chem. Soc.* **2011**, 133, 3381–3389.
- [4] L. Liu, D. A. Ruiz, D. Munz, G. Bertrand, *Chem* **2016**, 1, 147–153.
- [5] M. T. Nguyen, A. Van Keer, L. G. Vanquickenborne, *J. Org. Chem.* **1996**, 61, 20, 7077–7084.
- [6] J. D. Protasiewicz, *Coordination Chemistry Reviews*, **2000**, 210, 181–201
- [7] D. V. Partyka, M. P. Washington, J. B. Updegraff, R. A. Woloszynek, J. D. Protasiewicz, *Angew. Chem. - Int. Ed.* **2008**, 47, 7489–7492.
- [8] A. B. Burg, W. Mahler, *J. Am. Chem. Soc.* **1961**, 83, 2388–2389.
- [9] E. Reactions, P. Analogue, *Inorg. Chem.* **1980**, 19, 515–518.
- [10] A. B. Burg, *J. Inorg. Nucl. Chem.* **1971**, 33, 1575–1581.
- [11] G. Fritz, T. Vaahs, H. Fleischer, E. Matern, *Z. Anorg. Allg. Chem.* **1989**, 570, 54–66.
- [12] J. Olkowska-Oetzel, J. Pikies, *Appl. Organomet. Chem.* **2003**, 17, 28–35.
- [13] G. Fritz, T. Vaahs, H. Fleischer, E. Matern, *Angew. Chem.- Int. Ed. English* **1989**, 28, 315–316.
- [14] R. C. Smith, S. Shah, J. D. Protasiewicz, *J. Organomet. Chem.* **2002**, 646, 255–261.
- [15] R. C. Smith, S. Shah, E. Umezius, J. D. Protasiewicz, *J. Am. Chem. Soc.* **2003**, 125, 40–41.
- [16] P. Gupta, J. E. Siewert, T. Wellnitz, M. Fischer, W. Baumann, T. Beweries, C. Hering-Junghans, *Dalt. Trans.* **2021**, 50, 1838–1844.
- [17] E. Bergmann, *J. Am. Chem. Soc.* **1932**, 54, 3773–3782.
- [18] X. Li, D. Lei, M. Y. Chiang, P. P. Gaspar, *J. Am. Chem. Soc.* **1992**, 114, 8526–8531.
- [19] A. H. Cowley, F. Gabbaï, R. Schluter, D. Atwood, *J. Am. Chem. Soc.* **1992**, 114, 3142–3144.
- [20] M. Yoshifuji, T. Sato, N. Inamoto, *Chem. Lett.* **1988**, 17, 1735–1738.
- [21] B. Twamley, C. D. Sofield, M. M. Olmstead, P. P. Power, *J. Am. Chem. Soc.* **1999**, 121, 3357–3367.
- [22] R. Armbrust, M. Sanchez, R. Réau, U. Bergstrasser, M. Regitz, G. Bertrand, *J. Am. Chem. Soc.* **1995**, 117, 10785–10786.
- [23] M. Sanchez, M. Regitz, G. Bertrand, F. Chemie, D. U. V., D.- Kaiserslautern, *J. Am. Chem. Soc.* **1997**, 7863, 9720–9728.
- [24] F. F. Puschmann, D. Stein, D. Heift, C. Hendriksen, Z. A. Gal, H. F. Grützmacher, H. Grützmacher, *Angew. Chem. - Int. Ed.* **2011**, 50, 8420–8423.
- [25] M. M. Hansmann, R. Jazzaar, G. Bertrand, *J. Am. Chem. Soc.* **2016**, 138, 8356–8359.
- [26] S. Yao, Y. Xiong, T. Szilvási, H. Grützmacher, M. Driess, *Angew. Chem. - Int. Ed.* **2016**, 128, 4859–4863.
- [27] N. Del Rio, A. Baceiredo, N. Saffon-Merceron, D. Hashizume, D. Lutters, T. Müller, T. Kato, *Angew. Chem. - Int. Ed.* **2016**, 55, 4753–4758.
- [28] T. Lin, G. Lee, S. Peng, C. Chiu, H. Chen, *Polymer*, **2019**, 180, 121748
- [29] R. Guthardt, J. Oetzel, J. I. Schweizer, C. Bruhn, R. Langer, M. Maurer, J. Vícha, P. Shestakova, M. C. Holthausen, U. Siemeling, *Angew. Chem. - Int. Ed.* **2019**, 58, 1387–1391.
- [30] D. Heift, Z. Benko, H. Grützmacher, *Dalt. Trans.* **2014**, 43, 5920–5928.
- [31] D. Raiser, K. Eichele, H. Schubert, L. Wesemann, *Chem. - A Eur. J.* **2021**, 27, 14073–14080.
- [32] B. A. Surgenor, M. Bühl, A. M. Z. Slawin, J. D. Woollins, P. Kilian, *Angew. Chem. - Int. Ed.* **2012**, 124, 10297–10300.
- [33] D. Heift, Z. Benko, H. Grützmacher, A. R. Jupp, J. M. Goicoechea, *Chem. Sci.* **2015**, 6, 4017–4024.
- [34] P. Pyykkö, M. Atsumi, *Chem. - A Eur. J.* **2009**, 15, 12770–12779.
- [35] T. L. Cottrell, *The Strengths of Chemical Bonds*, **1958**.
- [36] J. McNulty, Y. Zhou, *Tetrahedron Lett.* **2004**, 45, 407–409.
- [37] A. B. Burg, R. I. Wagner, *J. Am. Chem. Soc.* **1953**, 75, 3872–3877.
- [38] S. Shah, G. P. A. Yap, J. D. Protasiewicz, **2000**, 608, 12–20.
- [39] P. P. Power, *Angew. Chem. - Int. Ed. English* **1990**, 29, 449–460.
- [40] A. Mayssara A. Abo Hassanin Supervised, *Pap. Knowl. . Towar. a Media Hist. Doc.* **2014**, 5,

2228–2230.

- [41] C. Y. Wong, R. McDonald, R. G. Cavell, *Inorg. Chem.* **1996**, *35*, 325–334.
- [42] H. Ishida, *Zeitschrift fur Naturforsch. - Sect. A J. Phys. Sci.* **2000**, *55*, 769–771.
- [43] R. W. Alder, J. G. E. Phillips, *Synthesis (Stuttg.)*. **1980**, *1*, 1–9.
- [44] Saul Patai, Carbon–Nitrogen Double Bonds, John Wiley & Sons Ltd., 1 january **1970**.
- [45] F. Uhlig, D. Dortmund, *Inorg. Chem.* **2000**, *2*, 208–222.
- [46] N. A. L. John Aurie Dean, in *Lange's Handb. Chem.*, **1999**.
- [47] B. D. Rekken, T. M. Brown, M. M. Olmstead, J. C. Fettinger, P. P. Power, *Inorg. Chem.* **2013**, *52*, *6*, 3054–3062.
- [48] N. Kano, N. Tokitoh, R. Okazaki, *Organometallics* **1997**, *16*, 4237–4239.

## **Experimental part**

Synthesis of chloroplumbylene **29**:



To a solution of iminophosphine (1.00 g, 2.0 mmol) in THF (20 mL), n-butyllithium was added dropwise (1.37 mL, 2.2 mmol, 1.6 M in hexanes) at -80 °C. The solution was warmed to room temperature. The reaction mixture was cooled again to – 80 °C, and lead dichloride (0.56 g, 2.0 mmol) in THF (10 mL) was added. The reaction mixture was warmed to room temperature. The solvent was removed under vacuum, and the solid residue was extracted with toluene (3 x 8 mL). Toluene was removed under vacuum. After washing the obtained solid with pentane (3 x 5 mL) the chloroplumbylene **29** was obtained as a yellow powder (1.72 g, yield = 77 %).

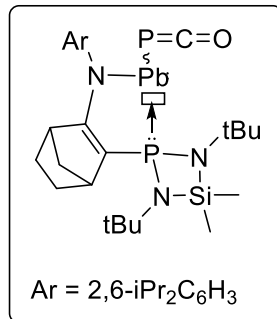
**$^1\text{H}$  NMR (300 MHz,  $\text{C}_6\text{D}_6$ , 25 °C):** 0.25 (s, 3H, SiCH<sub>3</sub>), 0.27 (s, 3H, SiCH<sub>3</sub>), 1.23 (s, 18H, CH<sub>3tBu</sub>), 1.24 (m, 6H, CH<sub>3iPr</sub>), 1.36 (m, 7H, CH<sub>3iPr</sub> + CH<sub>2</sub>), 1.44 (m, 1H, CH<sub>2</sub>), 1.70 (m, 3H, CH<sub>2</sub>), 1.87 (m, 1H, CH<sub>2</sub>), 2.51 (s, 1H, CH<sub>bridgehead</sub>), 2.98 (s, 1H, CH<sub>bridgehead</sub>), 3.50 (m, 1H, CH<sub>iPr</sub>), 3.68 (m, 1H, CH<sub>iPr</sub>), 7.15 (m, 3H, CH<sub>Ar</sub>).

**$^{13}\text{C}$  NMR (75 MHz,  $\text{C}_6\text{D}_6$ , 25 °C):** 4.4 (s, SiCH<sub>3</sub>), 7.4 (d,  $J_{CP}$  = 6.4 Hz, SiCH<sub>3</sub>), 24.5 (s, CH<sub>3iPr</sub>), 25.0 (s, CH<sub>3iPr</sub>), 26.1 (s, CH<sub>2</sub>), 26.5 (s, CH<sub>3iPr</sub>), 26.8 (s, CH<sub>3iPr</sub>), 27.8 (s, CH<sub>iPr</sub>), 27.9 (s, CH<sub>iPr</sub>), 29.5 (s, CH<sub>2</sub>), 33.0 (d,  $J_{CP}$  = 4.7 Hz, CH<sub>3tBu</sub>), 33.3 (d,  $J_{CP}$  = 4.1 Hz, CH<sub>3tBu</sub>), 42.5 (d,  $J_{CP}$  = 6.3 Hz, CH<sub>bridgehead</sub>), 43.9 (d,  $J_{CP}$  = 11.8 Hz, CH<sub>bridgehead</sub>), 48.1 (d,  $J_{CP}$  = 4.0 Hz, CH<sub>2</sub>), 51.1 (d,  $J_{CP}$  = 1.2 Hz, C<sub>tBu</sub>), 51.2 (s, C<sub>tBu</sub>), 115.0 (d,  $J_{CP}$  = 10.0 Hz, CP), 124.0 (s, CH<sub>Ar</sub>), 124.1 (s, CH<sub>Ar</sub>), 125.9 (s, CH<sub>Ar</sub>), 144.5 (d,  $J_{CP}$  = 0.8 Hz, NC<sub>Ar</sub>), 145.5 (s, C<sub>Ar</sub>iPr), 145.9 (s, C<sub>Ar</sub>iPr), 188.1 (d,  $J_{CP}$  = 35.6 Hz, CN).

**$^{31}\text{P}\{^1\text{H}\}$  NMR (122 MHz,  $\text{C}_6\text{D}_6$ , 25 °C):** 211.4 (s, PN2).

**$^{29}\text{Si}$  NMR (99 MHz,  $\text{C}_6\text{D}_6$ , 25 °C):** 10.6 (d,  $J$  = 4.1 Hz, SiCH<sub>3</sub>).

Synthesis of lead phosphaketene **30**:



Chloroplumbylene **29** (600 mg, 0.81 mmol) and 1 eq. of  $\text{Na(OCP)(dioxane)}_{2.4}$  (235 mg, 0.81 mmol) are solved in 6 ml of THF at  $-30^\circ\text{C}$ . After stirring for 1h all volatiles were removed under vacuum and the residue was extracted with cold DCM. The solid was washed with cold pentane and the product was obtained as orange powder (410 mg, yield = 66%).

**$^1\text{H NMR}$  (400 MHz,  $\text{CDCl}_3$ , -50 °C):** 0.58 (s, 3H,  $\text{SiCH}_3$ ), 0.60 (s, 3H,  $\text{SiCH}_3$ ), 0.61 (s, 6H, 2 x  $\text{SiCH}_3$ ), 1.18 (m, 1H,  $\text{CH}_2$ ), 1.28 (m, 1H,  $\text{CH}_2$ ), 1.15-1.35 (m, 24H, 8 x  $\text{CH}_{\text{iPr}}$ ), 1.37 (s, 9H,  $\text{CH}_{3\text{tBu}}$ ), 1.40 (s, 18H,  $\text{CH}_{3\text{tBu}}$ ), 1.41 (s, 9H,  $\text{CH}_{3\text{tBu}}$ ), 1.58 (m, 1H,  $\text{CH}_2$ ), 1.68 (m, 3H,  $\text{CH}_2$ ), 1.72 (m, 2H,  $\text{CH}_2$ ), 1.83 (m, 1H,  $\text{CH}_2$ ), 1.90 (m, 2H,  $\text{CH}_2$ ), 2.15 (m, 1H,  $\text{CH}_2$ ), 2.54 (s, 1H,  $\text{CH}_{\text{bridgehead}}$ ), 2.58 (s, 1H,  $\text{CH}_{\text{bridgehead}}$ ), 3.10 (s, 1H,  $\text{CH}_{\text{bridgehead}}$ ), 3.14 (s, 1H,  $\text{CH}_{\text{bridgehead}}$ ), 3.22 (sept,  $J_{HH} = 6.6$  Hz, 2H,  $\text{CH}_{\text{iPr}}$ ), 3.34 (sept,  $J_{HH} = 6.6$  Hz, 1H,  $\text{CH}_{\text{iPr}}$ ), 3.54 (sept,  $J_{HH} = 6.6$  Hz, 1H,  $\text{CH}_{\text{iPr}}$ ), 7.27 (m, 6H,  $\text{CH}_{\text{Ar}}$ ).

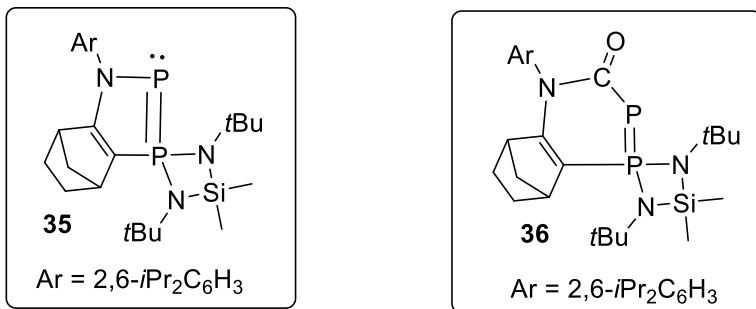
**$^{13}\text{C NMR}$  (101 MHz,  $\text{CDCl}_3$ -50 °C):** 4.3 (d,  $J_{\text{CP}} = 0.7$  Hz,  $\text{SiCH}_3$ ), 4.7 (d,  $J_{\text{CP}} = 1.0$  Hz,  $\text{SiCH}_3$ ), 7.9 (d,  $J_{\text{CP}} = 6.2$  Hz,  $\text{SiCH}_3$ ), 8.0 (d,  $J_{\text{CP}} = 5.8$  Hz,  $\text{SiCH}_3$ ), 23.9 (s,  $\text{CH}_{3\text{iPr}}$ ), 24.4 (s,  $\text{CH}_{3\text{iPr}}$ ), 25.3 (s,  $\text{CH}_{3\text{iPr}}$ ), 25.4 (s,  $\text{CH}_2$ ), 25.6 (s,  $\text{CH}_{3\text{iPr}}$ ), 25.7 (s,  $\text{CH}_{3\text{iPr}}$ ), 25.8 (s,  $\text{CH}_2$ ), 26.2 (s,  $\text{CH}_{3\text{iPr}}$ ), 26.9 (s,  $\text{CH}_{3\text{iPr}}$ ), 27.1 (d,  $J_{\text{CP}} = 7.0$  Hz,  $\text{CH}_{\text{iPr}}$ ), 27.2 (s,  $\text{CH}_{3\text{iPr}}$ ), 27.4 (d,  $J_{\text{CP}} = 7.0$  Hz,  $\text{CH}_{\text{iPr}}$ ), 27.7 (s,  $\text{CH}_{\text{iPr}}$ ), 27.5 (s,  $\text{CH}_{\text{iPr}}$ ), 28.9 (s,  $\text{CH}_2$ ), 29.2 (s,  $\text{CH}_2$ ), 32.5 (d,  $J_{\text{CP}} = 4.1$  Hz,  $\text{CH}_{3\text{tBu}}$ ), 32.8 (dd,  $J_{\text{CP}} = 5.1$  and 7.2 Hz,  $\text{CH}_{3\text{tBu}}$ ), 33.5 (d,  $J_{\text{CP}} = 4.1$  Hz,  $\text{CH}_{3\text{tBu}}$ ), 33.6 (d,  $J_{\text{CP}} = 5.5$  Hz,  $\text{CH}_{3\text{tBu}}$ ), 41.6 (d,  $J_{\text{CP}} = 5.3$  Hz,  $\text{CH}_{\text{bridgehead}}$ ), 41.8 (d,  $J_{\text{CP}} = 5.8$  Hz,  $\text{CH}_{\text{bridgehead}}$ ), 43.1 (d,  $J_{\text{CP}} = 11.6$  Hz,  $\text{CH}_{\text{bridgehead}}$ ), 43.4 (d,  $J_{\text{CP}} = 11.9$  Hz,  $\text{CH}_{\text{bridgehead}}$ ), 46.5 (d,  $J_{\text{CP}} = 4.5$  Hz,  $\text{CH}_2$ ), 48.6 (d,  $J_{\text{CP}} = 4.7$  Hz,  $\text{CH}_2$ ), 50.9 (d,  $J_{\text{CP}} = 4.4$  Hz,  $\text{C}_{\text{tBu}}$ ), 51.0 (d,  $J_{\text{CP}} = 2.1$  Hz,  $\text{C}_{\text{tBu}}$ ), 51.3 (d,  $J_{\text{CP}} = 4.3$  Hz,  $\text{C}_{\text{tBu}}$ ), 51.4 (d,  $J_{\text{CP}} = 3.5$  Hz,  $\text{C}_{\text{tBu}}$ ), 113.1 (d,  $J_{\text{CP}} = 12.9$  Hz, PC), 114.2 (d,  $J_{\text{CP}} = 17.4$  Hz, PC), 123.0 (s,  $\text{CH}_{\text{Ar}}$ ), 123.2 (s,  $\text{CH}_{\text{Ar}}$ ), 123.8 (s,  $\text{CH}_{\text{Ar}}$ ), 123.9 (s,  $\text{CH}_{\text{Ar}}$ ), 124.9 (s,  $\text{CH}_{\text{Ar}}$ ), 125.0 (s,  $\text{CH}_{\text{Ar}}$ ), 143.6 (d,  $J_{\text{CP}} = 1.0$  Hz,  $\text{C}_{\text{Ar}}$ ), 143.9 (s,  $\text{C}_{\text{Ar}}$ ), 144.1 (s,  $\text{C}_{\text{Ar}}$ ), 144.3 (s,  $\text{C}_{\text{Ar}}$ ), 145.8 (s,  $\text{C}_{\text{Ar}}$ ), 146.4 (s,  $\text{C}_{\text{Ar}}$ ), 181.7 (dd,  $^1J_{\text{CP}} = 95.0$  Hz,  $^2J_{\text{CP}} = 11.8$  Hz, PCO), 182.6 (dd,  $^1J_{\text{CP}} = 95.5$  Hz,  $^2J_{\text{CP}} = 12.4$  Hz, PCO), 187.5 (d,  $J_{\text{CP}} = 35.3$  Hz, NC), 188.0 (d,  $J_{\text{CP}} = 33.8$  Hz, NC).

**$^{31}\text{P}\{^1\text{H}\}$  NMR (161 MHz,  $\text{CDCl}_3$ , -50 °C):** 182.2 (d,  $J_{\text{PPb}} = 3716.1$  Hz,  $J_{\text{pp}} = 11.6$  Hz, PN2), -329.4 (d,  $J_{\text{PPb}} = 954.9$  Hz,  $J_{\text{pp}} = 11.6$  Hz, PCO), 189.9 (d,  $J_{\text{PPb}} = 3816.2$  Hz,  $J_{\text{pp}} = 5.5$  Hz, PN2), -333.2 (d,  $J_{\text{PPb}} = 989.6$  Hz, ,  $J_{\text{pp}} = 5.5$ , PCO).

**$^{29}\text{Si NMR}$  (80 MHz,  $\text{C}_6\text{D}_6$ , 25 °C):** 11.3 (d,  $J_{\text{SiP}} = 2.7$  Hz,  $\text{SiCH}_3$ ), 11.4 (d,  $J_{\text{SiP}} = 0.9$  Hz,  $\text{SiCH}_3$ ).

**$^{207}\text{Pb NMR}$  (104 MHz,  $\text{THF-d}_8$ , 0 °C):** 2227.2 (dd,  $^1J_{\text{PPb}} = 954.9$  and 3716.1 Hz), 2455.2 (dd,  $^1J_{\text{PPb}} = 989.6$  and 3816.2 Hz).

## Synthesis of (amino)phosphanylidene- $\sigma^4$ -phosphoranes **35** and **36**



The products **35** and **36** were synthesized by the following two methods (**A** or **B**) using either in-situ generated **30** from the chloroprumbylene **29** (method **A**) or isolated PCO-substituted plumbylene **30**. The former method (method **A** starting from the thermally stable **29**) is more convenient and generally give the products in better yield.

**Method A:** The solution of chloroplumbylene **29** (500 mg, 0.67 mmol) and 1 eq. of Na(OCP)(dioxane)2.6 (211 mg, 0.67 mmol) in toluene (6 ml) was heated for 4 h at 100 °C. The resulting solution was centrifuged and then separated from the solids by syringe. After filtration, all volatiles were evaporated in vacuo. The addition of pentane (10 ml) to the residue results the precipitation of **36**. Filtration and drying the solid under vacuum yielded **36** as a yellow powder (144 mg, yield = 39%). The resulting solution was then dried under vacuum and the residue was resolved in heptanes. Product **35** was obtained as colorless crystals from a concentrated solution of n-heptane at -30 °C (109 mg, yield = 31%).

**Method B:** The freshly prepared solution of **30** (103.2 mg, 0.13 mmol) in toluene (0.5 ml) was heated at 100 °C for 4 h. The resulting products **35** and **36** were isolated by the same preparation procedure as described for method **A** (4: 35.7 mg, yield = 26%, 5: 37.6 mg, 26%).

### NMR of **35**:

**<sup>1</sup>H NMR (500 MHz, THF-d<sub>8</sub>, 25 °C):** 0.46 (s, 3H, SiCH<sub>3</sub>), 0.50 (s, 3H, SiCH<sub>3</sub>), 1.12 (d, 3H, J<sub>HH</sub> = 7.0 Hz, CH<sub>3*i*Pr</sub>), 1.14 (d, 3H, J<sub>HH</sub> = 7.0 Hz CH<sub>3*i*Pr</sub>), 1.20 (d, 3H, J<sub>HH</sub> = 6.8 Hz, CH<sub>3*t*Bu</sub>), 1.26 (d, 3H, J<sub>HH</sub> = 6.8 Hz, CH<sub>3*t*Bu</sub>), 1.29 (m, 2H, CH<sub>2</sub>), 1.32 (d, 9H, J<sub>HH</sub> = 0.8 Hz, CH<sub>3*t*Bu</sub>), 1.37 (d, 9H, J<sub>HH</sub> = 0.8 Hz CH<sub>3*t*Bu</sub>), 1.46 (m, 1H, CH<sub>2</sub>), 1.69 (m, 1H, CH<sub>2</sub>), 1.84 (m, 2H, CH<sub>2</sub>), 2.52 (m, 1H, CH<sub>bridgehead</sub>), 2.90 (sept, J<sub>HH</sub> = 6.8 Hz, 1H, CH<sub>*i*Pr</sub>), 3.22 (sept, J<sub>HH</sub> = 6.8 Hz, 1H, CH<sub>*i*Pr</sub>), 3.25 (s, 1H, CH<sub>bridgehead</sub>), 7.10 (m, 2H, CH<sub>Ar</sub>), 7.21 (m, 1H, CH<sub>Ar</sub>).

**<sup>13</sup>C NMR (125 MHz, THF-d<sub>8</sub>, 25 °C):** 3.7 (d, J<sub>CP</sub> = 1.6 Hz, SiCH<sub>3</sub>), 4.9 (s, SiCH<sub>3</sub>), 24.1 (s, CH<sub>3*i*Pr</sub>), 24.2 (s, CH<sub>3*i*Pr</sub>), 26.1 (d, J<sub>CP</sub> = 1.4 Hz, CH<sub>3*i*Pr</sub>), 26.4 (d, J<sub>CP</sub> = 3.4 Hz, CH<sub>3*i*Pr</sub>), 27.2 (s, CH<sub>2</sub>), 28.4 (s, CH<sub>*i*Pr</sub>), 28.7 (s, CH<sub>*i*Pr</sub>), 29.8 (s, CH<sub>2</sub>), 33.1 (m, CH<sub>3*t*Bu</sub>), 42.3 (s, CH<sub>bridgehead</sub>), 43.2 (dd, <sup>1</sup>J<sub>CP</sub> = 3.6 Hz, <sup>2</sup>J<sub>CP</sub> = 14.2 Hz, CH<sub>bridgehead</sub>), 52.4 (d, J<sub>CP</sub> = 5.7 Hz, CH<sub>2</sub>), 53.0 (s, C<sub>*t*Bu</sub>), 100.4 (dd, <sup>1</sup>J<sub>CP</sub> = 80.2 Hz, <sup>2</sup>J<sub>CP</sub> = 8.7 Hz, PC), 124.2 (s, CH<sub>Ar</sub>), 128.6 (s, CH<sub>Ar</sub>), 137.8 (dd, <sup>1</sup>J<sub>CP</sub> = 6.8 Hz, <sup>2</sup>J<sub>CP</sub> = 10.6 Hz, NC<sub>Ar</sub>), 148.4 (d, J<sub>CP</sub> = 1.0 Hz, C<sub>Ar*i*Pr</sub>), 148.8 (d, J<sub>CP</sub> = 1.0 Hz, C<sub>Ar*i*Pr</sub>), 167.6 (d, J<sub>CP</sub> = 32.5 Hz, NC).

**<sup>31</sup>P{<sup>1</sup>H} NMR (162 MHz, THF-d<sub>8</sub>, 25 °C):** 75.5 (d, J<sub>PP</sub> = 518.0 Hz, PN2), 88.5 (d, J<sub>PP</sub> = 518.0 Hz, PN).

**<sup>29</sup>Si NMR (99 MHz, THF-d<sub>8</sub>, 25 °C):** -3.0 (s, SiCH<sub>3</sub>).

**HRMS (ESI/Q-TOF) m/z C29H49N3P2Si [M+H]<sup>+</sup>:** calculated 530.3252, found 530.3252.

**NMR of 36:**

**<sup>1</sup>H NMR (400 MHz, THF-d<sub>8</sub>, 25 °C):** 0.57 (s, 3H, SiCH<sub>3</sub>), 0.60 (s, 3H, SiCH<sub>3</sub>), 1.08 (d, 3H, J<sub>HH</sub> = 6.8 Hz, CH<sub>3*iPr*</sub>), 1.09 (d, 3H, J<sub>HH</sub> = 6.8 Hz, CH<sub>3*iPr*</sub>), 1.16 (d, 3H, J<sub>HH</sub> = 6.9 Hz, CH<sub>3*iPr*</sub>), 1.19 (d, 3H, J<sub>HH</sub> = 6.9 Hz, CH<sub>3*iPr*</sub>), 1.25 (m, 1H, CH<sub>2</sub>), 1.31 (m, 1H, CH<sub>2</sub>), 1.36 (s, 9H, CH<sub>3*tBu*</sub>), 1.41 (d, 9H, J<sub>HH</sub> = 0.7 Hz, CH<sub>3*tBu*</sub>), 1.60 (m, 1H, CH<sub>2</sub>), 1.67 (m, 2H, CH<sub>2</sub>), 1.85 (m, 1H, CH<sub>2</sub>), 2.46 (m, 1H, CH<sub>bridgehead</sub>), 2.73 (sept, J<sub>HH</sub> = 6.9 Hz, 1H, CH<sub>*iPr*</sub>), 2.89 (sept, J<sub>HH</sub> = 6.8 Hz, 1H, CH<sub>*iPr*</sub>), 3.37 (m, 1H, CH<sub>bridgehead</sub>), 7.17 (m, 2H, CH<sub>Ar</sub>), 7.22 (m, 1H, CH<sub>Ar</sub>).

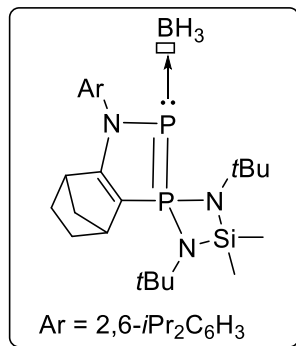
**<sup>13</sup>C NMR (125 MHz, THF-d<sub>8</sub>, 25 °C):** 4.5 (s, SiCH<sub>3</sub>), 5.1 (d, J<sub>CP</sub> = 2.2 Hz, SiCH<sub>3</sub>), 23.4 (s, CH<sub>3*iPr*</sub>), 23.5 (s, CH<sub>3*iPr*</sub>), 25.2 (s, CH<sub>3*iPr*</sub>), 25.7 (s, CH<sub>3*iPr*</sub>), 26.4 (d, J<sub>CP</sub> = 1.3 Hz, CH<sub>2</sub>), 28.1 (s, CH<sub>2</sub>), 29.5 (s, CH<sub>*iPr*</sub>), 29.6 (s, CH<sub>*iPr*</sub>), 32.7 (dd, <sup>1</sup>J<sub>CP</sub> = 3.2 Hz, <sup>2</sup>J<sub>CP</sub> = 5.4 Hz, CH<sub>3*tBu*</sub>), 33.0 (dd, <sup>1</sup>J<sub>CP</sub> = 3.1 Hz, <sup>2</sup>J<sub>CP</sub> = 5.1 Hz, CH<sub>3*tBu*</sub>), 43.7 (d, J<sub>CP</sub> = 1.8 Hz, CH<sub>bridgehead</sub>), 47.7 (d, J<sub>CP</sub> = 12.7 Hz, CH<sub>bridgehead</sub>), 48.2 (d, J<sub>CP</sub> = 5.3 Hz, CH<sub>2</sub>), 53.7 (s, C<sub>*tBu*</sub>), 102.9 (dd, <sup>1</sup>J<sub>CP</sub> = 5.4 Hz, <sup>2</sup>J<sub>CP</sub> = 78.6 Hz, CP), 124.2 (s, CH<sub>Ar</sub>), 124.3 (s, CH<sub>Ar</sub>), 129.2 (s, CH<sub>Ar</sub>), 138.8 (d, J<sub>CP</sub> = 2.2 Hz, NC<sub>Ar</sub>), 147.1 (s, C<sub>Ar*iPr*</sub>), 147.2 (s, C<sub>Ar*-iPr*</sub>), 162.5 (d, J<sub>CP</sub> = 19.3 Hz, CN), 187.9 (dd, <sup>1</sup>J<sub>CP</sub> = 4.8 Hz, <sup>2</sup>J<sub>CP</sub> = 76.9 Hz, C=O).

**<sup>31</sup>P{<sup>1</sup>H} NMR (162 MHz, THF-d<sub>8</sub>, 25 °C):** 69.8 (d, J<sub>PP</sub> = 482.0 Hz, PN2), -69.3 (d, J<sub>PP</sub> = 482 Hz, PC=O).

**<sup>29</sup>Si NMR (99 MHz, THF-d<sub>8</sub>, 25 °C):** 7.43 (SiCH<sub>3</sub>).

**HRMS (ESI/Q-TOF) m/z C30H49N3OP2Si [M+H]<sup>+</sup>:** calculated 558.3198, found 558.3201.

Synthesis of the borane adduct **45**:



To a solution of **35** (40.0 mg, 0.08 mmol) in toluene (0.5 mL),  $\text{BH}_3 \cdot \text{THF}$  (1.0 M, 0.075 mL, 0.08 mmol) was added at room temperature. All the volatiles were removed under vacuum and the residue was washed with heptane to give the complex **45** as white powder (15 mg, 37%). The crystals suitable for X-ray diffraction analysis were obtained from a concentrated ether solution at room temperature. Mp: 125 °C.

**$^1\text{H}$  NMR (400 MHz,  $\text{C}_6\text{D}_6$ , 25 °C):** 0.24 (s, 3H, SiCH<sub>3</sub>), 0.34 (s, 3H, SiCH<sub>3</sub>), 1.12 (d, 1H,  $J_{\text{HH}} = 8.4$  Hz, CH<sub>2</sub>), 1.19 (d, 3H,  $J_{\text{HH}} = 7.0$  Hz, CH<sub>3*i*Pr</sub>), 1.23 (d, 3H,  $J_{\text{HH}} = 7.0$  Hz, CH<sub>3*i*Pr</sub>), 1.51 (d, 3H,  $J_{\text{HH}} = 6.8$  Hz, CH<sub>3*t*Bu</sub>), 1.54 (d, 3H,  $J_{\text{HH}} = 6.8$  Hz, CH<sub>3*t*Bu</sub>), 1.30 (s, 9H, CH<sub>3*t*Bu</sub>), 1.33 (s, 9H, CH<sub>3*t*Bu</sub>), 1.41 (m, 1H, CH<sub>2</sub>), 1.60 (m, 2H, CH<sub>2</sub>), 1.73 (d, 1H,  $J_{\text{HH}} = 8.3$  Hz, CH<sub>2</sub>), 1.93 (dd, 3H,  $J_{\text{HP}} = 25.2$  and 10.0 Hz, BH<sub>3</sub>), 2.45 (d,  $J_{\text{HH}} = 2.9$  Hz, 1H, CH<sub>bridgehead</sub>), 3.06 (s, 1H, CH<sub>bridgehead</sub>), 3.28 (sept,  $J_{\text{HH}} = 7.1$  Hz, 1H, CH<sub>*i*Pr</sub>), 3.41 (sept,  $J_{\text{HH}} = 6.8$  Hz, 1H, CH<sub>*i*Pr</sub>), 7.15 (m, 3H, CH<sub>Ar</sub>).

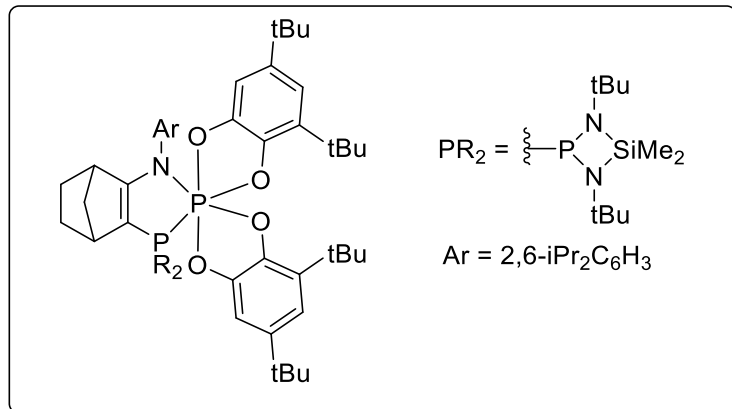
**$^{13}\text{C}\{^1\text{H}\}$  NMR (100 MHz,  $\text{C}_6\text{D}_6$ , 25 °C):** 3.8 (d,  $J_{\text{CP}} = 0.8$  Hz, SiCH<sub>3</sub>), 4.8 (dd,  $J_{\text{CP}} = 0.9$  and 1.8 Hz, SiCH<sub>3</sub>), 24.5 (s, CH<sub>3*i*Pr</sub>), 24.6 (s, CH<sub>3*i*Pr</sub>), 25.3 (s, CH<sub>3*i*Pr</sub>), 26.0 (d,  $J_{\text{CP}} = 3.3$  Hz, CH<sub>3*i*Pr</sub>), 28.8 (d,  $J_{\text{CP}} = 1.4$  Hz, CH<sub>2</sub>), 28.4 (d,  $J_{\text{CP}} = 2.9$  Hz, CH<sub>*i*Pr</sub>), 28.2 (s, CH<sub>*i*Pr</sub>), 25.7 (dd,  $J_{\text{CP}} = 1.4$  and 1.6 Hz, CH<sub>2</sub>), 32.6 (dd,  $J_{\text{CP}} = 5.2$  and 5.4 Hz, CH<sub>3*t*Bu</sub>), 32.8 (dd,  $J_{\text{CP}} = 2.1$  and 5.1 Hz, CH<sub>3*t*Bu</sub>), 43.2 (dd,  $J_{\text{CP}} = 2.5$  and 13.0 Hz, CH<sub>bridgehead</sub>), 49.9 (d,  $J_{\text{CP}} = 5.9$  Hz, CH<sub>2</sub>), 40.9 (d,  $J_{\text{CP}} = 1.2$  Hz, CH<sub>bridgehead</sub>), 52.3 (s, C<sub>*t*Bu</sub>), 52.6 (s, C<sub>*t*Bu</sub>), 97.32 (d,  $J_{\text{CP}} = 78.9$  Hz, PC), 128.9 (s, CH<sub>Ar</sub>), 124.2 (s, CH<sub>Ar</sub>), 124.3 (s, CH<sub>Ar</sub>), 135.4 (t,  $J_{\text{CP}} = 4.9$  Hz, NC<sub>Ar</sub>), 148.0 (s, C<sub>dipp-*i*Pr</sub>), 148.4 (s, C<sub>dipp-*i*Pr</sub>), 177.2 (d,  $J_{\text{CP}} = 29.2$  Hz, NC).

**$^{31}\text{P}\{^1\text{H}\}$  NMR (162 MHz,  $\text{C}_6\text{D}_6$ , 25 °C):** 10.1.0 (d,  $J_{\text{PP}} = 408.8$  Hz, PN2), 77.0 (d,  $J_{\text{PP}} = 408.3$  Hz, PBH<sub>3</sub>).

**$^{29}\text{Si}\{^1\text{H}\}$  NMR (79 MHz,  $\text{C}_6\text{D}_6$ , 25 °C):** 6.1 (s, SiCH<sub>3</sub>).

**$^{11}\text{B}\{^1\text{H}\}$  NMR (128.5 MHz,  $\text{C}_6\text{D}_6$ , 25 °C):** -32.4 (s, BH<sub>3</sub>).

Synthesis of the product **46**:



To a solution of **35** (40 mg, 0.08 mmol) in toluene (0.5 mL), 3, 5-di-tertbutyl-o-benzoquinone (33 mg, 0.16 mmol) was added. After 3 hours at room temperature, all the volatiles were removed under vacuum and the residue was extracted with pentane. Suitable crystals for X-ray of compound **46** were obtained by crystallization from heptane solution at RT (29 mg, 40%).

**$^1\text{H}$  NMR (500 MHz,  $\text{C}_6\text{D}_6$ , 25 °C):**

**Major isomer (78%):** 0.29 (s, 3H,  $\text{SiCH}_3$ ), 0.32 (s, 3H,  $\text{SiCH}_3$ ), 0.53 (d, 3H,  $^3J_{\text{HH}} = 6.5$  Hz,  $\text{CH}_{3\text{iPr}}$ ), 0.83 (s, 9H,  $\text{CH}_{3\text{tBu-Ar}}$ ), 1.09 (m, 1H,  $\text{CH}_2$ ), 1.13 (d, 3H,  $^3J_{\text{HH}} = 6.6$  Hz,  $\text{CH}_{3\text{iPr}}$ ), 1.16 (s, 9H,  $\text{CH}_{3\text{tBu-N}}$ ), 1.23 (s, 9H,  $\text{CH}_{3\text{tBu-Ar}}$ ), 1.31 (m, 2H,  $\text{CH}_2$ ), 1.39 (s, 9H,  $\text{CH}_{3\text{tBu-Ar}}$ ), 1.40 (d, 3H,  $^3J_{\text{HH}} = 6.9$  Hz,  $\text{CH}_{3\text{iPr}}$ ), 1.41 (s, 9H,  $\text{CH}_{3\text{tBu-Ar}}$ ), 1.51 (m, 2H,  $\text{CH}_2$ ), 1.62 (s, 9H,  $\text{CH}_{3\text{tBu-N}}$ ), 1.67 (m, 1H,  $\text{CH}_2$ ), 1.76 (m, 1H,  $\text{CH}_2$ ), 1.79 (d, 7H,  $^3J_{\text{HH}} = 6.6$  Hz,  $\text{CH}_{3\text{iPr}}$ ), 2.51 (s, 1H,  $\text{CH}_{\text{bridgehead}}$ ), 3.06 (s, 1H,  $\text{CH}_{\text{bridgehead}}$ ), 3.63 (sept,  $^3J_{\text{HH}} = 6.8$  Hz, 1H,  $\text{CH}_{\text{iPr}}$ ), 4.50 (sept,  $^3J_{\text{HH}} = 6.7$  Hz, 1H,  $\text{CH}_{\text{iPr}}$ ), 6.76 (m, 1H,  $\text{CH}_{\text{Ar}}$ ), 6.87 (m, 1H,  $\text{CH}_{\text{Ar}}$ ), 6.97 (m, 1H,  $\text{CH}_{\text{Ar}}$ ), 6.99 (m, 1H,  $\text{CH}_{\text{Ar}}$ ), 7.05 (m, 1H,  $\text{CH}_{\text{Ar}}$ ), 7.11 (m, 1H,  $\text{CH}_{\text{Ar}}$ ), 7.25 (m, 1H,  $\text{CH}_{\text{Ar}}$ ).

**Minor isomer (22%):** 0.31 (s, 3H,  $\text{SiCH}_3$ ), 0.35 (s, 3H,  $\text{SiCH}_3$ ), 0.50 (d, 3H,  $J_{\text{HH}} = 6.5$  Hz,  $\text{CH}_{3\text{iPr}}$ ), 0.82 (s, 9H,  $\text{CH}_{3\text{tBu-Ar}}$ ), 1.08 (d, 3H,  $J_{\text{HH}} = 6.6$  Hz,  $\text{CH}_{3\text{iPr}}$ ), 1.10 (s, 9H,  $\text{CH}_{3\text{tBu-N}}$ ), 1.21 (s, 9H,  $\text{CH}_{3\text{tBu-Ar}}$ ), 6 signals of  $\text{CH}_2$  not detected, 1.40 (s, 9H,  $\text{CH}_{3\text{tBu-Ar}}$ ), 1.42 (s, 9H,  $\text{CH}_{3\text{tBu-Ar}}$ ), 1.61 (s, 9H,  $\text{CH}_{3\text{tBu-N}}$ ), 1.79 (d, 3H,  $J_{\text{HH}} = 6.6$  Hz,  $\text{CH}_{3\text{iPr}}$ ), 2.48 (s, 1H,  $\text{CH}_{\text{bridgehead}}$ ), 3.09 (s, 1H,  $\text{CH}_{\text{bridgehead}}$ ), 3.63 (sept,  $J_{\text{HH}} = 6.8$  Hz, 1H,  $\text{CH}_{\text{iPr}}$ ), 4.34 (sept,  $J_{\text{HH}} = 6.7$  Hz, 1H,  $\text{CH}_{\text{iPr}}$ ), 6.79 (m, 1H,  $\text{CH}_{\text{Ar}}$ ), 6.85 (m, 1H,  $\text{CH}_{\text{Ar}}$ ), 7.01 (m, 2H,  $\text{CH}_{\text{Ar}}$ ), 7.08 (m, 1H,  $\text{CH}_{\text{Ar}}$ ), 7.11 (m, 1H,  $\text{CH}_{\text{Ar}}$ ), 7.25 (m, 1H,  $\text{CH}_{\text{Ar}}$ ).

**$^{13}\text{C}$  NMR (125 M Hz,  $\text{C}_6\text{D}_6$ , 25 °C):**

**Major isomer (78%):** 3.9 (d,  $J_{\text{CP}} = 1.8$  Hz,  $\text{SiCH}_3$ ), 8.1 (dd,  $^3J_{\text{CP}} = 10.0$  Hz,  $^4J_{\text{CP}} = 1.6$  Hz,  $\text{SiCH}_3$ ), 25.2 (s,  $\text{CH}_2$ ), 25.3 (s,  $\text{CH}_{3\text{iPr}}$ ), 25.8 (s,  $\text{CH}_{3\text{iPr}}$ ), 26.5 (s,  $\text{CH}_{3\text{iPr}}$ ), 26.7 (s,  $\text{CH}_{3\text{iPr}}$ ), 27.4 (s,  $\text{CH}_{\text{iPr}}$ ), 28.0 (s,  $\text{CH}_{\text{iPr}}$ ), 28.9 (s,  $\text{CH}_2$ ), 29.1 (s,  $\text{CH}_{3\text{tBu-Ar}}$ ), 30.7 (s,  $\text{CH}_{3\text{tBu-Ar}}$ ), 32.0 (s,  $\text{CH}_{3\text{tBu-Ar}}$ ), 32.1 (s,  $\text{CH}_{3\text{tBu-Ar}}$ ), 32.4 (dd,  $^3J_{\text{CP}} = 4.2$  Hz,  $^4J_{\text{CP}} = 1.5$  Hz,  $\text{CH}_{3\text{tBu-N}}$ ), 32.5 (dd,  $^3J_{\text{CP}} = 4.6$  Hz,  $^4J_{\text{CP}} = 1.6$  Hz,  $\text{CH}_{3\text{tBu-N}}$ ), 34.0 (s,  $\text{C}_{\text{tBu-Ar}}$ ), 34.5 (s,  $\text{C}_{\text{tBu-Ar}}$ ), 34.7 (s,  $\text{C}_{\text{tBu-Ar}}$ ), 34.8 (s,  $\text{C}_{\text{tBu-Ar}}$ ), 40.6 (dd,  $^3J_{\text{CP}} = 10.4$  Hz,  $^4J_{\text{CP}} = 3.2$  Hz,  $\text{CH}_{\text{bridgehead}}$ ), 46.2 (dd,  $^3J_{\text{CP}} = 7.7$  Hz,  $^4J_{\text{CP}} = 2.7$  Hz,  $\text{CH}_{\text{bridgehead}}$ ), 46.6 (d,  $J_{\text{CP}} = 7.8$  Hz,  $\text{CH}_2$ ), 53.4 (pseudo-t,  $J_{\text{PC}} = 1.5$  Hz,  $\text{C}_{\text{tBu-N}}$ ), 53.8 (d,  $J_{\text{CP}} = 1.3$  Hz,  $\text{C}_{\text{tBu}}$ ), 87.7 (dd,  $^1J_{\text{CP}} = 69.3$  Hz,  $^2J_{\text{CP}} = 67.7$  Hz, PC), 106.8 (dd,  $^5J_{\text{CP}} = 11.7$  Hz,  $^4J_{\text{CP}} = 1.3$  Hz,  $\text{CH}_{\text{Ar}}$ ), 107.3 (dd,  $^5J_{\text{CP}} = 11.0$  Hz,  $^4J_{\text{CP}} = 3.9$  Hz,  $\text{CH}_{\text{Ar}}$ ), 113.5 (s,  $\text{CH}_{\text{Ar}}$ ), 114.5 (s,  $\text{CH}_{\text{Ar}}$ ), 124.6 (s,  $\text{CH}_{\text{dipp}}$ ), 124.9 (s,  $\text{CH}_{\text{dipp}}$ ), 127.3 (s,  $\text{CH}_{\text{dipp}}$ ), 131.6 (dd,  $^4J_{\text{CP}} = 7.8$  Hz,  $^3J_{\text{CP}} = 2.7$  Hz,  $\text{tBu-C}_{\text{Ar}}$ ), 132.3 (d,  $^3J_{\text{CP}} = 12.9$  Hz,  $\text{tBu-C}_{\text{Ar}}$ ), 140.9 (s,  $\text{tBu-C}_{\text{Ar}}$ ), 141.5 (s,  $\text{tBu-C}_{\text{Ar}}$ ), 141.8 (dd,  $J_{\text{CP}} = 4.3$  and 7.3 Hz,  $\text{NC}_{\text{dipp}}$ ), 142.6 (d,  $^2J_{\text{CP}} = 3.1$  Hz,  $\text{OC}_{\text{Ar}}$ ), 144.0 (dd,  $^4J_{\text{CP}} = 3.0$  Hz,  $^3J_{\text{CP}} = 1.8$  Hz,  $\text{OC}_{\text{Ar}}$ ), 146.2 (dd,  $^4J_{\text{CP}} = 7.2$  Hz,  $^3J_{\text{CP}} = 3.8$  Hz,  $\text{OC}_{\text{Ar}}$ ), 147.2 (m,  $\text{OC}_{\text{Ar}}$ ), 147.7 (s,  $\text{iPr-C}_{\text{dipp}}$ ), 148.3 (d,  $J_{\text{CP}} = 1.6$  Hz,  $\text{iPr-C}_{\text{dipp}}$ ), 181.8 (dd,  $^3J_{\text{CP}} = 19.9$  Hz,  $^2J_{\text{CP}} = 14.7$  Hz,  $\text{NC}_{\text{dipp}}$ ).

**Minor isomer (22%):** 3.7 (d,  $J_{CP} = 1.9$  Hz, SiCH<sub>3</sub>), 8.0 (dd,  $J_{CP} = 1.8$  and  $J_{CP} = 10.2$  Hz, SiCH<sub>3</sub>), 23.6 (s, CH<sub>3*i*Pr</sub>), 24.9 (s, CH<sub>3*i*Pr</sub>), 26.8 (s, CH<sub>3*i*Pr</sub>), 26.9 (s, CH<sub>2</sub>), 27.6 (s, CH<sub>*i*Pr</sub>), 27.7 (s, CH<sub>*i*Pr</sub>), 28.5 (s, CH<sub>2</sub>), 29.2 (s, CH<sub>3*t*Bu-Ar</sub>), 30.4 (s, CH<sub>3*t*Bu-Ar</sub>), 32.1 (s, CH<sub>3*t*Bu-Ar</sub>), 32.2 (s, CH<sub>3*t*Bu-Ar</sub>), 32.4 (dd,  $J_{CP} = 1.9$  and 4.0 Hz, CH<sub>3*t*Bu-N</sub>), 32.6 (dd,  $^3J_{CP} = 4.6$  Hz,  $^4J_{CP} = 1.7$  Hz, CH<sub>3*t*Bu-N</sub>), 34.0 (s, C<sub>*t*Bu-Ar</sub>), 34.5 (s, C<sub>*t*Bu-Ar</sub>), 34.9 (s, C<sub>*t*Bu-Ar</sub>), 1 signal of C<sub>*t*Bu-Ar</sub> not detected, 41.2 (dd,  $^4J_{CP} = 10.4$  Hz,  $^3J_{CP} = 2.8$  Hz, CH<sub>bridgehead</sub>), 45.3 (dd,  $^4J_{CP} = 7.5$  Hz,  $^3J_{CP} = 2.8$  Hz, CH<sub>bridgehead</sub>), 46.4 (d,  $J_{CP} = 6.9$  Hz, CH<sub>2</sub>), 53.5 (d,  $J_{CP} = 1.3$  Hz, C<sub>*t*Bu-N</sub>), 1 signal of C<sub>*t*Bu-N</sub> not detected, 83.8 (dd,  $^1J_{CP} = 67.5$  Hz,  $^2J_{CP} = 70.0$  Hz, PC), 106.4 (dd,  $^5J_{CP} = 12.0$  Hz,  $^4J_{CP} = 1.1$  Hz, CH<sub>Ar</sub>), 107.4 (dd,  $^5J_{CP} = 11.1$  Hz,  $^4J_{CP} = 4.0$  Hz, CH<sub>Ar</sub>), 113.7 (s, CH<sub>Ar</sub>), 114.2 (s, CH<sub>Ar</sub>), 124.7 (s, CH<sub>dipp</sub>), 127.9 (s, CH<sub>dipp</sub>), 1 signal of C<sub>dipp</sub> not detected, 131.8 (dd,  $^5J_{CP} = 7.9$  Hz,  $^4J_{CP} = 2.8$  Hz, C<sub>Ar</sub>), 132.3 (d,  $^4J_{CP} = 13.1$  Hz, C<sub>Ar</sub>), 141.0 (s, tBu-C<sub>Ar</sub>), 1 signal of tBu-C<sub>Ar</sub> not detected, 141.3 (dd,  $^5J_{CP} = 6.8$  Hz,  $^4J_{CP} = 4.3$  Hz, NC<sub>dipp</sub>), 142.7 (d,  $^2J_{CP} = 3.1$  Hz, OC<sub>Ar</sub>), 144.2 (dd,  $J_{CP} = 1.5$  and 3.2 Hz, OC<sub>Ar</sub>), 146.3 (dd,  $^3J_{CP} = 6.9$  Hz,  $^2J_{CP} = 3.7$  Hz, OC<sub>Ar</sub>), 147.2 (pseudo-t,  $^3J_{CP} = 2.1$  Hz, OC<sub>Ar</sub>), 147.7 (s, iPr-C<sub>dipp</sub>), 1 signal of iPr-C<sub>dipp</sub> not detected, 182.6 (dd,  $^4J_{CP} = 19.7$  Hz,  $^3J_{CP} = 14.3$  Hz, NC<sub>dipp</sub>).

**<sup>31</sup>P{<sup>1</sup>H} NMR (202 MHz, C<sub>6</sub>D<sub>6</sub>, 25 °C):**

**Major isomer (78%):** 34.7 (d,  $J_{PP} = 690.1$  Hz, PN2), -104.8 (d,  $J_{PP} = 690.1$  Hz, PO<sub>4</sub>).

**Minor Isomer (22%):** 35.9 (d,  $J_{PP} = 683.0$  Hz, PN2), -104.6 (d,  $J_{PP} = 683.0$  Hz, PO<sub>4</sub>).

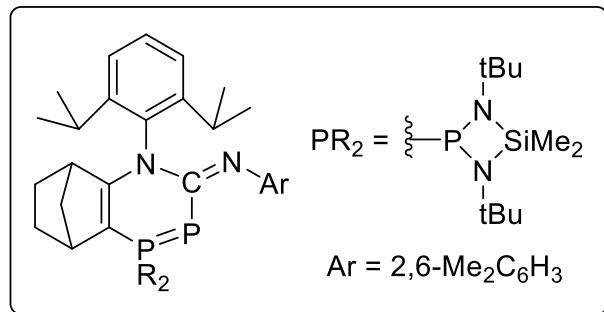
**<sup>29</sup>Si NMR (99 MHz, C<sub>6</sub>D<sub>6</sub>, 25 °C):**

**Major isomer (78%):** 12.4 (dd,  $J_{SiP} = 5.0$  Hz and 4.0 Hz, SiCH<sub>3</sub>).

**Minor isomer (22%):** 11.9 (dd,  $J_{SiP} = 5.4$  Hz and 3.9 Hz, SiCH<sub>3</sub>)

**HRMS (ESI/Q-TOF) m/z C57H89N3O4P2Si [M+H]+:** calculated 970.6176, found 970.6171

Synthesis of the product **47**



Phosphinidene **35** (20 mg, 0.038 mmol) and 1 eq. of 2,6-Dimethylphenyl isocyanide (5 mg, 0.038 mmol) are solved in 0.4 ml of heptane at room temperature. Suitable crystals of **47** for X-ray diffraction analysis were obtained from a concentrated heptane solution at room temperature (13.31 mg, yield = 53.3%).

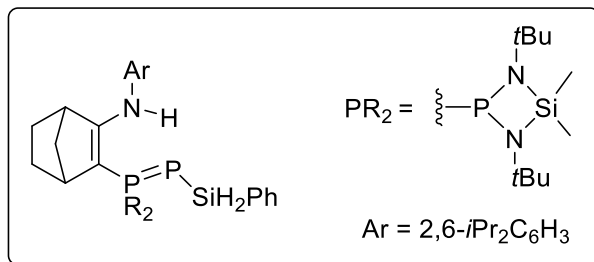
**$^1\text{H NMR}$  (500 MHz, THF- $\text{d}_8$ , 25 °C):** 0.19 (s, 3H, SiCH<sub>3</sub>), 0.22 (s, 3H, SiCH<sub>3</sub>), 0.91 (m, 1H, CH<sub>2</sub>), 1.25 (d, 9H,  $J_{\text{HH}} = 0.6$  Hz, CH<sub>3tBu</sub>), 1.26 (s, 9H, CH<sub>3tBu</sub>), 1.28 (d, 3H,  $J_{\text{HH}} = 6.8$  Hz, CH<sub>3iPr</sub>), 1.30 (d, 3H,  $J_{\text{HH}} = 6.8$  Hz, CH<sub>3iPr</sub>), 1.43 (d, 3H,  $J_{\text{HH}} = 6.6$  Hz, CH<sub>3iPr</sub>), 1.44 (d, 3H,  $J_{\text{HH}} = 6.7$  Hz, CH<sub>3iPr</sub>), 1.48 (m, 2H, CH<sub>2</sub>), 1.60 (m, 2H, CH<sub>2</sub>), 1.69 (m, 1H, CH<sub>2</sub>), 2.21 (s, 3H, ArCH<sub>3</sub>), 2.47 (m, 1H, CH<sub>bridgehead</sub>), 2.58 (s, 3H, ArCH<sub>3</sub>), 3.12 (m, 1H, CH<sub>bridgehead</sub>), 3.34 (sept,  $J_{\text{HH}} = 6.8$  Hz, 1H, CH<sub>iPr</sub>), 3.42 (sept,  $J_{\text{HH}} = 6.7$  Hz, 1H, CH<sub>iPr</sub>), 6.96 (m,  $J_{\text{HH}} = 7.4$  Hz, 1H, CH<sub>Ar</sub>), 7.06 (m, 1H, CH<sub>Ar</sub>), 7.21 (m, 3H, CH<sub>Ar</sub> and CH<sub>dipp</sub>), 7.28 (t,  $J_{\text{HH}} = 7.6$  Hz, 1H, CH<sub>dipp</sub>).

**$^{13}\text{C NMR}$  (125 M Hz, THF- $\text{d}_8$ , 25 °C):** 4.1 (s, SiCH<sub>3</sub>), 4.8 (dd,  $^3J_{\text{CP}} = 2.5$  Hz,  $^4J_{\text{CP}} = 0.9$  Hz, SiCH<sub>3</sub>), 19.2 (d,  $J_{\text{CP}} = 3.9$  Hz, ArCH<sub>3</sub>), 20.0 (d,  $J_{\text{CP}} = 3.5$  Hz, ArCH<sub>3</sub>), 25.0 (s, CH<sub>3iPr</sub>), 25.1 (s, CH<sub>3iPr</sub>), 25.7 (s, CH<sub>3iPr</sub>), 26.7 (s, CH<sub>3iPr</sub>), 27.0 (d,  $J_{\text{CP}} = 1.9$  Hz, CH<sub>2</sub>), 27.9 (s, CH<sub>2</sub>), 28.3 (s, CH<sub>iPr</sub>), 29.0 (s, CH<sub>iPr</sub>), 32.3 (dd,  $^3J_{\text{CP}} = 5.4$  Hz,  $^4J_{\text{CP}} = 3.4$  Hz, CH<sub>3tBu</sub>), 32.5 (dd,  $^3J_{\text{CP}} = 5.0$  Hz,  $^4J_{\text{CP}} = 3.4$  Hz, CH<sub>3tBu</sub>), 42.4 (d,  $J_{\text{CP}} = 1.6$  Hz, CH<sub>bridgehead</sub>), 46.6 (d,  $J_{\text{CP}} = 5.6$  Hz, CH<sub>2</sub>), 47.4 (d,  $J_{\text{CP}} = 11.6$  Hz, CH<sub>bridgehead</sub>), 52.6 (d,  $J_{\text{CP}} = 1.4$  Hz, C<sub>tBu</sub>), 52.7 (s, C<sub>tBu</sub>), 99.2 (dd,  $^1J_{\text{CP}} = 81.4$  Hz,  $^2J_{\text{CP}} = 5.6$  Hz, PC), 121.9 (s, CH<sub>Ar</sub>), 124.2 (s, CH<sub>dipp</sub>), 124.3 (s, CH<sub>dipp</sub>), 127.0 (d,  $J_{\text{CP}} = 3.1$  Hz, C<sub>Ar</sub>-CH<sub>3</sub>), 128.4 (s, CH<sub>Ar</sub>), 128.5 (s, CH<sub>dipp</sub>), 128.8 (s, CH<sub>Ar</sub>), 130.0 (d,  $J_{\text{CP}} = 2.1$  Hz, C<sub>Ar</sub>-CH<sub>3</sub>), 140.1 (d,  $J_{\text{CP}} = 2.3$  Hz, NC<sub>dipp</sub>), 146.0 (s, C<sub>dipp</sub>-iPr), 148.5 (s, C<sub>dipp</sub>-iPr), 149.6 (dd,  $^3J_{\text{CP}} = 15.1$  Hz,  $^4J_{\text{CP}} = 6.3$  Hz, CNC<sub>Ar</sub>), 164.9 (d,  $J_{\text{CP}} = 16.4$  Hz, NC), 170.9 (dd,  $^3J_{\text{CP}} = 100.5$  Hz,  $^4J_{\text{CP}} = 5.9$  Hz, NC<sub>isonitrile</sub>).

**$^{31}\text{P}\{\text{H}\}$  NMR (162 MHz, THF- $\text{d}_8$ , 25 °C):** 66.2 (d,  $J_{\text{PP}} = 483.0$  Hz, PN2), -87.6 (d,  $J_{\text{PP}} = 483.0$  Hz, PC<sub>isonitrile</sub>N).

**$^{29}\text{Si NMR}$  (99 MHz, THF- $\text{d}_8$ , 25 °C):** 5.3 (d,  $J = 2.3$  Hz, SiCH<sub>3</sub>).

Synthesis of the product **48** :



To a solution of **35** (20 mg, 0.04 mmol) in toluene (0.5 mL), Ph<sub>3</sub>SiH (40 mg, 0.37 mmol) was added at room temperature. Full conversion of **35** was observed after 20h at 80 °C. The product **48** was extracted with pentane. Then, after removal of all volatiles under reduced pressure, the residue was washed with acetonitrile to give the corresponding **48** as yellow powder (25 mg, 39%). Mp: 125 °C. Single crystals, suitable for X-ray diffraction analysis, were obtained from a saturated CH<sub>3</sub>CN/Ether solution at room temperature.

**<sup>1</sup>H NMR (500 MHz, C<sub>6</sub>D<sub>6</sub>, 25 °C):** 0.37 (s, 3H, SiCH<sub>3</sub>), 0.55 (s, 3H, SiCH<sub>3</sub>), 0.95 (d,  $J_{\text{HH}} = 8.3$  Hz, 1H, CH<sub>2</sub>), 1.20 (d, 3H,  $J_{\text{HH}} = 6.9$  Hz, CH<sub>3*i*Pr</sub>), 1.27 (d, 3H,  $J_{\text{HH}} = 6.9$  Hz, CH<sub>3*i*Pr</sub>), 1.28 (d, 3H,  $J_{\text{HH}} = 6.9$  Hz, CH<sub>3*t*Bu</sub>), 1.34 (d, 3H,  $J_{\text{HH}} = 6.9$  Hz, CH<sub>3*t*Bu</sub>), 1.40 (s, 9H, CH<sub>3*t*Bu</sub>), 1.44 (s, 9H, CH<sub>3*t*Bu</sub>), 1.50 (m, 3H, CH<sub>2</sub>), 1.64 (m, 1H, CH<sub>2</sub>), 1.70 (m, 1H, CH<sub>2</sub>), 2.59 (s, 1H, CH<sub>bridgehead</sub>), 3.26 (s, 1H, CH<sub>bridgehead</sub>), 3.61 (sept,  $J_{\text{HH}} = 6.9$  Hz, 1H, CH<sub>*i*Pr</sub>), 3.65 (sept,  $J_{\text{HH}} = 6.9$  Hz, 1H, CH<sub>*i*Pr</sub>), 5.43 (ddd,  $J_{\text{HH}} = 6.6$  Hz,  $^3J_{\text{HP}} = 11.8$  Hz,  $^2J_{\text{HP}} = 12.9$  Hz, 2H, SiH<sub>2</sub>), 7.16 (m, 6H, CH<sub>Ar</sub>), 7.99 (m, 2H, CH<sub>Ar</sub>), 8.76 (d,  $J_{\text{HH}} = 18.6$  Hz, 1H, NH).

**<sup>13</sup>C NMR (125 M Hz, C<sub>6</sub>D<sub>6</sub>, 25 °C):** 3.5 (d,  $J_{\text{CP}} = 2.2$  Hz, SiCH<sub>3</sub>), 5.4 (s, SiCH<sub>3</sub>), 22.8 (s, CH<sub>3*i*Pr</sub>), 23.1 (s, CH<sub>3*i*Pr</sub>), 25.4 (s, CH<sub>3*i*Pr</sub>), 25.9 (d,  $J_{\text{CP}} = 5.0$  Hz, CH<sub>3*i*Pr</sub>), 26.2 (d,  $J_{\text{CP}} = 1.4$  Hz, CH<sub>2</sub>), 28.4 (d,  $J_{\text{CP}} = 2.3$  Hz, CH<sub>*i*Pr</sub>), 28.6 (s, CH<sub>*i*Pr</sub>), 28.8 (s, CH<sub>2</sub>), 32.3 (dd,  $^4J_{\text{CP}} = 1.5$  and 5.3 Hz, CH<sub>3*t*Bu</sub>), 32.4 (dd,  $^4J_{\text{CP}} = 1.7$  and 5.2 Hz, CH<sub>3*t*Bu</sub>), 44.9 (dd,  $^4J_{\text{CP}} = 12.0$  Hz,  $^3J_{\text{CP}} = 1.1$  Hz, CH<sub>bridgehead</sub>), 45.3 (d,  $J_{\text{CP}} = 6.6$  Hz, CH<sub>2</sub>), 45.6 (pseudo t,  $J_{\text{CP}} = 6.5$  Hz, CH<sub>bridgehead</sub>), 52.1 (s, C<sub>*t*Bu</sub>), 52.7 (s, C<sub>*t*Bu</sub>), 101.5 (dd,  $^1J_{\text{CP}} = 95.4$  Hz,  $^2J_{\text{CP}} = 21.4$  Hz, PC), 123.5 (s, CH<sub>Ar</sub>), 124.0 (s, CH<sub>Ar</sub>), 127.6 (s, CH<sub>Ar</sub>), 127.9 (s, CH<sub>Ar</sub>), 128.4 (s, CH<sub>Ar</sub>), 129.1 (s, CH<sub>Ar</sub>), 136.2 (dd,  $^3J_{\text{CP}} = 16.7$  Hz,  $^2J_{\text{CP}} = 7.4$  Hz, Si-C<sub>Ar</sub>), 136.3 (d,  $J_{\text{CP}} = 4.0$  Hz, CH<sub>Ar</sub>), 136.6 (d,  $J_{\text{CP}} = 0.8$  Hz, NC<sub>Ar</sub>), 147.0 (s, C<sub>dipp-*i*Pr</sub>), 148.4 (s, C<sub>dipp-*i*Pr</sub>), 164.8 (dd,  $^3J_{\text{CP}} = 13.4$  Hz,  $^2J_{\text{CP}} = 1.4$  Hz, NC).

**<sup>31</sup>P{<sup>1</sup>H} NMR (202 MHz, C<sub>6</sub>D<sub>6</sub>, 25 °C):** 72.7 (d,  $J_{\text{PP}} = 526.1$  Hz, PN2), -216.4 (d,  $J_{\text{PP}} = 526.1$  Hz, PSiH<sub>2</sub>).

**<sup>29</sup>Si NMR (99 MHz, C<sub>6</sub>D<sub>6</sub>, 25 °C):** 5.2 (t,  $J_{\text{SiP}} = 1.5$  Hz, SiCH<sub>3</sub>), -38.9 (dd,  $J_{\text{SiP}} = 71.2$  and 10.0 Hz, PSiH<sub>2</sub>).

## **Chapter III: Synthesis and reactivity of cationic plumbylenes**

## I. Introduction

### I.I Hydroamination

Amines are a highly relevant class of compounds, since versatile natural occurring substances and biologically active molecules include amine functional group. They are widely applied in industry as synthons for the synthesis of pharmaceutical substances, bactericides, flotation auxiliaries, anti-foam agents, corrosion inhibitors, detergents and dyes.<sup>[1]</sup>

The hydroamination reactions, e.g. direct addition of the amine moiety to olefins, would be an elegant and simple waste-free approach to amines with high atom efficiency.<sup>[2]</sup> However, as other hydrofunctionalization reactions, hydroamination can give two isomers, Markovnikov and *anti*-Markovnikov products (Figure 1). Even though hydroamination reactions in theory can afford 100% atom efficiency, they cannot ensure “zero waste”.<sup>[3]</sup> It is therefore important to perform such reactions with high regio- and stereo-selectivity in terms of atom economy.

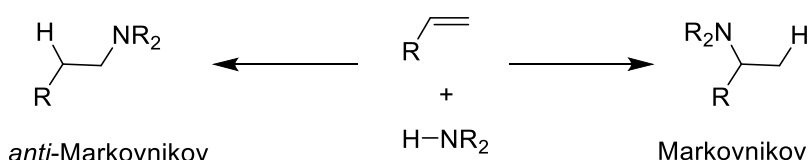


**Figure 1.** Hydroamination of olefins.

Another difficulty of the hydroamination reactions is the thermodynamic and kinetic restrictions of the direct nucleophilic addition of amines across inactivated CC-multiple bonds. Due to the electrostatic repulsion between electron-rich  $\pi$ -bond of the alkene or alkyne and the lone pair of amine nitrogen atom, a high activation barrier exists for the direct addition of amines.<sup>[4]</sup> For these reasons along with highly negative reaction entropy the direct hydroamination reaction is almost impossible in the absence of a catalyst.<sup>[2]</sup> Thus, hydroamination reactions can only be achieved in the presence of a catalyst, which would affect not only the selectivity of the reaction but also the mere possibility of the reaction proceeding.<sup>[4,5]</sup> Nowadays, various approaches used for efficient and selective catalysis of hydroamination reactions: acid-catalysts, base-catalysts, rare-earth metal based catalysis, TM-based catalysis (early-TM catalysts and late-TM catalysts).<sup>[6]</sup>

- Acid-catalyzed hydroamination of alkenes and alkynes

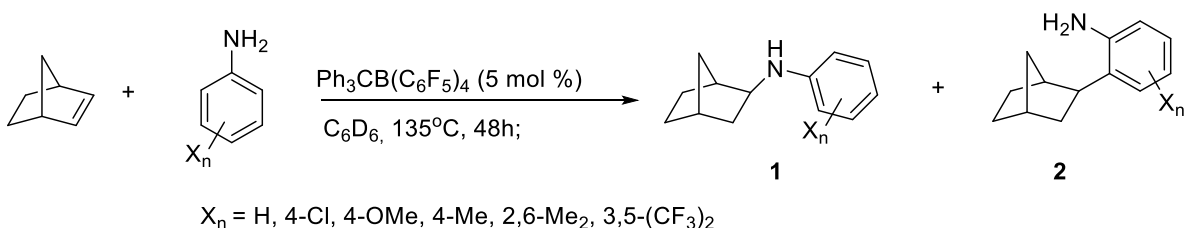
Acid-catalyzed hydroamination reactions most frequently are found among the industrial production of the amines using zeolites.<sup>[7]</sup> For example, the synthesis of *tert*-butylamine by the addition reaction of ammonia to isobutene (2-methylpropene) in the presence of zeolites gives the Markovnikov product (Scheme 1).<sup>[8–10]</sup> The reaction requires very drastic conditions, while the conversion of the substrate is only reasonable as regards industrial process (24 %). Besides, the recycling of the unreacted substrates (ammonia and isobutene) is rather expensive.



**Scheme 1.** Industrial synthesis of *tert*-butylamine using acid catalysis.

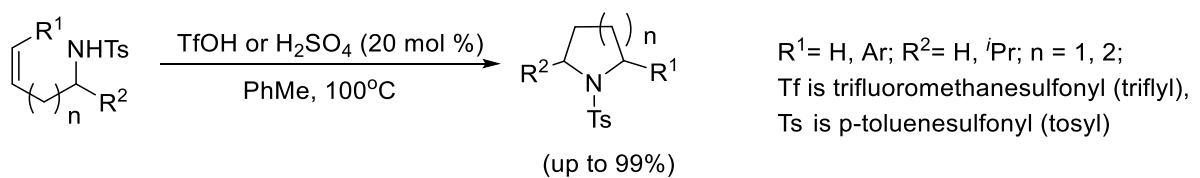
Another fairly recent example of amines preparation using zeolites was presented in a patent (2013 year) by T. Heidemann and J. Kehrer. They used lithium-doped boron zeolites for the catalysis of thereactions of alkenes with ammonia and primary or secondary amines, providing better results with higher efficiency and yields.<sup>[11]</sup>

Intermolecular hydroamination of norbornene with aniline derivatives was reported by Bergman et al.. They demonstrated that  $\text{Ph}_3\text{CB}(\text{C}_6\text{F}_5)_4$  was a good Lewis acid catalyst for both hydroamination and hydroarylation reactions. These two reactions are competitive, and the reaction pathway depends on the nature of the substrates. When  $X_n$  is an electron withdrawing substituent [4-Cl or 3,5-( $\text{CF}_3$ )<sub>2</sub>], the selective formation of product **1** was found (yields 55 % and 80 % respectively), while in the other cases, reactions are less selective [the ratio of products **1** and **2** depends on the nature of the substituents:  $X_n = \text{H}$  (1 : 1); 4-OMe (1 : 2); 2,6-Me<sub>2</sub> (2 : 3); N-Me (1 : 4)] (Scheme 2).<sup>[12]</sup>



**Scheme 2.** Intermolecular hydroamination of norbornene with aniline derivatives.

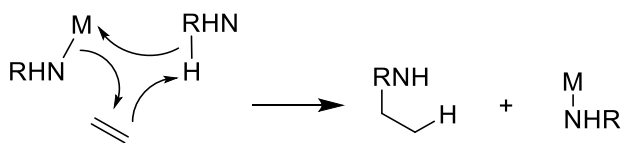
In contrast to Lewis acids, Bronsted acids didn't find a broad implementation in hydroamination reactions due to the protonation of more basic amines compared to unsaturated compounds leading the formation of stable and non-nucleophilic ammonium salts. It blocks the further nucleophilic attack of amine to unsaturated compounds. Nevertheless, it was found that catalytic amounts of Bronsted acids are able to catalyze hydroamination reactions.<sup>[13,14]</sup> For example, in 2002 Schlummer and Hartwig reported the cyclization of aminoalkenes catalyzed by Bronsted acids (Scheme 3), and excellent yields were obtained with triflic or sulfuric acids.<sup>[15]</sup>



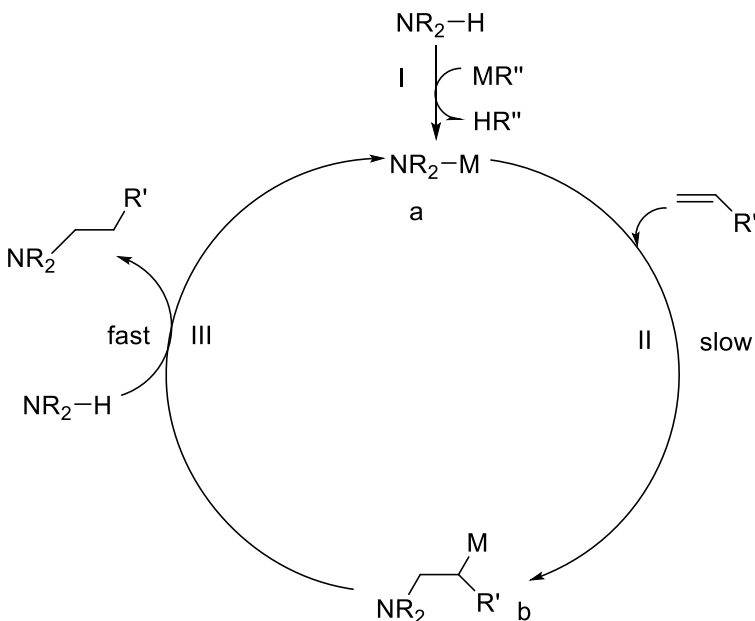
**Scheme 3.** Aminocyclisation catalyzed by triflic or sulfuric acid in toluene.

- Base-catalyzed hydroamination of alkenes and alkynes

Base catalysis of unsaturated compounds usually proceeds with alkali metal amides, such as rubidium and cesium amides, in the role of bases. Due to the electronic repulsion between nitrogen lone pair and  $\pi$ -electrons of unsaturated molecules, these reactions usually require drastic conditions.<sup>[2]</sup> Possible mechanisms for the base-catalyzed hydroamination reaction are represented in Scheme 4 and Scheme 5. In the case of a concerted mechanism (Scheme 4), the reaction proceeds in a single step (simultaneous bond breaking and forming).<sup>[2,16]</sup>



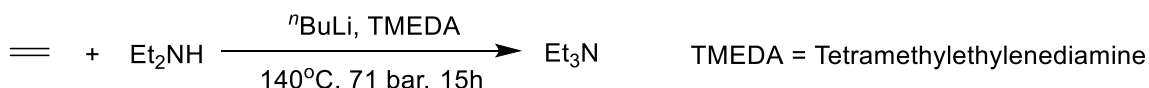
**Scheme 4.** Concerted mechanism for base-catalyzed hydroamination reactions.



**Scheme 5.** Catalytic cycle for the base-catalyzed hydroamination reactions mechanism.

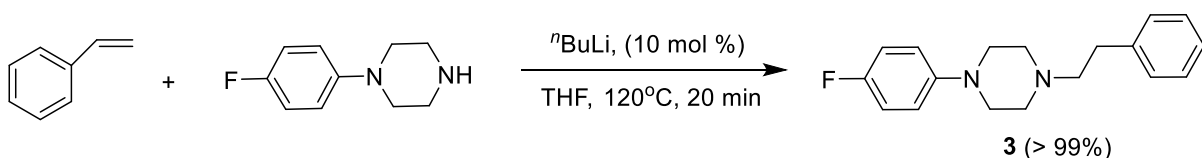
In the case of a multi-step process, the catalytic cycle probably starts with the deprotonation of the reacting amine by basic-catalyst (for example alkali metals or their alkyl or aryl salts, hydrides or appropriate amides). The metal amides formed in the step I possess a strongly nucleophilic character and thus, are able to react with olefins. However, the step II has a high activation energy and thus proceeds slowly (in the case of reactions with a non-activated olefin). This step leads to the formation of highly reactive nucleophilic 2-aminoalkyl metal complexes (**b**). This complex immediately regenerates the parent metal amide by fast protonation in the presence of the excess of the parent amine (step III). This step could be reversible depending on the reaction conditions as well as the type of substrates.

The first example of hydroamination of alkenes with primary amines in the presence of alkali metals or their hydrides was reported in 1954 by Howk et al.<sup>[17]</sup> This reaction requires drastic conditions and the addition of ammonia to ethylene was carried out at 175 – 200 °C and 800 - 1000 bar pressure. Another example of base-catalyzed hydroamination was reported by D. Reinehr in 1973. The addition of diethylamine to ethylene was catalyzed by *n*-butyllithium at 140 °C and 70 bar pressure (Scheme 6).<sup>[18]</sup>



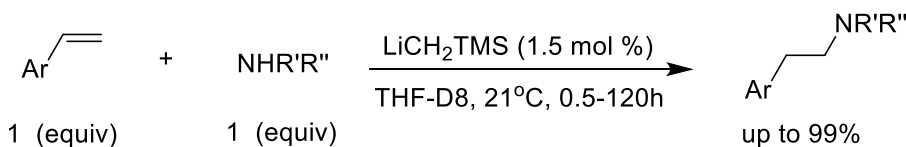
**Scheme 6.** *n*BuLi catalyzed addition of diethylamine to ethylene reported by D. Reinehr.

The base-catalyzed hydroamination reactions with more reactive alkenes such as styrenes proceed in much milder conditions. It was demonstrated by Beller and Breindl in 1998 that the reaction of styrene with piperazine derivative catalyzed by *n*BuLi proceeds at 120 °C to give the anti-Markovnikov product with a remarkable selectivity (> 99%) and high yield (> 99%) (Scheme 7).<sup>[19]</sup>



**Scheme 7.** Base-catalyzed hydroamination of styrene with piperazine derivative reported by Beller and Breindl (1998).

Among the most recent examples of base-catalyzed hydroamination reactions, which could proceed in mild conditions, is the anti-Markovnikov addition of simple secondary aliphatic amines to vinylarenes which takes place at room temperature (Scheme 8).<sup>[20]</sup>



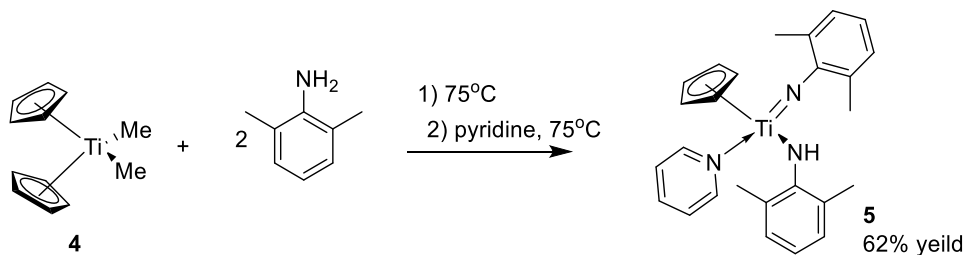
**Scheme 8.** Li-catalysed anti-Markovnikov hydroamination of the vinylarenes with secondary amines (Shulz and co-workers, 2017)

- Hydroamination reactions Catalyzed by transition metals

Over last decades, it was shown that hydroamination reactions can be catalyzed by early and late transition metals. Either CC-multiple bond, or N-H bond could be activated during the reaction depending on the nature of the catalyst. In general, early transition metals, similarly to alkali metals, activate N-H bonds, leading to the formation of the amido species. On the contrary, late-transition metals have a tendency to activate CC- $\pi$ -bonds of alkenes or alkynes via their coordination. However late-TM can activate also N-H moiety via an oxidative addition to the electron-rich metal center.<sup>[21]</sup> A goal of TM-catalyzed hydroamination reactions is to achieve the control of the diastereoselectivity and the regioselectivity.

#### ❖ Early Transition Metal-Catalyzed Hydroamination

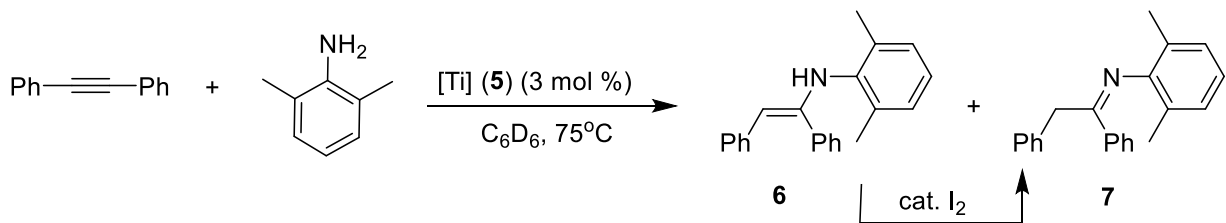
Bergman et al. found that Ti and Zr cyclopentadienyl complexes of type **4** are converted to the half-sandwich amido-imide complexes of type **5** (Scheme 9).



**Scheme 9.** Formation of the half sandwich amido-imide complex, which can catalyze the hydroamination of anilines with diphenylacetylene.

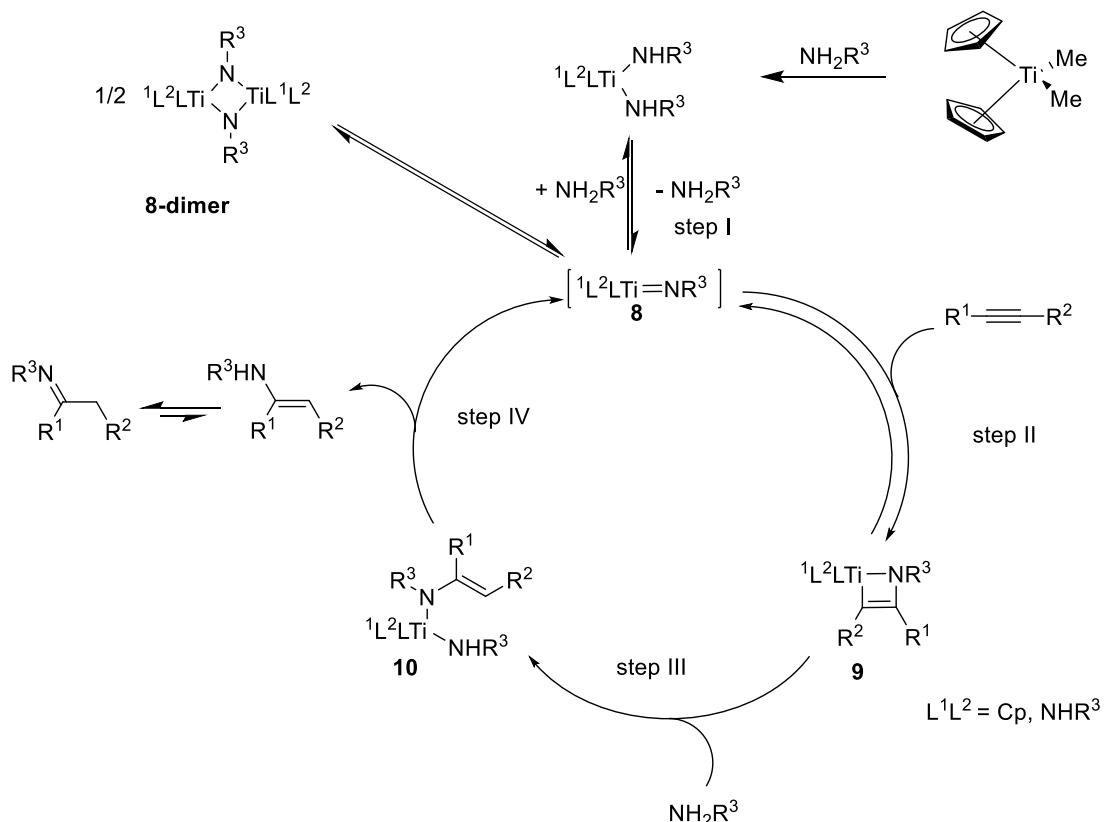
These complexes were found to be highly efficient hydroamination catalyst for alkynes and allenes. The reaction of phenylacetylene with anilines afforded enamine **6**, which isomerizes to imine **7** in the

presence of catalytic amounts of iodine (Scheme 10).<sup>[22]</sup>



**Scheme 10.** The reaction of anilines with diphenylacetylene, catalyzed by Ti-complex 5.

The mechanism of the hydroamination reactions catalyzed by Ti-cyclopentadienyl complexes has been investigated thoroughly (Scheme 11).<sup>[5]</sup> The first step of the catalytic cycle is the generation of the metal imido complex **8**, which is forming through reversible elimination of an amine from a bis(amido) precursor (Scheme 11). The catalytically active metal imido complex can possibly exist in the imido-bridged dimeric form **8-dimer**, depending on the steric hindrance of the ancillary ligands. The formed metal imido complex **8** then undergoes a reversible [2+2]-cycloaddition with CC-unsaturated bond of alkyne or alkene, forming azametallacyclobutene species **9** (step **II** on the scheme 11). This step is the rate-limiting step of the catalytic cycle. Further slow protonation of the azametallacyclobutene gives enamide amido complex **10** (step **III**), which subsequently undergoes elimination of the enamine (step **IV**). It leads to the fast regeneration of the catalyst and the formation of the hydroamination product.<sup>[14,23]</sup>



**Scheme 11.** Proposed mechanism for the early-TM (titanium) catalyzed addition of amines to alkynes.

#### ❖ Late Transition Metal-Catalyzed Hydroamination

Catalysts based on late-transition metals are the most investigated ones. They have a wide range of functional group tolerance, air and moisture insensitivity and high reactivity.<sup>[1]</sup> The mechanism of the hydroamination catalytic cycle, based on late-transition metal complexes, can be generally characterized by

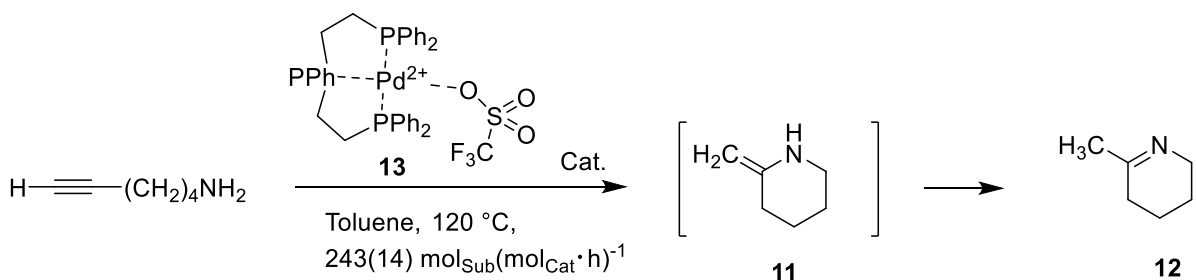
the four groups based on the step in which the regioselectivity is determined:

- 1) Nucleophilic attack of amine nitrogen atom on a coordinated alkene or alkyne,
- 2) Nucleophilic attack of amine nitrogen atom on allylic complexes,
- 3) Insertion of the alkene/alkyne into M-H bond,
- 4) Oxidative addition of the amine to electron-rich metal center.<sup>[14]</sup>

Thus, three first mechanistic models involve the activation of the unsaturated CC-bond, while the last one implies the amine activation.

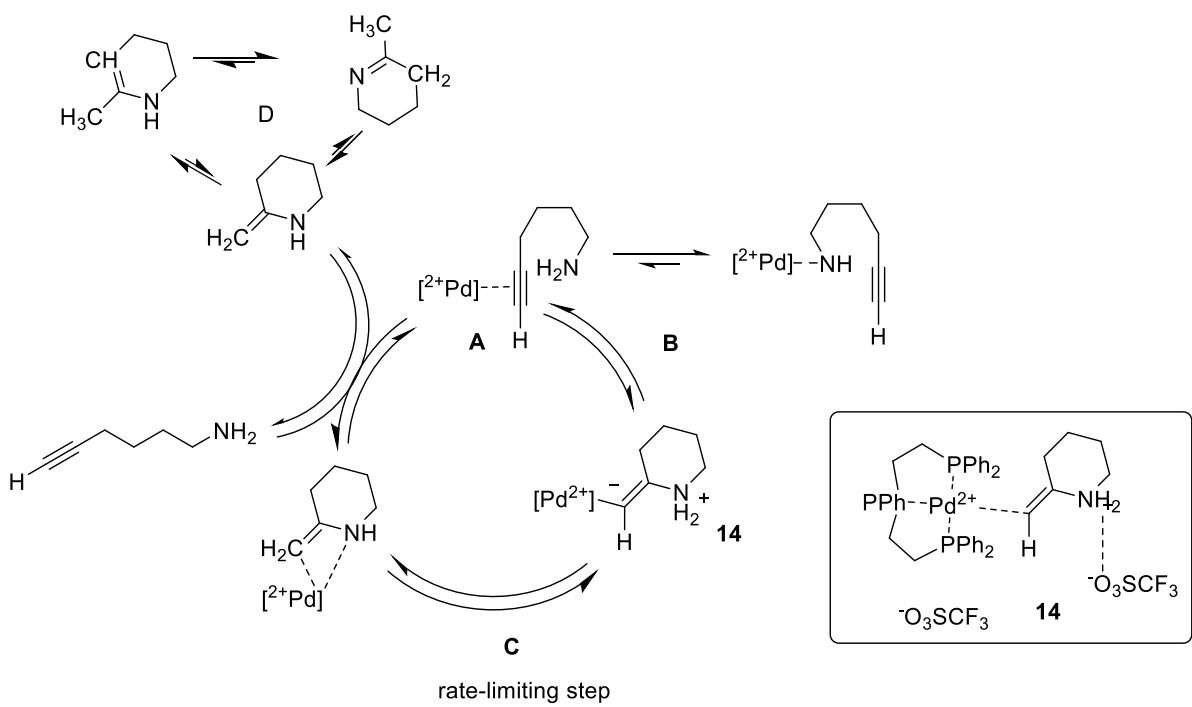
Nucleophilic attack of amine nitrogen atom on a coordinated alkene or alkyne

In 2001 Thomas E. Muller reported the palladium-catalyzed intramolecular cyclisation of the 6-aminohex-1-yne affording Markovnikov product **11** with an exocyclic double bond, which subsequently tautomerizes to a more stable isomeric imine **12** through 1,3-hydrogen shift (Scheme 12).<sup>[24]</sup> The highest catalytic activity was observed with the [Pd(Triphos)](CF<sub>3</sub>SO<sub>3</sub>)<sub>2</sub> complex **13** in toluene under reflux (243(14) mol<sub>Sub</sub>·(mol<sub>Cat</sub>·h)<sup>-1</sup>) (Scheme 12).



**Scheme 12.** Intramolecular cyclisation of the 6-aminohex-1-yne

According to <sup>31</sup>P-NMR studies<sup>[14,24,25]</sup> and DFT studies,<sup>[26]</sup> the regioselectivity of this reaction is determined by the step of nucleophilic attack of the amine on the  $\alpha$ -carbon atom of the coordinated alkyne, which is kinetically controlled at usual reaction temperatures.<sup>[27]</sup> The proposed catalytic cycle is presented in Scheme 13. The reaction starts with the initial coordination of the 6-aminohex-1-yne to the Pd atom through the amine moiety. Then, the complex isomerises and the CC-multiple bond is activated by its coordination to the Lewis acidic metal center (Step **A**, Scheme 13). Then, the nucleophilic attack of the amine nitrogen lone pair (step **B**) renders zwitterionic 2-ammonio-alkyl/alkenyl complex which subsequently undergoes the protolytic cleavage of the metal-carbon bond, giving the amine/enamine product (step **C**). The subsequent elimination from the metal center gives the hydroaminated product (Step **D**).

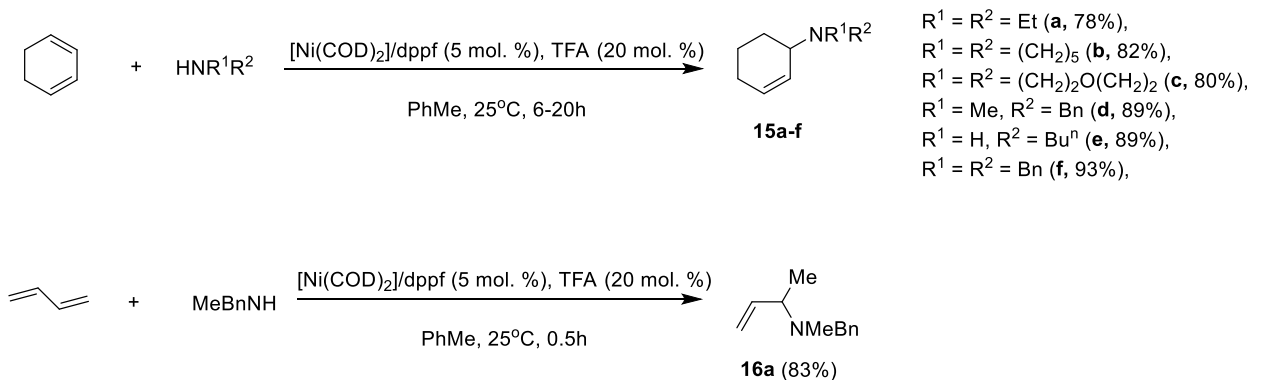


**Scheme 13.** Nucleophilic attack on a coordinated alkene/alkyne

Complex **14** was found to be the predominant palladium species (>99%) in the catalytic cycle, suggesting that the following step such as protolytic cleavage of the M-C bond (step **C**, Scheme 13) is the rate-determining step. Indeed, when 1 equivalent of trifluoromethane sulfonic acid, as source of protons, was added to the reaction mixture, the reaction rate doubled from 243(14) mol<sub>Sub.</sub>(mol<sub>Cat.</sub>h)<sup>-1</sup> to 435(15) mol<sub>Sub.</sub>(mol<sub>Cat.</sub>h)<sup>-1</sup>. In the case of the 100:1:100 mixture of the 6-aminohex-1-yne : [Pd(Triphos)](CF<sub>3</sub>SO<sub>3</sub>)<sub>2</sub> : CF<sub>3</sub>SO<sub>3</sub>H the reaction was complete with estimated reaction rate ca. 1800 mol<sub>Sub.</sub>(mol<sub>Cat.</sub>· h)<sup>-1</sup>.<sup>[24]</sup>

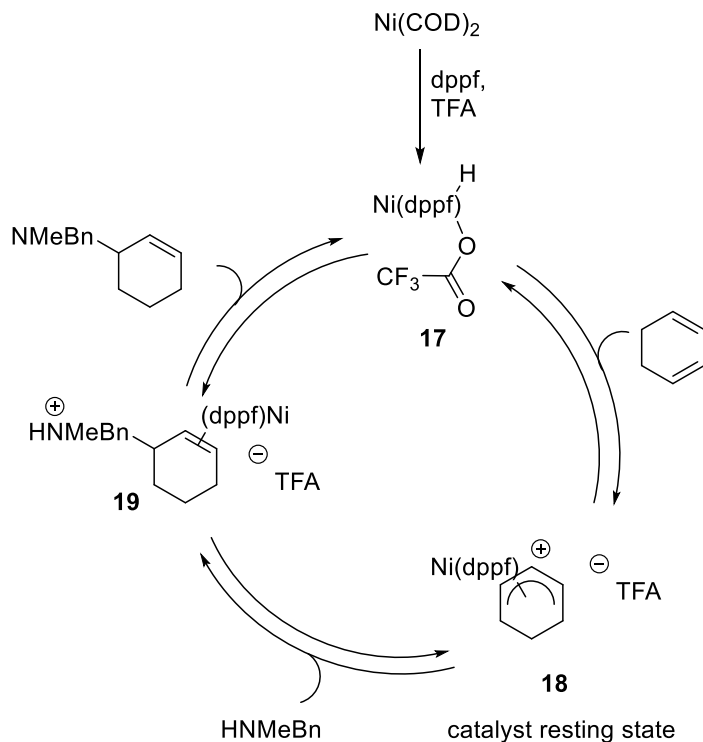
#### Nucleophilic attack of amine nitrogen atom on allylic complexes

In 2002, John F. Hartwig reported the hydroamination of 1,3-dienes with alkylamines catalyzed by nickel-complexes Ni(COD)<sub>2</sub> with dppf ligand in the presence of acid cocatalyst TFA (Scheme 14). Thus, trifluoroacetic acid serves for the generation of cationic nickel-hydride complex, which is the key-intermediate for the proposed catalytic cycle discussed below. The Markovnikov addition of primary amines to buta-1,3-diene using these conditions gave a major product **16a** with a high yield (83 %) without telomerisation.<sup>[28]</sup>



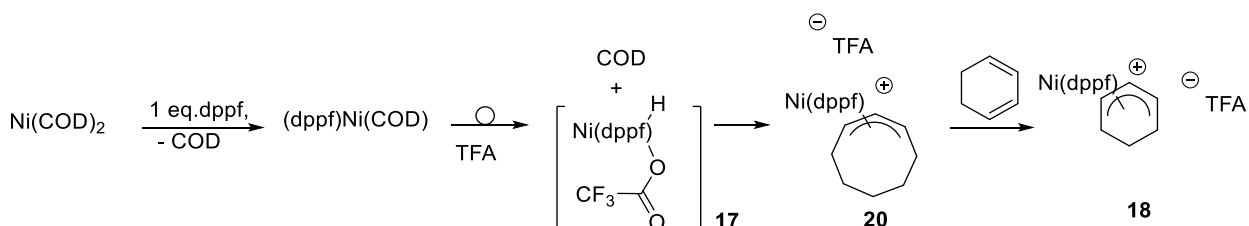
**Scheme 14.** Hydroamination of cyclohexa-1,3-diene and buta-1,3-diene with alkylamines.

The suggested mechanism involves the initial protonation of the Ni(dppf) complex (which is formed *in situ* from  $\text{Ni}(\text{COD})_2$  and dppf) by TFA and formation of the unstable nickel-hydride complex **17** (Scheme 15). Then, it reacts with 1,3-cyclohexadiene to form cationic  $\eta^3$ -allyl complex **18**, which subsequently undergoes to the attack of amine on the coordinated diene. In the last step of the catalytic cycle, the enamine is eliminated from the ammonium-nickel complex **19**, regenerating the initial Ni-hydride complex **17**.<sup>[14,28]</sup>



**Scheme 15.** Mechanistic model of the hydroamination proceeding through nucleophilic attack on allylic complexes.

To prove the suggested mechanism, the group of John F. Hartwig performed studies to generate and characterize the potential reaction intermediates. For the key-intermediate, the nickel hydride complex **17**, the  $\text{Ni}(\text{COD})_2$  was successively reacted with dppf and then with TFA. However, instead of the desired unstable **17**, the reaction afforded dppf-ligated nickel( $\eta^3$ -cyclooctenyl) complex **20** due to the reaction of **17** with a COD (Scheme 16).<sup>[28]</sup>

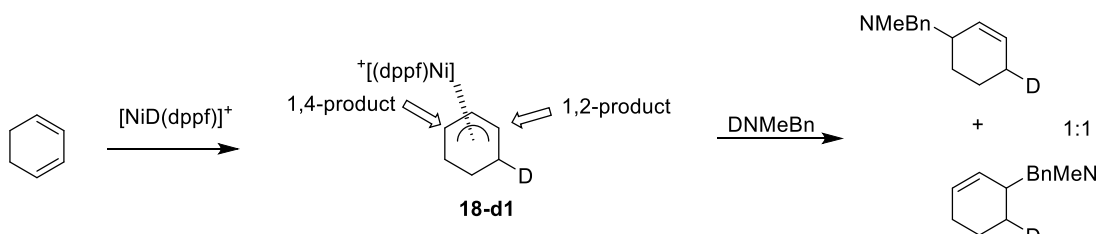


**Scheme 16.** An attempt for the generation of the nickel hydride complex **17** via the protonation by TFA of the  $(\text{dppf})\text{Ni}(\text{COD})$  generated *in situ*.

The compound **20** reacts with 1,3-cyclohexadiene and after 12 h at 50 °C to form the  $\eta^3$ -allyl complex **18**. This complex **18** could be independently isolated with 81 % yield via the reaction of the  $\text{Ni}(\text{COD})_2$ , dppf, TFA and 1,3-cyclohexadiene. The structure of **18** was confirmed by X-ray diffraction analysis. Besides, the isolated complexes **20** and **18** catalyzed the addition of the N-benzylmethylamine to the 1,3-

cyclohexadiene with similar rates compared to those reactions that were catalyzed by a species generated in situ from Ni(COD)<sub>2</sub>, dppf, and TFA.

In order to support the formation of the nickel allyl complex **18** as an intermediate in the course of the reaction, further experiments with deuterium labelling were done within the same group. The  $\eta^3$ -allyl complex **18-d1** was formed upon the reaction of the deuterated TFA-d1 and Ni(COD)<sub>2</sub> and dppf (Scheme 17). Further reaction with N-deutero, N-benzylmethylamine affords a 1:1 mixture of the 1,2 and 1,4-addition products, indicating that the reaction proceeds via the formation of the  $\eta^3$ -allyl complex **18-d1** instead of the simple olefin coordination to the Ni center (Scheme 17).<sup>[28]</sup>



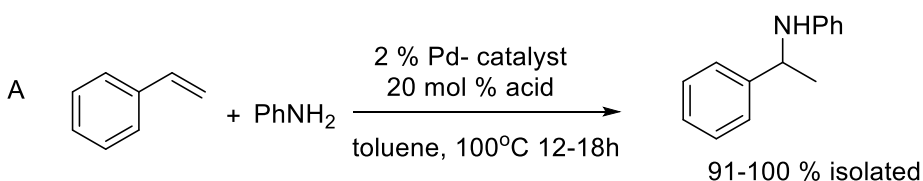
**Scheme 17.** Deuterium labelling experiments with cyclohexadiene and N-benzylmethylamine

In the last step of the catalytic cycle, the amine attacks on the nickel allyl complex **18**, and formation of the hydroamination product was found to be endothermic. Thus, the addition of an excess amount of diene substrate is necessary. The forming highly reactive unstable Ni-hydride complex **17** reacts with the diene in excess in the reaction mixture, forcing the next catalytic cycle. Using a stoichiometric amount of diene, the reversed reaction of oxidative addition of the allylic amine, formed in the reaction, to the Ni-complex **17** is favourable.

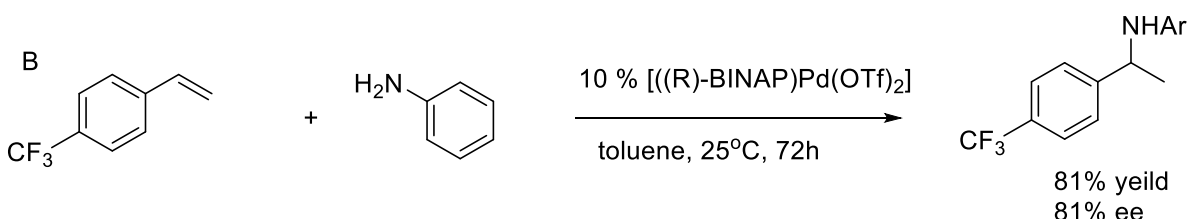
The same mechanism was proposed for hydroamination of dienes (Pd and Ni catalyzed)<sup>[28,29]</sup>, allenes (Pd catalyzed)<sup>[30,31]</sup>, and trienes (Pd catalyzed).<sup>[32]</sup>

#### Insertion of the alkene/alkyne into metal-hydride bond

The Markovnikov intermolecular hydroamination of styrenes with arylamines catalyzed by various palladium complexes in the presence of acid co-catalyst was reported by Hartwig in 2000 (Scheme 18, A).<sup>[33]</sup> When enantiopure  $[(R)\text{-BINAP}]\text{Pd}(\text{OSO}_2\text{CF}_3)_2$  complex was applied as catalyst for the enantioselective hydroamination of aniline with trifluoromethyl-styrene, which proceeds at near room temperature, the addition product was formed with 81 % yield and 81 % enantioselective excess (Scheme 18, B).<sup>[33–35]</sup>

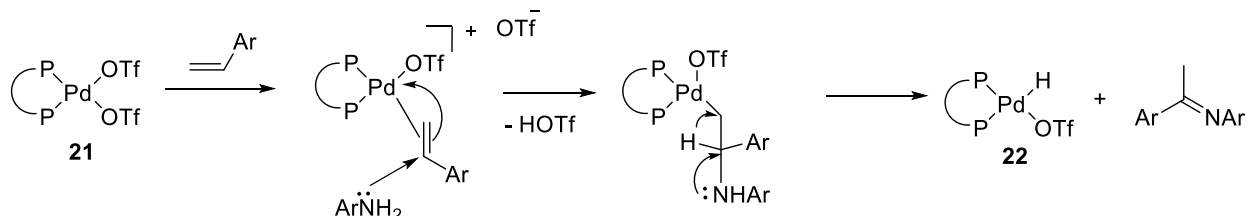


Palladium/ligand	Acid	Yield
2% $[\text{Pd}](\text{PPh}_3)_4$		0%
2% $[\text{Pd}(\text{PPh}_3)_4]$	20% TfOH	91%
2% $\text{Pd}(\text{TFA})_2/8\% \text{PPh}_3$	20% TfOH	68%
2% $[(\text{DPPF})\text{Pd}(\text{OTf})_2]$		100%



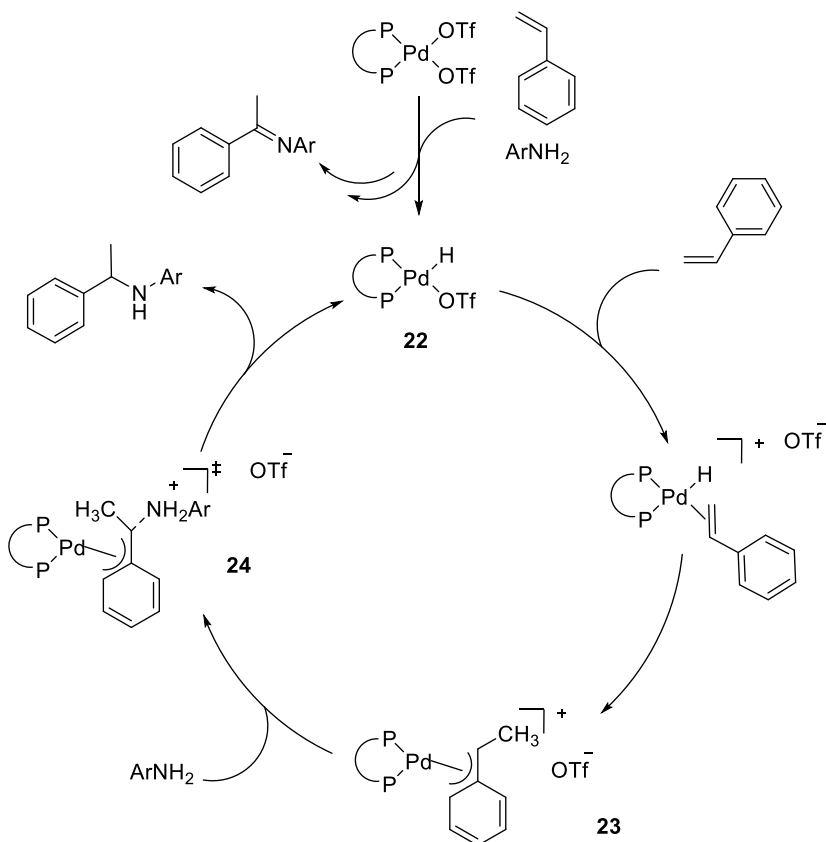
**Scheme 18.** The hydroamination of styrenes with cyclic amines catalyzed by various Pd complexes.

Pd(II) complex **21** was generated *in situ* when commercially available palladium trifluoroacetate was mixed with BINAP and TfOH as co-catalyst. According to GC analysis, the imine by-product is produced in a ratio 0.77-0.98 : 1 versus the palladium catalyst. Thus, the authors suggested that the catalytically active key-intermediate Pd-hydride **22** is forming upon a sequence of the nucleophilic attack of the amine on the coordinated olefin and subsequent  $\beta$ -hydride elimination in a Wacker-type oxidation processes (Scheme 19).<sup>[34,35]</sup>



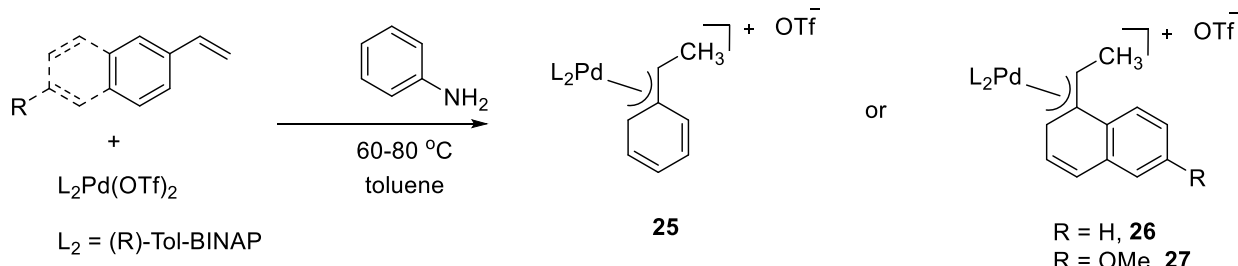
**Scheme 19.** Catalyst initiation via Wacker-type oxidation process.

After the first step of the catalytic cycle - catalyst initiation (Scheme 19), the alkene/alkyne inserts into Pd-H bond of the complex **22** forming the  $\eta^3$ -phenethyl complex **23** (Scheme 20). Subsequent attack of the amine on the benzylic carbon of the **23** affords ammonium salts complex **24**. In the last step of the catalytic cycle the palladium-hydride complex **22** regenerates via the proton transfer from the ammonium salts along with the release of the coordinated product.<sup>[34,35]</sup>



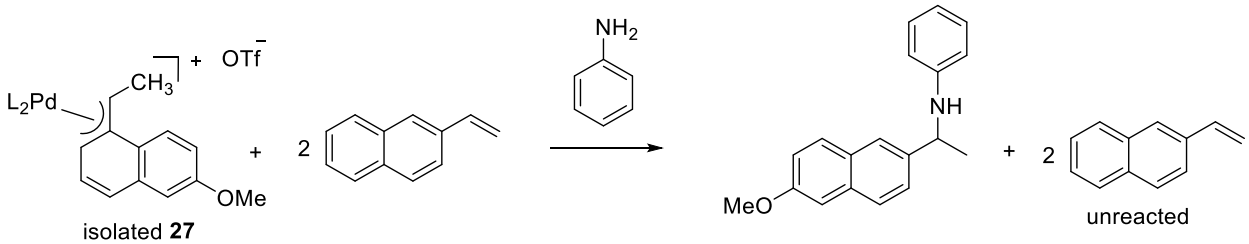
**Scheme 20.** Mechanistic model of the hydroamination reactions via insertion of the alkene/alkyne into metal-hydride bond.

To investigate the mechanism, the group of Hartwig synthesized and isolated a series of  $\eta^3$ -arylethyl complexes **25-27** as catalytic intermediates (Scheme 21) and checked their reactivity.<sup>[35]</sup>



**Scheme 21.** Reaction of various styrenes with aniline in the presence of Pd catalyst for the isolation of  $\eta^3$ -arylethyl complexes.

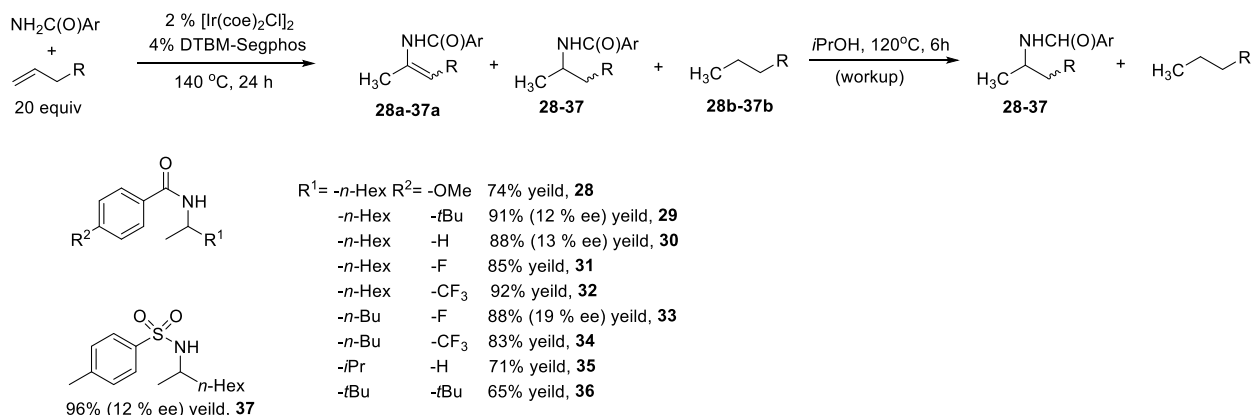
Indeed, the complex **27** reacts with aniline in presence of an excess of free 2-vinylnaphthalene to give the expected amine such as N-1-(6-methoxy-2-naphthyl)ethylaniline. If the vinylarene de-inserts from  $\eta^3$ -arylethyl complex **27** eliminating the palladium as an active catalyst, it would react with a free 2-vinylnaphthalene. However, such a reaction to form unsubstituted naphthylethyl-amine was observed. This supports the hypothesis of the transient formation of  $\eta^3$ -arylethyl complexes in the catalytic cycle (Scheme 22).<sup>[34,35]</sup> This type of catalytic cycle is referred for the palladium-driven hydroaminations (Scheme 21).<sup>[14,33,36]</sup>



**Scheme 22.** Reaction of the isolated **27** with aniline in the presence of an excess of free 2-vinylnaphthalene

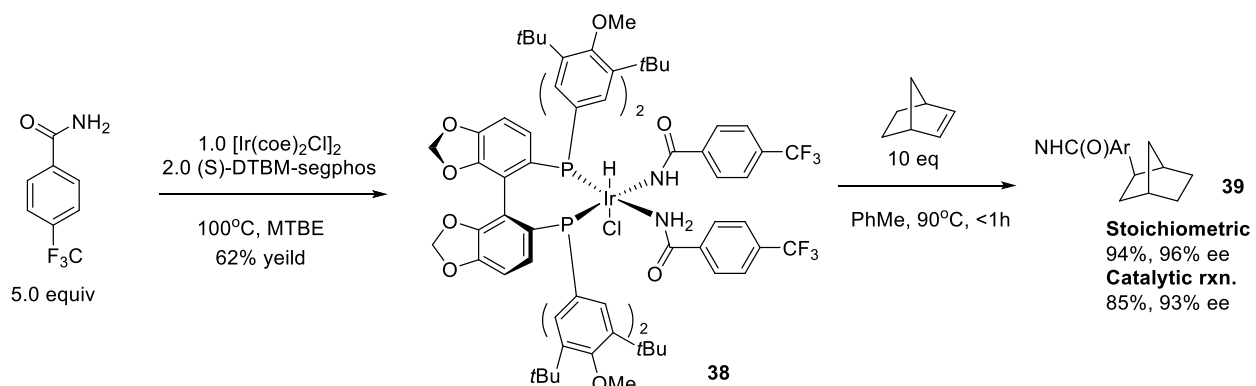
Oxidative addition of the amine to electron-rich metal center

In 2012, Hartwig reported Ir-catalyzed Markovnikov intermolecular hydroamination of unactivated  $\alpha$ -olefins (alkylated olefins) by amides and sulphonamides (Scheme 23).<sup>[37]</sup> The reactions were performed in neat alkenes (20 equivalents) with addition of 0.3 mmol of amide or sulfonamide which afforded the corresponding hydroamination products **28-37** along with enamides **28a-37a** and alkanes as by-products. In order to obtain single hydroamination products **28-37**, the corresponding enamide was reduced (hydrogenated) to alkylamide by treating the reaction mixture with an excess of isopropanol after the hydroamination.



**Scheme 23.** Ir-catalyzed intermolecular hydroamination of unactivated alkynes by amides and sulphonamides.

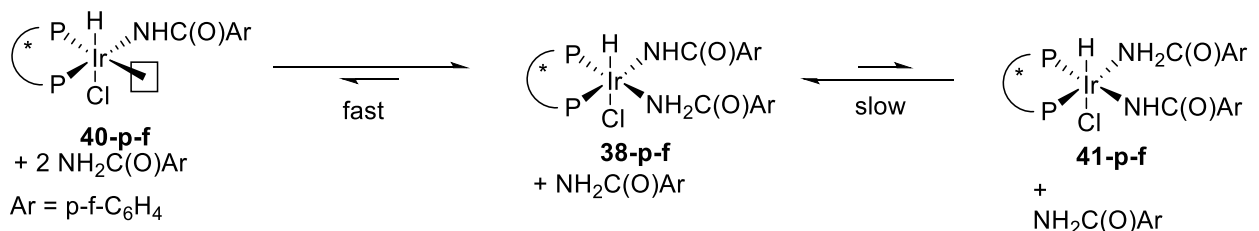
To investigate the reaction mechanism, commercially available Ir(I) complex  $[\text{Ir}(\text{coe})_2\text{Cl}]_2$  was reacted with (S)-DTBM-segphos ligand (DTBM = 3,5-di-tert-butyl-4-methoxy) and 4-CF<sub>3</sub>-benzamide at 100 °C in methyl *t*-butyl ether (Scheme 24), which afforded the complex **38**.<sup>[37]</sup>



**Scheme 24.** Synthesis of complex **38**.

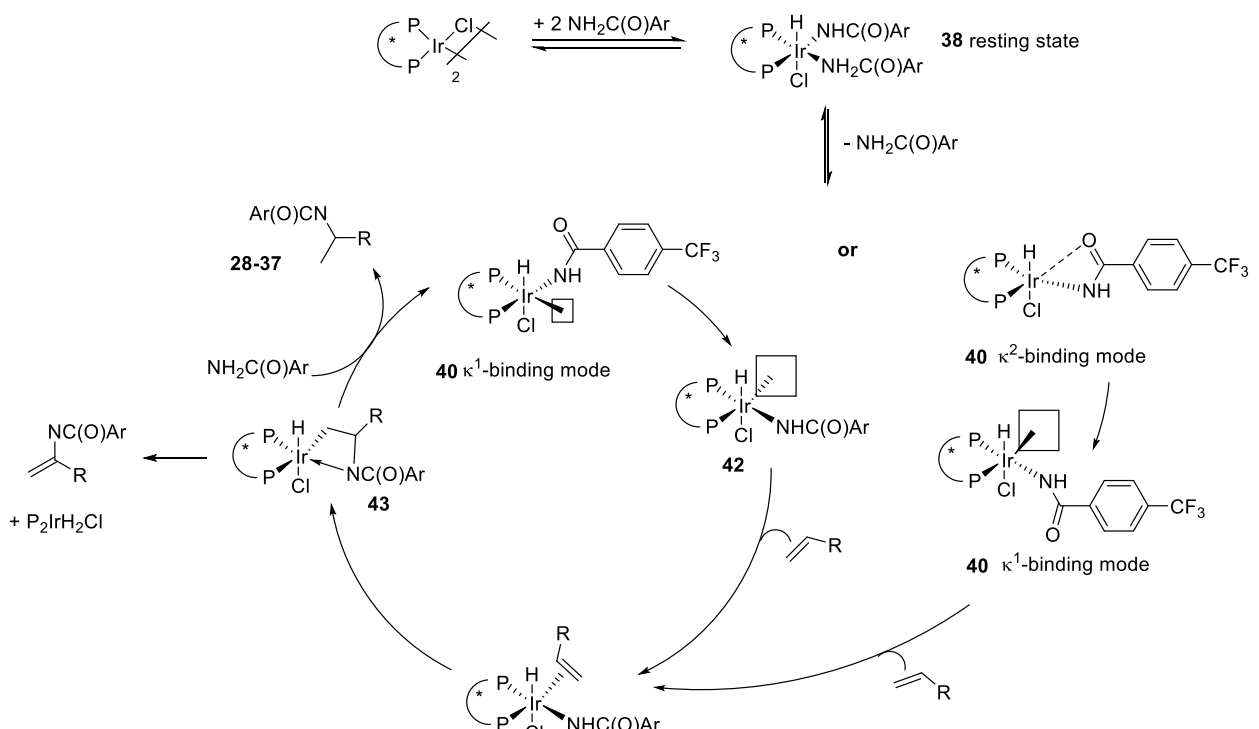
The formation of this complex **38** indicates that the reaction of Ir(I) complex with an amide starts

with an oxidative addition reaction of the N-H amide bond to the Ir(I) center. The  $^{31}\text{P}$  and  $^{19}\text{F}$  NMR data match with those observed for a complex **38** formed in a catalytic reaction at room temperature and 50 °C, which is evidencing that complex **38** is a catalyst resting state. The further reaction of 1 equivalent of the isolated **38** with 10 equivalents of norbornene at 90 °C for 1 hour afforded N-norbornylamide **39** in 94 % (96 % ee) yield (Scheme 24). When catalytic amounts of **38** were used for the same reaction, 95 % (93% ee) of N-norbornylamide was formed. Thus, these observations confirm that the observed complex **38** is a reaction intermediate in the catalytic hydroamination reaction of unactivated alkynes by amides and sulphonamides.



**Scheme 25.** Dynamic ligand exchange for **38-p-f**

Subsequent variable-temperature NMR spectroscopy experiments on a p-fluorobenzamide analogue of **38-p-f** aimed to gain information on dynamics of complex **38** were performed (Scheme 25). The Ir(III) complex **38-p-f** was mixed with 1 equivalent of free amide in toluene. Between room temperature and 60 °C an exchange between free amide and datively bonded amide was observed by  $^{19}\text{F}$  NMR spectroscopy (complex **40-p-f**). Above 60 °C slow exchange between amidate ligand and amide was detected (complex **41-p-f**). Thus, the process of the isomerisation of positions of the amidate-ligand and datively bonded amide ligand is slow, while the process of the dissociation of the neutral amide from **38-p-f** is fast. The subsequent intramolecular isomerisation could possibly reorganise the molecule in the way with more open coordination site (**40-p-f**), facilitating the subsequent olefin coordination.



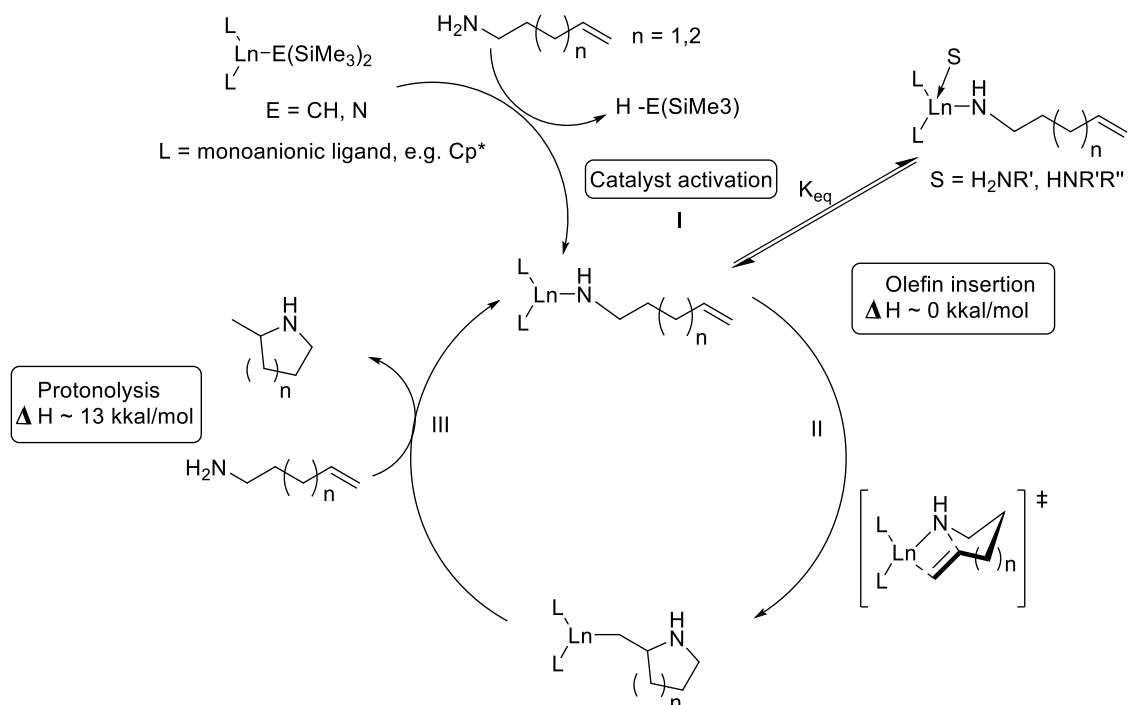
**Scheme 26.** Mechanism of catalytic hydroamination via oxidative addition of the amine.

According to these experimental evidences, the mechanism of the catalytic hydroamination via

oxidative addition of N–H bond of an arylamide was suggested (Scheme 26). On the first step of the catalytic cycle, the Ir(III) complex **38** is forming via the oxidative addition reaction of the N–H bond to the Ir(I) complex. Subsequent dissociation of the datively bonded amide ligand gives five-coordinate complex **40** with amidate ligand in the most open coordinative site of the molecule. Thus, subsequent intramolecular ligand reorganisation leads to the facile olefin coordination to the Ir(III) center. This intramolecular reorganisation could proceed either via the amidate ligand migration with formation of the unstable complex **42** with more open coordination site, either via shift of the amidate from a  $\kappa^2$  binding mode (18-electron intermediate) to a  $\kappa^1$  binding mode (16-electron intermediate). Then, alkene inserts into the Ir–N bond giving alkyliridium hydride complex **43**. Subsequent competitive C–H bond forming reductive elimination forms N-alkylamide products **28–37** and  $\beta$ -hydride elimination forms the enamide.

❖ Rare Earth Metal-Based Catalysts

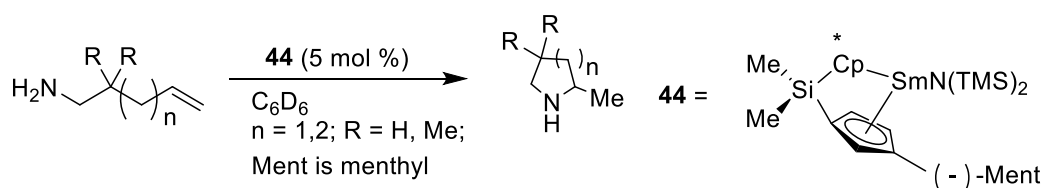
The high turnover frequencies and excellent stereoselectivity of organolanthanide complexes ( $\text{Ln} = \text{La, Nd, Sm, Dy, Er, Y, Lu}$ ) make them good candidates for the development of new hydroamination catalysts.<sup>[14]</sup> The mechanism of hydroaminations, catalyzed by organolanthanide complexes has been well studied. It is very different than the transformations catalysed by the late transition metal complexes and quite similar to the mechanisms reported for the alkaline earth metals. The major reason for it is that lanthanides have predominantly one stable oxidation state ( $3^+$ ) and therefore the oxidative addition/reductive elimination pathways are impossible, in contrast to the late-transition metals.<sup>[38]</sup> The hydroamination mechanism involves the catalyst activation by amide exchange (step I), the rate-limiting alkene insertion into Ln–N bond (step II) and the rapid protonolysis by other amine substrates with the regeneration of the active catalyst (step III) (Scheme 27).<sup>[14]</sup>



**Scheme 27.** Hydroamination of aminoalkenes with lanthanide complex catalysts.

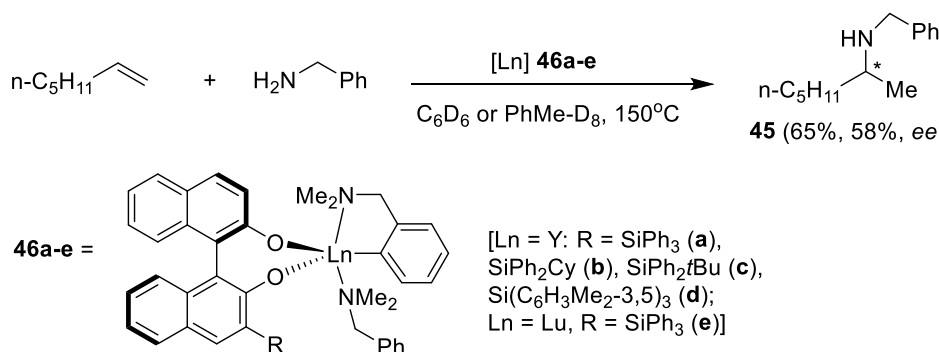
Over the last years, many successful examples of both intra- and intermolecular hydroamination reactions, catalyzed by lanthanide complexes were reported.<sup>[3]</sup> The first examples of organolanthanide-

catalyzed intramolecular hydroamination reactions of alkenes and alkynes were first described by Marks et al. in the late 1980s.<sup>[39–41]</sup>



**Scheme 28.** Hydroamination of 1-aminopent-4-ene ( $n=1$ ,  $R=H$ ) catalyzed by chiral samarium complex **44**.

The intramolecular hydroamination of 1-aminopent-4-ene ( $n=1$ ,  $R=H$ ) catalyzed by chiral samarium complex **44** gives 2-methylpyrrolidine with up to 72 % ee (Scheme 28).<sup>[38]</sup> When 1-aminohex-5-ene ( $n=2$ ,  $R=H$ ) is used, the 2-methylpiperidine is forming in the reaction. The degrees of the substrate conversion for all the reactions were more than 95 %.



**Scheme 29.** Intermolecular hydroamination catalyzed by chiral lanthanide complexes.

An example of intermolecular hydroamination was reported by Hultzsch and co-workers (Scheme 29).<sup>[42,43]</sup> Chiral yttrium and lutetium complexes catalyzed the hydroamination of non-activated alkenes with simple amines, affording Markovnikov products. The highest yields and enantiomeric excesses of the product **45** were obtained with catalyst **46a**. In summary, rare-earth metal complexes were found to be very efficient for hydroamination reactions. However, their sensitivity to oxygen and moisture has limited their application.<sup>[14]</sup>

To date, significant progress has been made in the field of catalytic hydroamination reactions. A vast diversity of catalysts has been applied for such reactions. The best results in the terms of selectivity and reaction rates were obtained with transition-metal catalysts.<sup>[5,6]</sup> However, due to the high cost of transition metals and limited natural resources, the development of an alternative to traditional transition metal based catalysts is an important challenge. Therefore, in this chapter, we will address this challenging topic using cationic Pb(II)-complexes as non-transition metal catalysts.

## **II. Results and discussion:**

- *Synthesis of cationic derivatives of plumbylenes*

Previously obtained chloroplumbylene complex **47** (Scheme 30) is a perfectly stable molecule, however it possesses a low reactivity. As we saw in the chapter 1 (section IV), the reactivity at the Pb center

in the complex could be increased dramatically by generation of the corresponding cationic plumbyliumylidene complex by removing a chloride anion (Figure 2).

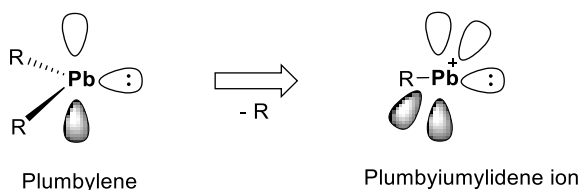
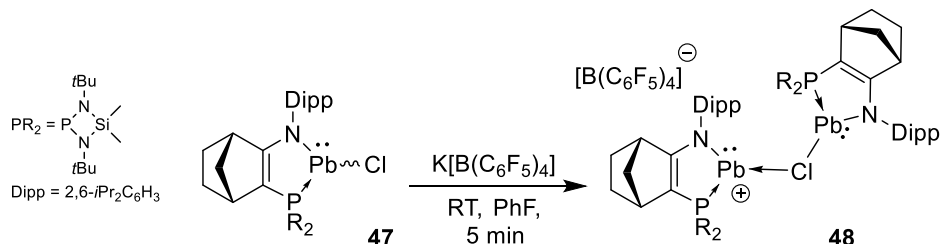


**Figure 2.** Strategy for increasing the reactivity of a plumbylene via converting it to a cationic complex (plumbyliumylidene).

The synthesis of the cationic plumbylene complex **48** was achieved via the chlorine abstraction of the corresponding chloroplumbylene complex **47** using a weakly Lewis acidic salt, such as potassium tetrakis(pentafluorophenyl)borate  $\text{K}[\text{B}(\text{C}_6\text{F}_5)_4]$  (Scheme 30). However, due to the high electrophilicity of the resulting cationic species, even with an excess amount of the Lewis acid (5 eq), the free dicoordinate  $\text{Pb}^+$  could not be obtained. Instead, the plumbyliumylidene complex **48**, stabilized by the coordination of the chlorine atom of chloroplumbylene **47** to the cationic lead center was obtained. In  $^{31}\text{P}$ -NMR spectrum, only one singlet signal at 255.5 ppm with two satellite peaks due to the  $^{207}\text{Pb}$  nuclei ( $I = \frac{1}{2}$ , natural abundance: 22 %) ( $^1J_{\text{Pb-P}} = 3755$  Hz) are observed, confirming the presence of a P-Pb-bond in the molecule. This signal is down-field shifted compared to the chloroplumbylene **47** (212 ppm,  $^1J_{\text{Pb-P}} = 3619$  Hz), probably owing to its cationic character.



**Scheme 30.** Synthesis of Plumbyliumylidene **48**.

Single crystals, suitable for XRD analysis, were obtained by José Miguel Léon Baeza, who continued this project, from saturated a fluorobenzene/pentane solution at -30 °C (Figure 3).

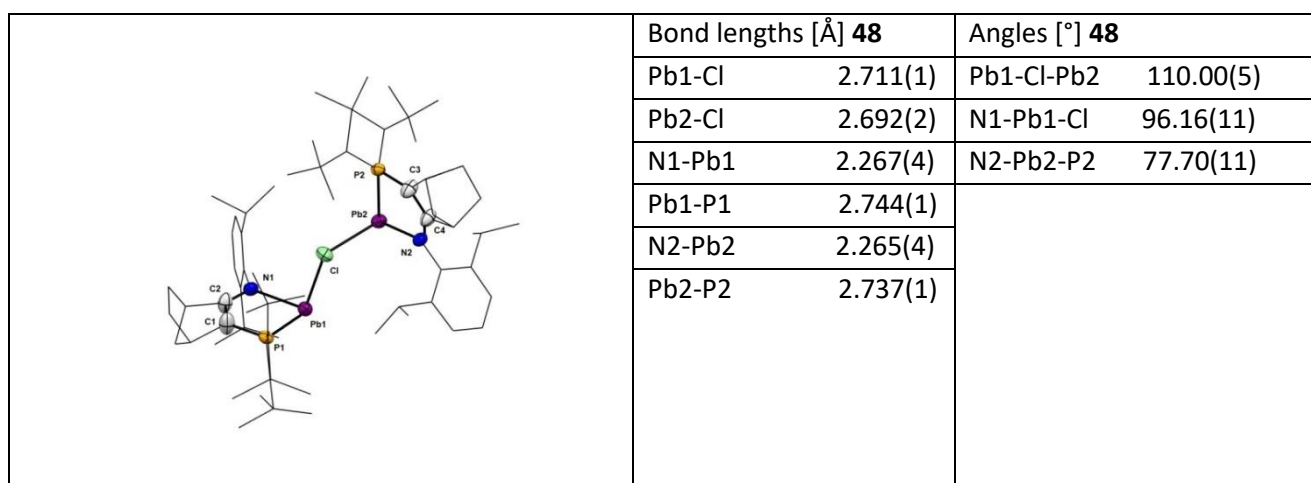


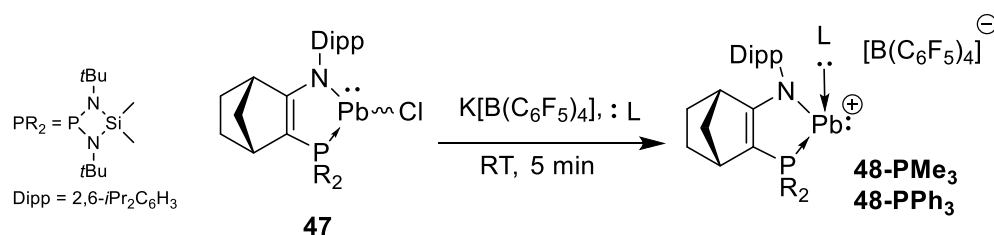
**Figure 3.** Molecular structure of **48** and selected bond lengths [ $\text{\AA}$ ] and angles [°]. Hydrogen and some distorted atoms, and counter-anions are omitted for clarity.

Due to the cationic character and the vacant p orbital on the same lead atom plumbyliumylidenes are extremely reactive and unstable. However, these Pb(II) cations can be isolated as stable complex **48-L** with an additional Lewis base ligand.

## II.I Stabilisation of plumbyliumylidenes with Lewis bases

- Cationic plumbyliumylidene stabilized by tertiary phosphines **48-PR<sub>3</sub>** (**R = Me, Ph**)

Chlorine abstraction from **47** in the presence of trimethylphosphine (PR<sub>3</sub>, R = Me), in fluorobenzene led to the formation of **48-PMe<sub>3</sub>** as an orange powder in 70 % yield (Scheme 31).



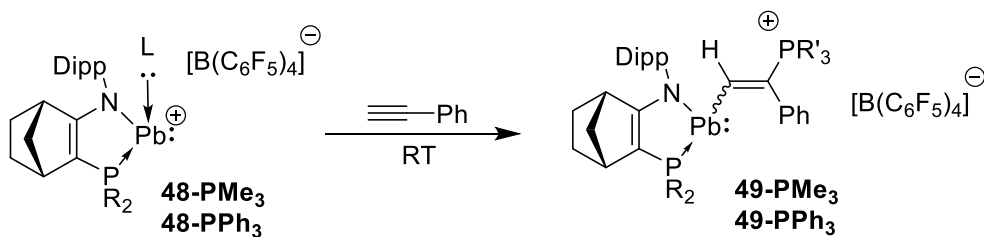
**Scheme 31.** Synthesis of cationic plumbylenes **48-PR<sub>3</sub>** (**R = Me, Ph**).

In the <sup>31</sup>P{<sup>1</sup>H} NMR spectrum at -95 °C, two AX-systems appeared at 211.6 (PR<sub>2</sub>) and 16.9 (PMe<sub>3</sub>) ppm with a <sup>2</sup>J<sub>P,P</sub> = 79.6 Hz. For both signals, satellites were observed with large lead-phosphorus coupling constants, <sup>1</sup>J<sub>Pb-P</sub> = 4017 Hz and 2622 Hz respectively, demonstrating the coordination of the two phosphorus atoms to the same lead centre. At RT, there is a broadening of these signals and they are becoming singlets with only one having lead satellites (PR<sub>2</sub>) (<sup>1</sup>J<sub>Pb-P</sub> = 3920 Hz), which suggests the labile nature of the PMe<sub>3</sub> ligand and a fast ligand-exchange. Indeed, this is confirmed by a shift of PMe<sub>3</sub> signal in the <sup>31</sup>P{<sup>1</sup>H} NMR spectrum of **48-PMe<sub>3</sub>** when an excess (3 eq) of PMe<sub>3</sub> was added to the reaction mixture. Moreover, a low-field shift (43.0 ppm) was observed, while the signals for the parent **48-PMe<sub>3</sub>** appears at 11.6 ppm and for the free trimethylphosphine at -63.6 ppm. When the excess of PMe<sub>3</sub> was removed under reduced pressure, the initial signal at 11.2 ppm was recovered. Probably due to this fast ligand-exchange the <sup>207</sup>Pb NMR signal was not observed. Thus, it suggests that the phosphine ligand is labile and could be easily replaced.

Similarly, with one equivalent of the triphenylphosphine (PPh<sub>3</sub>) in fluorobenzene the corresponding plumbyliumylidene complex **48-PPh<sub>3</sub>** was obtained as a dark red powder in 61 % yield. In the <sup>31</sup>P{<sup>1</sup>H} NMR spectrum of **48-PPh<sub>3</sub>**, similarly to the **48-PMe<sub>3</sub>** at RT, two singlet signals, appeared at 243.4 ppm (PR<sub>2</sub>) with two satellite peaks (<sup>1</sup>J<sub>Pb-P</sub> = 3778.6 Hz) and at 38.7 ppm (PPh<sub>3</sub>). It is worth noting that in contrast to the **48-PMe<sub>3</sub>**, in the case of the **48-PPh<sub>3</sub>**, these two phosphorus atoms are not coupled with each other even at -90 °C, probably as a consequence of the more labile character of PPh<sub>3</sub> ligand.

- Reactivity of complexes **48-PR<sub>3</sub>** (**R = Me, Ph**) with an alkyne.

The cationic complexes **48-PR<sub>3</sub>** (**R = Me, Ph**) were found to react with phenylacetylene at RT, affording vinyl plumbylene complexes **49-PR<sub>3</sub>** (Scheme 32).



**Scheme 32.** Reactions of complexes **48-PR<sub>3</sub>** (**R = Me, Ph**) with HC≡CPh.

When complex **48-PPh<sub>3</sub>** reacts with 1 equivalent of phenylacetylene at RT in fluorobenzene, the formation of **49-PPh<sub>3</sub>** through an insertion of acetylene into the Pb-PR<sub>3</sub> bond is observed. Phosphoniovinyll plumbylene product **49-PPh<sub>3</sub>** was isolated in good yield (60 %) as a yellow powder. It was also found that **48-PPh<sub>3</sub>** does not react with less electron-rich alkynes (HC≡CSiMe<sub>3</sub> or 1-hexyne), bulkier alkynes (Ph-C≡C-Ph, Et-C≡C-Et) or olefins (styrene, vinyltrimethylsilane). Complex **48-PMe<sub>3</sub>**, with a more electron-donating phosphine ligand, also reacts with phenylacetylene in a similar manner. According to the <sup>31</sup>P-NMR data, compound **49-PPh<sub>3</sub>** was obtained as a mixture of two diastereomers in a 60 : 40 ratio (Figure 4).

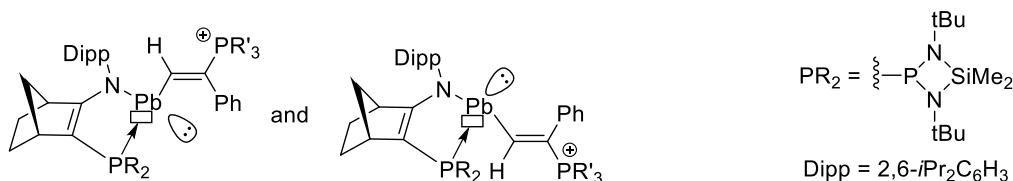


**Figure 4.** Two possible diastereomers of **49-PPh<sub>3</sub>**

For each isomer, two AX-systems are observed in the <sup>31</sup>P-NMR spectrum, confirming the presence of two types of phosphorus atoms in the molecule (phosphine ligand and phosphonio group) (table 1). The signals corresponding to the phosphine ligand (PR<sub>2</sub>) exhibit <sup>207</sup>Pb-satellite peaks with a classically large coupling constant <sup>1</sup>J<sub>Pb-P</sub> = 3655 (major) and <sup>1</sup>J<sub>Pb-P</sub> = 3627 (minor). The signals, corresponding to the PPh<sub>3</sub> moiety have also Pb-satellite peaks with smaller coupling constants (major isomer: <sup>3</sup>J<sub>Pb-P</sub> = 370 Hz, minor isomer: <sup>3</sup>J<sub>Pb-P</sub> = 362 Hz) (Figure 5).

<sup>31</sup> P- RMN	Major isomer (60 %)	Minor isomer (40 %)
Phosphine ( $\delta$ )	166.0	171.7
PPh <sub>3</sub> ( $\delta$ )	18.5	18.3
<sup>4</sup> J <sub>P-P</sub> (Hz)	10.5	10.6
<sup>1</sup> J <sub>Pb-P</sub> (Hz)	3655	3627
<sup>3</sup> J <sub>Pb-P</sub> (Hz)	370	362

**Table 1.** <sup>31</sup>P-NMR data for **49-PPh<sub>3</sub>**

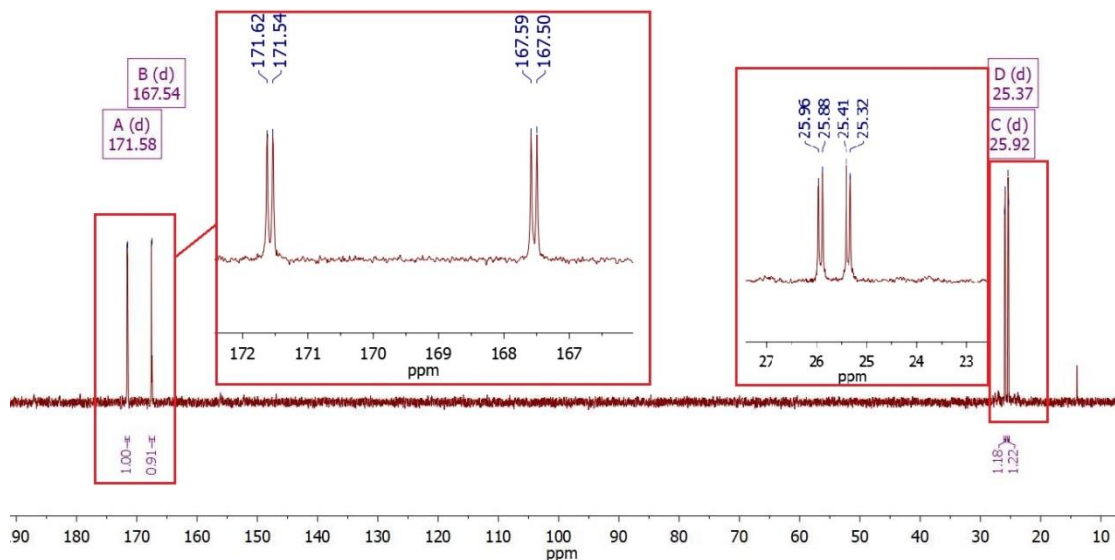


**Figure 5.**  $^{31}\text{P}$ -NMR spectrum of **49-PMe<sub>3</sub>**

The  $^{207}\text{Pb}$ -NMR spectrum displays two doublet of doublets at 1268 ppm (major) and 1799 ppm (minor), featuring the same P-Pb-coupling constants which are observed in the  $^{31}\text{P}\{\text{H}\}$ -NMR spectrum. In  $^{13}\text{C}$ -NMR spectrum, the signals corresponding to the vinyl carbon atom, bonded to Pb moiety, were observed as doublet of doublets at 239.3 ppm ( $^2J_{\text{C-P}} = 18.1$  Hz and 20.6 Hz) for major isomer and 238.7 ppm ( $^2J_{\text{C-P}} = 16.8$  Hz and 21.3 Hz) for minor isomer. The carbon atom, bonded to the phosphonio moiety was observed at higher field at 132.1 ppm ( $^1J_{\text{C-P}} = 51.7$  Hz and  $^4J_{\text{C-P}} = 8.7$  Hz) for major isomer and 132.6 ppm ( $^1J_{\text{C-P}} = 51.5$  Hz and  $^4J_{\text{C-P}} = 8.7$  Hz) for minor isomer. This shifting of the C3 carbon atom towards low field is probably due to the Pb(II) atom, bonded to it. In the  $^1\text{H}$ -NMR spectrum, the signals corresponding to the vinyl proton were observed at low field at 9.96 ppm ( $J_{\text{H-P}} = 1.8$  Hz and 35.0 Hz) and 10.0 ppm ( $J_{\text{H-P}} = 34.9$  Hz). Single crystals of **49-PPh<sub>3</sub>** suitable for X-ray diffraction analysis were obtained by the slow diffusion of a concentrated fluorobenzene solution of **49-PPh<sub>3</sub>** into a non-polar solvent (pentane) (Figure 6).

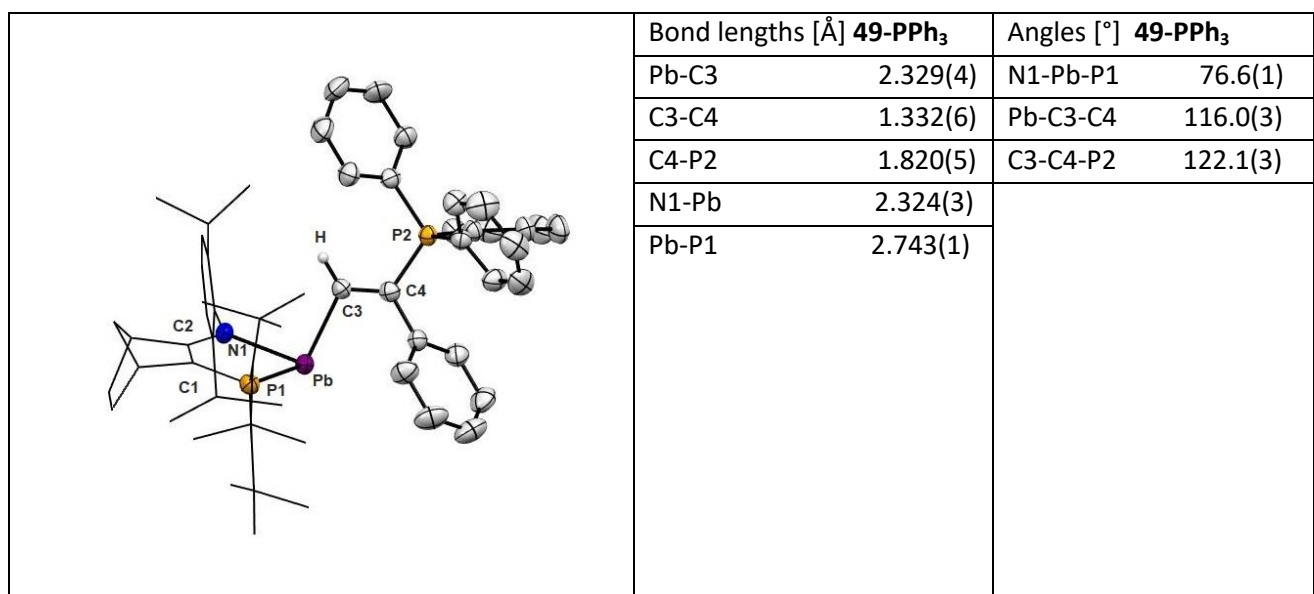
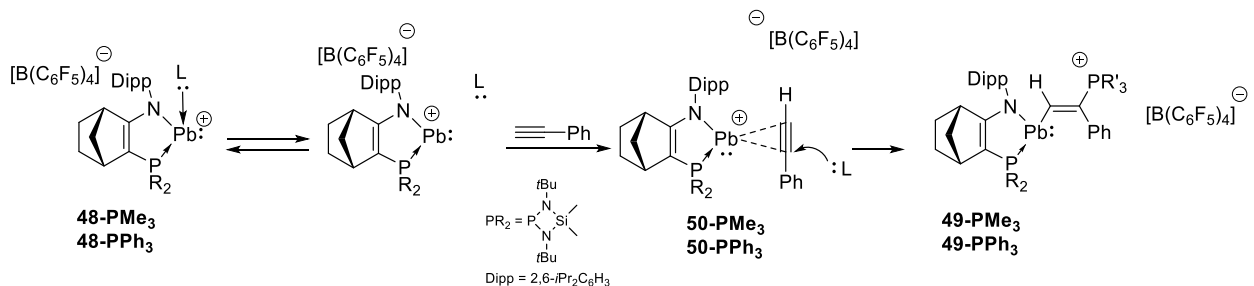


**Figure 6.** Molecular structure of **49-PPh<sub>3</sub>** and selected bond lengths [Å] and angles [°]. Hydrogen and some distorted atoms are omitted for clarity.

The structure confirms that the phenyl and phosphonio groups are attached to the  $\beta$ -position of the vinyl group. Phosphonio group possess a trans configuration relative to the Pb(II) atom. The C3-C4 bond

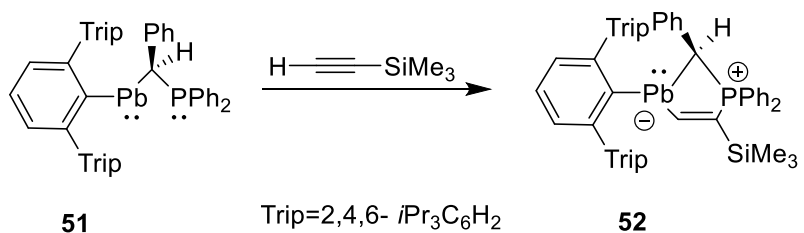
length [1.332(6) Å] is slightly shorter than the classical CC-double bond (1.34 Å). The Pb-N bond distance [2.324(3) Å] is significantly shorter compare to the Pb-N bond distance in the parent neutral tricoordinate chloroplumbylene **47** [2.3505(2) Å], however, it is still in the range of other typical Pb-N single bond lengths reported for other diaminoplumbbylenes (2.0 - 2.9 Å).<sup>[44,45]</sup> Besides, the tricoordinate lead center is strongly pyramidalized ( $\Sigma^\circ_{\text{Pb}} = 272.2^\circ$ ), suggesting the presence of the lone pair at the divalent Pb atom.



**Scheme 33.** Proposed mechanism for the alkyne insertion into Pb-P bond of **48-L** ( $L = PMe_3, PPh_3$ )

Thus, the reaction probably starts with the dissociation of the labile phosphine ligand from the Pb(II) and formation of the highly reactive free plumbyliumylidene cation. It readily reacts with phenylacetylene leading to a  $\pi$ -acetylene complex **50**, followed by the nucleophilic attack of the released phosphine on a less hindered part of the vinyl cation, affording therefore trans-vinyl plumbylene complex **49** (Scheme 33).

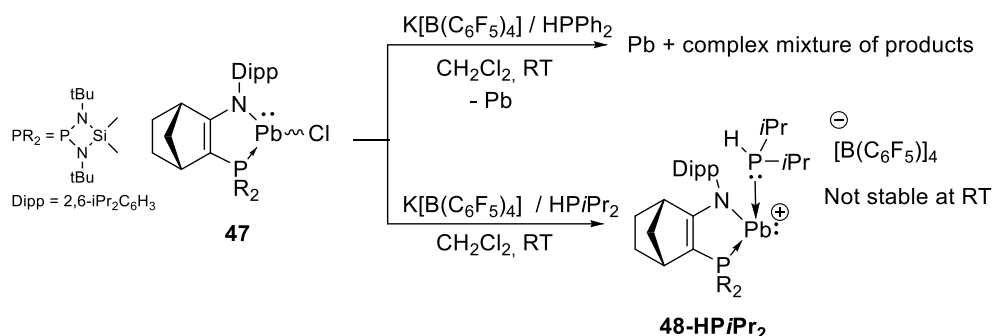
A similar alkyne insertion was reported by the group of Lars Wesemann in 2016.<sup>[46]</sup> A neutral phosphine-substituted plumbbylene **51** reacts with trimethylsilylacetylene at room temperature to give a cyclo-adduct **52** (Scheme 34). In <sup>207</sup>Pb-NMR spectrum a doublet signal was observed at 2111 ppm with a  $^3J_{\text{Pb}-\text{P}} = 52$  Hz, which is smaller than those observed with the **49-PPPh<sub>3</sub>** (major isomer:  $^3J_{\text{Pb}-\text{P}} = 370$  Hz, minor isomer:  $^3J_{\text{Pb}-\text{P}} = 362$  Hz) probably due to the cis-configuration. Similarly to **49-PPPh<sub>3</sub>**, the olefinic CH-moiety attached to Pb-atom appeared at low field at 12.31 ppm in <sup>1</sup>H-NMR spectrum and at 259.7 ppm ( $^3J_{\text{H}-\text{P}} = 74.4$  Hz) in the <sup>13</sup>C-NMR spectrum.



**Scheme 34.** Alkyne insertion into Pb-P of **51** reported by Lars Wesermann.

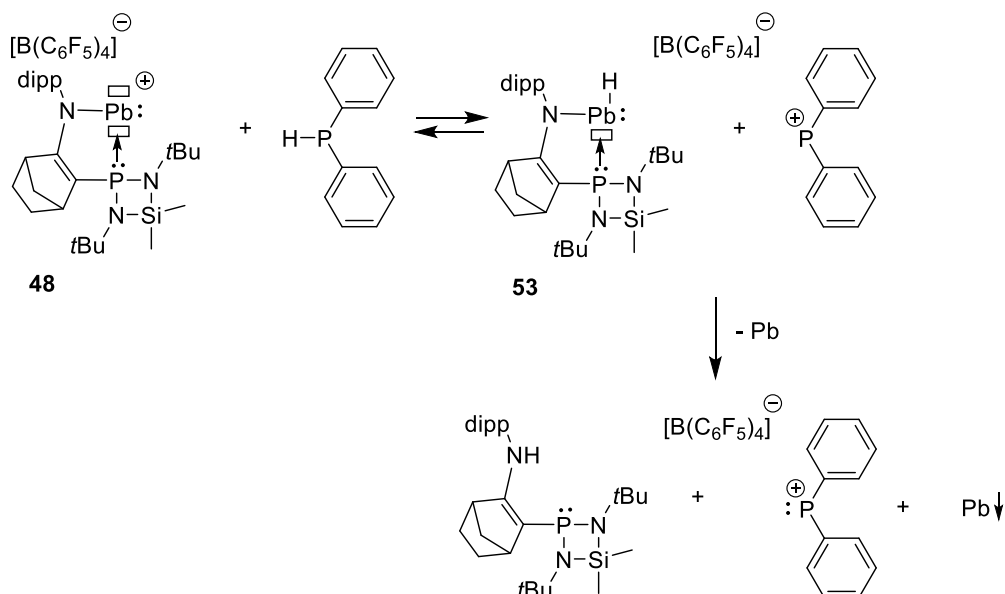
- Cationic plumbyliumylidenes stabilized by secondary phosphines **48-HPR<sub>2</sub>** ( $R = Ph, iPr$ )

The use of a secondary phosphine ligand ( $L = PHR_2$ ,  $R = Ph, iPr$ ) is more promising since it could be potentially used as hydrophosphination catalysts of alkynes. However, the reaction of chloroplumbylene **47** with diphenylphosphine  $HPPH_2$  in the presence  $K[B(C_6F_5)_4]$  at RT leads to the decomposition of the parent plumbylene and precipitation of metallic lead (Scheme 35).



**Scheme 35.** Synthesis of cationic plumbyliumylidene **48-HPiPr<sub>2</sub>**.

Probably, the initial step is the hydride abstraction by the plumbyliumylidene with the formation of an unstable lead-hydride complex **53** and the highly reactive phosphonium cation (Scheme 36). The resulting complex **53** releases metallic lead by its reductive elimination, while the protonated ligand and diphenylphosphonium cation reacts further, affording a complicated reaction mixture. Probably, the driving force of the reaction is the formation of the phosphonium cation ( $^+\text{PPh}_2$ ) which is efficiently stabilized by two phenyl substituents.

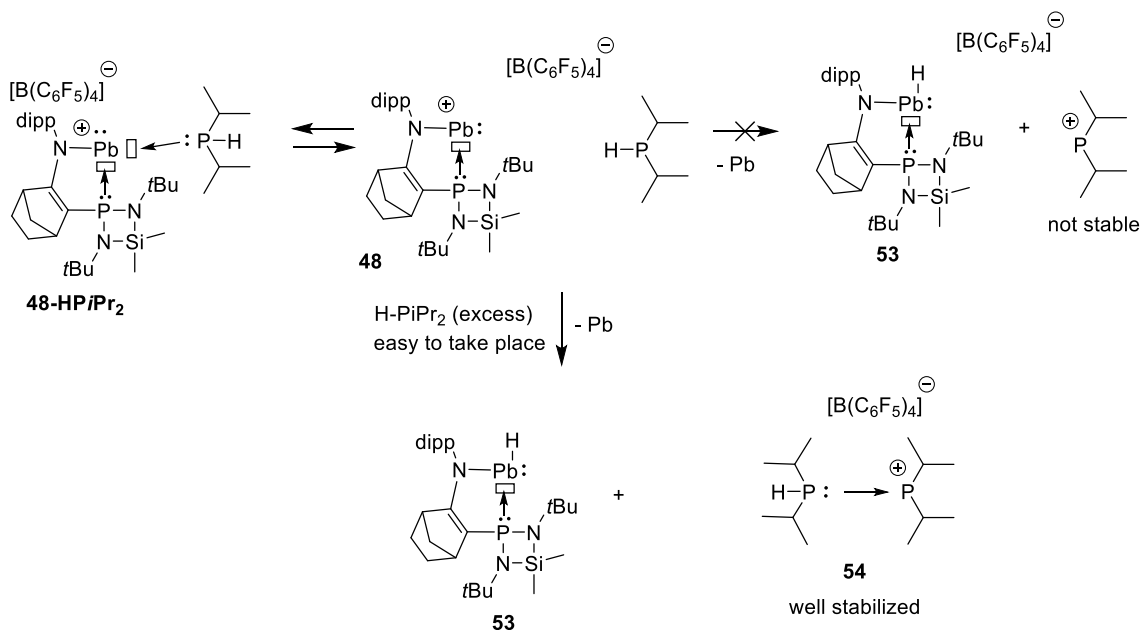


**Scheme 36.** Attempt to synthetize the **48-HPPh<sub>2</sub>** complex and its rapid decomposition.

In contrast, with diisopropylphosphine (HPiPr<sub>2</sub>), the hydride abstraction is hampered due to the instability of the resulting phosphonium cation ( $^+\text{PiPr}_2$ ). Indeed, the reaction of the plumbylene **47** with diisopropylphosphine in the presence of the  $\text{K}[\text{B}(\text{C}_6\text{F}_5)_4]$  at RT gives the desired complex **48-HPiPr<sub>2</sub>** as a dark red powder in 64 % yield (Scheme 37). In the  $^{31}\text{P}\{\text{H}\}$  spectrum two signals appeared at 213.3 ppm ( $\text{PN}_2$ ) and 51.3 ppm (HPiPr<sub>2</sub>). The  $^1\text{H-NMR}$  signal corresponding to the P-H moiety appeared as a doublet at 5.14 ppm ( $^1J_{\text{H-P}} = 312.43$  Hz).

This compound is relatively stable at RT, however, it decomposes slowly in solution, leading to the precipitation of metallic lead and formation of a complex mixture of unidentified products. It could be a consequence of the slow formation of the diisopropylphosphonium cation ( $^+\text{PiPr}_2$ ). Indeed, the use of an excess of diisopropylphosphine (HPiPr<sub>2</sub>) promotes the decomposition reaction via the hydride abstraction reaction. The excess of the HPiPr<sub>2</sub> stabilize the forming diisopropylphosphonium cation by its coordination and therefore promotes the formation of the stable phosphinephosphonium complex **54** (Scheme 37). Thus,

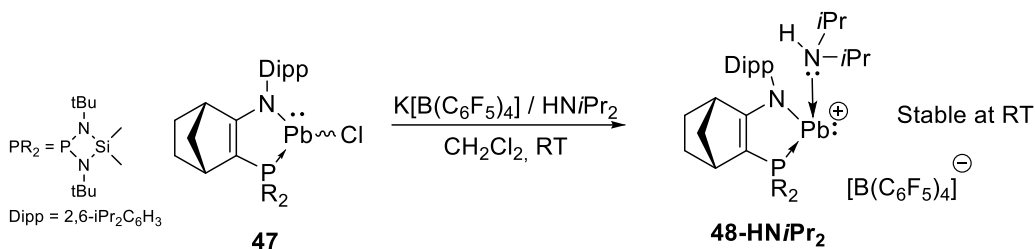
due to the instability of the **48-HP*i*Pr<sub>2</sub>** in the presence of an excess of phosphine, this model cannot be successfully applied in catalytic reactions.



**Scheme 37.** Reaction of **48** with diisopropyl phosphine

- Cationic plumbyliumylidene stabilized by secondary amines **48-HNR<sub>2</sub>** (*R* = *i*Pr)

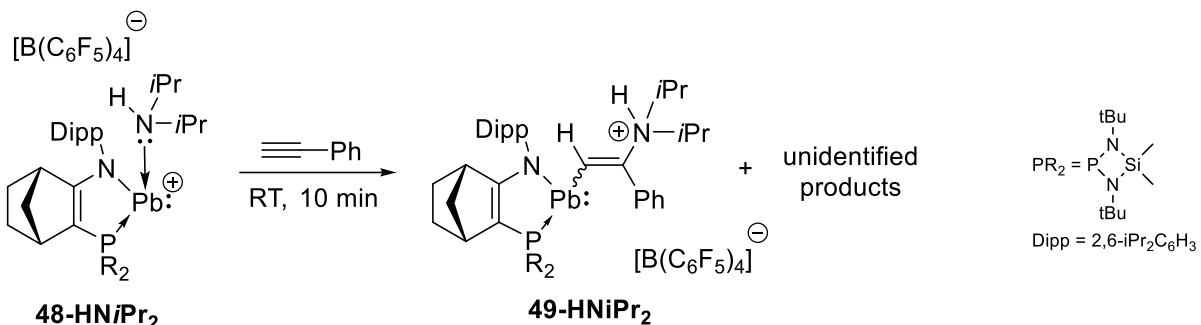
A possible strategy to overcome such problematic hydride transfer reaction is the use of secondary amines as ligands for the stabilization of the plumbyliumylidene species. Indeed, due to the inverted polarity of the N-H bond ( $N^{\delta-}H^{\delta+}$ ) and the instability of the nitrenium ion  $R_2N^+$ , the hydride transfer reaction is unlikely.



**Scheme 38.** Synthesis of the cationic plumbyliumylidene **48-HNi*i*Pr<sub>2</sub>**.

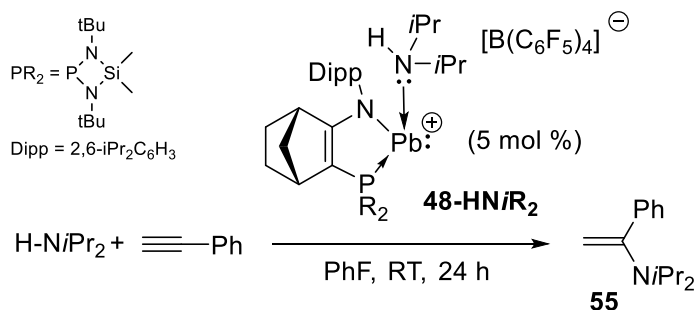
Thus, we synthesized **48-NH*i*Pr<sub>2</sub>** using the same strategy as with the other Lewis base stabilized cationic plumbylenes **48-L** (Scheme 38). As expected, compound **48-NH*i*Pr<sub>2</sub>** is stable even in the presence of an excess of amine. In the <sup>31</sup>P-NMR spectrum a singlet signal at 259.0 ppm appeared with satellites due to the <sup>207</sup>Pb atom with a typically large coupling constant  $^{1}\text{J}_{\text{P-Pb}} = 3915$  Hz. As in the previous cases, the <sup>207</sup>Pb-NMR could not be observed, probably due to the labile nature of the amine ligand. In <sup>1</sup>H-NMR spectrum the signal for CH-*i*Pr protons of the coordinated amine ligand was observed at 2.55 ppm with  $^{1}\text{J}_{\text{H-H}} = 6.3$  Hz, while the CH<sub>3</sub>-*i*Pr protons appeared at 0.67 ppm as a doublet with the same coupling constant ( $^{1}\text{J}_{\text{H-H}} = 6.3$  Hz). Thus, the shifts for the coordinated NH*i*Pr<sub>2</sub> in <sup>1</sup>H-NMR are slightly shifted to the high field compared to free diisopropylamine (CH-*i*Pr m, 2.70, CH<sub>3</sub>-*i*Pr 0.95, d,  $^{1}\text{J}_{\text{H-H}} = 5.0$  Hz) due to its coordination to the metal center.

- Reactivity of complex **48-NHiPr<sub>2</sub>** with alkynes.



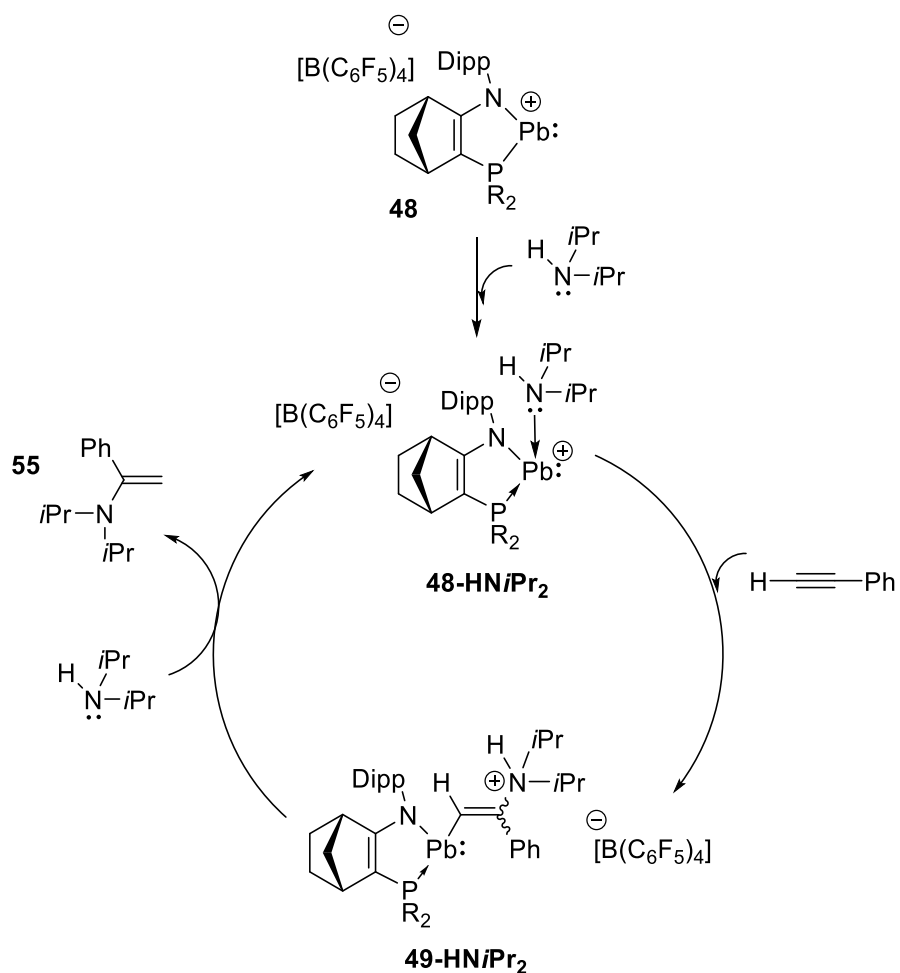
Scheme 39. Reaction of **48-NHiPr<sub>2</sub>** with  $\text{HC}\equiv\text{CPh}$ .

Similarly to the complex **48-PPh<sub>3</sub>**, **48-NHiPr<sub>2</sub>** readily reacts with 1 equivalent of phenylacetylene, giving the vinyl-plumbylene product **49-NHiPr<sub>2</sub>** with several unidentified products (Scheme 39). Indeed, the insertion reaction of the acetylene into Pb-N bond was observed by NMR spectroscopy. The <sup>31</sup>P-NMR spectrum of **49-NHiPr<sub>2</sub>** displays a singlet signal at 176.1 ppm with two satellites due to the lead atom (<sup>1</sup>J<sub>PbP</sub> = 2404 Hz). This signal appears at low field in the same region as the phosphine analogues discussed above (166 - 171 ppm). With an excess of diisopropylamine (10 eq), the signal of the parent **48-NHiPr<sub>2</sub>** appeared in the <sup>31</sup>P-NMR spectrum, suggesting a metathesis reaction. Indeed, it was found that the regioselective hydroamination of phenylacetylene could be catalysed by **48-NHiPr<sub>2</sub>** (5 mol %) (Scheme 40). However, the yield of the reaction remains low (< 22%), even after optimisation of the reaction, probably due to undesired side-reactions, which are killing the catalyst.



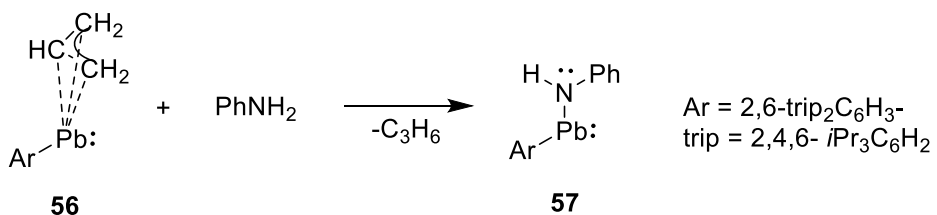
Scheme 40. Hydroamination of phenylacetylene catalyzed by **48-NHiPr<sub>2</sub>**.

The catalytic cycle starts with the generation of the **48-NHiPr<sub>2</sub>** via the coordination of diisopropylamine to the cationic plumbyliumylidene **48**. Then, the insertion of the phenylacetylene into Pb-N bond affords complex **49-NHiPr<sub>2</sub>** which then regenerate the active catalyst **48-NHiPr<sub>2</sub>** through a metathesis reaction with another equivalent of the amine, leading to the hydroamination product **55** in this last step (Scheme 41).



**Scheme 41.** Proposed catalytic cycle for the hydroamination of phenylacetylene catalyzed by the cationic plumbyliumlidene complex **48-HNiPr<sub>2</sub>**.

A similar Pb-C/N-H bond metathesis was reported in 2019 by the group of Lars Wesemann,<sup>[47]</sup> when the neutral allyl-plumbylene **56** reacts with aniline in C<sub>6</sub>D<sub>6</sub> (Scheme 42). After 24 h the formation of the monomeric plumbylene **57** was detected.

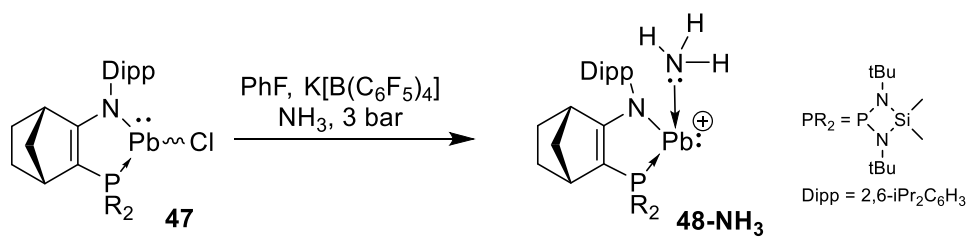


**Scheme 42.** Reaction of the allyl-plumbylene **56** with aniline

- Cationic c stabilized by ammonia **48-NH<sub>3</sub>**

Inspired by the previous results we considered the synthesis of the cationic plumbyliumlidene stabilized by ammonia **48-NH<sub>3</sub>**. To date, the hydroamination of abundant non-activated multiple bonded species with ammonia, the simplest amine, is considered as a Holy Grail in chemistry. However, even for transition metals such reactions remain limited.<sup>[48]</sup> Thus, we generated the cationic plumbyliumlidene **48** via chlorine abstraction from **47** with K[B(C<sub>6</sub>H<sub>5</sub>)<sub>4</sub>] and 3 bar of the ammonia were added at -30 °C to

synthesize complex **48-NH<sub>3</sub>** (Scheme 43). As expected, the <sup>31</sup>P-NMR spectrum of this compound displays a singlet signal at 217 ppm with two satellite signals due to the <sup>207</sup>Pb nuclei (<sup>1</sup>J<sub>Pb-P</sub> = 3985 Hz (Figure 7).



**Scheme 43.** Synthesis of the cationic plumbyliumylidene stabilized by ammonia **48-NH<sub>3</sub>**

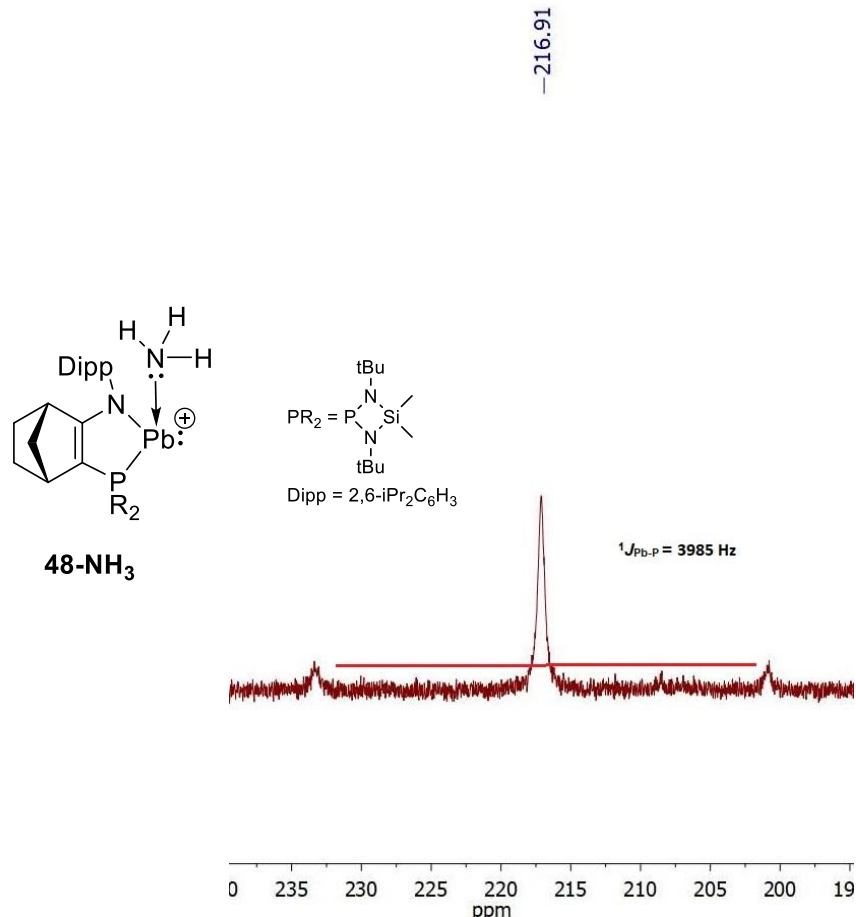
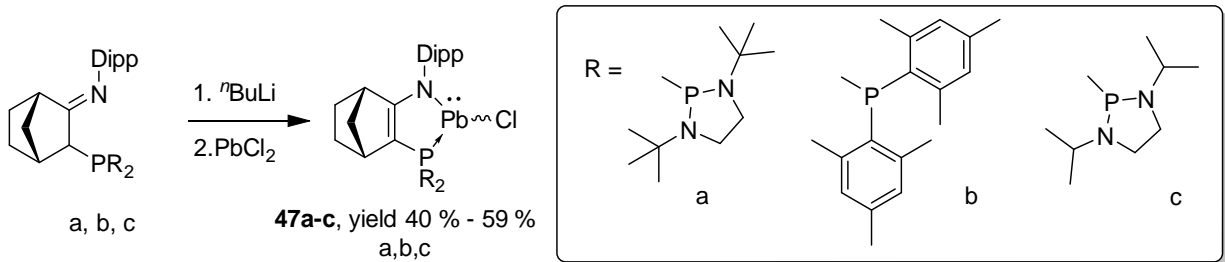


**Figure 7.** <sup>31</sup>P-NMR of **48-NH<sub>3</sub>**

However, when phenylacetylene was added to the freshly generated **48-NH<sub>3</sub>** no reaction was observed. Even after heating 2 h at 60 °C, we didn't observe any conversion. Probably, it could be a consequence of the bulky ligand system, which hampered the insertion of the acetylene moiety into the Pb-N bond of the **48-NH<sub>3</sub>**. Complex **48-NH<sub>3</sub>** is unstable at room temperature and decomposes after 1 night but it can be stored in solution under an inert atmosphere at -45 °C for three days.

Thus, several phosphine-stabilized chloroplumbbylenes featuring less hindered phosphines (**a**, **b**, **c**) have been prepared following the synthetic strategy already established in our group (Scheme 44). The deprotonation of the corresponding iminophosphine ligands by *n*-BuLi followed by addition of PbCl<sub>2</sub> in THF affords the corresponding chloroplumbbylenes **47a-c** in moderate yields (59 % for **47a**, 40 % for **47b**, 47 % for **47c**). These models are very fragile and start to decompose after one night in the glovebox at -30 °C.



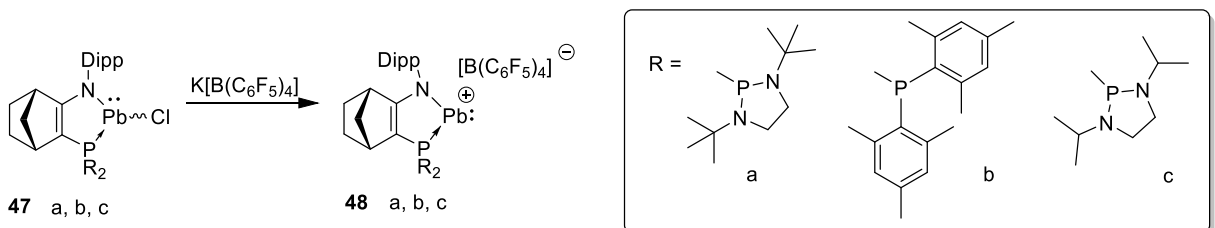
**Scheme 44.** Synthesis of plumbylenes **47a-c**.

$^{31}\text{P}\{^1\text{H}\}$ RMN	<b>47a</b>	<b>47b</b>	<b>47c</b>
Phosphine ( $\delta$ ) (ppm)	209	60	207
$^1J_{\text{Pb-P}}$ (Hz)	3807	2247	3916

**Table 2.**  $^{31}\text{P}\{^1\text{H}\}$  NMR of **47a-47c**

In the  $^{31}\text{P}\{^1\text{H}\}$  NMR spectrum, models **47a** and **47c** appears as singlets at 209 and 207 ppm with large  $^1J_{\text{Pb-P}}$  coupling constants (3807 and 3916 Hz) similarly to complex **47** (table 2). In contrast, the signal for plumbylene **47b** appears at higher field (60 ppm). Probably due to the electron deshielding of the phosphorus, caused by the presence of two nitrogen atoms, the chemical shifts of **47a** and **47c** in the  $^{31}\text{P}\{^1\text{H}\}$  NMR spectra appear at higher field, than in the case of **47b**. In this latter case such deshielding does not occur due to the absence of the nitrogen atoms in the ligand scaffold.

Once we obtained plumbylenes **47a-47c**, their cationic derivatives were prepared following the initial synthetic strategy used for **48** (Scheme 45). Thus, plumbylenes **47a-47c** were mixed with one equivalent of  $\text{K}[\text{B}(\text{C}_6\text{H}_5)_4]$  in fluorobenzene, and immediately the colour of the solutions was turned dark-red. In the  $^{31}\text{P}$ -NMR spectrum singlet signals featuring satellites, due to the P-Pb-coupling constant, were observed at lower field (table 3).

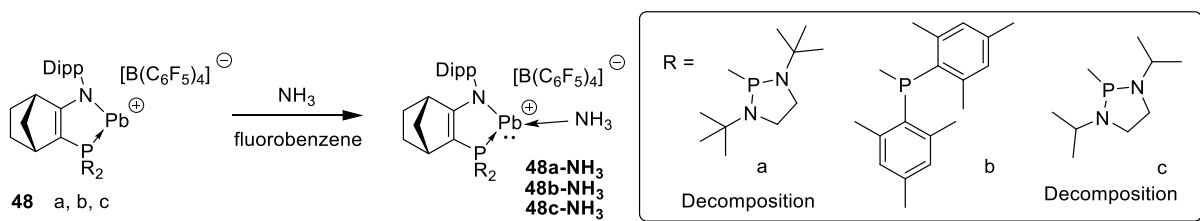


**Scheme 45.** Synthesis of cationic plumbyliumylidenes **48a-c**.

$^{31}\text{P}\{^1\text{H}\}$ RMN	<b>48a</b>	<b>48b</b>	<b>48c</b>
Phosphine ( $\delta$ ) (ppm)	251	97	252
$^1J_{\text{Pb-P}}$ (Hz)	3773	2487	3523

**Table 3.**  $^{31}\text{P}\{^1\text{H}\}$  NMR of **48a-c**

In the next step these plumbyliumylidenes were reacted with 3 bars of  $\text{NH}_3$  (Scheme 46). However, models **48a** and **48c** appeared to be very fragile and readily decompose as indicated by the immediate formation of a big amount of white precipitate and colour change from dark-red to pale yellow. Moreover, the  $^{31}\text{P}$ -NMR analysis of the mixture indicates the complete decomposition of **48a** and **48c** even at  $-30^\circ\text{C}$ . In contrast, **48b** cleanly reacts with  $\text{NH}_3$  leading to cationic plumbyliumylidene **48b-NH3**, and in the  $^{31}\text{P}$ -NMR spectrum a signal appeared at 48 ppm with lead-satellites with a large coupling constant ( $^1J_{\text{Pb-Pb}} = 1486$  Hz).



**Scheme 46.** Reaction of the cationic plumbylumidenes **48a-c** with 3 bar of ammonia.

Thus, the reaction of model **48b-NH<sub>3</sub>** was tested with alkynes. However, similarly to **48-NH<sub>3</sub>**, when 1 equivalent of phenylacetylene was added to **48b-NH<sub>3</sub>**, no clean reaction was observed after heating at 80 °C for 1.5 hours, and instead some unidentified products of decomposition were formed. Thus, we conclude that for successful hydroamination reactions with ammonia catalyzed by our catalytic system we need to find other better models.

### III. Conclusions and perspectives

In this chapter we have reported the synthesis of a new phosphine-stabilized plumbylumylidene **48**. This cationic species is extremely electrophilic and thus, must be stabilized by coordination of various Lewis-base ligands. However, despite the stabilization of the plumbylumylidene cation by two ligands, it remains reactive and readily reacts with phenylacetylene through an alkyne insertion into Pb-L bond. Notably, the amine-adduct **48-HNiPr<sub>2</sub>** could be applied as a catalyst for the hydroamination of phenylacetylene. However, our attempts to perform hydroaminations of unsaturated compounds with ammonia were fruitless for the moment. Hence, future work is directed to the possible application of the cationic lead complex **48** in catalysis.

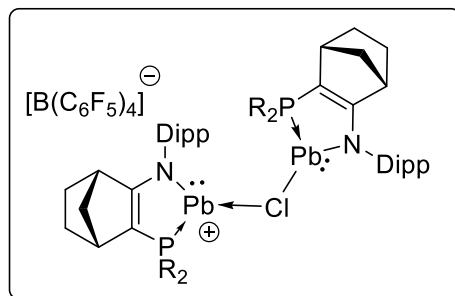
## **Bibliographic references**

- [1] K. C. Hultzsch, *Adv. Synth. Catal.* **2005**, 347, 367–391.
- [2] J. Seayad, A. Tillack, C. G. Hartung, M. Beller, *Adv. Synth. Catal.* **2002**, 344, 795–813.
- [3] I. P. Beletskaya, C. Nájera, M. Yus, *Russ. Chem. Rev.* **2020**, 89 (2), 250–274.
- [4] F. Pohlki, S. Doye, *Chem. Soc. Rev.* **2003**, 32, 104–114.
- [5] I. P. Beletskaya, C. Nájera, M. Yus, *Russ. Chem. Rev.* **2021**, 90, 70–93.
- [6] Irina P. Beletskaya et al., *Russ. Chem. Rev.* **2020**, 89, 250–274.
- [7] W. Hölderich, M. Hesse, F. Näumann, *Angew. Chem. - Int. Ed. English* **1988**, 27, 226–246.
- [8] W. D. D. M. Volker Dr. Taglieber, Wolfgang Dr. Hoelderich, Rudolf Dr. Kummer, *Process for Preparing Amines*, **1986**.
- [9] W. D. D. M. Volker Dr. Taglieber, Wolfgang Dr. Hoelderich, Rudolf Dr. Kummer, *Process for the Manufacture of Amines*, **1991**.
- [10] W. D. D. M. Volker Dr. Taglieber, Wolfgang Dr. Hoelderich, Rudolf Dr. Kummer, *Process for the Production of Amines*, **1987**.
- [11] T. H. Kehrer, *CATALYSTS AND METHOD FOR THE HYDROAMINATION OF OLEFINS*, **2013**.
- [12] L. L. Anderson, J. Arnold, R. G. Bergman, *J. Am. Chem. Soc.* **2005**, 127, 14542–14543.
- [13] J. Penzien, R. Q. Su, T. E. Müller, *J. Mol. Catal. A Chem.* **2002**, 182–183, 489–498.
- [14] T. E. Müller, K. C. Hultzsch, M. Yus, F. Foubelo, M. Tada, *Chem. Rev.* **2008**, 108, 3795–3892.
- [15] B. Schlummer, J. F. Hartwig, *Org. Lett.* **2002**, 4, 1471–1474.
- [16] G. P. Pez, J. E. Galle, *Pure Appl. Chem.* **1985**, 57, 1917–1926.
- [17] B. W. Howk, E. L. Little, S. L. Scott, G. M. Whitman, *J. Am. Chem. Soc.* **1954**, 76, 1899–1902.
- [18] E. S. Sa, H. Lehmkuhl, D. R. Mdheimfruhr, M. Kohlenforsehung, **1973**, 55, 215–220.
- [19] M. Belier, C. Breindl, *Tetrahedron* , **1998**, 54, 6359–6368.
- [20] S. Germain, M. Lecoq, E. Schulz, J. Hannedouche, *ChemCatChem* **2017**, 9, 1749 –1753
- [21] P. W. Roesky, T. E. Müller, *Angew. Chem. - Int. Ed.* **2003**, 42, 2708–2710.
- [22] J. S. Johnson, R. G. Bergman, *J. Am. Chem. Soc.* **2001**, 123, 2923–2924.
- [23] J. L. Polse, R. A. Andersen, R. G. Bergman, *J. Am. Chem. Soc.* **1998**, 120, 51, 13405–13414.
- [24] T. E. Mu, M. Berger, M. Grosche, E. Herdtweck, F. P. Schmidtchen, *Organometallics* **2001**, 4384–4393.
- [25] Björn Åkermark, Jan E. Bäckvall, Kirsti Siirala-Hanseen, Kjell Sjöberg, Krister Zetterberg *Tetrahedron Lett.* **1974**, 15, 1363–1366.
- [26] H. M. Senn, P. E. Blo, E. T. H. Zentrum, C.- Zu, *J. Am. Chem. Soc.* **2000**, 122, 4098–4107.
- [27] O. Jimenez, T. E. Müller, C. Sievers, A. Spirk, J. A. Lercher, *Chem. Commun.* **2006**, 2974–2976.
- [28] J. Pawlas, Y. Nakao, M. Kawatsura, J. F. Hartwig, *J. Am. Chem. Soc.* **2002**, 124, 3669–3679.
- [29] O. Löber, M. Kawatsura, J. F. Hartwig, *J. Am. Chem. Soc.* **2001**, 123, 4366–4367.
- [30] P. Pii, O. Resources, M. Chemistry, C. R. Science, **1997**, 38, 6071–6074.
- [31] M. Meguro, Y. Yamamoto, *Tetrahedron Letters*, **1998**, 39, 5421–5424.
- [32] Norio Sakai, André Ridder, and John F. Hartwig, *J. Am. Chem. Soc.*, **2006**, 128, 25, 8134–8135.
- [33] M. Kawatsura, J. F. Hartwig, *J. Am. Chem. Soc.* **2000**, 122, 9546–9547.
- [34] J. F. Hartwig, *Pure Appl. Chem.* **2004**, 76, 507–516.
- [35] U. Nettekoven, J. F. Hartwig, *J. Am. Chem. Soc.* **2002**, 124, 1166–1167.
- [36] C. Sievers, O. Jiménez, R. Knapp, X. Lin, T. E. Müller, A. Türler, B. Wierczinski, J. A. Lercher, *J. Mol. Catal. A Chem.* **2008**, 279, 187–199.
- [37] C. S. Sevov, J. Zhou, J. F. Hartwig, *J. Am. Chem. Soc.* **2012**, 136, 3200–3207.
- [38] S. Hong, T. J. Marks, *Acc. Chem. Res.* **2004**, 37, 673–686.
- [39] H. F. Yuen, T. J. Marks, *Organometallics* **2009**, 28, 2423–2440.
- [40] Michel R. Gagne and Tobin J. Marks, *J. Am. Chem. Soc.* **1989**, 111, 11, 4108–4109.
- [41] J. S. Ryu, T. J. Marks, F. E. McDonald, *J. Org. Chem.* **2004**, 69, 1038–1052.
- [42] A. L. Reznichenko, H. N. Nguyen, K. C. Hultzsch, *Angew. Chem. Int. Ed.*, **2010**, 49, 8984–8987.
- [43] A. L. Reznichenko, K. C. Hultzsch, *Organometallics*, **2013**, 32, 5, 1394–1408.
- [44] T. Lin, G. Lee, S. Peng, C. Chiu, H. Chen, *Polymer* **2019**, 180, 121748 [45] R. Guthardt, J. Oetzel, J. I. Schweizer, C. Bruhn, R. Langer, M. Maurer, J. Vícha, P. Shestakova, M. C.

- Holthausen, U. Siemeling, *Angew. Chem. - Int. Ed.* **2019**, *58*, 1387–1391.
- [46] J. Schneider, K. M. Krebs, S. Freitag, K. Eichele, H. Schubert, L. Wesemann, *Chem.Eur.J.*, **2016**, *22*, 9812–9826.
- [47] S. Weiß, M. Auer, K. Eichele, H. Schubert, L. Wesemann, *Organometallics* **2019**, *38*, *2*, 417–423.
- [48] S. Streiff, F. Jérôme, *Chem. Soc. Rev.* **2021**, *50*, 1512–1521.

## **Experimental part**

Synthesis of cationic derivative of plumbylene **48**:



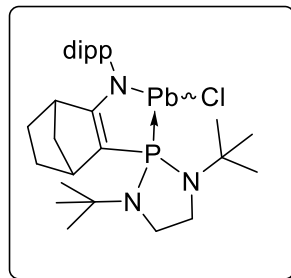
Chloroplumbylene **47** (100 mg, 0.134 mmol) was dissolved 3.5 ml of fluorobenzene inside the glovebox. K[B(C<sub>6</sub>F<sub>5</sub>)<sub>4</sub>] (98 mg, 0.134 mmol) was added to a solution and then stirred for 5 minutes at RT. The dark-red solution was filtrated inside the glovebox in order to eliminate the potassium salts. After washing the product with pentane, the product was obtained as dark red powder (138 mg, yield = 74 %). Mp: 159–163 °C (decomp.).

**<sup>1</sup>H NMR (400 MHz, CDCl<sub>3</sub>, 25 °C):** 0.57 (s br, 3H, SiCH<sub>3</sub>), 0.61 (s br, 3H, SiCH<sub>3</sub>), 1.11 (d, <sup>1</sup>J<sub>HH</sub> = 6.7 Hz, 3H CH<sub>3*i*Pr</sub>), 1.16 (d, <sup>1</sup>J<sub>HH</sub> = 6.7 Hz, 3H CH<sub>3*i*Pr</sub>), 1.20 (d, <sup>1</sup>J<sub>HH</sub> = 6.6 Hz, 3H CH<sub>3*i*Pr</sub>), 1.33 (s, 9H, CH<sub>3*t*Bu</sub>), 1.34 (s, 9H, CH<sub>3*t*Bu</sub>), 1.45 (m, 3H CH<sub>3*i*Pr</sub>), 1.71 (m, 3H, CH<sub>2</sub>), 1.91 (m, 1H, CH<sub>2</sub>), 2.27 (m, 1H, CH<sub>2</sub>), 2.51 (s, 1H, CH<sub>bridgehead</sub>), 3.04 (s, 1H, CH<sub>bridgehead</sub>), 3.15 (m, 2H, CH<sub>*i*Pr</sub>), 7.15 (m, 3H, CH<sub>Ar</sub>).

**<sup>13</sup>C NMR (102 MHz, C<sub>6</sub>D<sub>6</sub>, 25 °C):** **<sup>13</sup>C NMR (75 MHz, C<sub>6</sub>D<sub>6</sub>, 25 °C):** 4.3 (s, SiCH<sub>3</sub>), 7.62 (d, *J*<sub>CP</sub> = 5.6 Hz, SiCH<sub>3</sub>), 23.9 (s, CH<sub>3*i*Pr</sub>), 24.4 (s, CH<sub>3*i*Pr</sub>), 25.5 (s, CH<sub>2</sub>), 26.1 (s, CH<sub>3*i*Pr</sub>), 26.6 (s, CH<sub>3*i*Pr</sub>), 27.4 (s, CH<sub>*i*Pr</sub>), 27.6 (s, CH<sub>*i*Pr</sub>), 28.8 (s, CH<sub>2</sub>), 33.2 (d, *J*<sub>CP</sub> = 4.5 Hz, CH<sub>3*t*Bu</sub>), 33.4 (d, *J*<sub>CP</sub> = 4.9 Hz, CH<sub>3*t*Bu</sub>), 43.5 (d, *J*<sub>CP</sub> = 5.8 Hz, CH<sub>bridgehead</sub>), 43.9 (d, *J*<sub>CP</sub> = 11.4 Hz, CH<sub>bridgehead</sub>), 48.0 (d, *J*<sub>CP</sub> = 4.3 Hz, CH<sub>2</sub>), 50.0 (d, *J*<sub>CP</sub> = 3.5 Hz, C<sub>*t*Bu</sub>), 51.0 (d, *J*<sub>CP</sub> = 2.7 Hz, C<sub>*t*Bu</sub>), 122.2 (m, CP), 123.9 (s, CH<sub>Ar</sub>), 124.0 (s, CH<sub>Ar</sub>), 126.1 (s, CH<sub>Ar</sub>), 143.0 (s, NC<sub>Ar</sub>), 145.0 (s, C<sub>Ar</sub>*i*Pr), 145.1 (s, C<sub>Ar</sub>*i*Pr), 189.4 (d, *J*<sub>CP</sub> = 33.8 Hz, CN).

**<sup>31</sup>P{<sup>1</sup>H} NMR (162 MHz, CDCl<sub>3</sub>, 25 °C):** 252.3 (s, PN<sub>2</sub>)

Synthesis of the chloroplumbbylene **47a**



To a solution of iminophosphine (**a**) (300 mg, 0.64 mmol) in THF (3 ml) was added dropwise a solution of nBuLi 1.6 M in hexane (0.44 ml, 0.70 mmol) at -78°C. The solution was slowly warmed to RT and stirred for 1 h and added to a flask containing suspension of PbCl<sub>2</sub> (178 mg, 0.15 mmol) in THF. The resulting solution was warmed up to room temperature and stirred for 1 h, and then the solvent was removed under vacuum. Product was extracted with DCM. After washing with toluene, the product was obtained as pale yellow powder (268 mg, 59 %).

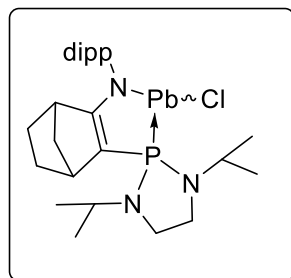
**<sup>1</sup>H NMR (500 MHz, CDCl<sub>3</sub>, 25 °C):** 1.16 (d, <sup>1</sup>J<sub>HH</sub> = 6.9 Hz, 3H, CH<sub>3*i*Pr</sub>), 1.21 (d, <sup>1</sup>J<sub>HH</sub> = 6.5 Hz, 3H, CH<sub>3*i*Pr</sub>), 1.23 (d, <sup>1</sup>J<sub>HH</sub> = 6.2 Hz, 3H, CH<sub>3*i*Pr</sub>) 1.31 (d, <sup>1</sup>J<sub>HH</sub> = 6.8 Hz, 3H, CH<sub>3*i*Pr</sub>), 1.34 (m, 1H, CH<sub>2</sub>), 1.42 (s, 9H, CH<sub>3*t*Bu</sub>), 1.46 (s, 9H, CH<sub>3*t*Bu</sub>), 1.62 (m, 1H, CH<sub>2</sub>), 1.73 (m, 1H, CH<sub>2</sub>), 1.83 (m, 1H, CH<sub>2</sub>), 2.06 (m, 1H, CH<sub>2</sub>), 2.47 (s, 1H, CH<sub>bridgehead</sub>), 2.98 (s, 1H, CH<sub>bridgehead</sub>), 3.18 (m, 2H, CH<sub>2</sub>), 3.25 (m, 1H, CH<sub>*i*Pr</sub>), 3.52 (m, 1H, CH<sub>2</sub>), 3.58 (m, 1H, CH<sub>*i*Pr</sub>), 3.76 (m, 1H, CH<sub>2</sub>), 7.17 (m, 3H, CH<sub>Ar</sub>).

**<sup>13</sup>C NMR (126 MHz, CDCl<sub>3</sub>, 25 °C):** 23.9 (s, CH<sub>3*i*Pr</sub>), 24.8 (s, CH<sub>3*i*Pr</sub>), 25.2 (s, CH<sub>2</sub>), 25.7 (s, CH<sub>3*i*Pr</sub>), 26.3 (s, CH<sub>3*i*Pr</sub>), 27.1 (s, CH<sub>*i*Pr</sub>), 27.5 (s, CH<sub>*i*Pr</sub>), 29.6 (d, J<sub>CP</sub> = 4.4 Hz, CH<sub>3*t*Bu</sub>), 30.2 (d, J<sub>CP</sub> = 3.2 Hz, CH<sub>3*t*Bu</sub>), 43.5 (d, J<sub>CP</sub> = 12.4 Hz, CH<sub>bridgehead</sub>), 44.1 (s, CH<sub>2</sub>), 44.3 (d, J<sub>CP</sub> = 7.0 Hz, CH<sub>bridgehead</sub>), 45.0 (d, J<sub>CP</sub> = 2.6 Hz, CH<sub>2</sub>), 48.2 (d, J<sub>CP</sub> = 4.4 Hz, CH<sub>2</sub>), 52.9 (d, J<sub>CP</sub> = 6.1 Hz, C<sub>*t*Bu</sub>), 53.1 (d, J<sub>CP</sub> = 10.6 Hz, C<sub>*t*Bu</sub>), 113.4 (d, J<sub>CP</sub> = 13.1 Hz, CP), 123.1 (s, CH<sub>Ar</sub>), 123.7 (s, CH<sub>Ar</sub>), 125.3 (s, CH<sub>Ar</sub>), 143.9 (s, NC<sub>Ar</sub>), 144.7 (s, C<sub>Ar*i*Pr</sub>), 146.2 (s, C<sub>Ar*i*Pr</sub>), 185.5 (d, J<sub>CP</sub> = 35.3 Hz, CN).

**<sup>31</sup>P{<sup>1</sup>H} NMR (202 MHz, CDCl<sub>3</sub>, 25 °C):** 209.6 (s, PN<sub>2</sub>).

**<sup>207</sup>Pb NMR (104 MHz, THF-d<sub>8</sub>, 0 °C):** 1932.2 (d, <sup>1</sup>J<sub>PPb</sub> = 3861.8 Hz).

Synthesis of the chloroplumbbylene **47c**



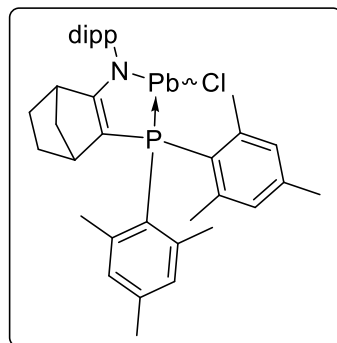
To a solution of iminophosphine (**c**) (300 mg, 0.68 mmol) in THF (3 ml) was added dropwise a solution of nBuLi 1.6 M in hexane (0.47 ml, 0.74 mmol) at -78°C. The solution was slowly warmed to RT and stirred for 1 h and added to a flask containing suspension of PbCl<sub>2</sub> (179 mg, 0.68 mmol) in THF. The solution was warmed to room temperature and stirred for 1 h. All the volatiles were removed under vacuum and the residue was extracted with DCM. After washing with pentane, the product was obtained as pale yellow powder (218 mg, 47 %).

**<sup>1</sup>H NMR (500 MHz, THF-d<sub>8</sub>, 0 °C):** 1.19 (d, <sup>1</sup>J<sub>HH</sub> = 6.9 Hz, 6H, CH<sub>3*iPr*</sub>), 1.20 (d, <sup>1</sup>J<sub>HH</sub> = 6.8 Hz, 6H, CH<sub>3*iPr*</sub>), 1.24 (d, <sup>1</sup>J<sub>HH</sub> = 3.3 Hz, 3H, CH<sub>3*iPr*</sub>), 1.29 (d, <sup>1</sup>J<sub>HH</sub> = 3.0 Hz, 3H, CH<sub>3*iPr*</sub>), 1.27 (d, <sup>1</sup>J<sub>HH</sub> = 3.3 Hz, 3H, CH<sub>3*iPr*</sub>), 1.29 (d, <sup>1</sup>J<sub>HH</sub> = 3.2 Hz, 3H, CH<sub>3*iPr*</sub>), 1.39 (m, 1H, CH<sub>2</sub>), 1.56 (m, 2H, CH<sub>2</sub>), 1.69 (m, 1H, CH<sub>2</sub>), 1.84 (m, 1H, CH<sub>2</sub>), 2.20 (m, 1H, CH<sub>2</sub>), 2.51 (s, 1H, CH<sub>bridgehead</sub>), 2.84 (s, 1H, CH<sub>bridgehead</sub>), 3.16 (m, 3H, CH<sub>*iPr*</sub>, CH<sub>2</sub>), 3.41 (m, 2H, CH<sub>*iPr*</sub>, CH<sub>2</sub>), 3.57 (m, 2H, CH<sub>*iPr*</sub>, CH<sub>2</sub>), 3.78 (m, 1H, CH<sub>*iPr*</sub>), 7.06 (m, 1H, CH<sub>Ar</sub>), 7.14 (m, 2H, CH<sub>Ar</sub>).

**<sup>13</sup>C NMR (126 MHz, THF-d<sub>8</sub>, 0 °C):** 20.6 (s, CH<sub>3*iPr*</sub>), 21.5 (s, CH<sub>3*iPr*</sub>), 23.2 (s, CH<sub>3*iPr*</sub>), 23.8 (s, CH<sub>3*iPr*</sub>), 25.3 (s, CH<sub>2</sub>), 25.6 (s, CH<sub>3*iPr*</sub>), 25.8 (s, CH<sub>3*iPr*</sub>), 27.1 (s, CH<sub>3*iPr*</sub>), 27.4 (s, CH<sub>3*iPr*</sub>), 29.9 (s, CH<sub>2</sub>), 40.8 (s, CH<sub>2</sub>), 42.9 (s, CH<sub>2</sub>), 42.7 (d, J<sub>CP</sub> = 11.3 Hz, CH<sub>bridgehead</sub>), 42.9 (d, J<sub>CP</sub> = 7.6 Hz, CH<sub>bridgehead</sub>), 44.7 (s, CH<sub>*iPr*</sub>), 44.8 (s, CH<sub>*iPr*</sub>), 47.8 (s, CH<sub>2</sub>), 109.8 (d, J<sub>CP</sub> = 13.7 Hz, CP), 122.9 (s, CH<sub>Ar</sub>), 123.3 (s, CH<sub>Ar</sub>), 124.5 (s, CH<sub>Ar</sub>), 144.5 (s, NC<sub>Ar</sub>), 144.9 (s, C<sub>Ar</sub>*iPr*), 145.1 (s, C<sub>Ar</sub>*iPr*), 192.0 (d, J<sub>CP</sub> = 36.5 Hz, CN).

**<sup>31</sup>P{<sup>1</sup>H} NMR (202 MHz, THF-d<sub>8</sub>, 0 °C):** 206.6 (s, PN<sub>2</sub>).

Synthesis of the chloroplumbbylene **47b**



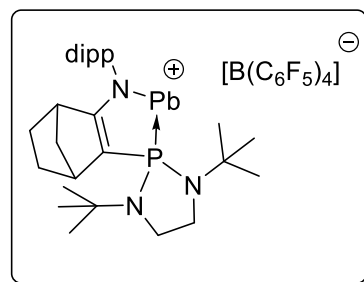
A n-BuLi (0.38 ml, 0.61 mmol, 1.6 M in hexane) solution was added dropwise to an iminophosphine (**b**) solution (300 mg, 0.56 mmol) in THF (3 mL) at -80 °C. The solution was slowly warmed to room temperature and added to a flask containing suspension of PbCl<sub>2</sub> (155 mg, 0.56 mmol) in THF. After stirring for 1 hour, all volatiles were removed under vacuum and the residue was extracted with DCM. The crude yellow solid was washed with pentane. **47b** was obtained as yellow powder (174 mg, 40 %).

**<sup>1</sup>H NMR (500 MHz, C<sub>6</sub>D<sub>6</sub>, 25 °C):** 0.54 (m, 1H, CH<sub>2</sub>), 1.24 (m, 5H, CH<sub>3*iPr*</sub>, CH<sub>2</sub>), 1.30 (d, <sup>1</sup>J<sub>HH</sub> = 6.8 Hz, 3H, CH<sub>3*iPr*</sub>), 1.38 (d, <sup>1</sup>J<sub>HH</sub> = 6.9 Hz, 3H, CH<sub>3*iPr*</sub>), 1.56 (m, 3H, CH<sub>3*iPr*</sub>), 1.96 (m, 1H, CH<sub>2</sub>), 2.01 (s, 9H, CH<sub>3Mes</sub>), 2.12 (s, 9H, CH<sub>3Mes</sub>), 2.03 (m, 2H, CH<sub>2</sub>), 2.45 (s, 1H, CH<sub>bridgehead</sub>), 2.93 (s, 1H, CH<sub>bridgehead</sub>), 3.54 (s, 1H, CH<sub>*iPr*</sub>), 3.95 (s, 1H, CH<sub>*iPr*</sub>), 6.66 (m, 3H, CH<sub>Ar</sub>), 6.89 (m, 1H, CH<sub>Ar</sub>), 7.17 (m, 2H, CH<sub>Ar</sub>), 7.32 (m, 1H, CH<sub>Ar</sub>).

**<sup>13</sup>C NMR (126 MHz, C<sub>6</sub>D<sub>6</sub>, 25 °C):** 20.5 (s, CH<sub>3*iPr*</sub>), 23.0 (s, CH<sub>3*iPr*</sub>), 23.1 (s, CH<sub>3*iPr*</sub>), 24.2 (s, CH<sub>3*iPr*</sub>), 24.3 (s, CH<sub>3*iPr*</sub>), 26.5 (s, CH<sub>3*iPr*</sub>), 26.7 (s, CH<sub>2</sub>), 27.1 (s, CH<sub>3*iPr*</sub>), 27.5 (s, CH<sub>*iPr*</sub>), 27.6 (s, CH<sub>*iPr*</sub>), 28.7 (s, CH<sub>2</sub>), 46.1 (d, *J*<sub>CP</sub> = 12.3 Hz, CH<sub>bridgehead</sub>), 47.2 (d, *J*<sub>CP</sub> = 4.0 Hz, CH<sub>bridgehead</sub>), 47.7 (d, *J*<sub>CP</sub> = 4.5 Hz, CH<sub>2</sub>), 86.3 (d, *J*<sub>CP</sub> = 43.0 Hz, CP), 124.7 (s, CH<sub>Ar</sub>), 125.4 (s, CH<sub>Ar</sub>), 129.3 (s, CH<sub>Ar</sub>), 129.9 (m, CH<sub>Ar</sub>), 130.0 (m, CH<sub>Ar</sub>), 130.9 (m, CH<sub>Ar</sub>), 131.2 (m, CH<sub>Ar</sub>), 131.2 (m, CP<sub>ArMes</sub>), 132.3 (d, *J*<sub>CP</sub> = 37.6 Hz, CP<sub>ArMes</sub>), 138.6 (s, C<sub>ArMes</sub>), 139.0 (s, C<sub>ArMes</sub>), 143.4 (s, NC<sub>Ar</sub>), 144.0 (s, C<sub>Ar*iPr*</sub>), 148.2 (s, C<sub>Ar*iPr*</sub>), 188.2 (d, *J*<sub>CP</sub> = 27.8 Hz, CN).

**<sup>31</sup>P{<sup>1</sup>H} NMR (202 MHz, C<sub>6</sub>D<sub>6</sub>, 25 °C):** 63.6 (s, PN<sub>2</sub>).

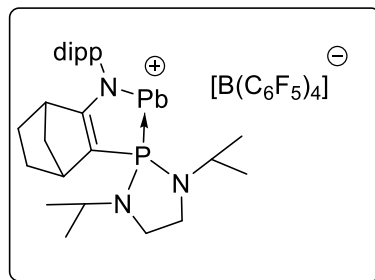
Synthesis of cationic derivative of plumbylene **48a**:



To a solution of Chloroplumbylene **47a** (70 mg, 0.09 mmol) in fluorobenzene was added K[B(C<sub>6</sub>F<sub>5</sub>)<sub>4</sub>] (65 mg, 0.09 mmol) at room temperature. After 5 minutes the crude solution was analysed by NMR spectroscopy.

<sup>31</sup>P{<sup>1</sup>H} NMR (122 MHz, THF-d<sub>8</sub>, 25 °C): 251.2 (s, PN<sub>2</sub>).

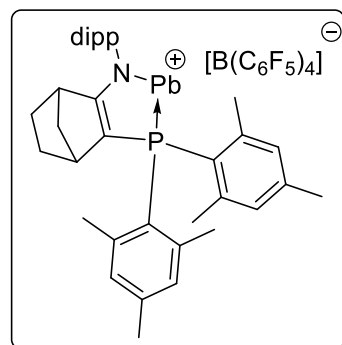
Synthesis of cationic derivative of plumbylene **48c**:



To a solution of Chloroplumbylene **47c** (70 mg, 0.10 mmol) in fluorobenzene was added K[B(C<sub>6</sub>F<sub>5</sub>)<sub>4</sub>] (71.82 mg, 0.10 mmol) at room temperature. After 5 minutes the crude solution was analysed by NMR spectroscopy.

<sup>31</sup>P{<sup>1</sup>H} NMR (122 MHz, tol-d<sub>8</sub>, -30 °C): 251.9 (s, PN<sub>2</sub>).

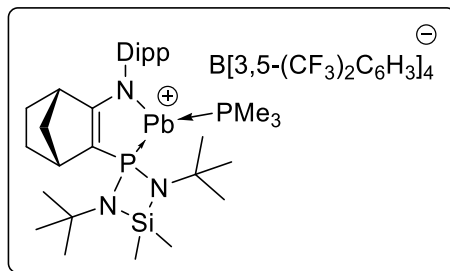
Synthesis of cationic derivative of plumbylene **48b**:



To a solution of chloroplumbylene **47b** (70 mg, 0.09 mmol) in fluorobenzene was added K[B(C<sub>6</sub>F<sub>5</sub>)<sub>4</sub>] (65 mg, 0.09 mmol) at room temperature. After 5 minutes the crude solution was analysed by NMR spectroscopy.

<sup>31</sup>P{<sup>1</sup>H} NMR (122 MHz, C<sub>6</sub>D<sub>6</sub>, 25 °C): 97.5 (s, PN<sub>2</sub>).

Synthesis of cationic derivative of plumbylene **48-PMe<sub>3</sub>**:



To a mixture of chloroplumbylene **47** (50 mg, 0.067 mmol) and NaB[3,5-(CF<sub>3</sub>)<sub>2</sub>C<sub>6</sub>H<sub>3</sub>]<sub>4</sub> (60 mg, 0.067 mmol) in C<sub>6</sub>H<sub>5</sub>F (0.5 ml) was added trimethylphosphine (1.0 M, 70.0 µL, 0.067 mmol) at room temperature. The mixture was stirred for 5 min then all volatiles were removed under vacuum. The residue was washed with heptane to give **48-PMe<sub>3</sub>** as orange powder (101 mg, yield = 91 %). Mp: 154–156 °C (decomp.).

**<sup>1</sup>H NMR (500 MHz, C<sub>6</sub>D<sub>6</sub> + C<sub>6</sub>H<sub>5</sub>F 25°C):** 0.26 (s, 3H, SiCH<sub>3</sub>), 0.33 (s, 3H, SiCH<sub>3</sub>), 0.90 (m, 9H, P(CH<sub>3</sub>)<sub>3</sub>), 1.06 (s, 9H, CH<sub>3tBu</sub>), 1.06 (overlapped, 3H, CH<sub>3iPr</sub>), 1.09 (overlapped, 3H, CH<sub>3iPr</sub>), 1.10 (s, 9H, CH<sub>3tBu</sub>), 1.11 (d, J<sub>HH</sub> = 6.8 Hz, 3H, CH<sub>3iPr</sub>), 1.16 (m, 1H, CH<sub>2</sub>), 1.42 (m, 1H, CH<sub>2</sub>), 1.54 (m, 2H, CH<sub>2</sub>), 1.66 (m, 1H, CH<sub>2</sub>), 1.89 (d, J<sub>HH</sub> = 8.8 Hz, 1H, CH<sub>2</sub>), 2.31 (s, 1H, CH<sub>bridgehead</sub>), 2.89 (br s, 1H, CH<sub>bridgehead</sub>), 2.89 (overlapped, 1H, CH<sub>iPr</sub>), 2.99 (sept, J<sub>HH</sub> = 6.7 Hz, 1H, CH<sub>iPr</sub>), 7.06 (m, 3H, CH<sub>Ar</sub>), 7.63 (s, 4H, CH<sub>ArF</sub>), 8.29 (s, 8H, CH<sub>ArF</sub>).

**<sup>13</sup>C{<sup>1</sup>H} NMR (125 MHz, C<sub>6</sub>D<sub>6</sub> + C<sub>6</sub>H<sub>5</sub>F, 25°C):** 3.6 (s, SiCH<sub>3</sub>), 7.2 (d, J<sub>CP</sub> = 4.3 Hz, SiCH<sub>3</sub>), 12.3 (d, J<sub>CP</sub> = 13.9 Hz, P(CH<sub>3</sub>)<sub>3</sub>), 24.1 (s, CH<sub>3iPr</sub>), 24.6 (s, CH<sub>3iPr</sub>), 25.4 (s, CH<sub>3iPr</sub>), 25.5 (s, CH<sub>3iPr</sub>), 25.8 (s, CH<sub>2</sub>), 28.0 (s, CH<sub>iPr</sub>), 28.1 (s, CH<sub>iPr</sub>), 28.9 (s, CH<sub>2</sub>), 32.8 (d, J<sub>CP</sub> = 5.8 Hz, CH<sub>3tBu</sub>), 32.8 (d, J<sub>CP</sub> = 5.5 Hz, CH<sub>3tBu</sub>), 43.4 (d, J<sub>CP</sub> = 5.7 Hz, CH<sub>bridgehead</sub>), 44.2 (d, J<sub>CP</sub> = 11.2 Hz, CH<sub>bridgehead</sub>), 48.2 (br s, CH<sub>2</sub>), 51.3 (d, J<sub>CP</sub> = 3.2 Hz, C<sub>tBu</sub>), 51.3 (d, J<sub>CP</sub> = 2.3 Hz, C<sub>tBu</sub>), 118.0 (br sept, J<sub>CF</sub> = 4.0 Hz, p-CH<sub>ArF4</sub>), 119.1 (d, J<sub>CP</sub> = 20.3 Hz, CP), 124.5 (s, CH<sub>Ar</sub>), 124.6 (s, CH<sub>Ar</sub>), 125.3 (q, J<sub>CF</sub> = 272.5 Hz, CF<sub>3</sub>), 127.3 (s, CH<sub>Ar</sub>), 129.9 (qq, J<sub>CF</sub> = 49.8 Hz, J<sub>CB</sub> = 2.8 Hz, m-C<sub>ArF</sub>), 135.4 (s, o-CH<sub>ArF</sub>), 143.0 (s, NC<sub>Ar</sub>), 144.6 (s, iPr-C<sub>Ar</sub>), 144.5 (s, iPr-C<sub>Ar</sub>), 162.9 (q, J<sub>CB</sub> = 49.8 Hz, B-C<sub>ArF4</sub>), 190.4 (d, J<sub>CP</sub> = 31.5 Hz, CN).

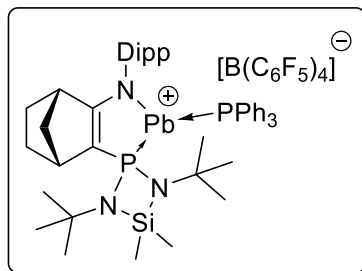
**<sup>31</sup>P{<sup>1</sup>H} NMR (202 MHz, C<sub>6</sub>D<sub>6</sub> + C<sub>6</sub>H<sub>5</sub>F, 25°C):** 218.7 (s, Pb-satellite: J<sub>PPb</sub> = 3960 Hz, PN), 11.6 (s, P(CH<sub>3</sub>)<sub>3</sub>). **<sup>29</sup>Si{<sup>1</sup>H} NMR (99 MHz, C<sub>6</sub>D<sub>6</sub> + C<sub>6</sub>H<sub>5</sub>F, 25°C):** 15.2 (d, J<sub>SiP</sub> = 3.8 Hz, SiCH<sub>3</sub>).

**<sup>11</sup>B{<sup>1</sup>H} NMR (160 MHz, C<sub>6</sub>D<sub>6</sub> + C<sub>6</sub>H<sub>5</sub>F, 25°C):** -6.0 (s, BAr<sub>4</sub>).

**<sup>19</sup>F NMR (470 MHz, C<sub>6</sub>D<sub>6</sub> + C<sub>6</sub>H<sub>5</sub>F, 25°C):** -62.2 (s, CF<sub>3</sub>).

**<sup>31</sup>P{<sup>1</sup>H} NMR (162 MHz, CD<sub>2</sub>Cl<sub>2</sub>, -90°C):** 210.4 (d, J<sub>PP</sub> = 79.6 Hz, Pb-satellite: J<sub>PPb</sub> = 4017 Hz, PN<sub>2</sub>), 17.1 (d, J<sub>PP</sub> = 79.6 Hz, Pb-satellite: J<sub>PPb</sub> = 2622 Hz, PMe<sub>3</sub>).

Synthesis of cationic derivative of plumbylene **48-PPh<sub>3</sub>**:



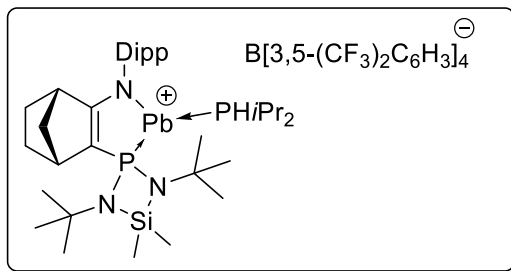
Chloroplumbylene **47** (200 mg, 0.27 mmol) was dissolved 2.0 ml of fluorobenzene inside the glovebox. K[B(C<sub>6</sub>F<sub>5</sub>)<sub>4</sub>] (213.1 mg, 0.29 mmol) and triphenylphosphine (70.73 mg, 0.27 mmol) was added to a solution and then stirred for 5 minutes at RT. The dark-red solution was filtrated inside the glovebox in order to eliminate the potassium salts. After washing the product with pentane, the product was obtained as dark red powder (295 mg, yield = 60.5 %). Mp: 165–168 °C (decomp.).

**<sup>1</sup>H NMR (300 MHz, C<sub>6</sub>D<sub>6</sub>, 25°C):** 0.48 (s, 3H, SiCH<sub>3</sub>), 0.50 (s, 3H, SiCH<sub>3</sub>), 1.12 (d, J = 6.8 Hz, 3H, CH<sub>3*i*Pr</sub>), 1.13 (d, <sup>1</sup>J<sub>HH</sub> = 6.7 Hz, 3H, CH<sub>3*i*Pr</sub>), 1.23 (d, <sup>1</sup>J<sub>HH</sub> = 5.6 Hz, 12H, CH<sub>3*i*Pr</sub>, CH<sub>3*t*Bu</sub>), 1.26 (s, 12H, CH<sub>3*i*Pr</sub>, CH<sub>3*t*Bu</sub>), 1.77 – 1.55 (m, 4H, CH<sub>2</sub>), 1.94 – 1.80 (m, 1H, ½ CH<sub>2</sub>), 2.16 (d, <sup>1</sup>J<sub>HH</sub> = 8.9 Hz, 1H, ½ CH<sub>2</sub>), 2.45 (s, 1H, CH<sub>bridgehead</sub>), 3.02 (s, 1H, CH<sub>bridgehead</sub>), 3.36 – 3.13 (m, <sup>1</sup>J<sub>HH</sub> = 6.9 Hz, 2H, CH<sub>*i*Pr</sub>), 7.17 – 6.85 (m, 854H, CH<sub>arPPh<sub>3</sub></sub>, CH<sub>arPhF</sub>), δ 7.41 – 7.17 (m, 26H, 3CH<sub>ar</sub>).

**<sup>13</sup>C NMR (75 MHz, C<sub>6</sub>D<sub>6</sub>, 25°C):** 7.3 (d, <sup>1</sup>J<sub>CP</sub> = 5.4 Hz, SiCH<sub>3</sub>), 3.8 (s, SiCH<sub>3</sub>), 24.0 (s, CH<sub>3*i*Pr</sub>), 25.8 (s, CH<sub>2</sub>), 24.5 (s, CH<sub>3*i*Pr</sub>), 25.9 (s, CH<sub>3*i*Pr</sub>), 26.0 (s, CH<sub>3*i*Pr</sub>), 28.0 (s, CH<sub>*i*Pr</sub>), 28.9 (s, CH<sub>2</sub>), 33.0 (d, <sup>1</sup>J<sub>CP</sub> = 5.0 Hz, CH<sub>3*t*Bu</sub>), 33.2 (d, <sup>1</sup>J<sub>CP</sub> = 5.1 Hz, CH<sub>3*t*Bu</sub>), 44.0 (d, <sup>1</sup>J<sub>CP</sub> = 6.1 Hz, NCCH), 44.4 (d, <sup>1</sup>J<sub>CP</sub> = 11.5 Hz, PCCH), 48.2 (d, <sup>1</sup>J<sub>CP</sub> = 3.7 Hz, CH<sub>2</sub>), 51.1 (d, <sup>1</sup>J<sub>CP</sub> = 3.0 Hz, C<sub>*t*Bu</sub>), 51.2 (d, <sup>1</sup>J<sub>CP</sub> = 2.5 Hz, C<sub>*t*Bu</sub>), 134.1 - 115.5 (s, C<sub>Ar</sub> PPh<sub>3</sub>, PhF, B(C<sub>6</sub>F<sub>5</sub>)<sub>4</sub>), 135.1 (s, PC), 129.2 (s, C<sub>Ar</sub>), 129.3 (s, C<sub>Ar</sub>), 130.0 (s, C<sub>Ar</sub>), 145.2 (s, CCH<sub>*i*Pr</sub>), 147.5 (s, CCH<sub>*i*Pr</sub>), 150.7 (s, NC<sub>Ar</sub>), 161.7 (s, CP<sub>PPh<sub>3</sub></sub>), 165.0 (s, CF<sub>PhF</sub>), δ 190.1 (d, <sup>1</sup>J<sub>CP</sub> = 35.5 Hz, NC).

**<sup>31</sup>P NMR (122 MHz, CDCl<sub>3</sub>, 25°C):** 14.69 (s, PPh<sub>3</sub>), 243.5 ppm (s, PR<sub>2</sub>).

Synthesis of cationic derivative of plumbylene **48-PHiPr<sub>2</sub>**:



Chloroplumbylene **47** (50 mg, 0.067 mmol) was dissolved 2.0 ml of fluorobenzene inside the glovebox. NaB[3,5-(CF<sub>3</sub>)<sub>2</sub>C<sub>6</sub>H<sub>3</sub>]<sub>4</sub> (60 mg, 0.067 mmol) and diisopropylphosphine solution in toluene (1.0 M, 70.0 µL, 0.067 mmol) was added to a solution and then stirred for 5 minutes at RT. The dark-red solution was filtrated inside the glovebox in order to eliminate the potassium salts. After stirring for 10 min at room temperature, the solution was filtrated. All volatiles were removed under vacuum (101 mg, yield = 91 %). Mp: 154–156 °C (decomp.).

**<sup>1</sup>H NMR (400 MHz, C<sub>7</sub>D<sub>8</sub> + C<sub>6</sub>H<sub>5</sub>F, -30°C):** 0.21 (s, 3H, SiCH<sub>3</sub>), 0.33 (s, 3H, SiCH<sub>3</sub>), 0.40 (m, 6H, CH<sub>3</sub>H<sub>PIPr2</sub>), 0.84 (m, 6H, CH<sub>3</sub>H<sub>PIPr2</sub>), 0.99 (br s, 3H, CH<sub>3iPr</sub>), 1.09 (s, 18H, CH<sub>3tBu</sub>), 1.10 (overlapped, 6H, CH<sub>3iPr</sub>), 1.20 (br s, 3H, CH<sub>3iPr</sub>), 1.43 (m, 2H, CH<sub>2</sub>), 1.52 (m, 1H, CH<sub>2</sub>), 1.62 (m, 3H, CH<sub>2</sub>), 1.79 (br s, 1H, CH<sub>HPIPr2</sub>), 1.99 (br s, 1H, CH<sub>HPIPr2</sub>), 2.37 (s, 1H, CH<sub>bridgehead</sub>), 2.91 (br s, 1H, CH<sub>bridgehead</sub>), 2.97 (br s, 2H, CH<sub>iPr</sub>), 5.13 (d, J<sub>HP</sub> = 313.61 Hz, 1H, P-H), 7.58 (s, 4H, CH<sub>ArF</sub>), 8.39 (s, 8H, CH<sub>ArF</sub>).

**<sup>13</sup>C{<sup>1</sup>H} NMR (100 MHz, C<sub>7</sub>D<sub>8</sub> + C<sub>6</sub>H<sub>5</sub>F, -30°C):** 3.4 (s, SiCH<sub>3</sub>), 6.9 (d, J<sub>CP</sub> = 5.0 Hz, SiCH<sub>3</sub>), 19.2 (s, CH<sub>3HPIPr2</sub>), 20.3 (s, CH<sub>3HPIPr2</sub>), 20.6 (s, CH<sub>3HPIPr2</sub>), 21.0 (d, J<sub>CP</sub> = 14.0 Hz, CH<sub>HPIPr2</sub>), 21.8 (d, J<sub>CP</sub> = 14.5 Hz, CH<sub>HPIPr2</sub>), 21.9 (s, CH<sub>3HPIPr2</sub>), 23.9 (s, CH<sub>3iPr</sub>), 25.1 (s, 2xCH<sub>3iPr</sub>), 25.4 (s, CH<sub>3iPr</sub>), 26.0 (s, CH<sub>2</sub>), 27.5 (s, CH<sub>iPr</sub>), 28.5 (s, CH<sub>iPr</sub>), 28.9 (s, CH<sub>2</sub>), 32.2 (s, CH<sub>3tBu</sub>), 32.8 (s, CH<sub>3tBu</sub>), 43.2 (s, CH<sub>bridgehead</sub>), 44.0 (d, J<sub>CP</sub> = 7.8 Hz, CH<sub>bridgehead</sub>), 46.2 (s, CH<sub>2</sub>), 51.1 (s, C<sub>tBu</sub>), 51.3 (s, C<sub>tBu</sub>), 118.0 (br s, p-CH<sub>ArF4</sub>), 124.6 (s, CH<sub>Ar</sub>), 124.7 (s, CH<sub>Ar</sub>), 125.2 (q, J<sub>CF</sub> = 272.3 Hz, CF<sub>3</sub>), 126.8 (s, CH<sub>Ar</sub>), 129.5 (br q, J<sub>CF</sub> = 31.5 Hz, m-C<sub>ArF</sub>), 135.3 (s, o-CH<sub>ArF</sub>), 143.3 (s, NC<sub>Ar</sub>), 143.4 (s, iPr-C<sub>Ar</sub>), 144.0 (s, iPr-C<sub>Ar</sub>), 162.9 (q, J<sub>CB</sub> = 49.5 Hz, B-C<sub>ArF4</sub>), 190.5 (d, J<sub>CP</sub> = 32.0 Hz, CN).

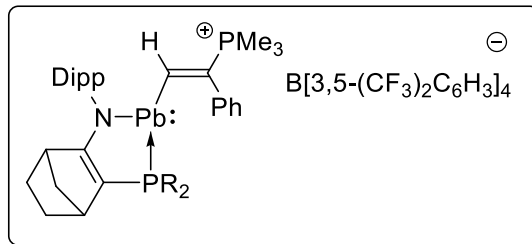
**<sup>31</sup>P{<sup>1</sup>H} NMR (161 MHz, C<sub>7</sub>D<sub>8</sub> + C<sub>6</sub>H<sub>5</sub>F, -30°C):** 211.8 (d, J<sub>PP</sub> = 65.5 Hz, Pb-satellite: J<sub>PPb</sub> = 3815 Hz, PN<sub>2</sub>), 51.4 (d, J<sub>PP</sub> = 65.5 Hz, Pb-satellite: J<sub>PPb</sub> = 2551 Hz, HPIPr<sub>2</sub>).

**<sup>29</sup>Si{<sup>1</sup>H} NMR (80 MHz, C<sub>7</sub>D<sub>8</sub> + C<sub>6</sub>H<sub>5</sub>F, -30°C):** 14.8 (s, SiCH<sub>3</sub>).

**<sup>11</sup>B{<sup>1</sup>H} NMR (128 MHz, C<sub>7</sub>D<sub>8</sub> + C<sub>6</sub>H<sub>5</sub>F, -30°C):** -6.3 (s, BAr<sub>4</sub>).

**<sup>19</sup>F{<sup>1</sup>H} NMR (282 MHz, C<sub>6</sub>D<sub>6</sub> + C<sub>6</sub>H<sub>5</sub>F, 25°C):** -62.6 (s, CF<sub>3</sub>).

Synthesis of cationic derivative of plumbylene **49-PPh<sub>3</sub>**:



To a solution of **48-PMe<sub>3</sub>** (with  $B[3,5-(CF_3)_2C_6H_3]_4$  as counter-anion) (50 mg, 0.067 mmol) in fluorobenzene (2 mL), a phenylacetylene (6.8 mg, 0.067 mmol) was added at room temperature. The solution was stirred for 10 minutes. Then all volatiles were removed under vacuum and the residue was dissolved in a mixture of pentane and fluorobenzene (1.5 ml, pentane: fluorobenzene = 3: 1). The red crystals were obtained after two days at -30 °C. (45 mg, yield = 79 %). Mp: 130–134 °C (decomp.). Major : Minor = 53 : 47.

**Major Isomer:**

**<sup>1</sup>H NMR (500 MHz, C<sub>6</sub>D<sub>6</sub> + C<sub>6</sub>H<sub>5</sub>F 25°C):** 0.38 (s, 3H, SiCH<sub>3</sub>), 0.39 (s, 3H, SiCH<sub>3</sub>), 0.85 (d,  $J_{HP} = 13.0$  Hz, 9H, P-CH<sub>3</sub>), 1.05 (d,  $J_{HH} = 6.9$  Hz, 3H, CH<sub>3iPr</sub>), 1.05 (s, 9H, CH<sub>3tBu</sub>), 1.13 (d,  $J_{HH} = 6.9$  Hz, 3H, CH<sub>3iPr</sub>), 1.16 (d,  $J_{HH} = 6.9$  Hz, 3H, CH<sub>3iPr</sub>), 1.18 (s, 9H, CH<sub>3tBu</sub>), 1.25 (d,  $J_{HH} = 6.9$  Hz, 3H, CH<sub>3iPr</sub>), 1.46 (m, 2H, CH<sub>2</sub>), 1.61 (m, 1H, CH<sub>2</sub>), 1.65 (m, 3H, CH<sub>2</sub>), 2.51 (s, 1H, CH<sub>bridgehead</sub>), 3.01 (s, 1H, CH<sub>bridgehead</sub>), 3.18 (sept,  $J_{HH} = 6.9$  Hz, 1H, CH<sub>iPr</sub>), 3.38 (sept,  $J_{HH} = 6.9$  Hz, 1H, CH<sub>iPr</sub>), 6.62–6.66 (m, 4H, CH<sub>Ar</sub>), 7.11–7.13 (m, 4H, CH<sub>Ar</sub>), 7.62 (s, 4H, CH<sub>ArF</sub>), 8.33 (m, 8H, CH<sub>ArF</sub>), 9.97 (dd,  $J_{HP} = 35.1$  and 2.0 Hz, 1H, C=C-H).

**<sup>13</sup>C{<sup>1</sup>H} NMR (125 MHz, C<sub>6</sub>D<sub>6</sub> + C<sub>6</sub>H<sub>5</sub>F 25°C):** 4.1 (d,  $J_{CP} = 1.2$  Hz, SiCH<sub>3</sub>), 7.2 (d,  $J_{CP} = 6.0$  Hz, SiCH<sub>3</sub>), 8.8 (d,  $J_{CP} = 55.2$  Hz, P-CH<sub>3</sub>), 24.1 (s, CH<sub>3iPr</sub>), 24.5 (s, CH<sub>3iPr</sub>), 25.7 (s, CH<sub>3iPr</sub>), 26.0 (s, CH<sub>2</sub>), 26.1 (s, CH<sub>3iPr</sub>), 27.5 (s, CH<sub>iPr</sub>), 27.9 (s, CH<sub>iPr</sub>), 29.4 (s, CH<sub>2</sub>), 32.6 (d,  $J_{CP} = 4.0$  Hz, CH<sub>3tBu</sub>), 32.8 (d,  $J_{CP} = 5.2$  Hz, CH<sub>3tBu</sub>), 42.2 (d,  $J_{CP} = 5.8$  Hz, CH<sub>bridgehead</sub>), 43.9 (d,  $J_{CP} = 11.0$  Hz, CH<sub>bridgehead</sub>), 46.9 (d,  $J_{CP} = 4.1$  Hz, CH<sub>2</sub>), 51.1 (d,  $J_{CP} = 3.4$  Hz, C<sub>tBu</sub>), 51.4 (d,  $J_{CP} = 4.6$  Hz, C<sub>tBu</sub>), 110.7 (d,  $J_{CP} = 15.0$  Hz, NC=C-P), 118.0 (br sept,  $J_{CF} = 3.7$  Hz, p-CH<sub>ArF4</sub>), 123.8 (s, CH<sub>Ar-Dip</sub>), 124.5 (s, CH<sub>Ar-Dip</sub>), 125.3 (q,  $J_{CF} = 272.3$  Hz, CF<sub>3</sub>), 126.0 (s, CH<sub>Ar-Dip</sub>), 128.3 (s, CH<sub>Ar-Ph</sub>), 129.5 (overlapped, CH<sub>Ar-Ph</sub>), 129.8 (qq,  $J_{CF} = 30.8$  Hz, J<sub>CB</sub> = 2.3 Hz, m-C<sub>ArF</sub>), 132.5 (dd,  $J_{CP} = 51.2$  and 7.0 Hz, P-C=CH), 135.0 (s, o-CH<sub>ArF</sub>), 135.9 (d,  $J_{CP} = 21.4$  Hz, CH=C-C<sub>Ar</sub>), 144.5 (s, NC<sub>Ar</sub>), 144.5 (s, iPr-C<sub>Ar</sub>), 144.7 (s, iPr-C<sub>Ar</sub>), 162.8 (q,  $J_{CB} = 49.7$  Hz, B-C<sub>ArF4</sub>), 188.2 (d,  $J_{CP} = 34.7$  Hz, CN), 236.8 (dd,  $J_{CP} = 21.0$  and 17.5 Hz, Pb-CH=C).

**<sup>31</sup>P{<sup>1</sup>H} NMR (202 MHz, C<sub>6</sub>D<sub>6</sub> + C<sub>6</sub>H<sub>5</sub>F 25°C):** 166.0 (d,  $J_{PP} = 10.6$  Hz, Pb-satellite:  $J_{PPb} = 3631$  Hz, PN<sub>2</sub>), 18.4 (d,  $J_{PP} = 10.6$  Hz, Pb-satellite:  $J_{PPb} = 370$  Hz, PMe<sub>3</sub>).

**<sup>29</sup>Si{<sup>1</sup>H} NMR (99 MHz, C<sub>6</sub>D<sub>6</sub> + C<sub>6</sub>H<sub>5</sub>F 25°C):** 11.3 (d,  $J_{SiP} = 4.2$  Hz, SiCH<sub>3</sub>).

**<sup>11</sup>B{<sup>1</sup>H} NMR (160 MHz, C<sub>6</sub>D<sub>6</sub> + C<sub>6</sub>H<sub>5</sub>F 25°C):** -6.0 (s, BAr<sub>4</sub>).

**<sup>19</sup>F NMR (470 MHz, C<sub>6</sub>D<sub>6</sub> + C<sub>6</sub>H<sub>5</sub>F 25°C):** -62.3 (s, CF<sub>3</sub>).

**<sup>207</sup>Pb{<sup>1</sup>H} NMR (105 MHz, C<sub>6</sub>D<sub>6</sub> + C<sub>6</sub>H<sub>5</sub>F 25°C):** 1627.2 (dd,  $J_{PbP} = 3625$  and 371 Hz, P-Pb).

**Minor Isomer:**

**<sup>1</sup>H NMR (500 MHz, C<sub>6</sub>D<sub>6</sub> + C<sub>6</sub>H<sub>5</sub>F 25°C):** 0.39 (s, 6H, SiCH<sub>3</sub>), 0.93 (d,  $J_{HP} = 13.0$  Hz, 9H, P-CH<sub>3</sub>), 1.05 (d,  $J_{HH} = 6.9$  Hz, 3H, CH<sub>3iPr</sub>), 1.10 (s, 9H, CH<sub>3tBu</sub>), 1.13 (overlapped, 3H, CH<sub>3iPr</sub>), 1.14 (s, 9H, CH<sub>3tBu</sub>), 1.17 (d,  $J_{HH} = 6.9$  Hz, 3H, CH<sub>3iPr</sub>), 1.25 (d,  $J_{HH} = 6.9$  Hz, 3H, CH<sub>3iPr</sub>), 1.46 (m, 2H, CH<sub>2</sub>), 1.60 (m, 1H, CH<sub>2</sub>), 1.79 (m, 3H, CH<sub>2</sub>), 2.43 (s, 1H, CH<sub>bridgehead</sub>), 3.02 (overlapped, 1H, CH<sub>bridgehead</sub>), 3.04 (sept,  $J_{HH} = 6.9$  Hz, 1H, CH<sub>iPr</sub>), 3.68 (sept,  $J_{HH} = 6.9$  Hz, 1H, CH<sub>iPr</sub>), 6.68–6.79 (m, 4H, CH<sub>Ar</sub>), 10.05 (d,  $J_{HP} = 34.8$  Hz, 1H, C=C-H).

**<sup>13</sup>C{<sup>1</sup>H} NMR (125 MHz, C<sub>6</sub>D<sub>6</sub> + C<sub>6</sub>H<sub>5</sub>F 25°C):** 4.1 (d,  $J_{CP} = 1.2$  Hz, SiCH<sub>3</sub>), 7.6 (d,  $J_{CP} = 6.4$  Hz, SiCH<sub>3</sub>), 8.9 (d,  $J_{CP} = 55.4$  Hz, P-CH<sub>3</sub>), 24.1 (s, CH<sub>3iPr</sub>), 24.8 (s, CH<sub>3iPr</sub>), 25.8 (s, CH<sub>3iPr</sub>), 25.8 (s, CH<sub>2</sub>), 25.9 (s, CH<sub>3iPr</sub>), 27.4 (s,

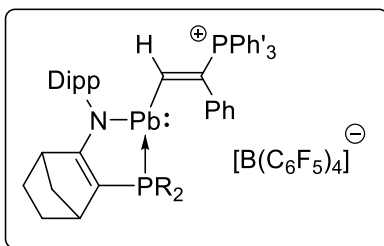
$\text{CH}_{\text{iPr}}$ ), 27.9 (s,  $\text{CH}_{\text{iPr}}$ ), 29.4 (s,  $\text{CH}_2$ ), 32.6 (d,  $J_{\text{CP}} = 5.4$  Hz,  $\text{CH}_{\text{3tBu}}$ ), 32.8 (d,  $J_{\text{CP}} = 3.9$  Hz,  $\text{CH}_{\text{3tBu}}$ ), 42.0 (d,  $J_{\text{CP}} = 5.8$  Hz,  $\text{CH}_{\text{bridgehead}}$ ), 43.7 (d,  $J_{\text{CP}} = 11.6$  Hz,  $\text{CH}_{\text{bridgehead}}$ ), 48.7 (d,  $J_{\text{CP}} = 5.8$  Hz,  $\text{CH}_2$ ), 51.1 (d,  $J_{\text{CP}} = 4.4$  Hz,  $\text{C}_{\text{tBu}}$ ), 51.5 (d,  $J_{\text{CP}} = 3.4$  Hz,  $\text{C}_{\text{tBu}}$ ), 111.6 (d,  $J_{\text{CP}} = 13.9$  Hz,  $\text{NC}=\text{C-P}$ ), 123.8 (s,  $\text{CH}_{\text{Ar-Dip}}$ ), 124.5 (s,  $\text{CH}_{\text{Ar-Dip}}$ ), 126.0 (s,  $\text{CH}_{\text{Ar-Dip}}$ ), 128.3 (s,  $\text{CH}_{\text{Ar-Ph}}$ ), 133.1 (dd,  $J_{\text{CP}} = 51.7$  and 7.1 Hz,  $\text{P-C=CH}$ ), 136.0 (d,  $J_{\text{CP}} = 21.4$  Hz,  $\text{CH}=\text{C-C}_{\text{Ar}}$ ), 144.3 (s,  $\text{NC}_{\text{Ar}}$ ), 144.8 (s,  $\text{iPr-C}_{\text{Ar}}$ ), 144.9 (s,  $\text{iPr-C}_{\text{Ar}}$ ), 187.8 (d,  $J_{\text{CP}} = 34.1$  Hz,  $\text{CN}$ ), 239.2 (dd,  $J_{\text{CP}} = 21.5$  and 16.8 Hz,  $\text{Pb-CH=C}$ ).

**$^{31}\text{P}\{\text{H}\}$  NMR (202 MHz,  $\text{C}_6\text{D}_6 + \text{C}_6\text{H}_5\text{F}$  25°C):** 171.7 (d,  $J_{\text{PP}} = 10.6$  Hz, Pb-satellite:  $J_{\text{PPb}} = 3656$  Hz,  $\text{PN}_2$ ), 18.3 (d,  $J_{\text{PP}} = 10.6$  Hz, Pb-satellite:  $J_{\text{PPb}} = 361$  Hz,  $\text{PMe}_3$ ).

**$^{29}\text{Si}\{\text{H}\}$  NMR (99 MHz,  $\text{C}_6\text{D}_6 + \text{C}_6\text{H}_5\text{F}$  25°C):** 11.0 (d,  $J_{\text{SiP}} = 4.2$  Hz,  $\text{SiCH}_3$ ).

**$^{207}\text{Pb}\{\text{H}\}$  NMR (105 MHz,  $\text{C}_6\text{D}_6 + \text{C}_6\text{H}_5\text{F}$  25°C):** 1780.5 (dd,  $J_{\text{PbP}} = 3659$  and 363 Hz, P-Pb).

Synthesis of cationic derivative of plumbylene **49-PPh<sub>3</sub>**:



To a mixture of chloroplumbylene **47** (50 mg, 0.067 mmol) and K[B(C<sub>6</sub>F<sub>5</sub>)<sub>4</sub>] (53.3 mg, 0.067 mmol) with triphenylphosphine (19 mg, 0.067 mmol) in fluorobenzene (2.0 ml) a phenylacetylene (6.8 mg, 0.067 mmol) was added at room temperature. The solution was stirred for 5 minutes and then filtrated to eliminate potassium salts. Then all volatiles were removed under vacuum and the residue was washed with pentane to give **49-PPh<sub>3</sub>** as dark yellow powder (295 mg, yield 60.5%). Crystals, suitable for X-ray diffraction analysis were obtained by a layering pentane on the fluorobenzene solution of **49-PPh<sub>3</sub>** at RT. Mp: 141–144 °C (decomp.). Major : Minor = 53 : 47.

**Major Isomer:**

**<sup>1</sup>H NMR (500 MHz, C<sub>6</sub>D<sub>6</sub> + C<sub>6</sub>H<sub>5</sub>F 25°C):** 0.38 (s, 3H, SiCH<sub>3</sub>), 0.40 (s, 3H, SiCH<sub>3</sub>), 0.53 (d, J<sub>HH</sub> = 6.9 Hz, 3H, CH<sub>3iPr</sub>), 1.03 (d, J<sub>HH</sub> = 6.9 Hz, 3H, CH<sub>3iPr</sub>), 1.07 (s, 9H, CH<sub>3tBu</sub>), 1.10 (d, J<sub>HH</sub> = 6.9 Hz, 3H, CH<sub>3iPr</sub>), 1.11 (d, J<sub>HH</sub> = 6.9 Hz, 3H, CH<sub>3iPr</sub>), 1.16 (s, 9H, CH<sub>3tBu</sub>), 1.26 (overlapped, 1H, CH<sub>2</sub>), 1.45 (m, 1H, CH<sub>2</sub>), 1.65 (m, 2H, CH<sub>2</sub>), 1.77 (m, 1H, CH<sub>2</sub>), 1.82 (d, J<sub>HH</sub> = 8.2 Hz, 1H, CH<sub>2</sub>), 2.44 (s, 1H, CH<sub>bridgehead</sub>), 3.02 (overlapped, 1H, CH<sub>bidgehead</sub>), 3.21 (sept, J<sub>HH</sub> = 6.9 Hz, 1H, CH<sub>iPr</sub>), 3.48 (sept, J<sub>HH</sub> = 6.9 Hz, 1H, CH<sub>iPr</sub>), 7.00-7.14 (m, 23H, CH<sub>Ar</sub>), 7.61 (s, 4H, CH<sub>ArF</sub>), 8.33 (m, 8H, CH<sub>ArF</sub>), 10.40 (d, J<sub>HP</sub> = 34.5 Hz, 1H, C=C-H).

**<sup>13</sup>C{<sup>1</sup>H} NMR (125 MHz, C<sub>6</sub>D<sub>6</sub> + C<sub>6</sub>H<sub>5</sub>F 25°C):** 4.2 (s, SiCH<sub>3</sub>), 7.7 (d, J<sub>CP</sub> = 5.6 Hz, SiCH<sub>3</sub>), 24.0 (s, CH<sub>3iPr</sub>), 24.5 (s, CH<sub>3iPr</sub>), 25.0 (s, CH<sub>3iPr</sub>), 25.9 (s, CH<sub>3iPr</sub>), 26.0 (s, CH<sub>2</sub>), 27.3 (s, CH<sub>iPr</sub>), 27.4 (s, CH<sub>iPr</sub>), 29.4 (s, CH<sub>2</sub>), 32.9 (d, J<sub>CP</sub> = 5.8 Hz, CH<sub>3tBu</sub>), 33.1 (d, J<sub>CP</sub> = 5.2 Hz, CH<sub>3tBu</sub>), 42.1 (d, J<sub>CP</sub> = 5.8 Hz, CH<sub>bridgehead</sub>), 44.0 (d, J<sub>CP</sub> = 11.0 Hz, CH<sub>bridgehead</sub>), 48.7 (d, J<sub>CP</sub> = 5.2 Hz, CH<sub>2</sub>), 51.2 (d, J<sub>CP</sub> = 3.9 Hz, C<sub>tBu</sub>), 51.4 (d, J<sub>CP</sub> = 4.0 Hz, C<sub>tBu</sub>), 118.0 (br sept, J<sub>CF</sub> = 4.0 Hz, p-CH<sub>ArF4</sub>), 111.2 (d, J<sub>CP</sub> = 15.0 Hz, NC=C-P), 119.1 (d, J<sub>CP</sub> = 84.5 Hz, P-C<sub>Ar</sub>), 123.7 (s, CH<sub>Ar-Dipp</sub>), 124.4 (s, CH<sub>Ar-Dipp</sub>), 125.3 (q, J<sub>CF</sub> = 272.3 Hz, CF<sub>3</sub>), 125.9 (s, CH<sub>Ar-Dip</sub>), 128.3 (s, CH<sub>Ar-Ph</sub>), 128.8 (s, CH<sub>Ar-Ph</sub>), 129.3 (s, CH<sub>Ar-Ph</sub>), 129.9 (d, J<sub>CP</sub> = 8.5 Hz, P-CH<sub>Ar</sub>), 129.9 (qq, J<sub>CF</sub> = 30.1 Hz, J<sub>CB</sub> = 2.3 Hz, m-C<sub>ArF</sub>), 131.9 (dd, J<sub>CP</sub> = 44.8 and 6.6 Hz, P-C=CH), 134.4 (d, J<sub>CP</sub> = 4.0 Hz, P-CH<sub>Ar</sub>), 135.0 (d, J<sub>CP</sub> = 4.6 Hz, P-CH<sub>Ar</sub>), 135.4 (s, o-CH<sub>ArF</sub>), 137.9 (d, J<sub>CP</sub> = 21.4 Hz, CH=C-C<sub>Ar</sub>), 144.5 (s, NC<sub>Ar</sub>), 144.9 (s, iPr-C<sub>Ar</sub>), 145.1 (s, iPr-C<sub>Ar</sub>), 162.8 (q, J<sub>CB</sub> = 49.8 Hz, B-C<sub>ArF4</sub>), 188.0 (d, J<sub>CP</sub> = 34.7 Hz, CN), 244.9 (dd, J<sub>CP</sub> = 20.8 and 18.8 Hz, Pb-CH=C).

**<sup>31</sup>P{<sup>1</sup>H} NMR (202 MHz, C<sub>6</sub>D<sub>6</sub> + C<sub>6</sub>H<sub>5</sub>F 25°C):** 171.4 (d, J<sub>PP</sub> = 11.0 Hz, Pb-satellite: J<sub>PPb</sub> = 3765 Hz, PN<sub>2</sub>), 25.0 (d, J<sub>PP</sub> = 11.0 Hz, Pb-satellite: J<sub>PPb</sub> = 382 Hz, PPh<sub>3</sub>).

**<sup>29</sup>Si{<sup>1</sup>H} NMR (99 MHz, C<sub>6</sub>D<sub>6</sub> + C<sub>6</sub>H<sub>5</sub>F 25°C):** 10.9 (d, J<sub>SiP</sub> = 3.6 Hz, SiCH<sub>3</sub>).

**<sup>11</sup>B{<sup>1</sup>H} NMR (160 MHz, C<sub>6</sub>D<sub>6</sub> + C<sub>6</sub>H<sub>5</sub>F 25°C):** -6.0 (s, BAr<sub>4</sub>).

**<sup>19</sup>F NMR (470 MHz, C<sub>6</sub>D<sub>6</sub> + C<sub>6</sub>H<sub>5</sub>F 25°C):** -62.3 (s, CF<sub>3</sub>).

**<sup>207</sup>Pb{<sup>1</sup>H} NMR (C<sub>6</sub>D<sub>6</sub> + C<sub>6</sub>H<sub>5</sub>F 25°C):** 1827.1 (dd, J<sub>PPb</sub> = 3769 and 380 Hz, P-Pb).

**Minor isomer:**

**<sup>1</sup>H NMR (500 MHz, C<sub>6</sub>D<sub>6</sub> + C<sub>6</sub>H<sub>5</sub>F 25°C):** 0.35 (s, 3H, SiCH<sub>3</sub>), 0.39 (s, 3H, SiCH<sub>3</sub>), 0.45 (d, J<sub>HH</sub> = 6.9 Hz, 3H, CH<sub>3iPr</sub>), 0.98 (d, J<sub>HH</sub> = 6.9 Hz, 3H, CH<sub>3iPr</sub>), 1.13 (s, 9H, CH<sub>3tBu</sub>), 1.13 (d, J<sub>HH</sub> = 6.9 Hz, 6H, CH<sub>3iPr</sub>), 1.21 (s, 9H, CH<sub>3tBu</sub>), 1.26 (overlapped, 1H, CH<sub>2</sub>), 1.45 (m, 1H, CH<sub>2</sub>), 1.58 (d, J<sub>HH</sub> = 8.4 Hz, 1H, CH<sub>2</sub>), 1.65 (m, 2H, CH<sub>2</sub>), 1.77

(m, 1H, CH<sub>2</sub>), 2.49 (s, 1H, CH<sub>bridgehead</sub>), 3.02 (overlapped, 1H, CH<sub>bridgehead</sub>), 3.05 (sept, *J<sub>HH</sub>* = 6.9 Hz, 1H, CH<sub>iPr</sub>), 3.20 (sept, *J<sub>HH</sub>* = 6.9 Hz, 1H, CH<sub>iPr</sub>), 7.00-7.14 (m, 23H, CH<sub>Ar</sub>), 10.37 (dd, *J<sub>HP</sub>* = 34.3 and 1.2 Hz, 1H, C=C-H).

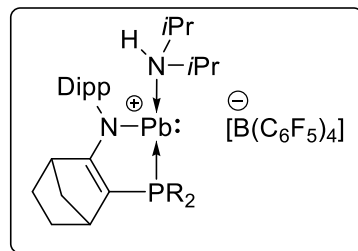
**<sup>13</sup>C{<sup>1</sup>H} NMR (125 MHz, C<sub>6</sub>D<sub>6</sub> + C<sub>6</sub>H<sub>5</sub>F 25°C):** 4.0 (s, SiCH<sub>3</sub>), 7.4 (d, *J<sub>CP</sub>* = 5.8 Hz, SiCH<sub>3</sub>), 23.8 (s, CH<sub>3iPr</sub>), 24.3 (s, CH<sub>3iPr</sub>), 25.0 (s, CH<sub>3iPr</sub>), 25.9 (s, CH<sub>3iPr</sub>), 26.0 (s, CH<sub>2</sub>), 27.8 (s, CH<sub>iPr</sub>), 27.9 (s, CH<sub>iPr</sub>), 29.5 (s, CH<sub>2</sub>), 32.6 (d, *J<sub>CP</sub>* = 4.1 Hz, CH<sub>3tBu</sub>), 33.1 (d, *J<sub>CP</sub>* = 4.1 Hz, CH<sub>3tBu</sub>), 42.0 (d, *J<sub>CP</sub>* = 5.8 Hz, CH<sub>bridgehead</sub>), 43.7 (d, *J<sub>CP</sub>* = 11.6 Hz, CH<sub>bridgehead</sub>), 46.9 (d, *J<sub>CP</sub>* = 4.6 Hz, CH<sub>2</sub>), 51.2 (overlapped, C<sub>tBu</sub>), 51.5 (d, *J<sub>CP</sub>* = 2.9 Hz, C<sub>tBu</sub>), 118.9 (d, *J<sub>CP</sub>* = 84.4 Hz, P-C<sub>Ar</sub>), 123.7 (s, CH<sub>Ar-Dip</sub>), 124.3 (s, CH<sub>Ar-Dip</sub>), 125.9 (s, CH<sub>Ar-Dip</sub>), 128.8 (s, CH<sub>Ar-Ph</sub>), 129.3 (s, CH<sub>Ar-Ph</sub>), 130.1 (d, *J<sub>CP</sub>* = 5.1 Hz, P-CH<sub>Ar</sub>), 132.1 (dd, *J<sub>CP</sub>* = 43.8 and 7.1 Hz, P-C=CH), 134.3 (d, *J<sub>CP</sub>* = 4.0 Hz, P-CH<sub>Ar</sub>), 135.0 (d, JCP = 4.7 Hz, P-CHAR), 138.3 (d, JCP = 22.0 Hz, CH=C-CAr), 144.4 (s, NCAr), 144.6 (s, iPr-CAr), 144.7 (s, iPr-C<sub>Ar</sub>), 188.1 (d, *J<sub>CP</sub>* = 33.8 Hz, CN), 242.3 (dd, *J<sub>CP</sub>* = 21.6 and 19.6 Hz, Pb-CH=C).

**<sup>1</sup>P{<sup>1</sup>H} NMR (202 MHz, C<sub>6</sub>D<sub>6</sub> + C<sub>6</sub>H<sub>5</sub>F 25°C):** 167.2 (d, *J<sub>PP</sub>* = 11.6 Hz, Pb-satellite: *J<sub>PPb</sub>* = 3711 Hz, PN<sub>2</sub>), 25.6 (d, *J<sub>PP</sub>* = 11.2 Hz, Pb-satellite: 386 Hz, PPh<sub>3</sub>).

**<sup>29</sup>Si{<sup>1</sup>H} NMR (99 MHz, C<sub>6</sub>D<sub>6</sub> + C<sub>6</sub>H<sub>5</sub>F 25°C):** 11.3 (d, *J<sub>SiP</sub>* = 4.2 Hz, SiCH<sub>3</sub>).

**<sup>207</sup>Pb{<sup>1</sup>H} NMR (C<sub>6</sub>D<sub>6</sub> + C<sub>6</sub>H<sub>5</sub>F 25°C):** 1677.0 (dd, *J<sub>PbP</sub>* = 3715 and 395 Hz, P-Pb).

Synthesis of cationic derivative of plumbylene **48-NH*i*Pr<sub>2</sub>**:



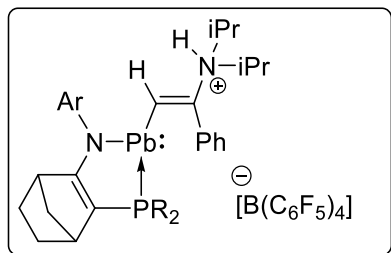
Chloroplumbylene **47** (30 mg, 0.04 mmol) was dissolved in 0.5 ml of fluorobenzene inside the glovebox. K[B(C<sub>6</sub>F<sub>5</sub>)<sub>4</sub>] (31.96 mg, 0.04 mmol) and diisopropylamine (6.2  $\mu$ l, 0.04 mmol) was added to a solution and then stirred for 5 minutes at RT. The dark-red solution was filtrated inside the glovebox in order to eliminate the potassium salts. After washing the product with pentane, the product **48-NH*i*Pr<sub>2</sub>** was obtained as dark red powder (303 mg, yield = 50%). Mp: 136–139 °C (decomp.).

**<sup>1</sup>H NMR (300 MHz, C<sub>6</sub>D<sub>6</sub>, 25 °C):** 0.09 (s, 3H, SiCH<sub>3</sub>), 0.13 (s, 3H, SiCH<sub>3</sub>), 0.03 (s, broad, NH<sub>iPr2</sub>), 0.67 (d, <sup>2</sup>J<sub>HH</sub> = 6.3 Hz, 12H, CH<sub>3iPr</sub>-amine), 0.81 (m, 1H, CH<sub>2</sub>), 0.90 (m, 12H, CH<sub>3iPr</sub>), 0.91 (s, 9H, CH<sub>3tBu</sub>), 0.92 (s, 9H, CH<sub>3tBu</sub>), 1.33 (m, 4H, CH<sub>2</sub>), 1.71 (d, <sup>1</sup>J<sub>HH</sub> = 8.5 Hz, 1H, CH<sub>2</sub>), 2.08 (s, CH<sub>bridgehead</sub>), 2.55 (sept, <sup>2</sup>J<sub>HH</sub> = 6.3 Hz, 2H, CH<sub>iPramine</sub>), 2.65 (s, CH<sub>bridgehead</sub>), 2.89 (m, 2H, CH<sub>iPr</sub>), 7.10 - 6.60 (m, 3H, CH<sub>Ar</sub>).

**<sup>13</sup>C NMR (102 MHz, C<sub>6</sub>D<sub>6</sub>, 25 °C):** 3.4 (s, SiCH<sub>3</sub>), 6.76 (d, J<sub>CP</sub> = 5.8 Hz, SiCH<sub>3</sub>), 22.9 (s, CH<sub>3iPr</sub>-amine x 4), 23.6 (s, CH<sub>3iPr</sub>), 24.2 (s, CH<sub>3iPr</sub>), 25.3 (s, CH<sub>2</sub>), 25.6 (s, CH<sub>3iPr</sub>), 25.8 (s, CH<sub>3iPr</sub>), 27.3 (s, CH<sub>iPr</sub>), 27.6 (s, CH<sub>iPr</sub>), 28.5 (s, CH<sub>2</sub>), 33.7 (m, CH<sub>3tBu</sub>), 33.8 (m, CH<sub>3tBu</sub>), 43.4 (d, J<sub>CP</sub> = 6.2 Hz, CH<sub>bridgehead</sub>), 43.9 (d, J<sub>CP</sub> = 11.2 Hz, CH<sub>bridgehead</sub>), 45.6 (s, CH<sub>iPramine</sub> x 2), 47.2 (s, CH<sub>2</sub>), 50.7 (m, C<sub>tBu</sub> x 2), 1119.6 (d, J<sub>CP</sub> = 15.8 Hz, CP), 123.9 (s, C<sub>Ar</sub>), 124.0 (s, C<sub>Ar</sub>), 126.3 (s, C<sub>Ar</sub>), 142.9 (s, CH<sub>Ar</sub>), 144.6 (s, CH<sub>Ar</sub>), 144.8 (s, CH<sub>Ar</sub>), 189.2 (d, J<sub>CP</sub> = 33.4 Hz, CN).

**<sup>31</sup>P{<sup>1</sup>H} NMR (162 MHz, C<sub>6</sub>D<sub>6</sub>, 25 °C):** 251.1 (s, PN<sub>2</sub>)

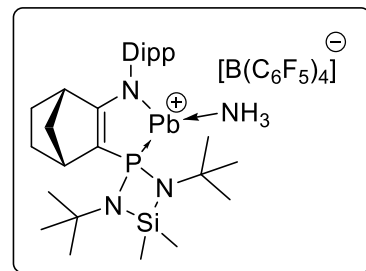
Synthesis of cationic derivative of plumbylene **49-NH*i*Pr<sub>2</sub>**:



To a mixture of chloroplumbylene **47** (200 mg, 0.27 mmol) and K[B(C<sub>6</sub>F<sub>5</sub>)<sub>4</sub>] (213.1 mg, 0.29 mmol) with diisopropylamine (41.85  $\mu$ l, 0.27 mmol) in 2.0 ml of fluorobenzene, phenylacetylene (30.30 mg, 0.27 mmol) was added at room temperature. The solution was stirred for 5 minutes and then filtrated to eliminate potassium salts. After removal of solvent under vacuum, **49-HN*i*Pr<sub>2</sub>** was obtained as a red powder, and was analyzed without any further purification due to its low stability.

<sup>31</sup>P NMR (121 MHz, C<sub>6</sub>D<sub>6</sub> + C<sub>6</sub>H<sub>5</sub>F, 25°C): 176.3 ppm (PR<sub>2</sub>, s, <sup>1</sup>J<sub>PbP</sub> = 2404 Hz).

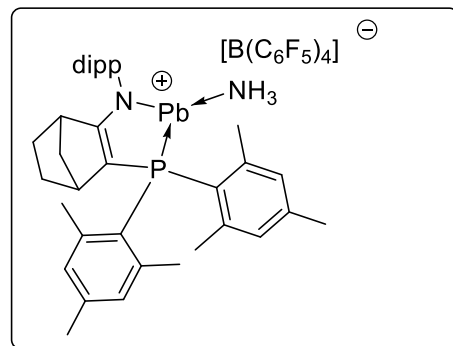
Synthesis of cationic derivative of plumbylene **48-NH<sub>3</sub>**:



The mixture of chloroplumbylene **47** (30 mg, 0.04 mmol) and K[B(C<sub>6</sub>F<sub>5</sub>)<sub>4</sub>] (31.96 mg, 0.04 mmol) was dissolved in C<sub>6</sub>H<sub>5</sub>F (0.5 ml) with one drop of C<sub>6</sub>D<sub>6</sub>. Then solution was cooled at -30°C and 3 bars of NH<sub>3</sub> was added. After 5 minutes the crude solution was analysed by NMR spectroscopy.

**<sup>31</sup>P NMR (122 MHz, C<sub>6</sub>D<sub>6</sub>)**: 217 ppm (PR<sub>2</sub>, s, <sup>1</sup>J<sub>Pb-P</sub> = 3953 Hz).

Synthesis of cationic derivative of plumbylene **48b-NH<sub>3</sub>**:



The mixture of chloroplumbylene **47b** (30 mg, 0.04 mmol) and K[B(C<sub>6</sub>F<sub>5</sub>)<sub>4</sub>] (31.96 mg, 0.04 mmol) was dissolved in C<sub>6</sub>H<sub>5</sub>F (0.5 ml) with one drop of C<sub>6</sub>D<sub>6</sub>. Then solution was cooled at -30°C and 3 bars of NH<sub>3</sub> was added. After 5 minutes the crude solution was analysed by NMR spectroscopy.

**<sup>31</sup>P NMR (122 MHz, CDCl<sub>3</sub>):** 48 ppm (PR<sub>2</sub>, s, <sup>1</sup>J<sub>Pb-P</sub> = 1486 Hz).

## **General conclusion**

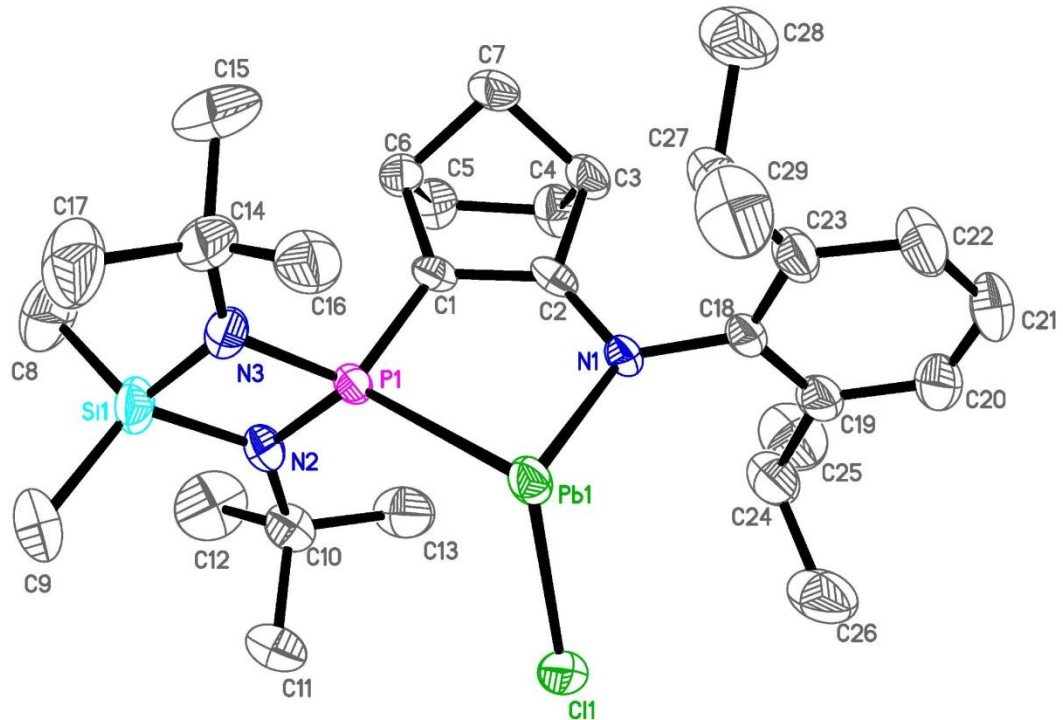
## General conclusion

Encouraged by the work done in our group concerning phosphine-stabilized silylenes and germylenes, we have developed the synthesis of an original stable phosphine-stabilized chloroplumbylene. Interestingly, the nucleophilic substitution of chlorine atom by NaPCO affords a new phosphaketene functionalized plumbylene. In contrast to the lighter analogues, this new phosphaketene-substituted plumbylene evolves in an unusual manner by reductive elimination at the divalent lead center, giving new phosphanylidene- $\sigma^4$ -phosphoranes and metallic lead. The five-membered (amino)phosphanylidene- $\sigma^4$ -phosphorane has a unique reactivity as an imine-stabilized phosphinidene due to the highly polarized phospha-ylide function and the labile P(II)-N bond. A mechanistic study demonstrated that the reaction proceeds via reductive elimination at the Pb(II) center, leading to new amino- and phosphonio-phosphaketene derivatives, which evolve to give the phosphanylidene phosphoranes obtained experimentally. Notably, the amino-phosphaketene evolves by CO removal to generate a phosphinidene intermediate that is stabilized by phosphine coordination to produce the cyclic phosphanylidene phosphorane. These results suggest that plumbylene-substituted phosphaketenes may be useful phosphinidene precursors, since the only by-products are inert molecules (metallic Pb and CO gas).

The reactivity of the parent chloroplumbylene complex can be significantly enhanced by abstraction of chlorine atom affording a new cationic phosphine-stabilized plumbylumylidene. These Pb(II)<sup>+</sup> cations are extremely electrophilic and can be stabilized by the coordination of various Lewis base ligands. Despite the stabilization of the plumbylene cation by two ligands, it still remains reactive and readily reacts with phenylacetylene via alkyne insertion into the Pb-L bond (L = PR<sub>3</sub>, NR<sub>3</sub>). Notably, the Pb<sup>+</sup> stabilized by a secondary amine (HNiPr<sub>2</sub>) can be used as a catalyst for the hydroamination of phenylacetylene. However, hydroamination attempts of unsaturated compounds with ammonia have failed so far and therefore the models should be redesigned to improve their performances.

## **Annexe**

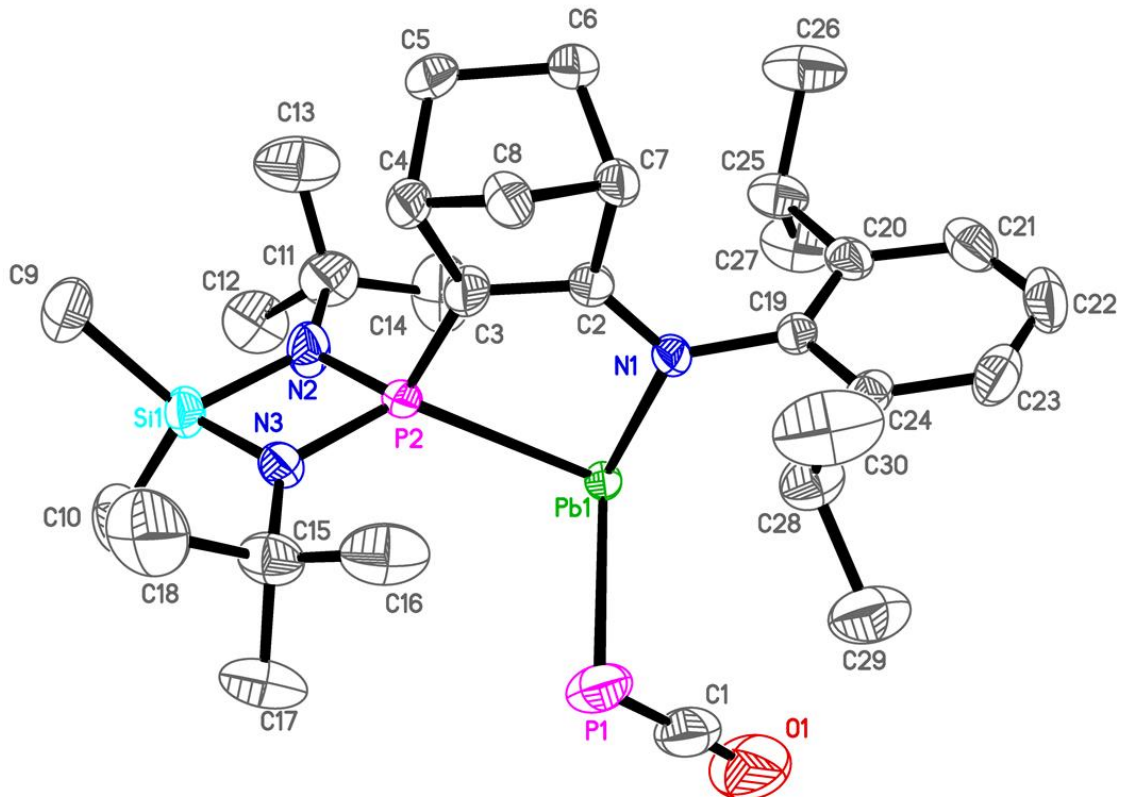
Chapter 2, compound 29 :



Empirical formula	C <sub>29</sub> H <sub>49</sub> ClN <sub>3</sub> PbSi		
Formula weight	741.41		
Temperature	193(2) K		
Wavelength	0.71073 Å		
Crystal system	Triclinic		
Space group	P-1		
Unit cell dimensions	a = 10.2600(3) Å	α = 73.4280(12)°.	
	b = 13.0876(4) Å	β = 80.2052(12)°.	
	c = 13.8636(5) Å	γ = 73.8722(12)°.	
Volume	1705.67(10) Å <sup>3</sup>		
Z	2		
Density (calculated)	1.444 Mg/m <sup>3</sup>		
Absorption coefficient	5.127 mm <sup>-1</sup>		
F(000)	744		
Crystal size	0.180 x 0.160 x 0.120 mm <sup>3</sup>		
Theta range for data collection	2.705 to 28.324°.		
Index ranges	-13<=h<=12, -17<=k<=17, -18<=l<=18		
Reflections collected	49276		
Independent reflections	8491 [R(int) = 0.0443]		
Completeness to theta = 25.242°	99.9 %		
Absorption correction	Semi-empirical from equivalents		

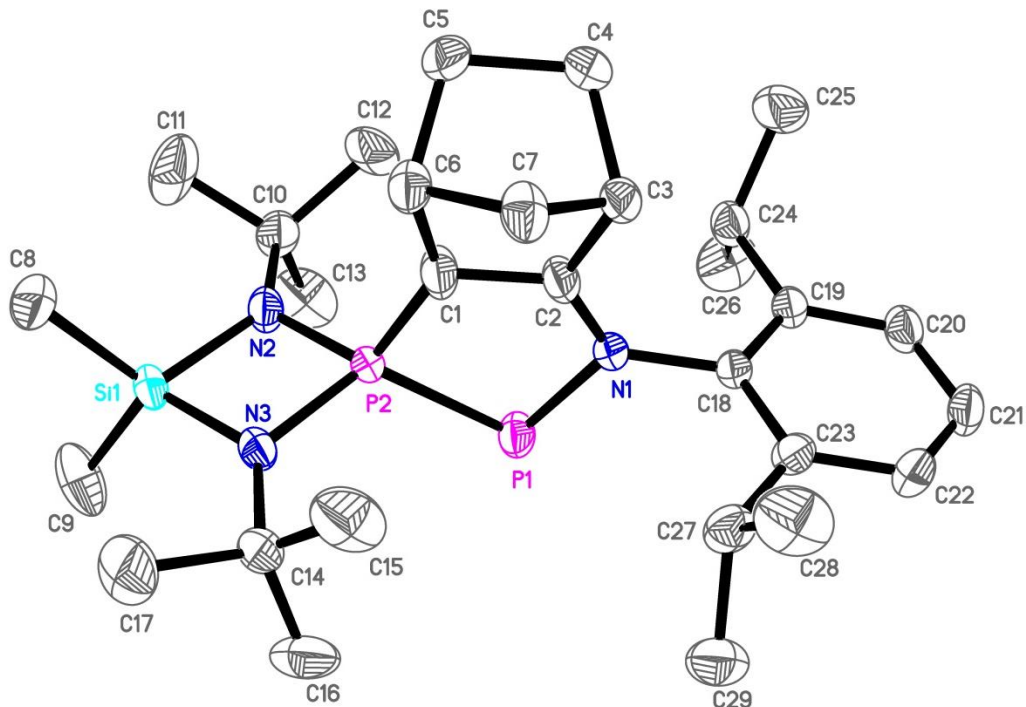
Max. and min. transmission	0.7457 and 0.6217
Refinement method	Full-matrix least-squares on F <sup>2</sup>
Data / restraints / parameters	8491 / 317 / 401
Goodness-of-fit on F <sup>2</sup>	1.049
Final R indices [I>2sigma(I)]	R1 = 0.0228, wR2 = 0.0406
R indices (all data)	R1 = 0.0341, wR2 = 0.0434
Extinction coefficient	n/a
Largest diff. peak and hole	1.071 and -0.757 e.Å <sup>-3</sup>

Chapter 2, compound 30 :



Empirical formula	C <sub>30</sub> H <sub>49</sub> N <sub>3</sub> O <sub>2</sub> P <sub>2</sub> PbSi		
Formula weight	764.94		
Temperature	193(2) K		
Wavelength	0.71073 Å		
Crystal system	Monoclinic		
Space group	P <sub>2</sub> /c		
Unit cell dimensions	a = 10.7130(7) Å	α = 90°.	
	b = 16.5676(8) Å	β = 96.446(2)°.	
	c = 19.1860(11) Å	γ = 90°.	
Volume	3383.8(3) Å <sup>3</sup>		
Z	4		
Density (calculated)	1.502 Mg/m <sup>3</sup>		
Absorption coefficient	5.142 mm <sup>-1</sup>		
F(000)	1536		
Crystal size	0.150 x 0.140 x 0.080 mm <sup>3</sup>		
Theta range for data collection	2.420 to 28.319°.		
Index ranges	-14≤h≤14, -22≤k≤22, -25≤l≤25		
Reflections collected	154386		
Independent reflections	8413 [R(int) = 0.0811]		
Completeness to theta = 25.242°	99.9 %		
Absorption correction	Semi-empirical from equivalents		

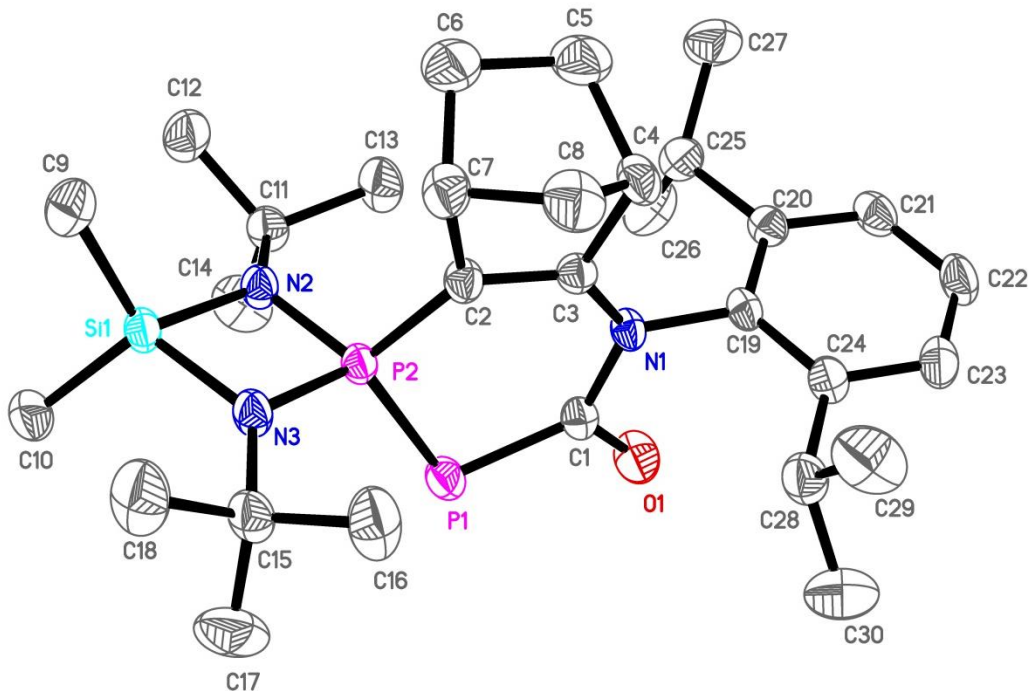
Max. and min. transmission	0.7457 and 0.6621
Refinement method	Full-matrix least-squares on F <sup>2</sup>
Data / restraints / parameters	8413 / 398 / 463
Goodness-of-fit on F <sup>2</sup>	1.064
Final R indices [I>2sigma(I)]	R1 = 0.0283, wR2 = 0.0534
R indices (all data)	R1 = 0.0429, wR2 = 0.0576
Extinction coefficient	n/a
Largest diff. peak and hole	0.616 and -0.440 e.Å <sup>-3</sup>



Empirical formula	C <sub>29</sub> H <sub>49</sub> N <sub>3</sub> P <sub>2</sub> Si		
Formula weight	529.74		
Temperature	193(2) K		
Wavelength	0.71073 Å		
Crystal system	Triclinic		
Space group	P-1		
Unit cell dimensions	a = 10.5392(7) Å	α = 95.982(3)°.	
	b = 12.2753(9) Å	β = 107.687(3)°.	
	c = 13.3336(9) Å	γ = 96.217(3)°.	
Volume	1616.6(2) Å <sup>3</sup>		
Z	2		
Density (calculated)	1.088 Mg/m <sup>3</sup>		
Absorption coefficient	0.192 mm <sup>-1</sup>		
F(000)	576		
Crystal size	0.300 x 0.200 x 0.170 mm <sup>3</sup>		
Theta range for data collection	2.992 to 28.371°.		
Index ranges	-14≤h≤14, -16≤k≤16, -17≤l≤17		
Reflections collected	50400		
Independent reflections	8025 [R(int) = 0.0810]		

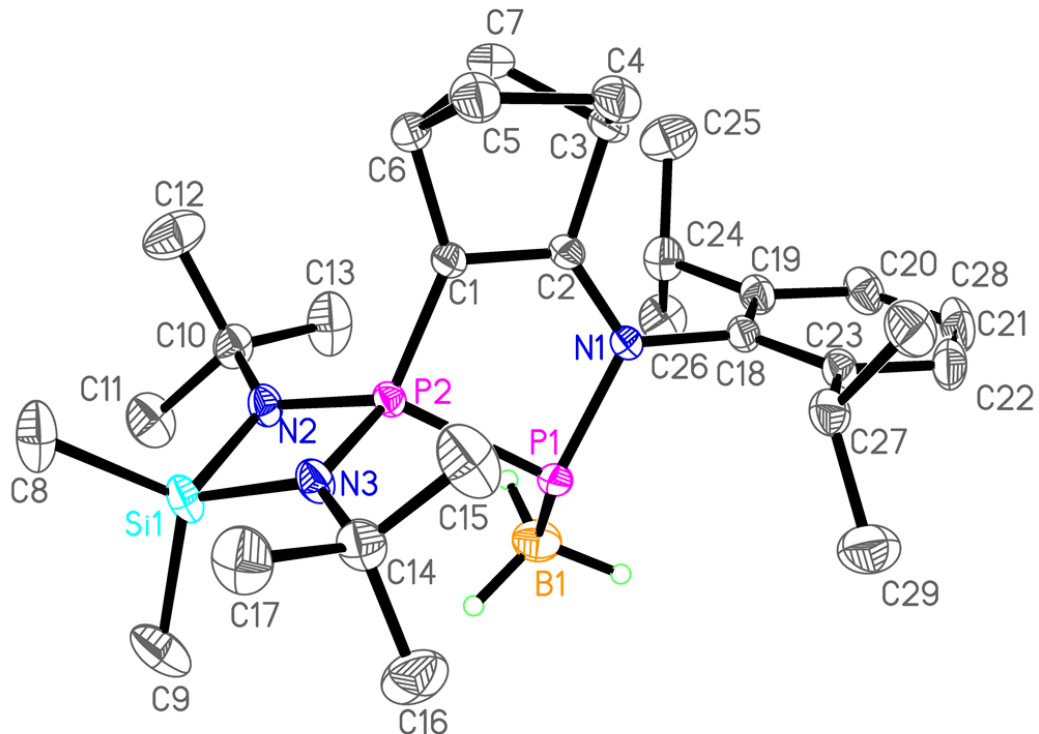
Completeness to theta = 25.242°	99.8 %
Absorption correction	Semi-empirical from equivalents
Max. and min. transmission	0.7457 and 0.7069
Refinement method	Full-matrix least-squares on F <sup>2</sup>
Data / restraints / parameters	8025 / 350 / 424
Goodness-of-fit on F <sup>2</sup>	1.025
Final R indices [I>2sigma(I)]	R1 = 0.0594, wR2 = 0.1402
R indices (all data)	R1 = 0.1048, wR2 = 0.1639
Extinction coefficient	n/a
Largest diff. peak and hole	0.463 and -0.332 e.Å <sup>-3</sup>

Chapter 2, compound 36 :



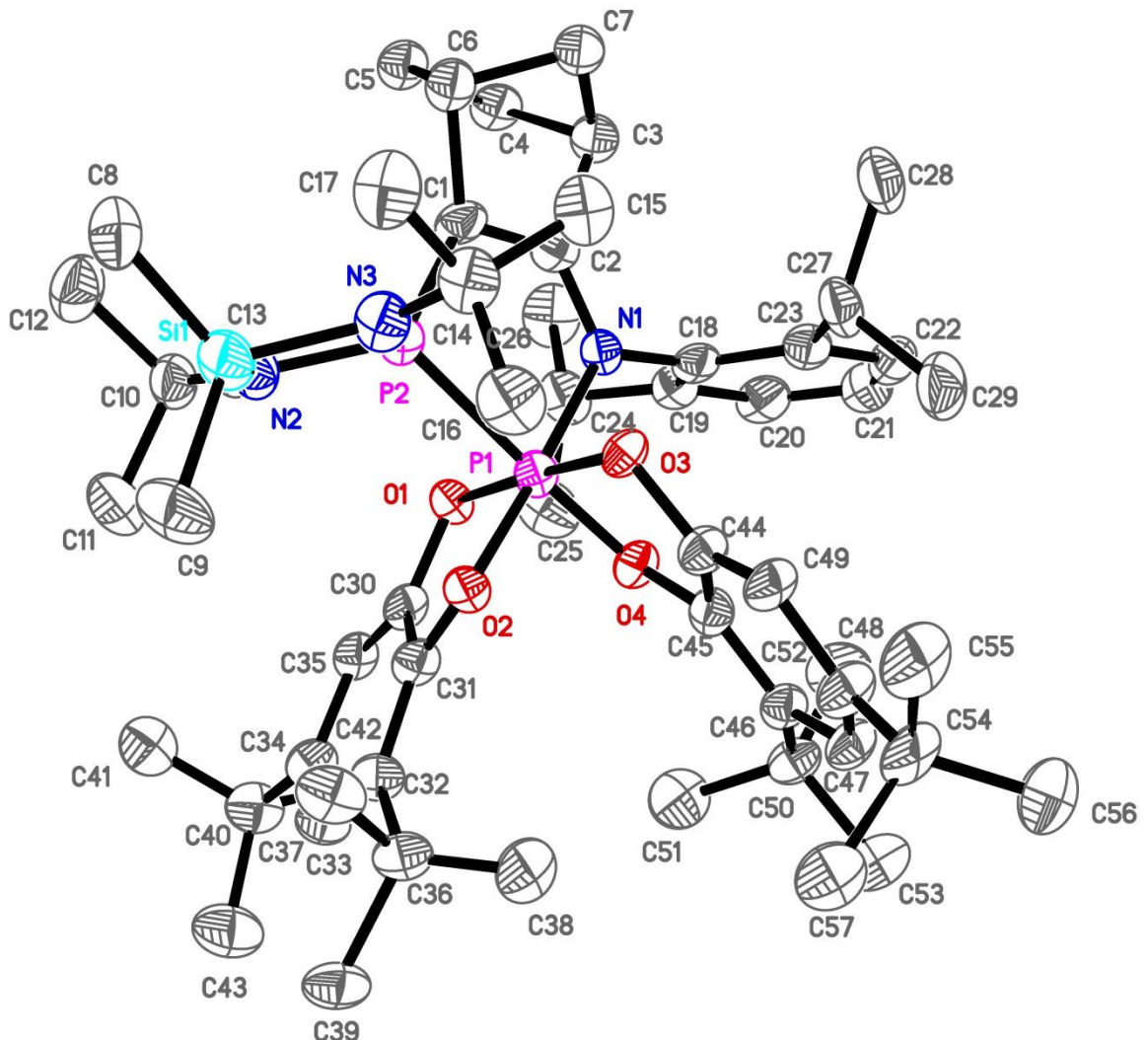
Empirical formula	C <sub>30</sub> H <sub>49</sub> N <sub>3</sub> O P <sub>2</sub> Si		
Formula weight	557.75		
Temperature	193(2) K		
Wavelength	0.71073 Å		
Crystal system	Monoclinic		
Space group	P <sub>2</sub> /c		
Unit cell dimensions	a = 16.4412(6) Å	α = 90°.	
	b = 11.8509(4) Å	β = 114.4634(11)°.	
	c = 18.3093(7) Å	γ = 90°.	
Volume	3247.2(2) Å <sup>3</sup>		
Z	4		
Density (calculated)	1.141 Mg/m <sup>3</sup>		
Absorption coefficient	0.197 mm <sup>-1</sup>		
F(000)	1208		
Crystal size	0.180 x 0.160 x 0.150 mm <sup>3</sup>		
Theta range for data collection	2.806 to 29.596°.		
Index ranges	-22<=h<=22, -16<=k<=16, -25<=l<=25		
Reflections collected	137610		

Independent reflections	9106 [R(int) = 0.0880]
Completeness to theta = 25.242°	99.9 %
Absorption correction	Semi-empirical from equivalents
Max. and min. transmission	0.7454 and 0.7016
Refinement method	Full-matrix least-squares on F <sup>2</sup>
Data / restraints / parameters	9106 / 0 / 346
Goodness-of-fit on F <sup>2</sup>	1.043
Final R indices [I>2sigma(I)]	R1 = 0.0492, wR2 = 0.1190
R indices (all data)	R1 = 0.0780, wR2 = 0.1354
Extinction coefficient	n/a
Largest diff. peak and hole	0.918 and -0.273 e.Å <sup>-3</sup>



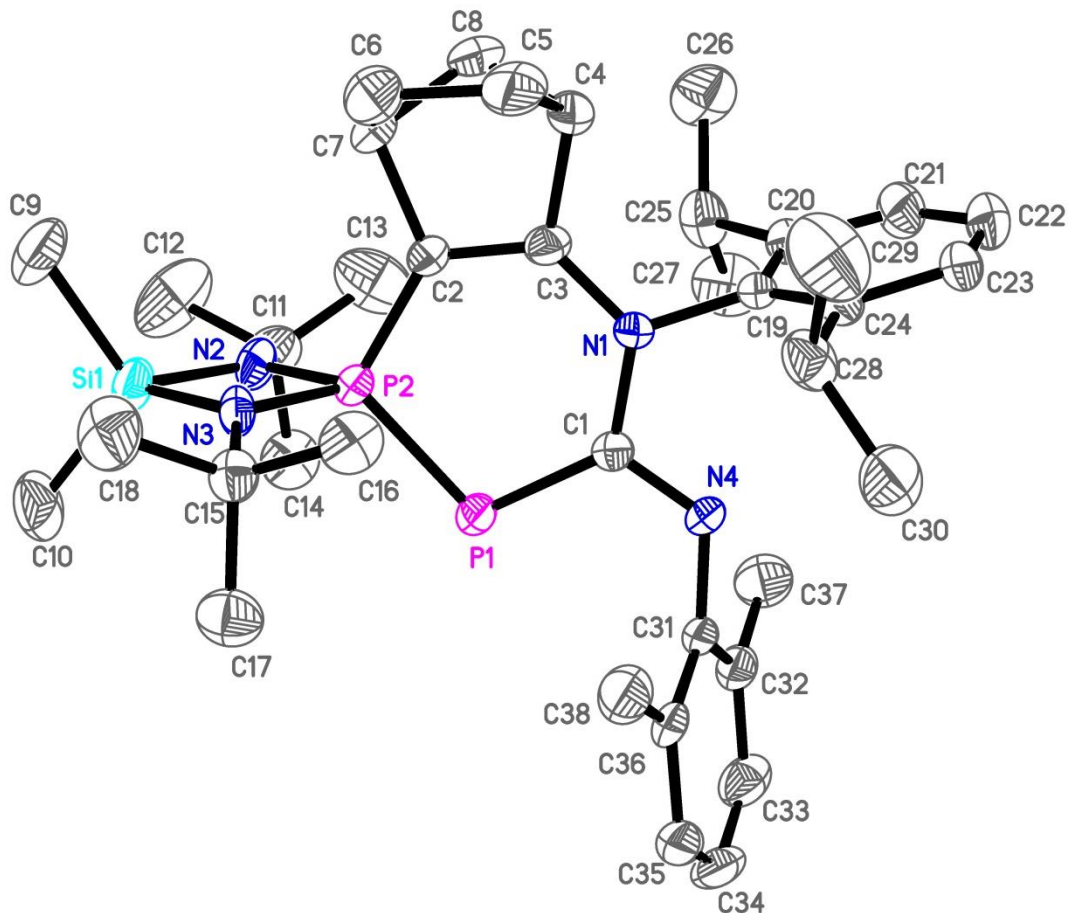
Empirical formula	C <sub>29</sub> H <sub>52</sub> B <sub>1</sub> N <sub>3</sub> P <sub>2</sub> Si		
Formula weight	543.57		
Temperature	193(2) K		
Wavelength	0.71073 Å		
Crystal system	Triclinic		
Space group	P-1		
Unit cell dimensions	a = 10.7735(5) Å	α = 67.9234(18)°.	
	b = 17.2017(9) Å	β = 85.5619(18)°.	
	c = 20.4495(10) Å	γ = 72.9133(18)°.	
Volume	3354.5(3) Å <sup>3</sup>		
Z	4		
Density (calculated)	1.076 Mg/m <sup>3</sup>		
Absorption coefficient	0.186 mm <sup>-1</sup>		
F(000)	1184		
Crystal size	0.500 x 0.300 x 0.200 mm <sup>3</sup>		
Theta range for data collection	2.646 to 28.343°.		
Index ranges	-12≤h≤14, -22≤k≤22, -27≤l≤27		
Reflections collected	112722		
Independent reflections	16667 [R(int) = 0.0291]		

Completeness to theta = 25.242°	99.4 %
Absorption correction	Semi-empirical from equivalents
Max. and min. transmission	0.7457 and 0.6913
Refinement method	Full-matrix least-squares on F <sup>2</sup>
Data / restraints / parameters	16667 / 258 / 772
Goodness-of-fit on F <sup>2</sup>	1.021
Final R indices [I>2sigma(I)]	R1 = 0.0446, wR2 = 0.1203
R indices (all data)	R1 = 0.0544, wR2 = 0.1289
Extinction coefficient	n/a
Largest diff. peak and hole	0.597 and -0.646 e.Å <sup>-3</sup>



Empirical formula	C <sub>57</sub> H <sub>89</sub> N <sub>3</sub> O <sub>4</sub> P <sub>2</sub> Si		
Formula weight	970.34		
Temperature	193(2) K		
Wavelength	0.71073 Å		
Crystal system	Monoclinic		
Space group	P <sub>2</sub> <sub>1</sub> /n		
Unit cell dimensions	a = 12.368(3) Å	α = 90°.	
	b = 23.744(7) Å	β = 96.690(7)°.	
	c = 19.528(5) Å	γ = 90°.	
Volume	5696(3) Å <sup>3</sup>		
Z	4		
Density (calculated)	1.132 Mg/m <sup>3</sup>		
Absorption coefficient	0.143 mm <sup>-1</sup>		
F(000)	2112		

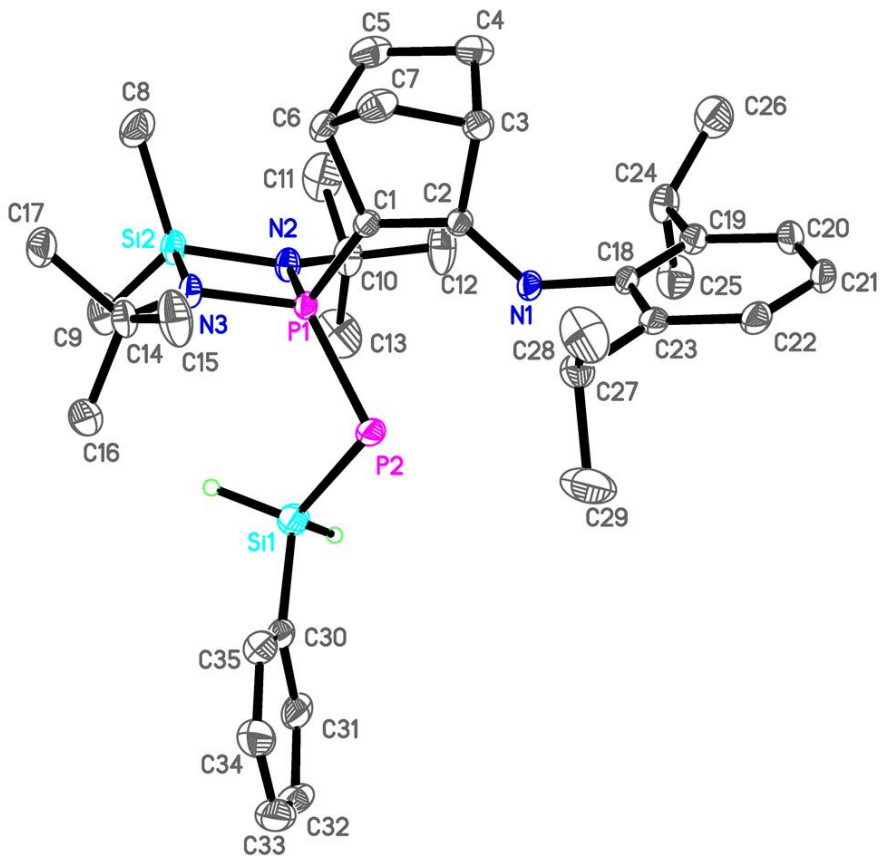
Crystal size	0.080 x 0.050 x 0.030 mm <sup>3</sup>
Theta range for data collection	2.528 to 25.218°.
Index ranges	-14<=h<=14, -28<=k<=28, -23<=l<=22
Reflections collected	104014
Independent reflections	10212 [R(int) = 0.3485]
Completeness to theta = 25.218°	99.3 %
Absorption correction	Semi-empirical from equivalents
Max. and min. transmission	0.5858 and 0.4394
Refinement method	Full-matrix least-squares on F <sup>2</sup>
Data / restraints / parameters	10212 / 1037 / 877
Goodness-of-fit on F <sup>2</sup>	1.015
Final R indices [I>2sigma(I)]	R1 = 0.1133, wR2 = 0.2285
R indices (all data)	R1 = 0.2880, wR2 = 0.3181
Extinction coefficient	n/a
Largest diff. peak and hole	0.324 and -0.396 e.Å <sup>-3</sup>



Empirical formula	C <sub>38</sub> H <sub>58</sub> N <sub>4</sub> P <sub>2</sub> Si	
Formula weight	660.91	
Temperature	193(2) K	
Wavelength	0.71073 Å	
Crystal system	Orthorhombic	
Space group	Pbcn	
Unit cell dimensions	a = 33.244(4) Å	α = 90°.
	b = 13.1020(14) Å	β = 90°.
	c = 18.125(2) Å	γ = 90°.
Volume	7894.4(15) Å <sup>3</sup>	
Z	8	
Density (calculated)	1.112 Mg/m <sup>3</sup>	
Absorption coefficient	0.170 mm <sup>-1</sup>	
F(000)	2864	
Crystal size	0.200 x 0.030 x 0.020 mm <sup>3</sup>	

Theta range for data collection	2.904 to 25.505°.
Index ranges	-40<=h<=40, -13<=k<=15, -21<=l<=21
Reflections collected	181663
Independent reflections	7247 [R(int) = 0.3479]
Completeness to theta = 25.242°	99.6 %
Absorption correction	Semi-empirical from equivalents
Max. and min. transmission	0.6971 and 0.6297
Refinement method	Full-matrix least-squares on F <sup>2</sup>
Data / restraints / parameters	7247 / 0 / 420
Goodness-of-fit on F <sup>2</sup>	1.022
Final R indices [I>2sigma(I)]	R1 = 0.0654, wR2 = 0.1235
R indices (all data)	R1 = 0.1570, wR2 = 0.1636
Extinction coefficient	n/a
Largest diff. peak and hole	0.322 and -0.277 e.Å <sup>-3</sup>

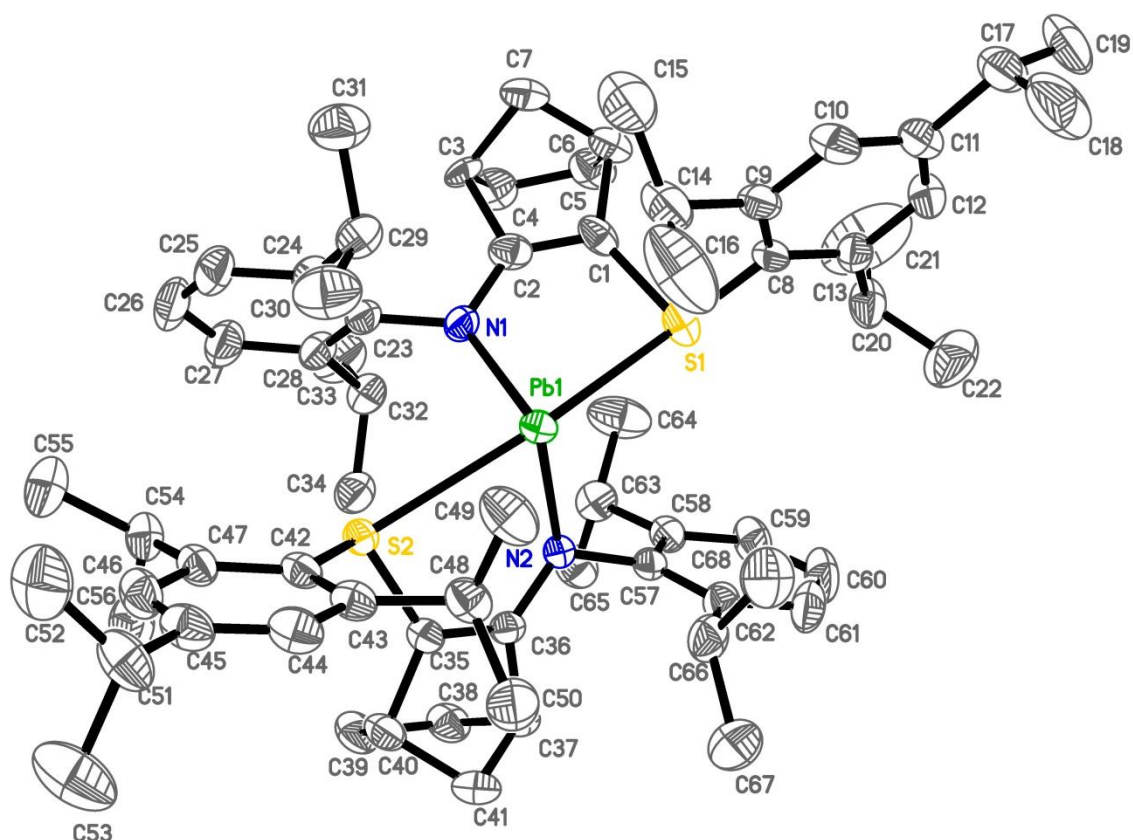
Chapter 2, compound 48



Empirical formula	C <sub>35</sub> H <sub>57</sub> N <sub>3</sub> P <sub>2</sub> Si <sub>2</sub>		
Formula weight	637.95		
Temperature	193(2) K		
Wavelength	0.71073 Å		
Crystal system	Monoclinic		
Space group	P2 <sub>1</sub> /c		
Unit cell dimensions	a = 9.1808(4) Å	α= 90°.	
	b = 33.9156(14) Å	β= 105.5158(14)°.	
	c = 12.6790(5) Å	γ = 90°.	
Volume	3804.0(3) Å <sup>3</sup>		
Z	4		
Density (calculated)	1.114 Mg/m <sup>3</sup>		
Absorption coefficient	0.204 mm <sup>-1</sup>		
F(000)	1384		
Crystal size	0.300 x 0.200 x 0.150 mm <sup>3</sup>		
Theta range for data collection	2.924 to 26.478°.		
Index ranges	-11≤h≤11, -42≤k≤42, -15≤l≤15		

Reflections collected	131339
Independent reflections	7829 [R(int) = 0.0719]
Completeness to theta = 25.242°	99.8 %
Absorption correction	Semi-empirical from equivalents
Max. and min. transmission	0.7415 and 0.7123
Refinement method	Full-matrix least-squares on F <sup>2</sup>
Data / restraints / parameters	7829 / 0 / 403
Goodness-of-fit on F <sup>2</sup>	1.110
Final R indices [I>2sigma(I)]	R1 = 0.0511, wR2 = 0.1114
R indices (all data)	R1 = 0.0679, wR2 = 0.1194
Extinction coefficient	n/a
Largest diff. peak and hole	0.433 and -0.255 e.Å <sup>-3</sup>

Chapter 2, compound 54



Empirical formula	C <sub>68</sub> H <sub>96</sub> N <sub>2</sub> PbS <sub>2</sub>		
Formula weight	1212.77		
Temperature	193(2) K		
Wavelength	0.71073 Å		
Crystal system	Monoclinic		
Space group	P2 <sub>1</sub> /c		
Unit cell dimensions	a = 19.4548(10) Å	α = 90°.	
	b = 17.6108(10) Å	β = 97.983(2)°.	
	c = 18.6436(10) Å	γ = 90°.	
Volume	6325.7(6) Å <sup>3</sup>		
Z	4		
Density (calculated)	1.273 Mg/m <sup>3</sup>		
Absorption coefficient	2.773 mm <sup>-1</sup>		
F(000)	2528		
Crystal size	0.200 x 0.200 x 0.120 mm <sup>3</sup>		
Theta range for data collection	2.491 to 28.297°.		
Index ranges	-25≤h≤25, -23≤k≤23, -24≤l≤24		
Reflections collected	270766		
Independent reflections	15681 [R(int) = 0.0458]		
Completeness to theta = 25.242°	99.8 %		

Absorption correction	Semi-empirical from equivalents
Max. and min. transmission	0.7457 and 0.6572
Refinement method	Full-matrix least-squares on F <sup>2</sup>
Data / restraints / parameters	15681 / 371 / 768
Goodness-of-fit on F <sup>2</sup>	1.102
Final R indices [I>2sigma(I)]	R1 = 0.0218, wR2 = 0.0492
R indices (all data)	R1 = 0.0367, wR2 = 0.0575
Extinction coefficient	n/a
Largest diff. peak and hole	1.211 and -0.638 e. $\text{\AA}^{-3}$

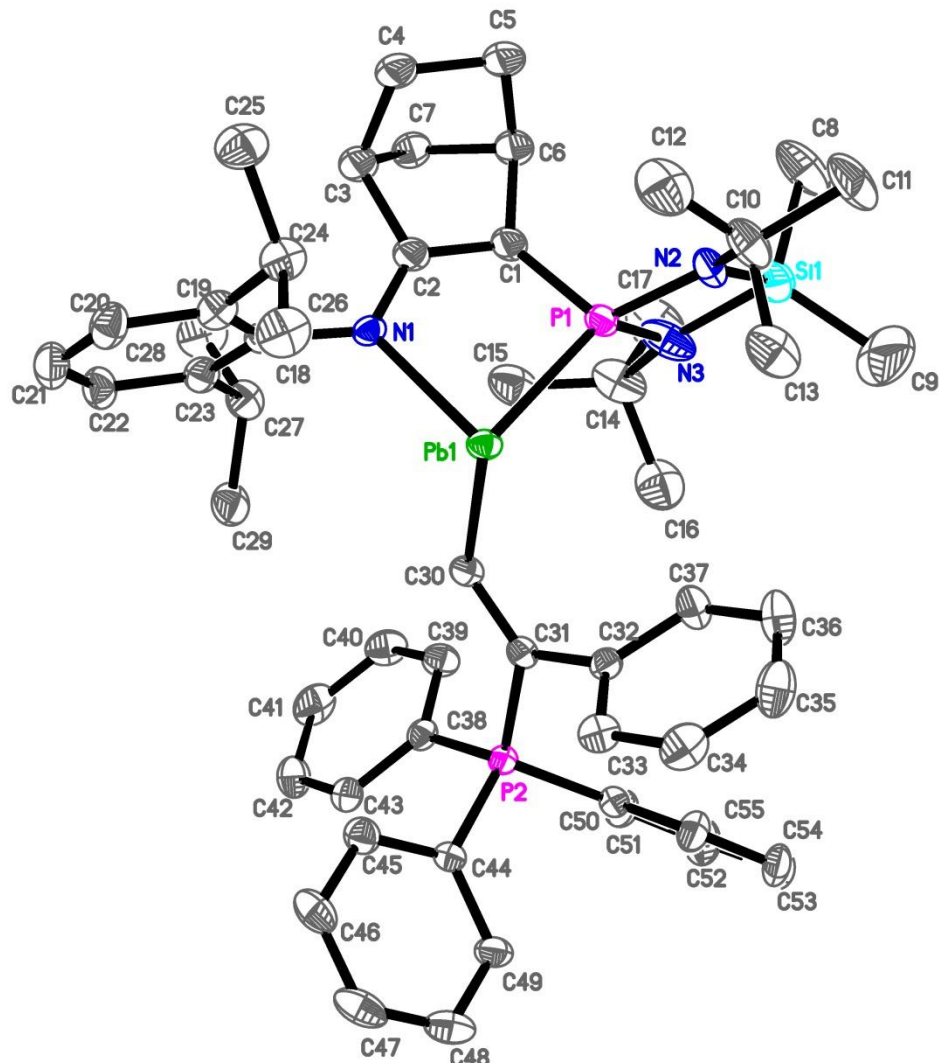


Table 1. Crystal data and structure refinement for ASWIN030320\_a.

Identification code	ASWIN030320_a		
Empirical formula	C82	H72.50	B F20.50 N3 P2 Pb Si
Formula weight	1797.46		
Temperature	193(2)	K	
Wavelength	0.71073	Å	
Crystal system	Monoclinic		
Space group	P2 <sub>1</sub> /c		
Unit cell dimensions	a = 18.2204(10) Å	α = 90°.	
	b = 27.3719(16) Å	β = 93.5337(19)°.	
	c = 17.4612(9) Å	γ = 90°.	
Volume	8691.8(8) Å <sup>3</sup>		

Z	4
Density (calculated)	1.374 Mg/m <sup>3</sup>
Absorption coefficient	2.077 mm <sup>-1</sup>
F(000)	3604
Crystal size	0.300 x 0.060 x 0.050 mm <sup>3</sup>
Theta range for data collection	2.453 to 28.304°.
Index ranges	-24<=h<=24, -36<=k<=36, -22<=l<=23
Reflections collected	264184
Independent reflections	21580 [R(int) = 0.1126]
Completeness to theta = 25.242°	99.8 %
Absorption correction	Semi-empirical from equivalents
Max. and min. transmission	0.7457 and 0.6327
Refinement method	Full-matrix least-squares on F <sup>2</sup>
Data / restraints / parameters	21580 / 828 / 1253
Goodness-of-fit on F <sup>2</sup>	1.042
Final R indices [I>2sigma(I)]	R1 = 0.0458, wR2 = 0.1093
R indices (all data)	R1 = 0.0892, wR2 = 0.1301
Extinction coefficient	n/a
Largest diff. peak and hole	1.300 and -0.699 e.Å <sup>-3</sup>

# Résumé du projet : Plombylènes stabilisés par des phosphines : précurseurs de nouveaux phosphinidènes et cations plombyliumylidènes

## I. Introduction

Ces dernières années ont vu une résurgence majeure de la chimie des éléments du groupe principal en raison du développement de composés de basse valence présentant un comportement de métal de transition. Parmi ces espèces, les carbènes et leurs analogues plus lourds, les tétrylènes, qui possèdent un faible écart HO-BV et des orbitales frontières semblables à celles des métaux de transition, sont des candidats prometteurs pour remplacer les complexes organométalliques coûteux. En effet, ces composés de basse valence sont capables d'activer de petites molécules par une étape d'addition oxydante. Cependant, les tétrylènes ont tendance à former des adduits à haut degré d'oxydation (IV) très stables, ce qui complique l'étape d'élimination réductrice permettant de reformer l'espèce active à bas degré d'oxydation.

La stabilité relative des bas degrés d'oxydation des espèces du groupe 14 augmente avec le numéro atomique de l'élément correspondant, et ainsi, les plombylènes sont parmi les tétrylènes les plus stables. En outre, les liaisons Pb-C étant particulièrement faibles, les substituants sur l'atome de Pb sont labiles et peuvent être facilement échangés. Ainsi, théoriquement, les plombylènes devraient être les candidats les plus adaptées pour la catalyse. De plus, la réactivité des plombylènes pourrait être exaltée en les transformant en espèces cationiques, les ions plombyliumylidène, qui possèdent une orbitale p vacante supplémentaire et une charge cationique, ce qui devrait les rendre plus électrophiles et donc extrêmement réactifs.

Cependant, l'étude des plombyliumylidènes et de leur réactivité reste pour l'instant très peu développée. Cette thèse vise à combler cette lacune en développant de nouveaux plombylènes et cations plombyliumylidènes stabilisés par un ligand amido-phosphine original développé par notre groupe, et à étudier leur chimie, en visant de nouvelles propriétés spécifiques et une réactivité qui ne peuvent pas être induites par d'autres systèmes de ligands.

## II. Synthèse d'un phosphacétène substitué par un fragment plombylène et réaction de décarbonylation

Les plombylènes ( $R_2Pb:$ ) sont les analogues les plus lourds des carbènes parmi les tétrylènes (figure 1). La stabilité des tétrylènes (état divalent) augmente lorsque le nombre quantique principal ( $n$ ) augmente en raison des effets relativistes. Cela signifie que parmi tous les tétrylènes, les plombylènes montrent une plus grande stabilité. Ceci n'est pas un handicap, car la plus grande stabilité de l'état divalent fait des plombylènes les espèces les plus prometteuses pour la catalyse, puisque l'étape d'élimination réductrice devrait être, théoriquement, plus facile.

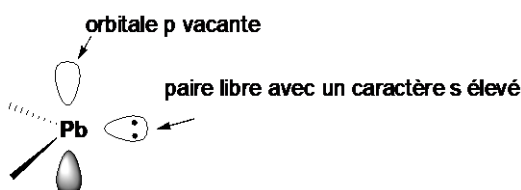
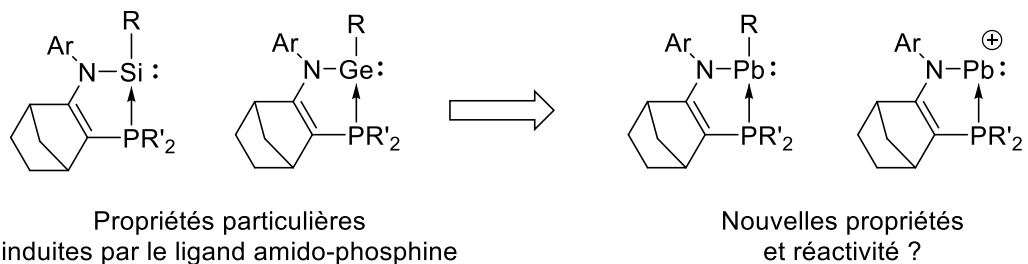


Figure 1. État fondamental singulet des plombylènes.

Ainsi, comme les tétrylènes, les plombylènes ont une orbitale p vacante et une paire d'électrons libre ayant un caractère s renforcé sur le même atome. En raison de la déficience électronique élevée (il manque 2 électrons pour satisfaire la règle de l'octet) et de la présence d'une paire d'électrons libre, les plombylènes sont très réactifs, ce qui rend leur synthèse en tant qu'espèces stables difficile.

Pour stabiliser ces plombylènes, nous avons envisagé l'utilisation d'un ligand amido-phosphine original développé par notre groupe, qui nous a déjà permis de préparer d'autres métallylènes stables (silylènes et germylènes). Une caractéristique clé de ce ligand est la structure bicyclique insaturée rigide qui relie les fragments amido et phosphine. Grâce à sa rigidité, malgré la labilité de la coordination du fragment P au site réactif des métallylènes (l'interaction labile  $P \rightarrow Si$  et  $P \rightarrow Ge$ ), le ligand reste sur le centre réactif du métallylène pour le stabiliser. D'autre part, le ligand

amido-phosphine possède un niveau élevé d'encombrement stérique grâce au substituant amido volumineux (Ar) et au ligand phosphine ( $\text{PR}_2$ ), ce qui permet une stabilisation cinétique efficace.



## II.I Synthèse et caractérisation d'un chloroplombylène stabilisé par une iminophosphine 1

Le chloroplombylène **1** stabilisé par la phosphine a été préparé en suivant la stratégie de synthèse déjà établie dans notre groupe (Schéma 1). L'avantage de celle-ci est que la synthèse ne nécessite pas d'équipement spécial et qu'elle peut être réalisée à grande échelle (50 - 100 g). De plus, cette synthèse est remarquablement modulable, puisqu'à chaque étape, chaque réactif (cétone, amine et phosphine) peut être changé pour ajuster et optimiser l'encombrement stérique, la nature de la base de Lewis, ou même changer la base de Lewis elle-même, sans modification conséquente des conditions expérimentales. La synthèse commence par la réaction de condensation d'une aryl-amine primaire avec le norcamphor pour donner l'imine **2** correspondante. Ensuite, la position  $\alpha$  de l'imine subit une déprotonation avec du n-butyl-lithium à  $-80^\circ\text{C}$  dans le THF, suivie par l'addition d'un équivalent de chlorophosphine donnant l'iminophosphine **3** avec un rendement de 93%. L'addition du ligand iminophosphine lithié à une suspension de  $\text{PbCl}_2$  dans le THF conduit à la formation du chloroplombylène **1** correspondant avec un rendement de 77 % (schéma 1).

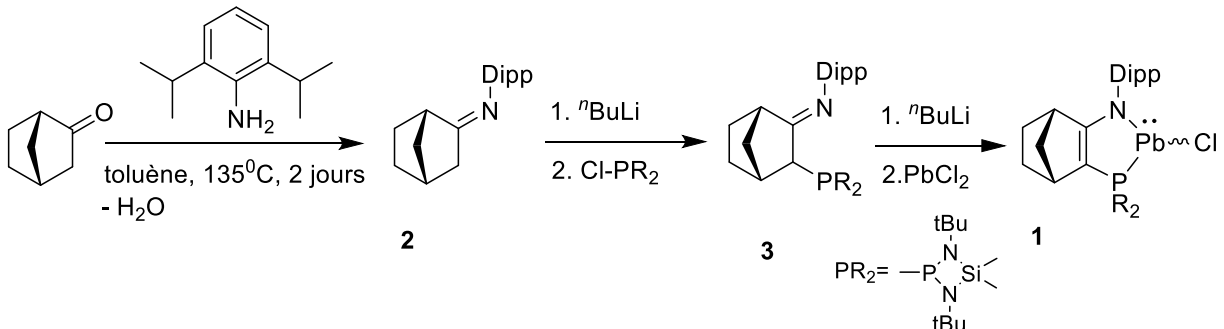


**Schéma 1.** Synthèse du chloroplombylène **1**.

Le plombylène **1** a été caractérisé par spectroscopie RMN en solution et par diffraction des rayons X à l'état solide. En RMN  $^{31}\text{P}\{\text{H}\}$ , **1** apparaît sous la forme d'un singulet à 212,3 ppm, présentant deux satellites avec une grande constante de couplage Pb-P ( $^1J_{\text{PbP}} = 3619,2 \text{ Hz}$ ) en accord avec une liaison Pb-P directe. Dans le spectre RMN  $^1\text{H}$  de **1**, le signal en  $\alpha$  du P a disparu, tandis que l'atome de carbone correspondant, en RMN  $^{13}\text{C}$  s'est déplacé de 66,6 ppm à 114,9 ppm. Le signal de l'atome de carbone situé en  $\alpha$  de l'azote en RMN  $^{13}\text{C}$  s'est déplacé vers 188,1 ppm, mettant ainsi en évidence la formation de la fonction énamine. La structure moléculaire du composé **1** a été confirmée par diffraction des rayons X (figure 2). La distance de la liaison Pb-N [2,3505(2) Å] se situe dans la gamme des liaisons simples Pb-N observées pour d'autres diaminoplombylénies (2,0 - 2,9 Å). La structure possède une géométrie pyramidale autour du centre Pb divalent ( $\Sigma^\circ\text{Pb} = 272.03^\circ$ ), ce qui indique la présence d'une paire libre sur ce centre (figure 2).

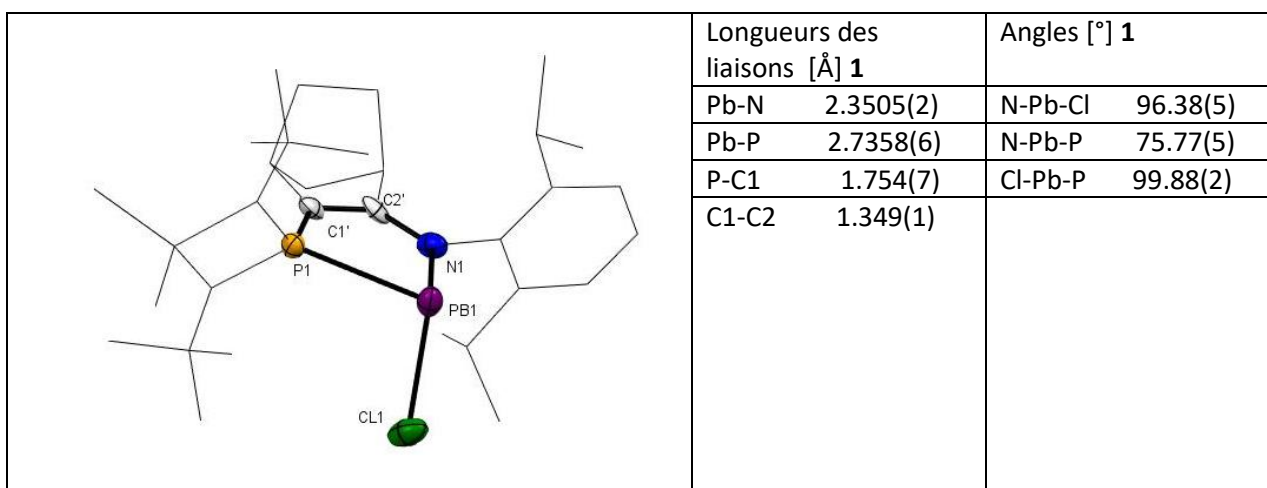


**Figure 2.** Structure moléculaire du chloroplumbylene **1** et longueurs de liaison [Å] et angles [°] sélectionnés.

## II.II Synthèse et caractérisation d'un phosphacétène de plombyle stabilisé par une iminophosphine **4**

La réaction du chloroplumbylene **1** stabilisé par une iminophosphine avec un équivalent de phosphéthynolate de sodium  $\text{Na(OCP)(dioxane)}_{2,4}$  conduit à la formation du phosphacétène de plomb **4** souhaité, qui a été isolé sous forme de poudre orange avec un rendement modéré (66%) (Schéma 2).

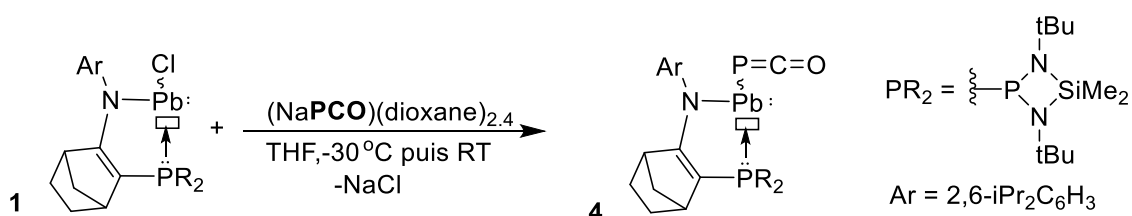


**Schéma 2.** Synthèse du phosphacétène substitué par un fragment plombyle **4**.

Le phosphacétène **4** a été obtenu sous forme d'un mélange de deux diastéréoisomères (55 : 45), en raison de la présence de deux centres chiraux dans la molécule (le fragment bicyclique asymétrique et l'atome de plomb pyramidal tricoordiné) (figure 3).

Pour chaque isomère, dans le spectre RMN  $^{31}\text{P}\{\text{H}\}$ , apparaissent deux systèmes AX dus à la présence de deux types d'atomes de phosphore (le ligand phosphine et le fragment phosphacétène). Tous les signaux présentent des satellites avec de grandes constantes de couplage P-Pb (isomère majeur:  $J_{\text{PPb}} = 3716,1$  Hz, isomère mineur :  $J_{\text{PPb}} = 3816,2$  Hz), ce qui indique l'interaction directe P-Pb (tableau 1).

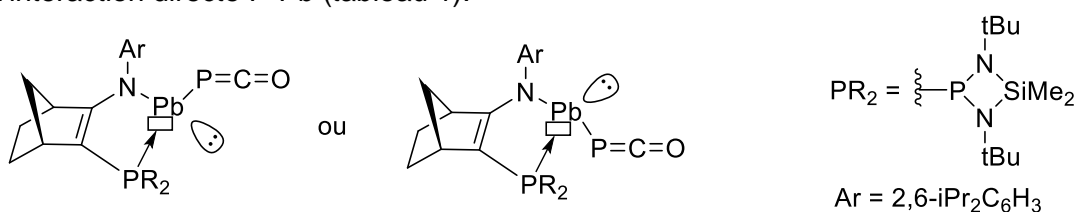


**Figure 3.** Les deux diastéréoisomères possibles du phosphacétène **4**.

Les signaux, dans le spectre RMN  $^{31}\text{P}\{\text{H}\}$ , pour les parties  $-\text{P}=\text{C}=\text{O}$  (- 329,4 et -333,2 ppm) sont décalés à champ faible par rapport au réactif NaPCO (- 392,0 ppm). Cette même tendance a déjà été observée pour d'autres phosphacétènes (tableau 1). Le spectre RMN  $^{207}\text{Pb}$  présente deux doublets de doublets à 2460 ppm (majeur) et 2233 ppm (mineur), dans la région typique des atomes de Pb(II) tricoordinés, avec des constantes de couplage P-Pb identiques à celles observées dans le spectre RMN  $^{31}\text{P}\{\text{H}\}$ .

<sup>31</sup> P{ <sup>1</sup> H} NMR				$\text{Ph}_3\text{Ge-P=C=O}$ <b>7</b> <sup>[30]</sup>	NaPCO
( $\delta$ ) PR <sub>2</sub>	182.2 / 189.9	90.7 / 90.1	-	-	
( $\delta$ ) -P=C=O	-329.4 / -333.2	-317.3 / -315.9	-298.9	-344	-392.0
<sup>2</sup> J <sub>P-P</sub> (Hz)	11.6 / 5.5	32.4 / 34.9			
<sup>1</sup> J <sub>P-Pb</sub> (Hz)	3716.1 / 3816.2				

**Tableau 1.** Déplacements chimiques et constantes de couplage en RMN <sup>31</sup>P des phosphacétènes préparés.

La structure de **4** a été confirmée par diffraction des rayons X sur monocristal (figure 4), et elle présente un centre Pb fortement pyramidalisé ( $\Sigma^{\circ}\text{Pb}=268,07^\circ$ ) et un cycle PbNCCP presque plan ( $\Sigma\alpha = 535^\circ$ ). La distance C1-C2 (1,387 Å) est légèrement plus longue qu'une double liaison classique (1,34 Å) tandis que les longueurs de liaison P1-C1 (1,715 Å) et C2-N1 (1,318 Å) sont plus courtes que des liaisons simples classiques (1,84 Å et 1,47 Å, respectivement). Ces données structurales sont similaires à celles observées dans le cas du Ge-phosphacétène **5** apparenté et suggèrent une délocalisation des électrons de la paire libre de l'azote (figure 5). En outre, la structure présente un angle Pb-P2-C3 aigu [87,3(3) $^\circ$ ] similaire à celui des analogues du germylène Ge-P-C [86,01(12) $^\circ$ ].

Longueurs des liaisons [Å] <b>4</b>	Angles [°] <b>4</b>
Pb-P2	2.761(5)
Pb-N1	2.315(2)
Pb-P1	2.747(1)
P1-C1	1.715(3)
C1-C2	1.387(4)
C2-N1	1.318(4)
P2-C3	1.591(8)
C3-O	1.176(9)
C2-N1-Pb	116.1(2)
Pb-P2-C3	87.3(3)
P2-C3-O	177.1(8)
N1-Pb-P1	76.6(1)
N1-Pb-P2	98.4(2)
P2-Pb-P1	93.1(1)
Pb-P1-C1	94.9(1)
P1-C1-C2	122.5(2)
C1-C2-N1	128.5(3)

**Figure 4.** Structure moléculaire de **4** et longueurs de liaison [Å] et angles [°] sélectionnés.

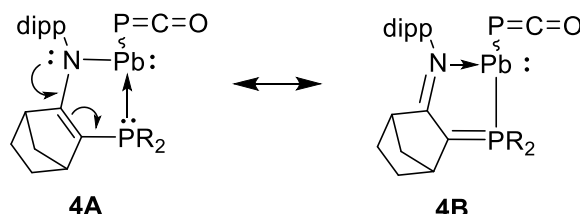


**Figure 5.** Formes mésomères du phosphacétène de plomb **4**.

### II.III. Réaction de décarbonylation du phosphacétène de plomb **4**

Nous avons ensuite étudié la thermolyse du phosphacétène de plomb **4**. Le suivi de la réaction par spectroscopie RMN <sup>31</sup>P indique que la molécule **4** commence à évoluer à 80°C. De façon particulièrement intéressante, la réaction conduit à la précipitation du plomb métallique et à la

formation d'un mélange de deux dérivés phosphanylidène-4-phosphorane **8** et **9** sans atome de plomb dans les molécules (Schéma 3). Le rapport entre ces deux produits dépend de la température et la température la plus basse favorise la formation de **8** [**8** : **9** = 80 : 20 ( $T = 80^\circ\text{C}$ ) et 50 : 50 ( $T=100^\circ\text{C}$ )]. Afin d'éviter d'isoler le composé **4** thermiquement instable, sa thermolyse peut être réalisée *in situ*, ce qui est un procédé plus efficace.

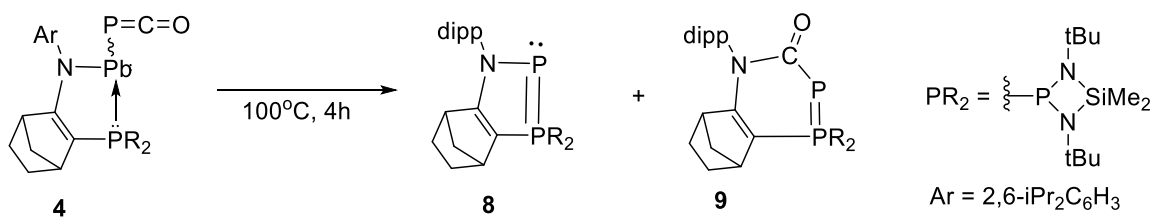


**Schéma 3.** Thermolyse du phosphacétène de plomb **4**.

Le produit minoritaire **9** a été isolé par précipitation sous la forme d'une poudre jaune à partir d'une solution pentanique du mélange (rendement 39 %), puis le produit majoritaire **8** a été isolé par cristallisation à partir d'une solution dans l'heptane à  $-30^\circ\text{C}$  avec un rendement modéré (31 %). Le spectre RMN  $^{31}\text{P}\{\text{H}\}$  de **8** montre un système AX ( $\delta = 88,5$  et 75,5 ppm) avec une grande constante de couplage PP ( $^1J_{\text{PP}} = 518,0$  Hz) confirmant que les deux atomes de phosphore sont directement liés. En général, le signal de l'atome de phosphore dicoordonné des phosphanylidène phosphoranes apparaît à un champ élevé en raison de la liaison ylure  $\text{R}_3\text{P}^{\delta+}=\text{P}^{\delta-}\text{R}$  fortement polarisée, ce qui est conforme au signal RMN  $^{31}\text{P}\{\text{H}\}$  du dérivé cyclique à 5 chaînons **9** (tableau 2). Le signal de l'atome  $\sigma^4\text{-P}$  apparaît dans la gamme typique des déplacements chimiques pour les atomes de phosphore tétracoordonnés.

$^{31}\text{P}\{\text{H}\}$ RMN				
	<b>8</b>	<b>9</b>	<b>10</b> <sup>[4]</sup>	<b>11</b> <sup>[5]</sup>
$\sigma^2\text{-P}$ ( $\delta$ ) (ppm)	88.5	-69.3	-244.3	-157.7
$\sigma^4\text{-P}$ ( $\delta$ ) (ppm)	75.5	69.8	56.7	76.7
$^1J_{\text{PP}}$ (Hz)	518.0	482	531.0	479.6

**Tableau 2.** Données RMN  $^{31}\text{P}\{\text{H}\}$  pour les produits **8** et **9** et certains phosphanylidène phosphoranes.

Les calculs DFT réalisés sur **8** indiquent qu'une des paires libres du  $\sigma^2\text{-P}$  est impliquée dans la délocalisation cyclique (figure 6).

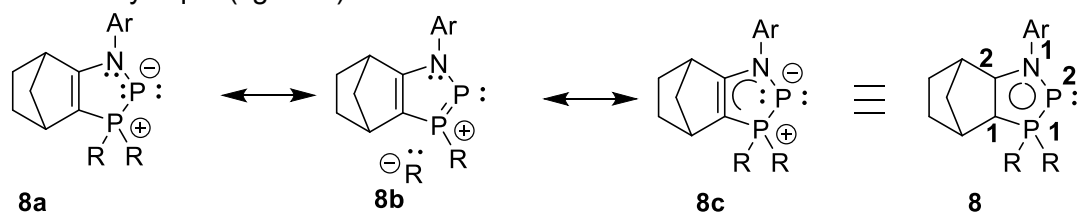
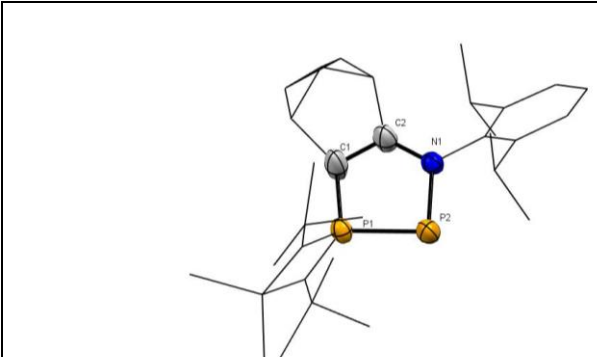


**Figure 6.** Quelques structures canoniques du phosphanylidène-4-phosphorane cyclique **8**.

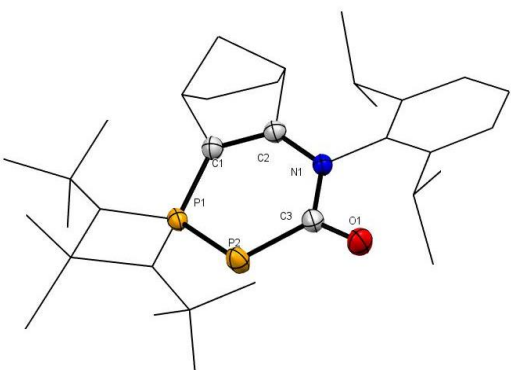
Selon l'analyse par diffraction X monocristalline, la structure moléculaire de **8** montre un cycle C2P2N à cinq membres presque plan ( $\Sigma\alpha = 537^\circ$ ) avec la distance de liaison N1-P2 (1,778 Å) significativement plus longue qu'une double liaison N=P (1,61 Å) (figure 7). Une longueur de liaison N-P similaire (1,779 Å) pour l'anion 1,4,2-diazaphospholidine-3,5-dione a été décrite par Grützmacher et Goicoechea.<sup>[6]</sup> Les longueurs des liaisons P1-C1 [1,715(3) Å] et C2-N1 [1,320(3) Å] sont légèrement plus courtes que celles de **9** substitué par CO (P1-C1 : 1,741 Å, C2-N1 : 1,376

Å, C1-C2 : 1,360 Å), tandis que la distance P1-P2 dans le **8** [2.119(8) Å] est intermédiaire entre les liaisons PP simples et doubles (2,22 Å et 2,04 Å) (figure 11).<sup>[7]</sup> La longueur de la liaison P1=P2 dans **9** est similaire à cette valeur [2,1006(7) Å] (figure 8). Ces résultats suggèrent une délocalisation cyclique des électrons 6π à travers le cycle C2P2N dans le cas de **8**.



Longueurs des liaisons [Å] <b>8</b>		Angles [°] <b>8</b>	
N1-P2	1.778(2)	N1-P2-P1	92.1(1)
P2-P1	2.119(1)	P2-P1-C1	95.5(1)
P1-C1	1.715(3)	P1-C1-C2	114.7(2)
C1-C2	1.368(3)	C1-C2-N1	121.8(2)
C2-N1	1.320(3)	C2-N1-P2	115.9(1)

Figure 7. Structure moléculaire de **8** et longueurs de liaison sélectionnées [Å] et angles [°].



Longueurs des liaisons [Å] <b>9</b>		Angles [°] <b>9</b>	
N1-C3	1.437(2)	C3-P2-P1	102.6(8)
C3-P1	1.798(2)	C1-P1-P2	107.1(6)
P1-P2	2.100(7)	C2-N1-C3	124.8(1)
P1-C1	1.741(2)	N1-C3-P2	126.6(6)
C1-C2	1.360(2)	C2-C1-P1	125.7(7)
C2-N1	1.376(2)	C1-C2-N1	129.1(2)

Figure 8. Structure moléculaire de **9** et longueurs de liaison sélectionnées [Å] et angles [°].

Nous avons ensuite étudié le mécanisme de la réaction. Pour expliquer la formation de deux dérivés **8** et **9**, nous avons d'abord envisagé la formation d'un des produits à partir de l'autre, soit par l'ajout ou l'élimination de CO. Nous avons donc vérifié la réaction de **8** sous 3 bar de CO à 100 °C ainsi que la réaction d'élimination du CO à partir de **9** sous vide à 100 °C (schéma 4). Cependant, aucune de ces deux réactions n'a lieu, ce qui indique que ces deux produits se forment par deux voies différentes.

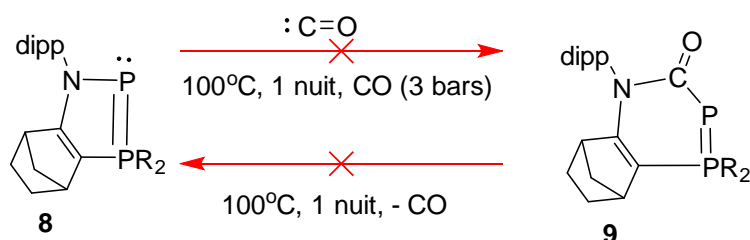


Schéma 4. Tests réalisés : (i) réaction thermique de **8** avec CO, et (ii) élimination thermique de CO à partir de **9**.

Étant donné la formation de Pb métallique pendant la thermolyse du plombyle 4 substitué par la fonction phosphacétène, la réaction commence probablement par une élimination réductrice de Pb, soit pour former une liaison P-N afin de générer un intermédiaire N-phosphacétène **12**, soit pour former une liaison P-P conduisant à un intermédiaire P-phosphacétène **13**. Les deux

intermédiaires **12** et **13** seraient les précurseurs des produits finaux **8** et **9**. En effet, une évolution supplémentaire de **12** par élimination du CO induite par une attaque de la phosphine sur l'atome P du phosphacétène donne le phosphanylidène phosphorane **8** ou une évolution par attaque de la phosphine sur l'atome C du phosphacétène donne **9**. De même, l'attaque de la fonction imine sur l'atome P ou N du phosphacétène en **13** conduit à la formation de **8** ou **9** respectivement.

Deux possibilités peuvent donc être envisagées :

- 1) L'un des deux intermédiaires (**12** ou **13**) est le précurseur des deux produits finaux (**8** et **9**).
- 2) Chaque intermédiaire est le précurseur spécifique de chacun des produits finaux.

Des études mécanistiques indiquent que dans ce cas, chaque intermédiaire est le précurseur spécifique de chacun des produits finaux. La réaction commence par l'élimination réductrice du Pb métallique pour former de nouveaux dérivés amino- et phosphonio-phosphacétènes qui évoluent ensuite pour donner les phosphanylidènes phosphoranes **8** et **9** obtenus expérimentalement. En particulier, l'amino-phosphacétène **12** évolue par élimination du CO pour générer un intermédiaire phosphinidène qui est stabilisé par la coordination de la phosphine conduisant au phosphanylidène phosphorane cyclique **8**. Etant donné que ce processus ne produit que des sous-produits inertes tels que le Pb métallique et le gaz CO, le phosphacétène **4** peut être considéré comme un excellent précurseur de phosphinidène (schéma 5).

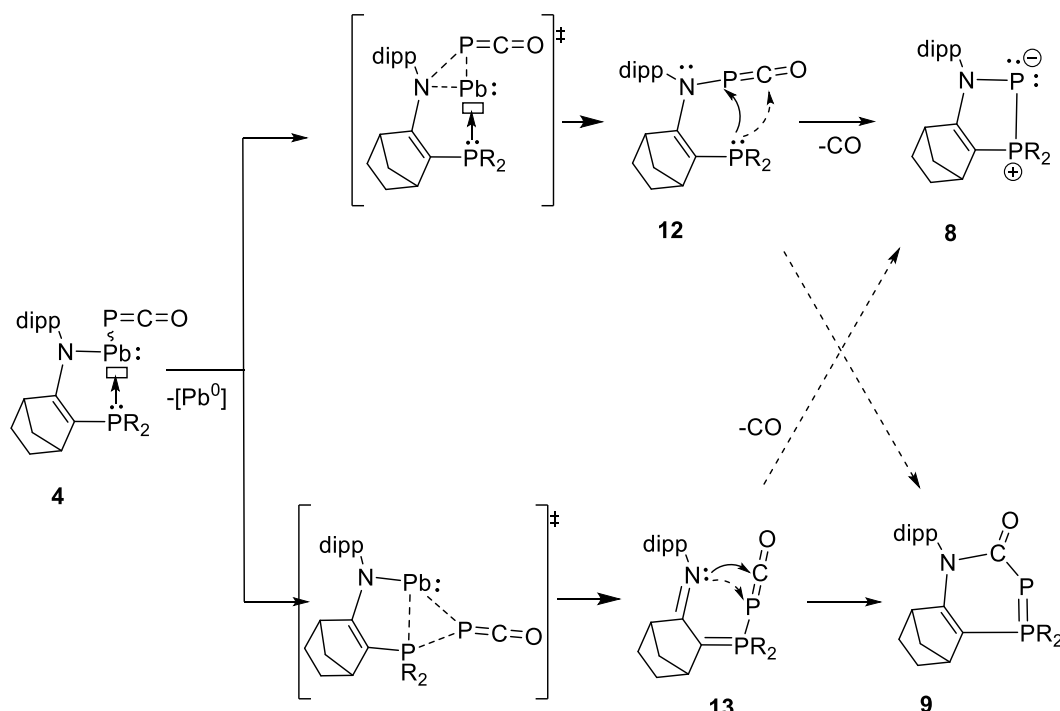


**Schéma 5.** Voies de réaction proposées pour la thermolyse du plombylène-phosphacétène **4**.

- *Réactivité de l'(amino)phosphanylidène- $\alpha^4$ -phosphorane **8***

Comme le suggèrent les calculs DFT, la liaison P2-N1 dans **8** est labile et les réactions impliquant la rupture de cette liaison peuvent être favorisées. En effet, **8** réagit avec le 1,3-diméthylbenzo isonitrile ambiphile via une réaction d'insertion dans la liaison P2-N1 pour donner un nouveau phosphanylidène phosphorane **14** (Schéma 6).

La labilité de la liaison P2-N1 dans **8** est également démontrée par la réaction avec le phénylsilane qui résulte en une métathèse formelle des liaisons Si-H/P-N pour donner un nouveau phosphanylidène phosphorane P-silylé **15** (Schéma 6).

L'addition du complexe borane-tétrahydrofurane, BH<sub>3</sub>·THF, à une solution de **8** dans le toluène à température ambiante a permis la formation du complexe donneur-accepteur correspondant **16** qui a été isolé sous forme cristalline avec un rendement modéré de 37 % (schéma 6).

La réaction de **8** avec deux équivalents de 3,5-di-tertbutyl-o-benzoquinone (TCBQ) dans le toluène conduit au produit phosphoré hexa-coordonné correspondant **17** qui a été isolé sous forme

d'un solide blanc avec un rendement modéré de 40 % (schéma 6).

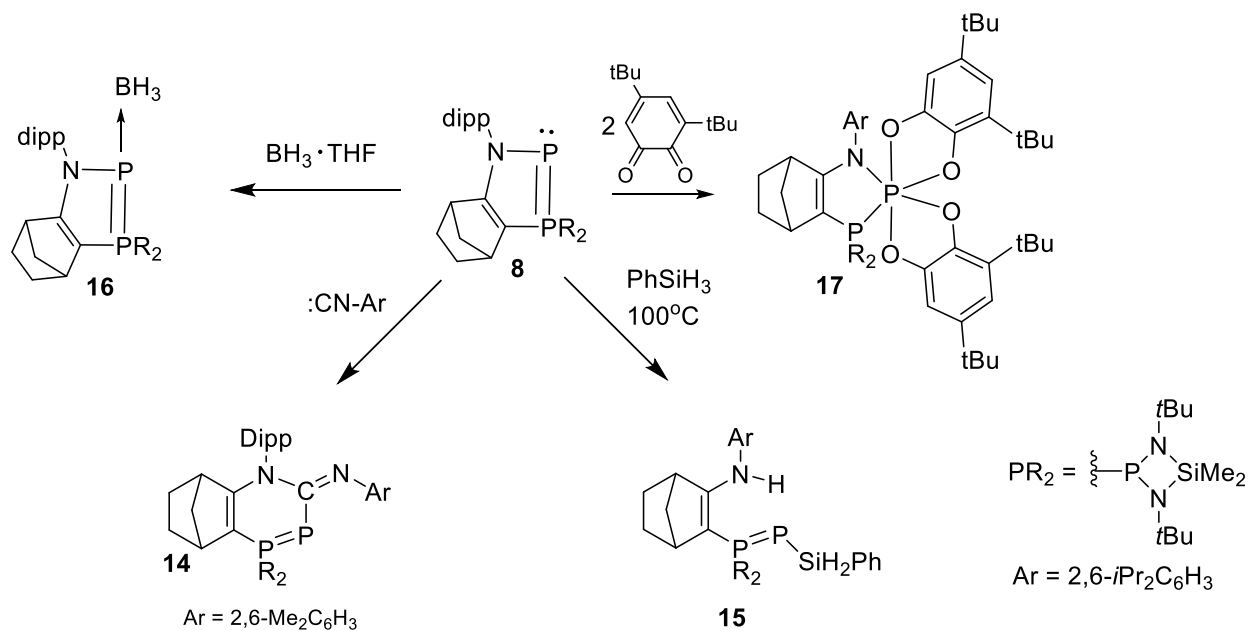
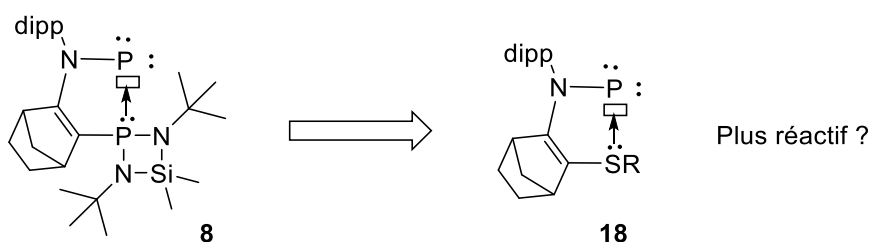


**Schéma 6.** Réactivité du phosphanylidène- $\sigma^4$ -phosphorane **8**.

- Premières tentatives de synthèse d'un phosphinidène **18** stabilisé par des sulfures

Le phosphanylidène- $\sigma^4$ -phosphorane **8** possède une liaison PP persistante, ce qui réduit son comportement en tant que phosphinidène. Ceci est probablement dû au fort caractère nucléophile du ligand diaminophosphine ainsi qu'à une importante rétrodonation conduisant à un fort caractère de double liaison P=P dans **8**. Afin d'augmenter la réactivité, nous avons envisagé de remplacer le ligand phosphine (l'énergie de dissociation de la liaison P-P est de 490(11) kJ/mol)<sup>[8]</sup> par un ligand moins donneur tel qu'un sulfure (l'énergie de dissociation de la liaison P-S est de 346.0(17) kJ/mol).<sup>[8]</sup>



Pour synthétiser un tel phosphinidène **18** stabilisé par un sulfure, nous avons envisagé d'utiliser la même stratégie de synthèse : la thermolyse du phosphacétène correspondant substitué par un plombylène **19** stabilisé par un sulfure. Nous pouvons facilement imaginer que le précurseur **19** peut être facilement préparé par la réaction du chloroplombylène **20** stabilisé par un sulfure correspondant et du NaPCO. Par conséquent, nous avons d'abord envisagé la synthèse du chloroplombylène **20** (Schéma 7).

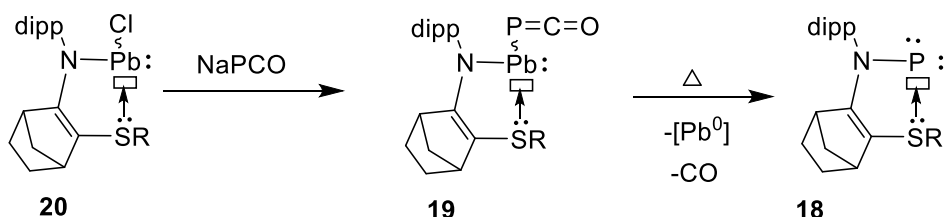


**Schéma 7.** Stratégie de synthèse pour la synthèse du nouveau phosphinidène **18** stabilisé par un sulfure.

Tout d'abord, nous avons considéré la synthèse du chloroplombulène **20** stabilisé par le soufre avec un groupe aryle volumineux ( $R = \text{groupe 2,4,6-triisopropylphényle}$ ) sur l'atome de S. La synthèse a commencé par la préparation du ligand iminosulfure **21** par la réaction du disulfure de bis(2,4,6-triisopropylphényle) avec l'imine lithiée **22**. Le composé **21** a été obtenu avec un rendement relativement bon (schéma 8). L'iminosulfure **21** est insoluble dans le méthanol et peut donc être facilement séparé du thiolate de 2,4,6-triisopropylphényle comme sous-produit par précipitation. L'analyse RMN indique que le composé a été obtenu sous forme d'un mélange de deux diastéréoisomères dans un rapport de 67 : 33. Dans le spectre de RMN  $^1\text{H}$ , le signal du proton du fragment CH-S a été observé à 3,67 ppm (majeur) et 3,16 ppm (mineur).

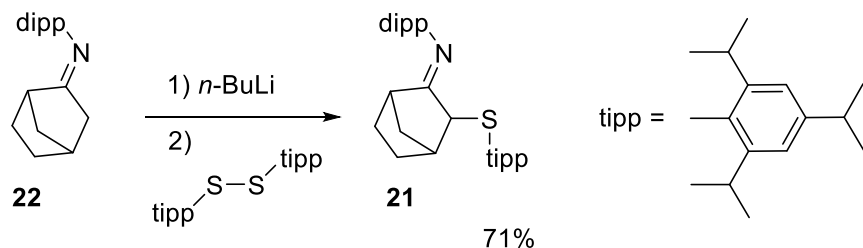


Schéma 8. Synthèse de l'iminosulfure **21**.

Ensuite, le ligand lithié, préparé par la réaction de **21** avec  $n\text{BuLi}$ , a été mis en réaction avec un équivalent de  $\text{PbCl}_2$  en espérant obtenir la formation du chloroplombulène correspondant stabilisé par un sulfure. Cependant, au lieu du chloroplombulène **18**, cette réaction au diaminoplombulène **23** avec deux fragments de la fraction énaminosulfure sous la forme d'un mélange de deux diastéréoisomères (schéma 9).

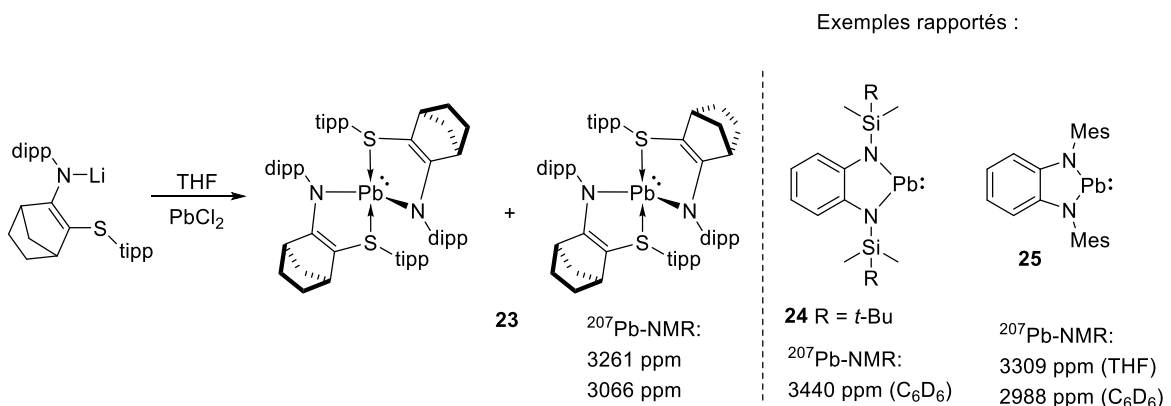
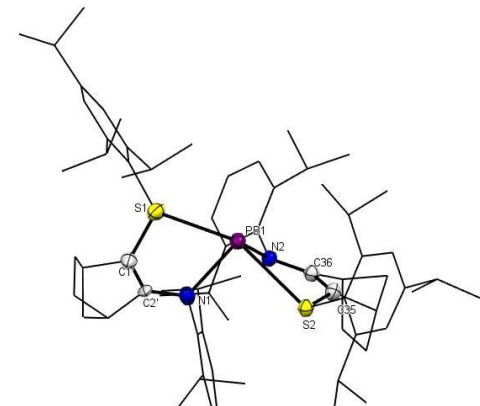


Schéma 9. La réaction de l'énaminosulfure lithié avec le dichlorure de plomb.

Le spectre RMN  $^{207}\text{Pb}$  montre deux singulets à 3261 ppm et 3066 ppm, qui apparaissent dans la même gamme que les diaminoplombulènes dicoordonnés décrits précédemment. Le remplacement du solvant  $\text{C}_6\text{D}_6$  par le THF conduit à un déplacement à champ élevé de ces signaux ( $\delta = 2988$  ppm) (schéma 9).

La structure de **23** a effectivement été confirmée par diffraction des rayons X (schéma 10). Les deux diastéréoisomères de **23** ont co-cristallisé et, par conséquent, nous avons pu confirmer les structures des diastéréoisomères, comme le montre la figure 10. Les longueurs de liaison Pb-N(1) et Pb-N(2) dans **23** sont dans la gamme des longueurs de liaison simple Pb-N décrites pour d'autres diaminoplombulènes (2,0 - 2,9 Å).<sup>[9,10]</sup> Les longueurs des liaisons Pb-S(1) et Pb-S(2) sont significativement plus longues que les distances rapportées pour d'autres valeurs de liaisons simples covalentes Pb-S de thiolates de plomb(II) dicoordonnés (2,49 - 2,56 Å), ce qui indique le caractère datif de ces liaisons.<sup>[11,12]</sup>



Longueurs des liaisons [Å] 23		Angles [°] 23	
Pb – N(1)	2.290(18)	N(1)-Pb(1)-S(2)	86.85(5)
Pb – N(2)	2.324(17)	N(1)-Pb(1)-S(2)	86.85(5)
Pn-S(1)	2.9838(6)	N(2)-Pb(1)-S(2)	73.19(4)
Pb – S(2)	2.9541(5)	N(1)-Pb(1)-S(1)	73.91(5)
		N(2)-Pb(1)-S(1)	90.23(4)
		N(1)-Pb-N(2)	103.75(7)
		S(1)-Pb-S(2)	150.99(15)

Figure 10. Structure moléculaire de **23** et longueurs de liaison [Å] et angles [°].

Ces résultats suggèrent que la stabilisation du chloroplombylène par le ligand aryl-sulfure (*tipp*-S) **21** n'est pas assez efficace, et par conséquent, il réagit ensuite avec un second équivalent de ligand lithié pour donner les dérivés diaminoplombylène **23** obtenus expérimentalement (Schéma 10).

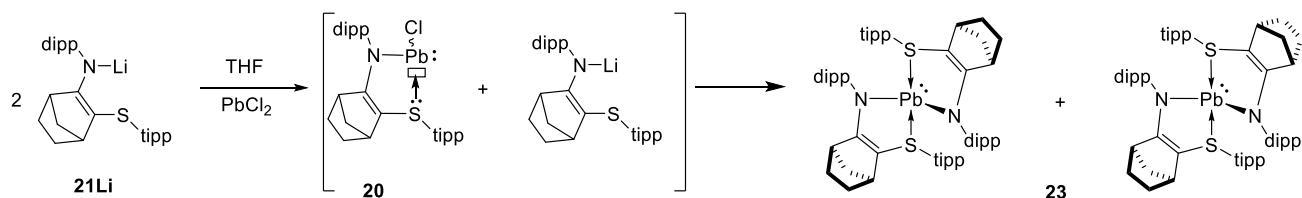


Schéma 10. Mécanisme proposé pour la réaction du **21Li** avec **20**.

En tenant compte de ces résultats, pour augmenter la stabilité des plombylènes, nous pouvons considérer comme modèles alternatifs : (i) un ligand amino-sulfure plus nucléophile conduisant au modèle **A** qui devrait être thermodynamiquement stabilisé, (ii) et un ligand aryl-sulfure plus encombré, conduisant au modèle **B** cinétiquement stabilisé (Schéma 10).

La synthèse de chloroplombylènes stables avec de tels systèmes de ligands (modèles **A** et **B**) pourrait donner un accès facile aux phosphacétènes correspondants substitués par Pb(II) stabilisés par des sulfures et donc aux phosphinidènes correspondants.

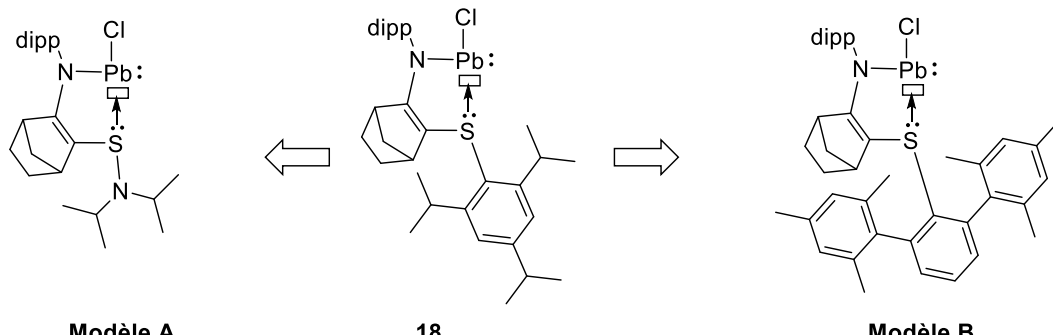
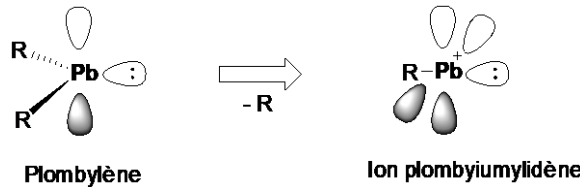


Figure 11. Méthodes proposées pour améliorer la capacité de stabilisation du ligand iminosulfure.

### III. Synthèse et réactivité des plombylènes cationiques

Le complexe **1** de chloroplombylène obtenu précédemment (schéma 1) est une molécule parfaitement stable, mais sa réactivité reste faible. Celle-ci pourrait être augmentée de façon importante en passant au complexe plombyliumylidène cationique correspondant par abstraction d'un chlorure (Figure 11).



**Figure 11.** Stratégie pour augmenter la réactivité d'un plumbylene en le convertissant en un complexe cationique (plumbiumylidène).

La synthèse du complexe de plumbylene cationique **26** a été réalisée via l'abstraction de chlore du chloroplumbylene **1** en utilisant le tétrakis(pentafluorophényl)borate de potassium  $K[B(C_6F_5)_4]$  (Schéma 11). Cependant, en raison de l'électrophilie élevée de l'espèce cationique résultante, même avec un excès d'acide de Lewis (5 eq), le  $Pb^+$  dioordonné libre n'a pas pu être obtenu. En fait, on obtient le complexe **26**, stabilisé par la coordination de l'atome de chlore du chloroplumbylene **1** sur le centre cationique formé. Dans le spectre RMN  $^{31}P$ , un seul signal singulet à 255,5 ppm avec deux satellites dus aux noyaux  $^{207}Pb$  ( $I = \frac{1}{2}$ , abondance naturelle : 22 %) ( $^1J_{Pb-P} = 3755$  Hz) est observé, confirmant la présence d'une liaison P-Pb dans la molécule. Ce signal est décalé à champ faible par rapport au chloroplumbylene **1** (212 ppm,  $^1J_{Pb-P} = 3619$  Hz), probablement en raison de son caractère cationique.

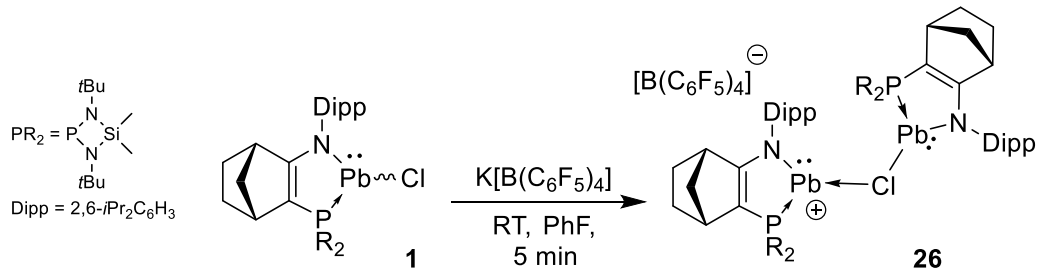


**Schéma 11.** Synthèse du Plumbiumylidène **26**.

Des monocristaux de **26**, adaptés à l'analyse XRD, ont été obtenus par José Miguel Léon Baeza, qui a poursuivi ce projet, à partir d'une solution saturée de fluorobenzène/pentane à -30 °C (Figure 12).

Longueurs des liaisons [Å] <b>26</b>	Angles [°] <b>26</b>
Pb1-Cl 2.711(1)	Pb1-Cl-Pb2 110.00(5)
Pb2-Cl 2.692(2)	N1-Pb1-Cl 96.16(11)
N1-Pb1 2.267(4)	N2-Pb2-P2 77.70(11)
Pb1-P1 2.744(1)	
N2-Pb2 2.265(4)	
Pb2-P2 2.737(1)	

**Figure 12.** Structure moléculaire de **26** et longueurs de liaison [Å] et angles [°] sélectionnés.

En raison du caractère cationique et de l'orbitale p vacante sur le même atome de plomb, les plumbiumylidènes sont extrêmement réactifs et instables. Cependant, ces cations  $Pb(II)$  peuvent être isolés sous forme de complexe **26-L** stable avec un ligand base de Lewis supplémentaire.

### III.I Stabilisation de plombyliumylidènes par des bases de Lewis

- Plombyliumylidènes cationiques stabilisés par des phosphines tertiaires **26-PR<sub>3</sub>** (*R* = Me, Ph)

L'abstraction du chlore de **1** en présence de triméthylphosphine PMe<sub>3</sub>, dans le fluorobenzène a conduit à la formation de **26-PMe<sub>3</sub>** sous la forme d'une poudre orange avec un rendement de 70 % (Schéma 12).

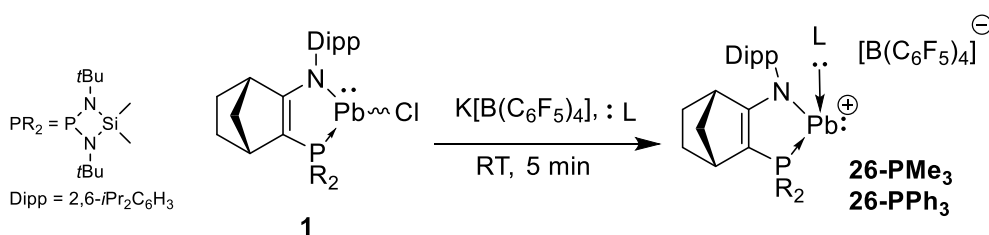


**Schéma 12.** Synthèse des plombyliènes cationiques **26-PR<sub>3</sub>** (*R* = Me, Ph).

Dans le spectre de RMN <sup>31</sup>P{<sup>1</sup>H} à - 95 °C, deux systèmes AX sont apparus à 211,6 (PR<sub>2</sub>) et 16,9 (PMe<sub>3</sub>) ppm avec une constante de couplage <sup>2</sup>J<sub>P-P</sub> = 79,6 Hz. Pour les deux signaux, des satellites ont été observés avec de grandes constantes de couplage Pb-P, <sup>1</sup>J<sub>Pb-P</sub> = 4017 Hz et 2622 Hz respectivement, démontrant la coordination des deux atomes de phosphore au même centre Pb. À la température ambiante, ces signaux s'élargissent et deviennent des singulets dont un seul possède des satellites dus au plomb (PR<sub>2</sub>) (<sup>1</sup>J<sub>Pb-P</sub> = 3920 Hz), ce qui suggère la nature labile du ligand PMe<sub>3</sub> et un échange rapide de ligands. En effet, ceci est confirmé par un déplacement du signal PMe<sub>3</sub> dans le spectre RMN <sup>31</sup>P{<sup>1</sup>H} de **26-PMe<sub>3</sub>** lorsque un excès (3 eq) de PMe<sub>3</sub> a été ajouté au mélange réactionnel. De plus, un déplacement à bas champ (43,0 ppm) a été observé, alors que les signaux pour le composé parent **26-PMe<sub>3</sub>** apparaissent à 11,6 ppm et pour la triméthylphosphine libre à -63,6 ppm. Lorsque l'excès de PMe<sub>3</sub> est éliminé sous pression réduite, le signal initial à 11,2 ppm est retrouvé. Probablement, en raison de cet échange rapide de ligands, le signal RMN de <sup>207</sup>Pb n'a pas été observé. Ces données suggèrent que le ligand phosphine est labile et pourrait être facilement remplacé.

De même, avec un équivalent de triphénylphosphine (PPh<sub>3</sub>) dans le fluorobenzène, le complexe plombyliumylidène correspondant **26-PPh<sub>3</sub>** a été obtenu sous la forme d'une poudre rouge foncé avec un rendement de 61 %. Dans le spectre de RMN <sup>31</sup>P{<sup>1</sup>H} **26-PPh<sub>3</sub>**, comme pour le **26-PMe<sub>3</sub>** à la température ambiante, deux signaux singuliers apparaissent à 243,4 ppm (PR<sub>2</sub>) avec des satellites (<sup>1</sup>J<sub>Pb-P</sub> = 3778,6 Hz) et à 38,7 ppm (PPh<sub>3</sub>). Il est intéressant de noter que, contrairement à **26-PMe<sub>3</sub>**, dans le cas de **26-PPh<sub>3</sub>**, les deux atomes de phosphore ne sont pas couplés l'un à l'autre, même à -90 °C, probablement en raison du caractère plus labile du ligand PPh<sub>3</sub>.

- Réactivité des complexes **26-PR<sub>3</sub>** (*R* = Me, Ph) avec un alcyne.

On a constaté que les complexes cationiques **26-PR<sub>3</sub>** (*R* = Me, Ph) réagissaient avec le phénylacétylène à la température ambiante, pour former des complexes de plombyliène vinylique **27-PR<sub>3</sub>** (schéma 13).

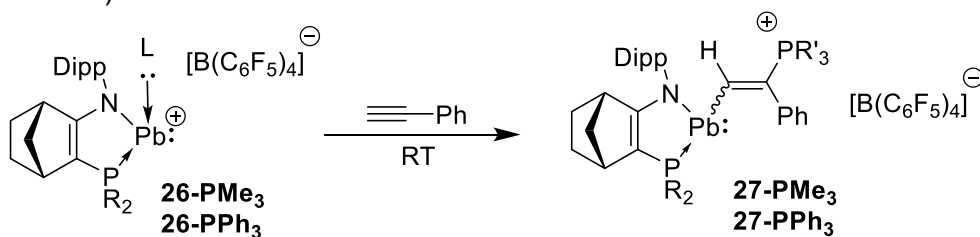


**Schéma 13.** Réactions des complexes **26-PR<sub>3</sub>** (*R* = Me, Ph) avec HC≡CPh.

Lorsque le complexe **26-PPh<sub>3</sub>** réagit avec 1 équivalent de phénylacétylène à température ambiante dans le fluorobenzène, on observe la formation de **27-PPh<sub>3</sub>** par une insertion d'acétylène dans la liaison Pb-PR<sub>3</sub>. Le produit phosphoniovinyplombylène **27-PPh<sub>3</sub>** a été isolé avec un bon rendement (60 %) sous forme de poudre jaune. Il a également été constaté que **26-PPh<sub>3</sub>** ne réagit pas avec les alcynes moins riches en électrons (HC≡CSiMe<sub>3</sub> ou 1-hexyne), les alcynes plus encombrés (Ph-C≡C-Ph, Et-C≡C-Et) ou les oléfines (styrène, vinyltriméthylsilane). Le complexe **26-PMe<sub>3</sub>**, dont le ligand phosphine est plus donneur d'électrons, réagit de façon similaire avec le phénylacétylène. D'après les données RMN <sup>31</sup>P, le composé **27-PPh<sub>3</sub>** a été obtenu sous la forme d'un mélange de deux diastéréoisomères dans un rapport 60 : 40 (Figure 13).

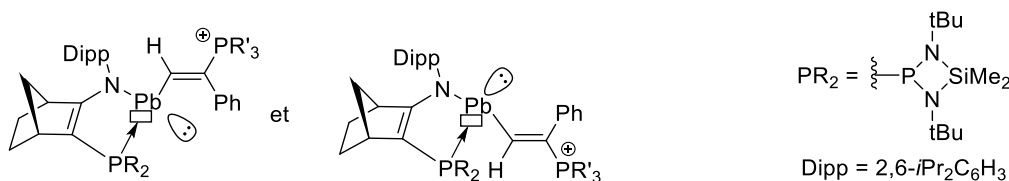


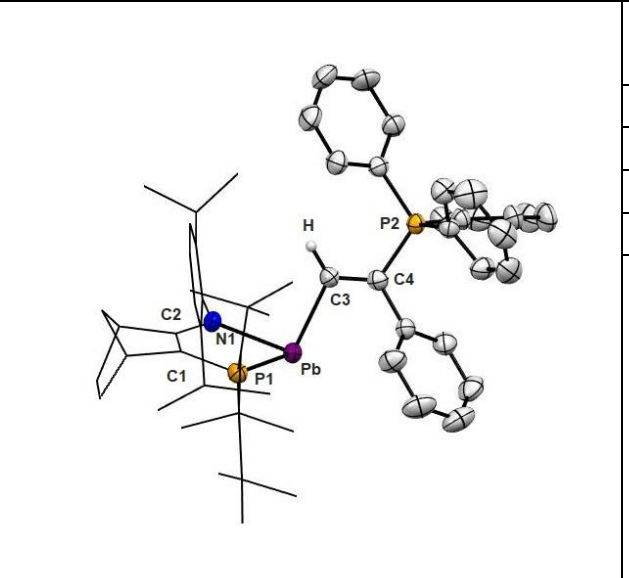
**Figure 13.** Les deux diastéréoisomères possibles de **27-PPh<sub>3</sub>**.

Pour chaque isomère, deux systèmes AX sont observés dans le spectre RMN <sup>31</sup>P, confirmant la présence de deux types d'atomes de phosphore dans la molécule (ligand phosphine et groupe phosphonio) (tableau 3). Les signaux correspondant au ligand phosphine (PR<sub>2</sub>) présentent des satellites <sup>207</sup>Pb avec une grande constante de couplage <sup>1</sup>J<sub>Pb-P</sub> = 3655 (majeur) et <sup>1</sup>J<sub>Pb-P</sub> = 3627 (mineur). Les signaux correspondant à la partie PPh<sub>3</sub> présentent également des satellites Pb avec des constantes de couplage plus faibles (isomère majeur : <sup>3</sup>J<sub>Pb-P</sub> = 370 Hz, isomère mineur : <sup>3</sup>J<sub>Pb-P</sub> = 362 Hz).

<sup>31</sup> P- RMN	Isomère principal (60 %)	Isomère mineur (40 %)
Phosphine ( $\delta$ )	166.0	171.7
PPh <sub>3</sub> ( $\delta$ )	18.5	18.3
<sup>4</sup> J <sub>P,P</sub> (Hz)	10.5	10.6
<sup>1</sup> J <sub>Pb-P</sub> (Hz)	3655	3627
<sup>3</sup> J <sub>Pb-P</sub> (Hz)	370	362

**Tableau 3.** Données RMN <sup>31</sup>P pour **27-PPh<sub>3</sub>**

Le spectre RMN <sup>207</sup>Pb présente deux doublets de doublets à 1268 ppm (majeur) et 1799 ppm (mineur), présentant les mêmes constantes de couplage P-Pb que celles observées dans le spectre RMN <sup>31</sup>P{<sup>1</sup>H}. Dans le spectre RMN <sup>13</sup>C, les signaux correspondant à l'atome de carbone vinylique, lié à la partie Pb, ont été observés sous forme de doublet de doublets à 239,3 ppm (<sup>2</sup>J<sub>C-P</sub> = 18,1 Hz et 20,6 Hz) pour l'isomère majeur et 238,7 ppm (<sup>2</sup>J<sub>C-P</sub> = 16,8 Hz et 21,3 Hz) pour l'isomère mineur. L'atome de carbone, lié à la partie phosphonio, a été observé à un champ plus élevé à 132,1 ppm (<sup>1</sup>J<sub>C-P</sub> = 51,7 Hz et <sup>4</sup>J<sub>C-P</sub> = 8,7 Hz) pour l'isomère majeur et 132,6 ppm (<sup>1</sup>J<sub>C-P</sub> = 51,5 Hz et <sup>4</sup>J<sub>C-P</sub> = 8,7 Hz) pour l'isomère mineur. Ce décalage de l'atome de carbone C3 vers les champs faibles est probablement dû à l'atome de Pb(II) qui lui est lié. Dans le spectre RMN <sup>1</sup>H, les signaux correspondant au proton vinyle ont été observés à faible champ à 9,96 ppm ( $J_{H-P}$  = 1,8 Hz et 35,0 Hz) et 10,0 ppm ( $J_{H-P}$  = 34,9 Hz). Des monocristaux de **27-PPh<sub>3</sub>** adaptés à l'analyse par diffraction des rayons X ont été obtenus par diffusion lente d'une solution concentrée de **27-PPh<sub>3</sub>** dans le fluorobenzène dans un solvant non polaire (pentane) (Figure 14).



Longueurs des liaisons [Å]	Angles [°] <b>27-PPh<sub>3</sub></b>	
<b>27-PPh<sub>3</sub></b>		
Pb-C3	2.329(4)	N1-Pb-P1 76.6(1)
C3-C4	1.332(6)	Pb-C3-C4 116.0(3)
C4-P2	1.820(5)	C3-C4-P2 122.1(3)
N1-Pb	2.324(3)	
Pb-P1	2.743(1)	

**Figure 14.** Structure moléculaire de **27-PPh<sub>3</sub>** et longueurs de liaison [Å] et angles [°] sélectionnés.

La structure confirme que les groupes phényle et phosphonio sont attachés à la position 2 du groupe vinyle. Le groupe phosphonio est en position trans par rapport à l'atome de Pb(II). La longueur de la liaison C3-C4 [1.332(6) Å] est légèrement plus courte qu'une double liaison CC classique (1.34 Å). La distance de la liaison Pb-N [2,324(3) Å] est nettement plus courte que la liaison Pb-N dans le chloroplombylène neutre tricordonné précurseur **1** [2,3505(2) Å], cependant, elle se situe toujours dans la gamme des autres longueurs de liaison simple Pb-N typiques décrites pour d'autres diaminoplumbylènes (2,0 - 2,9 Å).<sup>[9,10]</sup> En outre, le centre de plomb tricordonné est fortement pyramidal (<sup>3</sup>Pb = 272,2°), ce qui suggère la présence de la paire solitaire sur cet atome.

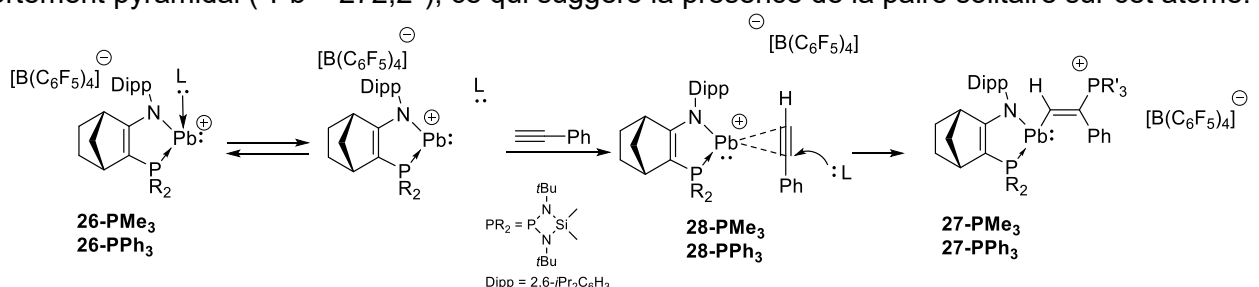


**Schéma 14.** Mécanisme proposé pour l'insertion de l'alcyne dans la liaison Pb-P de **26-L** (L = PMe<sub>3</sub>, PPh<sub>3</sub>).

La réaction commence probablement par la dissociation du ligand phosphine labile du Pb(II) et la formation du cation plombyliumylidène libre très réactif. Celui-ci réagit facilement avec le phénylacétylène, pour former un complexe  $\pi$ -acétylène **28**, suivi par l'attaque nucléophile de la phosphine libérée sur la partie moins encombrée du cation vinyle, et former ainsi le complexe trans-vinylplombylène **27** (schéma 14).

- *Plombyliumylidènes cationiques stabilisés par des phosphines secondaires 26-HPR<sub>2</sub> (R = Ph, *i*Pr)*

L'utilisation d'un ligand phosphine secondaire (L = PHR<sub>2</sub>, R = Ph, *i*Pr) serait plus prometteuse car cela permettrait potentiellement de réaliser des réactions d'hydrophosphination d'alcynes catalytiques. Cependant, la réaction du chloroplombylène **1** avec la diphenylphosphine HPPH<sub>2</sub> en présence de K[B(C<sub>6</sub>F<sub>5</sub>)<sub>4</sub>] à température ambiante conduit à la décomposition du plombylène **1** et à la précipitation de plomb métallique (Schéma 15).

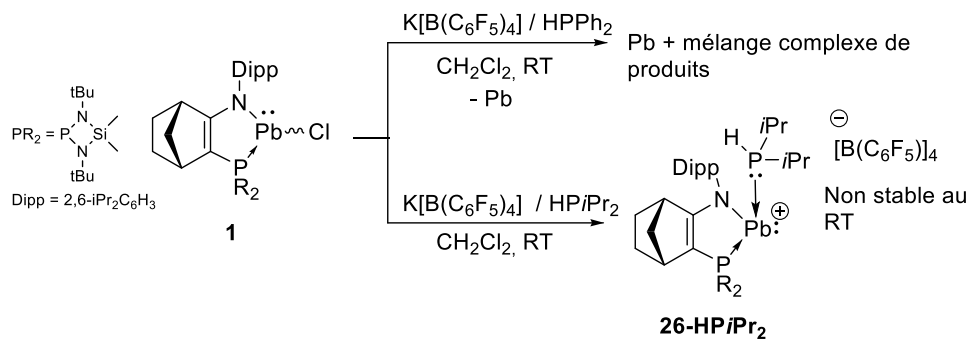


**Schéma 15.** Synthèse du plombyliumylidène cationique **26-HP*i*Pr<sub>2</sub>**.

Probablement, la décomposition du complexe de plombyliène **1** dans le cas où il réagit avec la diphénylphosphine HPPPh<sub>2</sub> en présence de K[B(C<sub>6</sub>F<sub>5</sub>)<sub>4</sub>] commence par l'abstraction d'hydrure par le plombyliumylidène avec la formation d'un complexe Pb-hydride instable **29** et un sel de phosphénium hautement réactif (Schéma 16). Le complexe **29** résultant libère le plomb métallique par élimination réductrice, tandis que le ligand protoné et le cation phosphénium réagissent encore, ce qui donne un mélange réactionnel compliqué. La force motrice de la réaction est probablement la formation du cation phosphénium (+PPh<sub>2</sub>) qui est efficacement stabilisé par deux substituants phényles.

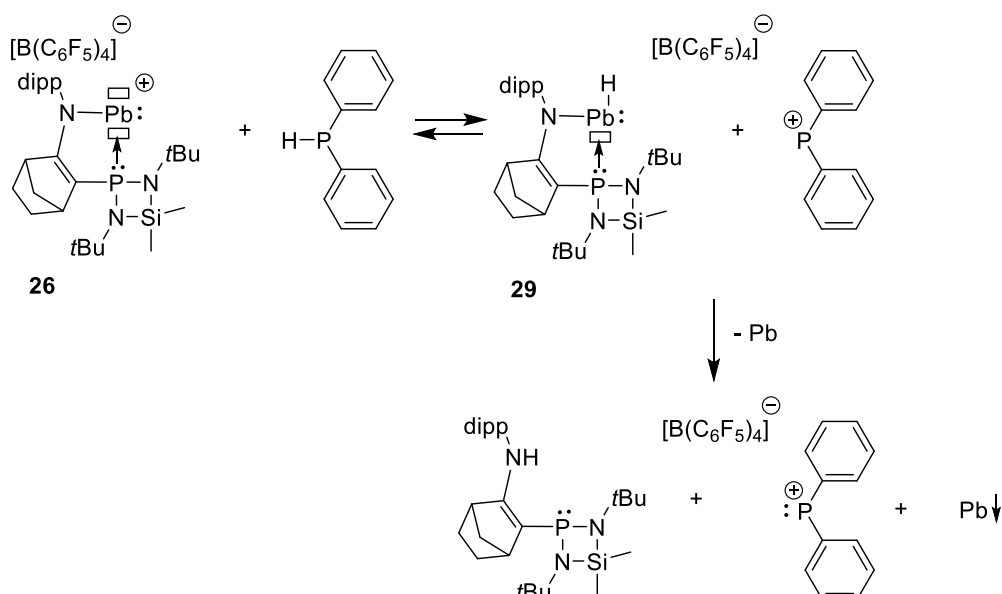


**Schéma 16.** Tentative de synthèse du complexe **26-PPh<sub>2</sub>** et sa décomposition rapide.

En revanche, avec la diisopropylphosphine (HP*i*Pr<sub>2</sub>), l'abstraction de l'hydrure est entravée en raison de l'instabilité du cation phosphénium résultant (<sup>+</sup>P*i*Pr<sub>2</sub>). En effet, la réaction du plombyliène **1** avec la diisopropylphosphine en présence du K[B(C<sub>6</sub>F<sub>5</sub>)<sub>4</sub>] à température ambiante donne le complexe attendu **26-HP*i*Pr<sub>2</sub>** sous la forme d'une poudre rouge foncé avec un rendement de 64 % (schéma 17). Dans le spectre RMN <sup>31</sup>P{<sup>1</sup>H}, deux signaux apparaissent à 213,3 ppm (PN<sub>2</sub>) et 51,3 ppm (HP*i*Pr<sub>2</sub>). Le signal RMN <sup>1</sup>H correspondant à la fonction P-H est apparu sous la forme d'un doublet à 5,14 ppm (<sup>1</sup>J<sub>H-P</sub> = 312,43 Hz).

Ce composé est relativement stable à la température ambiante, cependant, il se décompose lentement en solution, ce qui entraîne la précipitation de plomb métallique et la formation d'un mélange complexe de produits non identifiés. Cela pourrait être une conséquence de la lenteur de la formation du cation diisopropylphosphénium (<sup>+</sup>P*i*Pr<sub>2</sub>). En effet, l'utilisation d'un excès de diisopropylphosphine (HP*i*Pr<sub>2</sub>) favorise la réaction de décomposition via la réaction d'abstraction d'hydrure. L'excès de HP*i*Pr<sub>2</sub> stabilise le cation diisopropylphosphénium en formation par sa coordination et favorise donc la formation du complexe phosphinephosphénium stable **30** (Schéma 17). Ainsi, en raison de l'instabilité de **26-HP*i*Pr<sub>2</sub>** en présence d'un excès de phosphine, ce modèle

ne peut pas être appliquée avec succès dans les réactions catalytiques.

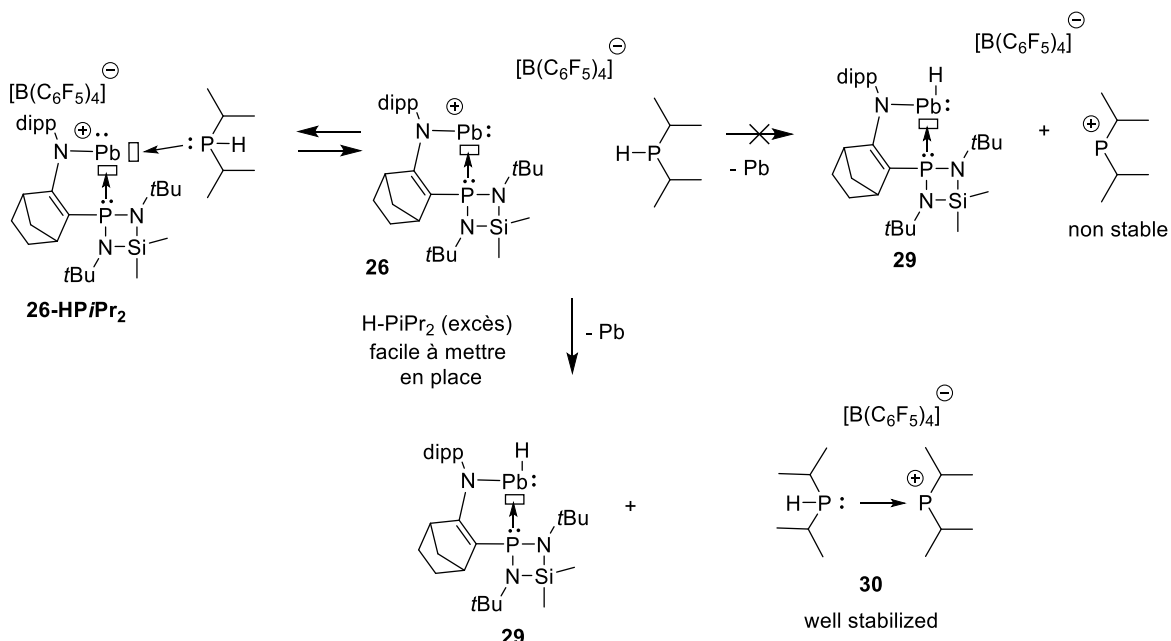


Schéma 17. Réaction de 26 avec la diisopropylphosphine

- *Plombyliumylidènes cationiques stabilisés par des amines secondaires 26-HNR<sub>2</sub> (R = iPr)*

Une stratégie possible pour éviter cette réaction problématique de transfert d'hydrure est l'utilisation d'amines secondaires comme ligands pour la stabilisation des espèces de plombyliumylidène. En effet, en raison de la polarité inversée de la liaison N-H ( $N^{\delta-}H^{\delta+}$ ) et de l'instabilité de l'ion nitrenium  $R_2N^+$ , la réaction de transfert d'hydrure est peu probable.

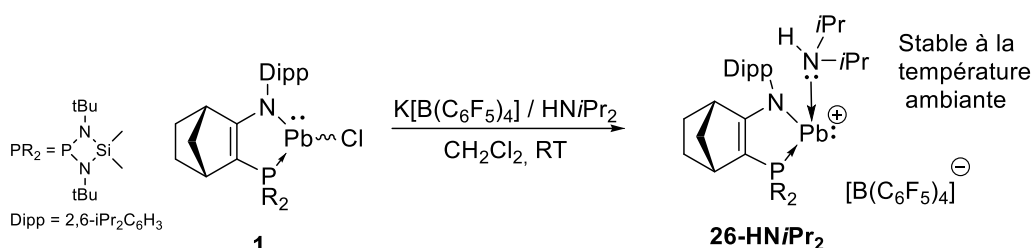


Schéma 18. Synthèse du plombylidène cationique 26-HNiPr<sub>2</sub>.

Nous avons donc synthétisé **26-NHiPr<sub>2</sub>** en utilisant la même stratégie que pour les autres plombyliènes cationiques **26-L** stabilisés par une base de Lewis (Schéma 18). Comme prévu, le composé **26-NHiPr<sub>2</sub>** est stable même en présence d'un excès d'amine. Dans le spectre RMN <sup>31</sup>P, un singulet à 259,0 ppm est apparu avec des satellites dus à l'atome <sup>207</sup>Pb avec une constante de couplage typiquement grande  $^1J_{P-Pb} = 3915$  Hz. Comme dans les cas précédents, le signal en RMN <sup>207</sup>Pb n'a pas pu être observé, probablement en raison de la nature labile du ligand amine. Dans le spectre RMN <sup>1</sup>H, le signal des protons CH-*i*Pr du ligand amine coordonné a été observé à 2,55 ppm avec une constante de couplage  $^1J_{H-H} = 6,3$  Hz, tandis que les protons CH<sub>3</sub>-*i*Pr sont apparus à 0,67 ppm sous la forme d'un doublet avec la même constante de couplage ( $^1J_{H-H} = 6,3$  Hz). Ainsi, les décalages pour le NH*i*Pr<sub>2</sub> coordonné en RMN-<sup>1</sup>H sont légèrement décalés vers les hauts champs par rapport à la diisopropylamine libre (CH-*i*Pr m, 2,70, CH<sub>3</sub>-*i*Pr 0,95, d,  $^1J_{H-H} = 5,0$  Hz) en raison de la coordination au centre métallique.

- Réactivité du complexe **26-NHiPr<sub>2</sub>** avec les alcynes.

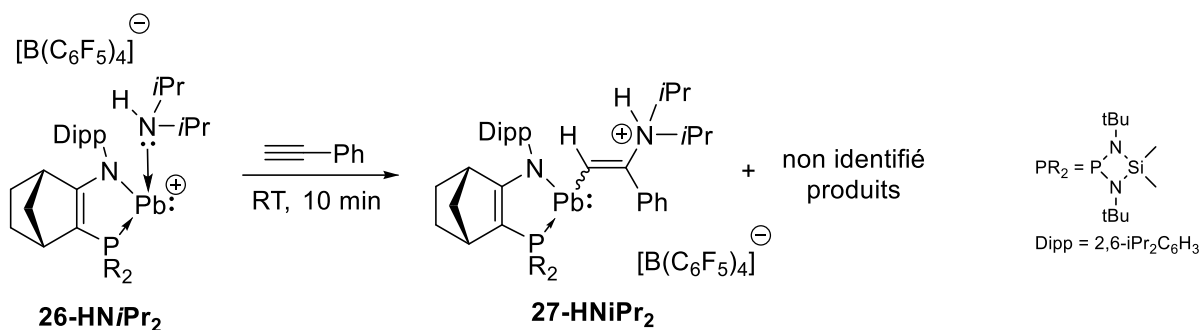


Schéma 19. Réaction de **26-HNiPr<sub>2</sub>** avec  $\text{HC}\equiv\text{CPh}$ .

Comme le complexe **26-PPh<sub>3</sub>**, **26-NHiPr<sub>2</sub>** réagit facilement avec 1 équivalent de phénylacétylène, donnant le produit vinyl-plombyle 27-HNiPr<sub>2</sub> avec plusieurs produits non identifiés (Schéma 19). En effet, la réaction d'insertion de l'acétylène dans la liaison Pb-N a été observée par spectroscopie RMN. Le spectre RMN <sup>31</sup>P présente un signal singulet à 176,1 ppm avec deux satellites dus à l'atome de plomb (<sup>1</sup>J<sub>PbP</sub> = 2404 Hz). Ce signal apparaît à bas champ dans la même région que les analogues avec la phosphine discutés ci-dessus (166 - 171 ppm). Avec un excès de diisopropylamine (10 eq), le signal de **26-NHiPr<sub>2</sub>** est apparu dans le spectre RMN <sup>31</sup>P, suggérant une réaction de métathèse. En effet, il a été constaté que l'hydroamination régiosélective du phénylacétylène pouvait être catalysée par **26-NHiPr<sub>2</sub>** (5 mol %) (Schéma 20). Cependant, le rendement de la réaction reste faible (< 22%), même après optimisation de la réaction, probablement en raison de réactions secondaires indésirables, qui désactivent le catalyseur.

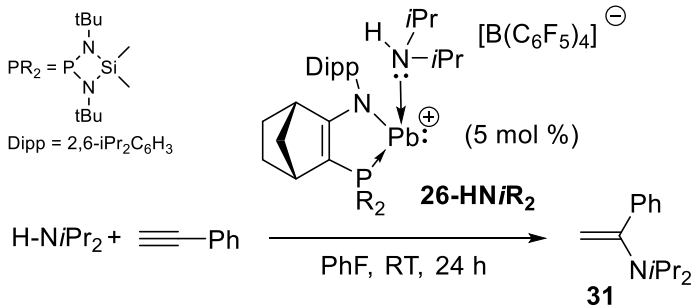
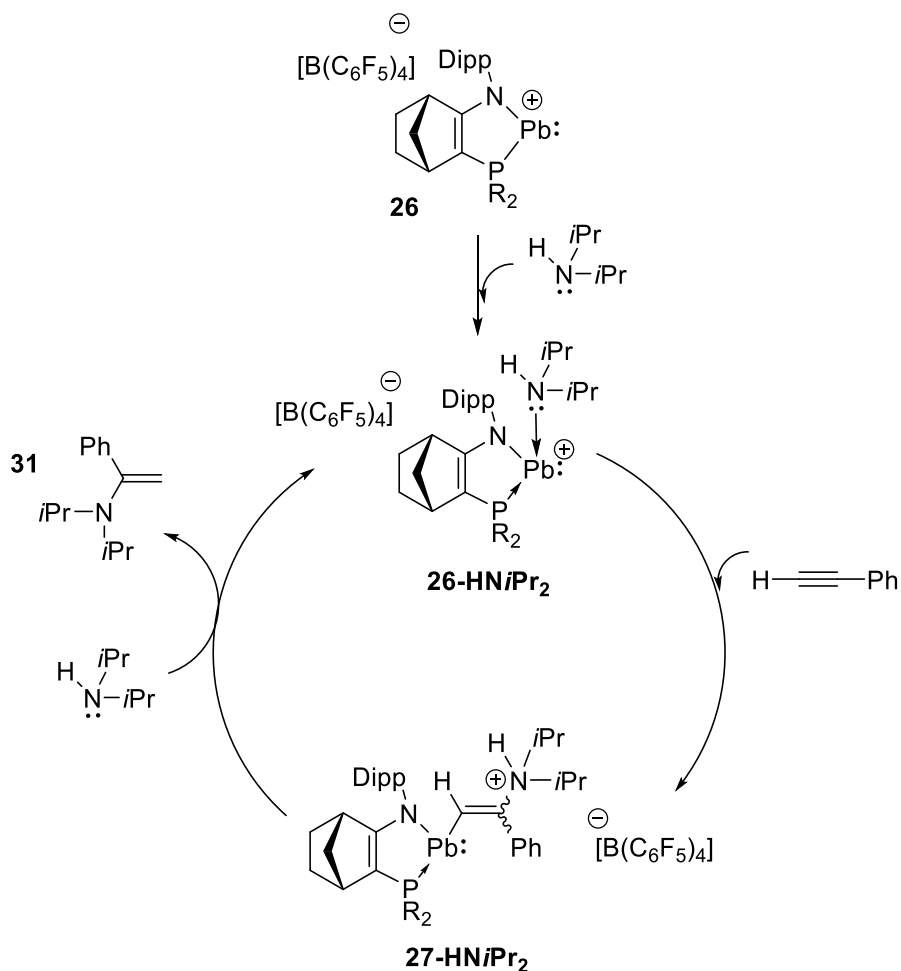


Schéma 20. Hydroamination du phénylacétylène catalysée par **26-HNiPr<sub>2</sub>**.

Le cycle catalytique commence par la génération du **26-HNiPr<sub>2</sub>** via la coordination de la diisopropylamine au plombbyliumylidène cationique **26**. Ensuite, l'insertion du phénylacétylène dans la liaison Pb-N donne le complexe **27-HNiPr<sub>2</sub>** qui régénère ensuite le catalyseur actif **26-HNiPr<sub>2</sub>** par une réaction de métathèse avec un autre équivalent de l'amine, conduisant au produit d'hydroamination **31** dans cette dernière étape (Schéma 21).



**Schéma 21.** Proposition de cycle catalytique pour l'hydroamination du phénylacétylène catalysée par le complexe plombyliumylidène cationique **26-HNiPr<sub>2</sub>**.

Inspirés par les résultats précédents, nous avons considéré la synthèse du plombyliumylidène cationique stabilisé par l'ammoniac **26-NH<sub>3</sub>**. A ce jour, l'hydroamination de nombreuses espèces insaturées non activées avec l'ammoniac, l'amine la plus simple, est considérée comme un Graal en chimie. Cependant, même pour les métaux de transition, de telles réactions restent limitées.<sup>[13]</sup> Ainsi, nous avons préparé le plombyliumylidène cationique **26-NH<sub>3</sub>** via l'abstraction du chlore de **1** avec K[B(C<sub>6</sub>H<sub>5</sub>)<sub>4</sub>] et 3 bar d'ammoniac, ajoutés à -30 °C (Schéma 22). Comme prévu, le spectre RMN <sup>31</sup>P de ce composé présente un signal singulet à 217 ppm avec deux satellites dus aux noyaux <sup>207</sup>Pb <sup>1</sup>J<sub>Pb-P</sub> = 3985 Hz.

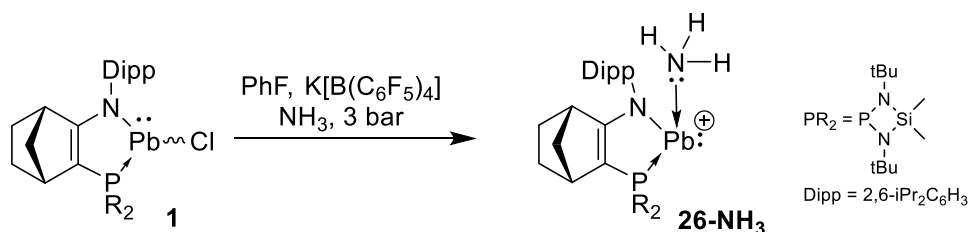


**Schéma 22.** Synthèse du plombyliumylidène cationique stabilisé par l'ammoniac **26-NH<sub>3</sub>**.

Cependant, lorsque le phénylacétylène a été ajouté au **26-NH<sub>3</sub>** fraîchement préparé, aucune réaction n'a été observée. Même après un chauffage de 2 h à 60 °C, nous n'avons pas observé de conversion. Cela pourrait probablement être une conséquence du système de ligand volumineux, qui empêche l'insertion de la partie acétylène dans la liaison Pb-N du **26-NH<sub>3</sub>**. Le complexe **26-NH<sub>3</sub>** est instable à température ambiante et se décompose après une nuit, mais il peut être conservé en solution sous une atmosphère inerte à -45 °C pendant trois jours.

Plusieurs chloroplombylènes stabilisés par différents types de phosphines plus ou moins

encombrées (a, b, c) ont été préparés en suivant la stratégie de synthèse déjà établie dans notre groupe (Schéma 23). La déprotonation des ligands iminophosphine correspondants par n-BuLi suivie de l'addition de PbCl<sub>2</sub> dans le THF donne les chloroplombylènes **1a-c** correspondants avec des rendements modérés (59 % pour **1a**, 40 % pour **1b**, 47 % pour **1c**). Ces modèles sont très fragiles et commencent à se décomposer après une nuit dans la boîte à gants à -30 °C.

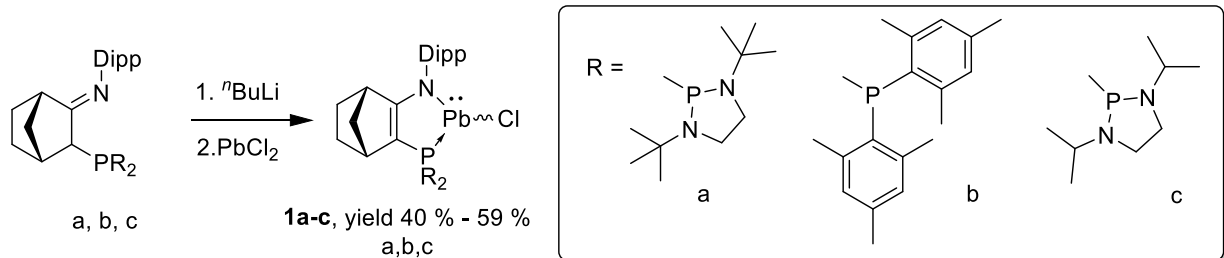


Schéma 23. Synthèse des plombylènes **1a-c**.

<sup>31</sup> P{ <sup>1</sup> H} RMN	<b>1a</b>	<b>1b</b>	<b>1c</b>
Phosphine ( $\delta$ ) (ppm)	209	60	207
$^1J_{\text{Pb-P}}$ (Hz)	3807	2247	3916

Tableau 4 : RMN <sup>31</sup>P{<sup>1</sup>H} de **1a-1c**.

Dans le spectre RMN <sup>31</sup>P{<sup>1</sup>H}, les modèles **1a** et **1c** apparaissent sous la forme de singulets à 209 et 207 ppm avec de grandes constantes de couplage  $^1J_{\text{Pb-P}}$  (3807 et 3916 Hz) comme pour le complexe **1** (tableau 4). En revanche, le signal du plombylène **1b** apparaît à un champ plus élevé (60 ppm).

Probablement à cause des groupement amino sur l'atome de P, les déplacements chimiques de **1a** et **1c** en RMN <sup>31</sup>P{<sup>1</sup>H} apparaissent à champ plus faible que dans le cas de **1b**.

A partir des plombylènes **1a-1c**, leurs dérivés cationiques ont été préparés en suivant la stratégie de synthèse initiale utilisée pour **26** (Schéma 24). Ainsi, les plombylènes **1a-1c** ont été mis en réaction avec un équivalent de K[B(C<sub>6</sub>F<sub>5</sub>)<sub>4</sub>] dans du fluorobenzène, et immédiatement la couleur des solutions est devenue rouge foncé. Dans les spectres RMN <sup>31</sup>P, des signaux singulets comportant des satellites, dus à la constante de couplage P-Pb, ont été observés à champ faible (tableau 5).

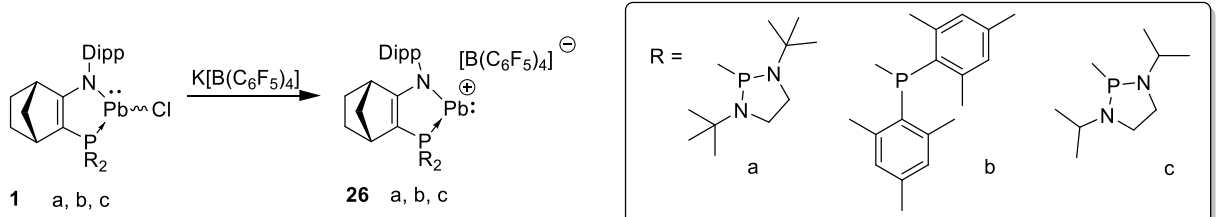
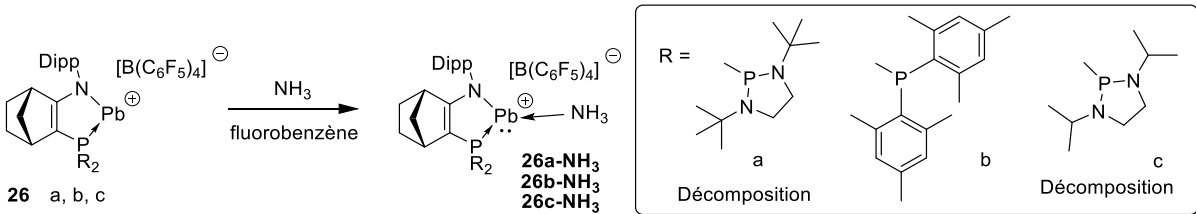


Schéma 24. Synthèse des plombyliumylidènes cationiques **26a-c**.

<sup>31</sup> P{ <sup>1</sup> H} RMN	<b>26a</b>	<b>26b</b>	<b>26c</b>
Phosphine ( $\delta$ ) (ppm)	251	97	252
$^1J_{\text{Pb-P}}$ (Hz)	3773	2487	3523

Tableau 5. RMN <sup>31</sup>P{<sup>1</sup>H} de **26a-c**.

Dans l'étape suivante, ces plombyliumylidènes ont été mis en réaction avec 3 bar de NH<sub>3</sub> (Schéma 25). Cependant, les modèles **26a** et **26c** sont apparus très fragiles et se décomposent facilement comme l'indique la formation immédiate d'une grande quantité de précipité blanc et le changement de couleur du rouge foncé au jaune pâle. De plus, l'analyse RMN <sup>31</sup>P du mélange indique la décomposition complète de **26a** et **26c** même à -30 °C. En revanche, **26b** réagit proprement avec NH<sub>3</sub>, conduisant au plombyliumylidène cationique **26b-NH<sub>3</sub>**, comme le montre le spectre RMN <sup>31</sup>P, avec un nouveau signal à 48 ppm avec les satellites dus au plomb avec une grande constante de couplage ( $^1J_{\text{P-Pb}} = 1486$  Hz).



**Schéma 25.** Réaction des plombyliumylidènes cationiques **26a-c** avec 3 bar d'ammoniac.

La réactivité du modèle **26b-NH<sub>3</sub>** a ensuite été testée avec des alcynes. Cependant, comme pour le modèle **26-NH<sub>3</sub>**, lorsque 1 équivalent de phénylacétylène est ajouté à **26b-NH<sub>3</sub>**, aucune réaction propre n'a été observée après chauffage à 80 °C pendant 1,5 heures, et à la place, certains produits de décomposition non identifiés ont été formés.

Compte tenu de ces résultats, pour réaliser des réactions d'hydroamination avec l'ammoniac catalysées par notre système catalytique, il est évident que le système devra être amélioré.

#### IV. Conclusions et perspectives

Encouragés par les travaux réalisés dans notre groupe concernant les silylènes et les germylènes stabilisés par notre système de ligand original (amino-Phosphine), nous avons développé la synthèse d'un chloroplombylène stable original stabilisé par le même système de ligand. De manière intéressante, la substitution nucléophile de l'atome de chlore par le NaPCO permet d'obtenir un nouveau plombylène fonctionnalisé par un fragment phosphacétène. Contrairement aux analogues plus légers, ce nouveau plombylène substitué par un phosphacétène évolue de manière inhabituelle par élimination réductrice au niveau du centre de plomb divalent, conduisant à de nouveaux phosphanylidène- $\sigma^4$ -phosphoranes et du plomb métallique. L'(amino)phosphanylidène- $\sigma^4$ -phosphorane à cinq chaînons présente une réactivité unique en tant que phosphinidène stabilisé par l'imine en raison de la fonction phospha-ylure hautement polarisée et de la liaison P(II)-N labile. Une étude mécanistique a démontré que la réaction se déroule par élimination réductrice au niveau du centre Pb(II), conduisant à de nouveaux dérivés amino- et phosphonio-phosphacétènes, qui évoluent pour donner les phosphanylidènes phosphoranes obtenus expérimentalement. Notamment, l'amino-phosphacétène évolue par élimination du CO pour générer un intermédiaire phosphinidène qui est stabilisé par coordination de la phosphine pour former le phosphanylidène phosphorane cyclique. Ces résultats suggèrent que les phosphacétènes substitués par un fragment plombylène peuvent être des précurseurs privilégiés de phosphinidène, puisque les seuls sous-produits sont des molécules inertes (Pb métallique et gaz CO).

La réactivité du complexe chloroplombylène parent peut être considérablement améliorée par l'abstraction de l'atome de chlore, conduisant à un nouveau plombyliumylidène cationique stabilisé par une phosphine. Ces cations Pb(II)<sup>+</sup> sont extrêmement électrophiles et peuvent être stabilisés par la coordination de divers ligands de type base de Lewis. Malgré la stabilisation du cation plombylène par deux ligands, il reste réactif et réagit facilement avec le phénylacétylène par insertion d'alcyne dans la liaison Pb-L (L = PR<sub>3</sub>, NR<sub>3</sub>). Notamment, le Pb<sup>+</sup> stabilisé par une amine secondaire (HN/Pr<sub>2</sub>) peut être utilisé comme catalyseur pour l'hydroamination du phénylacétylène. Cependant, les tentatives d'hydroamination de composés insaturés avec l'ammoniac ont échoué jusqu'à présent et les modèles doivent donc être repensés pour améliorer leurs performances.

#### V. Références bibliographiques

- [1] N. Del Rio, A. Baceiredo, N. Saffon-Merceron, D. Hashizume, D. Lutters, T. Müller, T. Kato, *Angew. Chemie - Int. Ed.* **2016**, *55*, 4753–4758.
- [2] S. Yao, Y. Xiong, T. Szilvási, H. Grützmacher, M. Driess, *Angew. Chemie* **2016**, *128*, 4859–4863.
- [3] D. Heift, Z. Benko, H. Grützmacher, *Dalt. Trans.* **2014**, *43*, 5920–5928.
- [4] D. Raiser, K. Eichele, H. Schubert, L. Wesemann, *Chem. - A Eur. J.* **2021**, *27*, 14073–14080.
- [5] B. A. Surgenor, M. Bühl, A. M. Z. Slawin, J. D. Woollins, P. Kilian, *Angew. Chemie* **2012**, *124*, 10297–10300.
- [6] D. Heift, Z. Benko, H. Grützmacher, A. R. Jupp, J. M. Goicoechea, *Chem. Sci.* **2015**, *6*, 4017–4024.
- [7] P. Pyykkö, M. Atsumi, *Chem. - A Eur. J.* **2009**, *15*, 12770–12779.

- [8] John Aurie Dean, Norbert Adolph Lange, Lange's Handbook of Chemistry, 15, **1999**.
- [9] T. Lin, G. Lee, S. Peng, C. Chiu, H. Chen, Polymer, 121748 **2019**, *180*.
- [10] R. Guthardt, J. Oetzel, J. I. Schweizer, C. Bruhn, R. Langer, M. Maurer, J. Vícha, P. Shestakova, M. C. Holthausen, U. Siemeling, *Angew. Chemie - Int. Ed.* **2019**, *58*, 1387–1391.
- [11] B. D. Rekken, T. M. Brown, M. M. Olmstead, J. C. Fettinger, P. P. Power, *Inorg. Chem.* **2013**, *52*, *6*, 3054–3062
- [12] N. Kano, N. Tokitoh, R. Okazaki, *Organometallics* **1997**, *16*, 4237–4239.
- [13] S. Streiff, F. Jérôme, *Chem. Soc. Rev.* **2021**, *50*, 1512–1521.

## Abstract

This thesis focuses on the synthesis and reactivity of new low valent lead species: (i) phosphine-stabilized plumbylenes and (ii) the corresponding cationic plumbyliumylidene derivatives featuring two empty formal orbitals. The stabilization of these highly electrophilic species will be considered by the coordination of two Lewis bases to the lead cationic center.

The first chapter presents a bibliographic overview of the state of the art in the field of heavier carbene analogues capable of activating small molecules (e.g. H<sub>2</sub>, NH<sub>3</sub>, CO, ethylene...). Particular emphasis has been put on the structure-reactivity relationship of these derivatives.

The second chapter presents the synthesis and characterization of the first stable phosphine-stabilized plumbylene substituted by a phosphaketene function via the reaction of chloroplumbylene and NaPCO and fully characterized in solution and in the solid state. This phosphaketene thermally evolves in an unusual manner via a reductive elimination at the divalent lead center, affording new phosphanylidene- $\sigma^4$ -phosphoranes, and lead metal. Particularly the five-membered cyclic phosphanylidene phosphorane shows a unique reactivity due to the highly polarized phospha-ylide function and labile P(II)-N bond. Mechanistic studies indicate that the reaction starts with the reductive eliminaton of Pb metal to form new amino- and phosphonio-phosphaketene derivatives which evolve further to give the experimentally obtained phosphanylidene phosphoranes. Particularly, the amino-phosphaketene evolves via CO-elimination to generate a phosphinidene intermediate which stabilized by the coordination of phosphine to produce the cyclic phosphanylidene phosphorane. Since this process produces only inert by-products such as Pb metal precipitate and CO gas, the plumbylene-substituted phosphaketene can be a useful phosphinidene precursor.

The last chapter concerns the synthesis of new phosphine-stabilized plumbyliumylidene cations. These cationic species are extremely electrophilic and can therefore be stabilized by coordination of different Lewis base ligands. Of particular interest, despite the stabilization of the plumbylene cation by two ligands, it still remains reactive and readily reacts with phenylacetylene by alkyne insertion into the Pb-L bond (L = PR<sub>3</sub>, NR<sub>3</sub>). Notably, the amine adduct efficiently catalyse the hydroamination of phenylacetylene. However, our attempts to prepare the hydroamination of unsaturated compounds with ammonia were not successful and the catalyst designs should be modified to improve their performance.